Comparing the group-contribution SAFT-γ Mie equation of state with SAFT-VR Mie

by

Ruan Martin Hurter

Thesis presented in partial fulfilment
of the requirements for the Degree

of

MASTER OF ENGINEERING
(CHEMICAL ENGINEERING)

in the Faculty of Engineering
at Stellenbosch University

The financial assistance of the National Research Foundation (NRF) towards this research is hereby acknowledged. Opinions expressed and conclusions arrived at are those of the author and are not necessarily to be attributed to the NRF.

Supervisor
Prof. A.J. Burger

Co-Supervisor
Dr J.T. Cripwell

December 2019

Declaration

By submitting this thesis electronically, I declare that the entirety of the work contained therein is my own, original work, that I am the sole author thereof (save to the extent explicitly otherwise stated), that reproduction and publication thereof by Stellenbosch University will not infringe any third party rights and that I have not previously in its entirety or in part submitted it for obtaining any qualification.

Date: December 2019

Plagiarism Declaration

1. Plagiarism is the use of ideas, material and other intellectual property of another's work and to present is as my own.

2. I agree that plagiarism is a punishable offence because it constitutes theft.

3. I also understand that direct translations are plagiarism.

4. Accordingly, all quotations and contributions from any source whatsoever (including the internet) have been cited fully. I understand that the reproduction of text without quotation marks (even when the source is cited) is plagiarism.

5. I declare that the work contained in this thesis, except where otherwise stated, is my original work and that I have not previously (in its entirety or in part) submitted it for obtaining any qualification.

Student number: _____

Initials and surname: _____

Signature: _____

Date: _____

Abstract

Group-contribution methods (GCMs) allow engineers to reduce time and other resources spent on conducting experiments for parameterisation of thermodynamic models, because GCMs grant users the ability to build new model fluids using previously parameterised functional groups (FGs). GCMs have widely been applied to semi-empirical cubic equations of state (EoS), activity coefficient models, and simpler variants of statistical associating fluid theory (SAFT) EoS, yet these models remain limited in regard to the types of systems and properties they can describe.

The rigorous SAFT-VR Mie EoS has a variable-range Mie-potential reference fluid and a complex dispersion term that enable it to accurately model second-derivative dependent properties, and properties in the near-critical region, but its model parameters are specific to components. The latter trait poses a problem when no pure-component data are available. A group-contribution (GC) variant of SAFT-VR Mie, SAFT-γ Mie, was recently developed in an attempt to combine the convenience of a GC model with the holistic predictions of SAFT-VR Mie. However, this model is relatively new and prior to this investigation, effects of the GC approach in the SAFT-VR Mie framework had not been evaluated in detail. The purpose of this project was to investigate whether assumptions made by the GC approach benefit or deteriorate different applications of this complex SAFT formulation.

A general comparison between SAFT-γ Mie and SAFT-VR Mie was done to identify characteristics posing a unique challenge to SAFT-γ Mie by modelling components of increasing complexity: nonpolar, non-associating *n*-alkanes and 1-alkenes; polar, non-self-associating *n*-alkyl acetates; and polar, self-associating 1-alcohols. It was found that SAFT-γ Mie is able to model alkanes, alkenes, and acetates accurately, but it failed to produce equally accurate results for 1-alcohols, suggesting that the modelling of small polar molecules poses a problem for SAFT-γ Mie. This notion cannot be verified without doing a comparison involving a larger sample of polar, non-self-associating components.

Ketones and esters were modelled to evaluate the performance of SAFT-γ Mie for polar components. This part of the study also provided the opportunity to evaluate the performance of the pseudo-association approach used to account for dipolar interactions, as well as the consistency in modelling accuracy between linear isomers. SAFT-VR Mie with the Gross & Vrabec (GV) polar term was used as a benchmark. SAFT-γ Mie cannot distinguish between structural isomers using exactly the same functional groups; therefore, new groups were defined for 2-ketones, 3-ketones, and *n*-alkyl propanoates. Results mirrored the 1-alcohol results, indicating

that the modelling of smaller, more polar molecules poses a challenge for SAFT-γ Mie likely due to the disregarding of proximity effects — a change in functional group characteristics based on its environment, i.e. its surrounding groups or atoms. One likely solution to the problem is to introduce second-order group contributions to act as adjustments to first-order contributions, but this empirical adjustment would reduce the model's fundamental predictive capability.

Besides proximity effects, SAFT-γ Mie also disregards structural considerations such as steric hindrance and the order of intramolecular bond formation; this is also expected to have an impact on SAFT-γ Mie's performance. It was found that these structural considerations are vital for accurate modelling of branched alkanes, and that significant differences can be observed in properties of branched alkane isomers. While SAFT-VR Mie models all of the considered branched alkanes accurately, SAFT-γ Mie does not. It was found that the homosegmented approach followed in SAFT-γ Mie's chain term prevents the model from making any distinctions based on a molecule's layout.

A new heterosegmented chain term was proposed: Bonding contributions would be calculated between segments of unique groups instead of between approximated molecular-average segments. Different methods for weighing the contributions of intra- and intergroup bonds were discussed. Although preliminary results suggest that a heterosegmented chain term would allow the model to distinguish between isomers, further investigation is required to evaluate the consequences of the proposed changes.

Uittreksel

Met behulp van groepsbydraemetodes (GCM's) spaar ingenieurs tyd en ander hulpbronne wat op eksperimente vir die parameterisering van termodinamiese modelle bestee sou word, want GCM's laat die gebruiker toe om nuwe vloeiers met voorheen geparameteriseerde funksionele groepe (FG's) te bou. Die toepassing van GCM's in semi-empiriese kubiese toestandsvergelykings (EoS), aktiwiteitskoëffisiëntmodelle en eenvoudiger weergawes van *statistical associating fluid theory* (SAFT) EoS is algemeen, tog bly hierdie modelle beperk ten opsigte van die tipes sisteme en eienskappe wat beskryf kan word.

Die breedvoerige SAFT-VR Mie EoS maak gebruik van 'n reëlbare rekwydte Mie-potensiaal verwysingsvloeier en komplekse dispersie term wat dit in staat stel om eienskappe wat afhanklik is van tweede-orde afgeleides, asook eienskappe naby aan die kritiese gebied, meer akkuraat te voorspel. Die modelparameters is egter eie aan chemiese komponente, wat problematies is indien suiwerkomponentdata nie beskikbaar is nie. 'n Groepsbydrae (GC) weergawe van SAFT-VR Mie, SAFT-γ Mie, is onlangs ontwikkel om die gerieflikheid van 'n GC model met die holistiese modellering van SAFT-VR Mie te kombineer. SAFT-γ Mie is egter nuut, en geen vorige ondersoeke het die uitwerkings van die GC benadering in die SAFT-VR Mie raamwerk deeglik bestudeer nie. Die doel van hierdie projek was om te ondersoek of aannames wat deur die GC benadering gemaak word, verskeie toepassings van hierdie komplekse SAFT formulering bevoordeel of verswak.

'n Algemene vergelyking is tussen SAFT-γ Mie en SAFT-VR Mie getref om te bepaal watter molekulêre eienskappe uitdagings vir SAFT-γ Mie stel. Die vergelyking bestaan uit voorspellings vir komponente met toenemende kompleksiteit: niepolêre, nie-assosiërende *n*-alkane en 1-alkene; polêre, nie-self-assosiërende *n*-alkielasetate; en polêre, self-assosiërende 1-alkohole. Daar is bevind dat SAFT-γ Mie alkane, alkene, en asetate akkuraat kan modelleer, maar dat dit nie ewe akkurate resultate vir 1-alkohole lewer nie, wat moontlik aandui dat die modellering van klein polêre molekule uitdagend vir SAFT-γ Mie is. Hierdie voorstel kan egter nie bevestig word sonder om 'n vergelyking te tref met 'n groter steekproef van polêre, nie-self-assosiërende komponente nie.

Ketone en esters is gemodelleer om SAFT-γ Mie se mate van akkuraatheid vir polêre komponente te evalueer. Hierdie deel van die studie het ook die geleentheid gebied om die akkuraatheid van pseudo-assosiasie, 'n benadering wat gebruik word om dipolêre interaksies in ag te neem, sowel as die konsekwentheid van modellering tussen lineêre isomere te evalueer. SAFT-VR Mie met die Gross & Vrabec (GV) polêre term is as maatstaf gebruik. SAFT-γ Mie kan nie

onderskei tussen strukturele isomere wat presies dieselfde FG's gebruik nie, daarom is nuwe groepe vir 2-ketone, 3-ketone, en *n*-alkielpropanoate gedefinieer. Resultate weerspieël die resultate van 1-alkohole, wat aandui dat die modellering van kleiner, meer polêre molekule moontlik 'n uitdaging vir SAFT-γ Mie is omdat nabyheidseffekte nie in ag geneem word nie. Nabyheidseffekte verwys na 'n verandering in die eienskappe van 'n FG as gevolg van interaksies met omliggende groepe. 'n Moontlike oplossing vir die probleem is om tweede-orde groepsbydraes by te voeg om die eerste-orde groepsbydraes aan te pas, maar hierdie empiriese aanpassing sal die model se fundamentele voorspellingsvermoë verminder.

SAFT-γ Mie ignoreer ook strukturele oorwegings soos steriese verhindering en die orde van intramolekulêre verbindings; dit sal na verwagting ook 'n uitwerking op SAFT-γ Mie se voorspellingsvermoë hê. Daar is bevind dat die bogenoemde strukturele oorwegings noodsaaklik is om vertakte alkane akkuraat te modelleer, en dat beduidende verskille tussen die eienskappe van vertakte alkaan-isomere waargeneem kan word. SAFT-VR Mie kan al die vertakte alkane akkuraat modelleer, maar SAFT-γ Mie kan nie. Die homogesegmenteerde benadering wat in SAFT-γ Mie se kettingterm gevolg word, verhoed dat die model onderskeidings op grond van molekulêre uitleg maak.

'n Nuwe heterogesegmenteerde kettingterm is voorgestel: Die bydraes van intramolekulêre verbindings word sodoende tussen unieke groepe, in plaas van beraamde gemiddelde molekulêre segmente, bereken. Verskillende metodes om die bydraes van intra- en intergroepverbindings te weeg, is bespreek. Alhoewel voorlopige resultate dui dat 'n heterogesegmenteerde kettingterm die model sal toelaat om tussen isomere te onderskei, is verdere ondersoek nodig om die uitwerkings van die voorgestelde veranderinge te evalueer.

Acknowledgements

This work is based on the research supported in part by the National Research Foundation (NRF) of South Africa (UID: 116925) and Sasol (Pty) Ltd. Opinions expressed and conclusions arrived at are those of the author and are not necessarily to be attributed to the sponsors.

The support of the following people carried me through this project. I express my thanks to:

- Prof. A. J. Burger for his excellent guidance, and for constantly helping me to improve my work.
- Dr J. T. Cripwell for sharing insightful ideas and diligent feedback, which contributed greatly to my understanding of SAFT.
- Dr A. J. de Villiers and the other researchers who invested much effort to create and expand upon the software used in this work.
- Ms Sonja Smith and Mr Riccardo Swanepoel for enduring my constant querying about grammar, and for always being keen to discuss technical details.
- the close friends whom I have met during my studies and those who have been there all along. Thank you for your humour, encouragement, shared celebration, and for being next to me when I needed someone to lift my spirits.
- my parents, Martin and Lourette. Ek kon nie vra vir beter mense om my te bring tot waar ek nou is nie. Dankie vir jul eindelose liefde en ondersteuning.

Contents

Nomenclature

Roman Symbols

Symbol	Description	Symbol	Description
a_1, a_2, a_3	dispersion energy perturbations	N_{G}	number of different functional groups
A	Helmholtz energy	N_{P}	number of data points
C	Mie potential prefactor	N_{ST}	number of different hydrogen-bonding sites
C_P	isobaric heat capacity	P	pressure
C_V	isochoric heat capacity	P^{vap}	saturated vapour pressure
d	temperature-dependent segment diameter	r	radial distance
f_{obj}	objective function	r_{ab}^{c}	association range
F	reduced Helmholtz energy state function	r_{ab}^{d}	association distance
H	enthalpy	R	gas constant
H^{vap}	heat of vaporisation	S_k	shape factor
k_{B}	Boltzmann's constant	T	temperature
k_{ij}	binary interaction parameter	u	speed of sound
K_{ab}	association volume	V	volume
m_{s}	SAFT-VR Mie segment number	w	regression weight
n_a	number of type a hydrogen-bonding sites	x_{s}	segment fraction
n_i	number of moles of component i	x	mole fraction
n_{p}	number of polar segments	X_a	fraction of unbonded type a hydrogen-bonding sites
N	number of molecules	z	molecular functional-group fraction
N_{C}	number of components		

Greek Symbols

Symbol	Description	Symbol	Description
Δ_{ab}	association bonding strength	ν_k^*	SAFT-γ Mie segment number
ϵ	dispersion energy parameter	ρ	number density
$\epsilon_{ab}^{\mathrm{HB}}$	association energy parameter	ρ^{sat}	saturated liquid density
λ^{a}	potential well attractive exponent	σ	segment diameter
λ^{r}	potential well repulsive exponent	Φ^{Mie}	Mie potential function
μ	dipole moment	Φ^{SW}	square-well potential function
$\nu_{k,i}$	number of times group k appears in component i	$\boldsymbol{\Omega}$	model parameter vector

Superscripts

Superscript	Description
Assoc	association
Disp	dispersion
E	excess property
HB	hydrogen bonding
HS	hard-sphere
Mono	monomeric segments
res	residual property
sat	saturation / saturated
Seg	segment
vap	vaporisation / vapour

Subscripts

Subscript	Description
a, b, c, d	association site indices
C	critical
calc	calculated
exp	experimental
i, j	component indices
k, l	functional-group indices
m	perturbation index
s	segment

Abbreviations

Abbreviation	Description	Abbreviation	Description
AAD	absolute average deviation	LJ	Lennard-Jones
BH	Barker and Henderson	LMA	Levenberg Marquart algorithm
BIP	binary interaction parameter	NRTL	nonrandom two-liquid
CPA	cubic-plus-association	OF	objective function
CR	combining rule	RDF	radial distribution function
DIPPR	Design Institute for Physical Properties	SAFT	statistical associating fluid theory
EoS	equation(s) of state	sPC-SAFT	simplified perturbed chain statistical associating fluid theory
FG	functional group	SW	square well
GC	group contribution	TPT1	Wertheim's first-order thermodynamic perturbation theory
GCM	group-contribution method	TS	traditionally structured
GV	Gross and Vrabec	UNIFAC	UNIQUAC functional-group activity coefficients
HB	hydrogen bonding	UNIQUAC	universal quasichemical activity coefficients
HS	hard-sphere	VLE	vapour–liquid equilibrium
JC	Jog and Chapman	VR	variable range

Functional Groups

Symbol	Description	Example
C	quaternary carbon group	2,2-dimethylpropane; $CH_3C(CH_3CH_3)CH_3$
CH	tertiary carbon group	2-methylbutane; $CH_3CH(CH_3)\ CH_2CH_3$
CH=	methylidyne group	propene; $CH_2{=}{=}CHCH_3$
CH_2	bridging methylene group	propane; $CH_3CH_2CH_3$
CH_2=	methylene end-group	propene; $CH_2{=}{=}CHCH_3$
CH_2CO	nonterminal ketone group	3-pentanone; $CH_3CH_2COCH_2CH_3$
CH_2OH	1-alcohol group	ethanol; CH_3CH_2OH
CH_3	methyl group	propane; $CH_3CH_2CH_3$
CH_3CO	terminal ketone group (methyl + carbonyl groups)	2-butanone; $CH_3COCH_2CH_3$
CO	alternate ketone group (carbonyl group)	2-butanone; $CH_3COCH_2CH_3$
COO	carboxylate group for acetate esters	ethyl acetate; $CH_3CH_2COOCH3$
COO (pr.)	carboxylate group for propanoate esters	ethyl propanoate; $CH_3CH_2COOCH_2CH3$

Chapter 1: Introduction

1.1 Background

1.1.1 Applications of Thermodynamic Modelling

Process design and optimisation greatly rely on the ability to make accurate predictions for a variety of thermodynamic properties using models, because design through trial and error is often not practical or economical. The industrial application of phase-equilibrium calculations makes vapour–liquid equilibrium (VLE) and liquid–liquid equilibrium (LLE) predictions particularly desirable; however, modern modelling applications increasingly include a variety of properties such as density, speed of sound, and heat capacities [1]. Furthermore, advanced problems in the pharmaceutical and petrochemical industry (e.g., hydrate formation) require thermodynamic models to determine the most stable configuration out of a number of different phase combinations where various solids, liquids and gases may exist simultaneously [2].

The models used most frequently in industry today are cubic equations of state (EoS) (viz. Soave-Redlich-Kwong [3] and Peng-Robinson [4]), and activity coefficient models (viz. nonrandom two-liquid (NRTL) [5], universal quasichemical activity coefficients (UNIQUAC) [6], and UNIQUAC functional-group activity coefficients (UNIFAC) [7]) [1]. For decades, researchers have been dedicated to parameterising and improving these models because they are relatively simple and effective at predicting phase equilibria, but due to their simplicity they remain limited in their applications — activity coefficient models are restricted to the liquid phase and require experimental data for system-specific parameterisation, and the basic cubic EoS are only effective for the vapour phase of near-ideal species. Moreover, thermodynamic properties that are calculated using second derivatives of thermodynamic potentials (viz. heat capacities, compressibilities, thermal expansivity, and speed of sound) can generally not be modelled accurately using the previously mentioned thermodynamic methods [8]. These properties are often estimated using empirical correlations such as those available in *Perry's Chemical Engineers' Handbook* [9], and the parameterisation of these correlations requires experimental data.

The perfect EoS should be able to provide holistic thermodynamic predictions for different phases of both pure components and mixtures without the need for continuous experimentation. The developers of EoS based on the statistical associating fluid theory (SAFT) aim to create such an EoS based on fundamental physical principles. Different variations of SAFT, SAFT-VR Mie in particular, have provided promising advances in recent years [10].

1.1.2 Statistical Associating Fluid Theory

SAFT EoS are based on Wertheim's first-order thermodynamic perturbation theory (TPT1) [11]–[15]. The Helmholtz energy of a system consisting of one or more components is given as a summation of different terms, where each term represents a specific type of interaction between segments — the spherical building blocks of molecules. The first time a SAFT EoS appeared in the familiar form was in an article by Chapman et al. [16] where the dimensionless residual Helmholtz energy is given by the following equation:

$$\frac{A^{\mathrm{res}}}{Nk_{\mathrm{B}}T} = \frac{A^{\mathrm{Seg}}}{Nk_{\mathrm{B}}T} + \frac{A^{\mathrm{Chain}}}{Nk_{\mathrm{B}}T} + \frac{A^{\mathrm{Assoc}}}{Nk_{\mathrm{B}}T} \tag{1.1}$$

where A^{Seg}, the Helmholtz energy of the segments, equals the sum of the hard-sphere (A^{HS}) and dispersion (A^{Disp}) contributions. The contribution of chain formation is denoted by A^{Chain} and association interactions by A^{Assoc}. This version is now often referred to as "the original SAFT". Figure 1.1 illustrates the functions of the different terms:

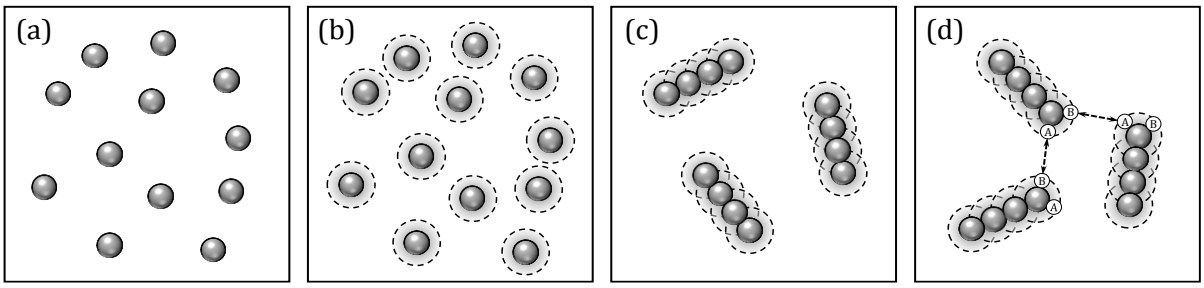

Figure 1.1: Illustration of the Helmholtz contribution of (a) ideal segments, (b) dispersion interactions, (c) chain formation, and (d) association interactions.

Each of the individual contributions are formulated using statistical mechanics while remaining grounded in the fundamental principles. While the chain and association contributions remain mostly based on theories presented by Wertheim, several alterations have been made to the dispersion contribution and intermolecular potential functions, giving rise to different variations of SAFT [1]. One such variation, the recently developed SAFT-VR Mie of 2013 by Lafitte et al. [10], boasts accurate descriptions of second-derivative and phase-behaviour properties. Its success is credited to: (i) the more rigorous Mie potential function [17] that is used to characterise intermolecular interactions instead of a simpler approximation, e.g., hard-sphere (HS) or square-well (SW); and (ii) the third-order Barker and Henderson (BH) high-temperature perturbation expansion of the dispersion contribution that allows for a better description of the near-critical region. Note that SAFT-VR Mie was first introduced in 2006 by Lafitte et al. [18] without the third-order expansion, but throughout the rest of this study the term "SAFT-VR Mie" will refer to the modified 2013 variant. Besides modifications to the potential function and dispersion term

formulation, SAFT has also been modified by adding new terms to account for different intermolecular interactions. One modified SAFT variant that makes use of a dipolar term is SAFT-VR Mie + GV [19]. Dipolar extensions to SAFT are further discussed in Section 2.1.3.

1.1.3 Predictive Capability and the Group-Contribution Method

Predictive capability refers to the ability to model a wide array of properties or components without needing excessive experimental data for correlation. Predictive capability on a *property level* is demonstrated by SAFT EoS with their ability to retain a good degree of accuracy for binary and multi-component phase-equilibrium predictions, despite normally being parameterised on pure-component data alone. Typical examples of predictive capability on a *component level* are group contribution (GC) models which move the focus of model parameterisation from components to functional groups (FGs). These groups are seen as the building blocks of molecules, and each is comprised of one or more atomic descriptors. In group-contribution methods (GCMs), it is assumed that the individual contributions of FGs can be added to obtain the overall properties of a system. The term *solution-of-groups*, made popular by the analytical solution of groups (ASOG) model [20] (one of the first GC models), captures the essence of GCMs well by emphasising that systems are seen as collections of groups and not molecules.

The group-contribution method was proposed for the modelling of pure components in the work of van Krevelen in 1972 [21], and shortly thereafter Fredenslund et al. [7] used the GC method to develop the UNIFAC activity coefficient model, a GC variant of UNIQUAC. UNIFAC and its modified variants saw successful application in industry and remain popular today [1], [22]; however, activity coefficient models are limited to liquid-phase applications and a small variety of property predictions. Therefore, the GC method has more recently been used in the development of various EoS such as the predictive Peng-Robinson (or PPR78) [23], and Copolymer PC-SAFT [24].

The strength of a GC EoS is being able to transfer model parameters between components and systems. This characteristic is particularly desirable in the modern application of thermodynamic property modelling for polymers and biomolecules [25]. Consequences of small changes to the chemical composition of product streams or the chemical structure of complex molecules can easily be investigated with a robust GC model without additional parameter generation. GCMs also provide the ability to predict the composition of a system with certain desired properties by regressing the number of occurrences of expected functional groups. This falls under the field of computer-aided molecular design (CAMD) [26].

1.1.4 Group-Contribution Method in a Complex SAFT Framework

As a result of its complexity, the parameterisation of SAFT-VR Mie is a challenge because associating species usually require the regression of a large number component-specific parameters. Several studies have aimed to determine the most effective parameterisation methods for component-oriented SAFT variants ([27]–[29]); however, it remains a time consuming exercise that largely relies on the availability and integrity of experimental data for different thermodynamic properties of each chemical component to be modelled.

In an attempt to increase the predictive capability of SAFT-VR Mie, Papaioannou et al. [30] developed a GC variant called SAFT-γ Mie. This new model makes use of a heteronuclear molecular model where each functional group consists of distinct monomeric segments, as opposed to a homonuclear model such as GC-SAFT [31], [32]. In homonuclear models, FG parameters are used to create component parameters that can be applied in a standard framework where all of the reference fluid segments are identical. Despite the successful applications of SAFT-γ Mie reported in various sources ([30], [33]–[35]), this GC approach makes the potentially limiting structural-independence assumption: A certain functional-group's contribution to the Helmholtz terms, as in Eq. (1.1), is independent of the overall structure of the molecule and also the location of the group inside the molecule. For example, the individual CH_3 and CH_2 group interactions are expected to be equally strong in both a short-chain alkane (e.g., C_3H_8) and a long-chain alkane (e.g., $C_{30}H_{62}$). GC models that make the structural-independence assumption are also unable to distinguish between isomers.

The single-component and binary mixture predictions of SAFT-γ Mie for *n*-alkanes and *n*-alkyl esters are compared to that of SAFT-γ Square-Well (SW) [36], [37] and UNIFAC (Dortmund) [38] in the original article by Papaioannou et al. [30], and comparisons were made for phase-equilibrium predictions between SAFT-γ Mie and UNIFAC in Sadeqzadeh et al. [39]. The performance of SAFT-γ Mie is yet to be evaluated against that of its non-GC predecessor, SAFT-VR Mie. Hence, the following questions remain unanswered in the open literature:

(i) Is the GC variant flexible enough to remain accurate for a wide range of properties and components?

(ii) To what extent does the structural-independence assumption influence the accuracy of the model?

(iii) Does the GC approach offer some advantages in terms of model accuracy?

(iv) Given that experimental data are still needed to validate the reliability of SAFT-γ Mie predictions, is it worth moving away from SAFT-VR Mie in exchange for the benefits of a GC approach?

1.2 Aim and Hypotheses

The aim of this study is to investigate the feasibility of the GC approach in an advanced SAFT framework by doing a comprehensive comparison between the performance of SAFT-γ Mie and that of its non-GC predecessor, SAFT-VR Mie. The following hypotheses are formulated to guide the project, each followed by an objective or objectives:

1. By assuming that the characteristics of a functional group are independent of its environment, the accuracy of SAFT-γ Mie becomes generally limited, whereas the component-specific regression procedure of SAFT-VR Mie allows it to remain accurate.
   (i) Identify which molecular characteristics pose a challenge when using SAFT-γ Mie by generating predictions with existing parameters for molecules with increasingly nonideal interactions, viz. *n*-alkanes, 1-alkenes, *n*-alkyl acetates, and 1-alcohols.
   (ii) Model short-chain dipolar molecules, such as ketones and esters, and identify whether SAFT-γ Mie has any advantages or disadvantages compared to SAFT-VR Mie + GV. These components are well suited to test the above hypothesis because proximity effects (a change in a group's nature due to the influence of its neighbouring groups) are associated with strong polarity. Additionally, this objective will allow one to investigate the modelling consistency between isomers containing the same functional groups, and the need for an explicit polar contribution in SAFT-γ Mie.
2. Ignoring the physical structure of the molecule in which groups occur compromises SAFT-γ Mie's accuracy for components with nonlinear structures.
   (i) Determine the characteristics of branched components that benefit or hinder SAFT-γ Mie's ability to model their properties accurately.

Chapter 2: Statistical Associating Fluid Theory

2.1 SAFT-VR Mie

The formulation of SAFT-VR Mie by Lafitte et al. [10] is similar to CK-SAFT [40] (a revised version of the original SAFT by Chapman et al. [41]) except for its rigorous Mie potential function and third-order BH perturbation expansion. The eight component-specific parameters of this EoS are: segment number (m_s), segment diameter (σ), dispersion energy (ϵ), attractive exponent (λ^a), repulsive exponent (λ^r), association energy (ϵ_{ab}^{HB}), association distance (r_{ab}^{d}), and association range (r_{ab}^{c}). Each parameter is put into context in the following subsections, but not all of the model equations are given. The complete set of equations that make up SAFT-VR Mie can be found in the appendix of its seminal article by Lafitte et al. [10].

2.1.1 Potential Function

Thermodynamic properties are largely determined by the nonideal interactions of intermolecular forces between the molecules of a pure component or mixture [1]. In the field of molecular physics, these forces are characterised by intermolecular potential functions that provide a way to qualitatively understand fluid properties and phase behaviour [42]. Several different types of intermolecular forces have been theorised, namely, permanent dipole and multipole forces, induced dipole forces (also called London dispersion forces), nonpolar electrostatic forces (e.g., attraction between a nucleus and electron cloud or repulsion between electron clouds), and specific chemical forces (e.g., association through hydrogen bonding). The reader is referred to Chapter 2, Table 2.1 in Kontogeorgis & Folas [1] for a summary of the different intermolecular potential expressions for various nonspecific chemical forces.

The interactions between atoms / molecules of a species that has no permanent polarity, e.g., between noble-gas atoms, are referred to as van der Waals forces. Gustav Mie presented a mathematical formula for these interactions in 1903 [17], known as the Mie potential function, even before the description of induced dipoles by London in 1930 [43]. The Mie potential function is given by the following equation (adaptation by Papaioannou et al. [30]):

$$\Phi^{Mie}(r) = C\epsilon\left[\left(\frac{\sigma}{r}\right)^{\lambda^r} - \left(\frac{\sigma}{r}\right)^{\lambda^a}\right] \tag{2.1}$$

and

$$C = \frac{\lambda^{\mathrm{r}}}{\lambda^{\mathrm{r}} - \lambda^{\mathrm{a}}}\left(\frac{\lambda^{\mathrm{r}}}{\lambda^{\mathrm{a}}}\right)^{\frac{\lambda^{\mathrm{a}}}{\lambda^{\mathrm{r}}-\lambda^{\mathrm{a}}}} \tag{2.2}$$

where C denotes a pre-factor that ensures that the minimum of the function is equal to $-\epsilon$. Figure 2.1 illustrates the Mie potential function:

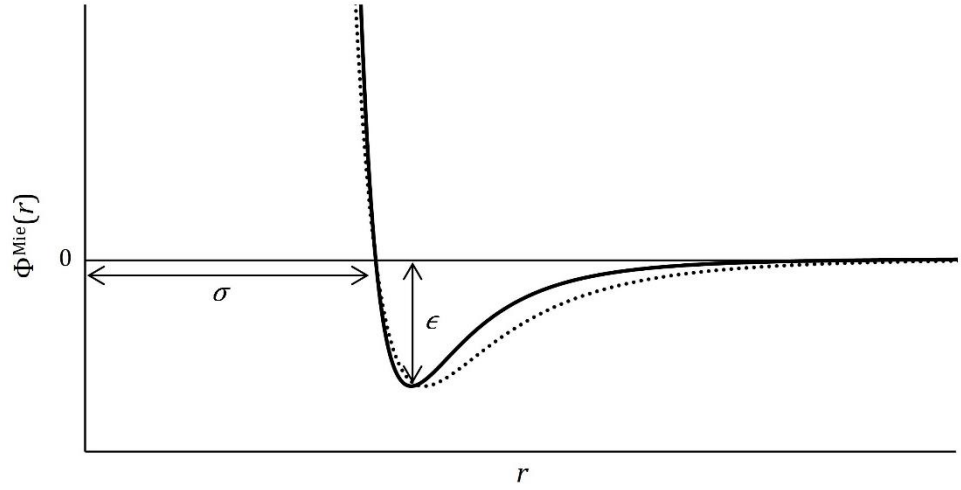

Figure 2.1: Mie potential function. The repulsive exponent of the solid line function is equal to 12 and the dotted line function repulsive exponent is 7. The σ and ϵ annotations are given for the solid line function.

The dispersion energy parameter, ϵ, represents the depth of the potential, and the segment diameter, σ, represents the centre-to-centre distance between segments or where the potential is equal to zero. The repulsive and attractive exponents determine the steepness of the potential function, as illustrated by the two different curves in Figure 2.1. Note that the attractive exponent is fixed to 6 — this value corresponds to the attraction interaction of induced dipoles, and was confirmed by London's theory of dispersion in 1937 [44].

While the Mie potential is the rigorous form of the dispersion potential function, several simplifications exist. The potential function where the repulsive and attractive exponents are fixed to 12 and 6, respectively, is known as the Lennard-Jones (LJ) potential [45]. Another popular simplification is the square-well (SW) potential function, as illustrated in Figure 2.2.

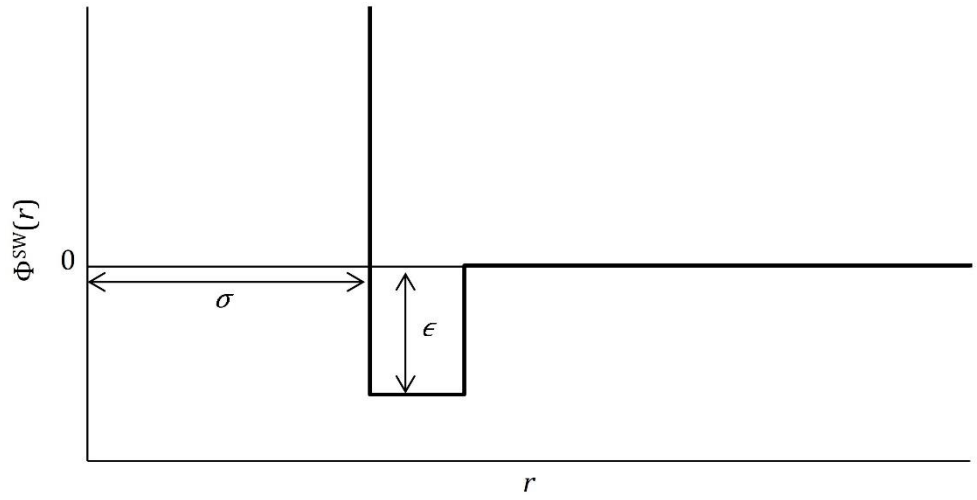

Figure 2.2: Square-well potential function.

Both the SAFT-VR Mie and SAFT-γ Mie EoS use the Mie potential function to express dispersion interactions. In the former model, hydrogen bonding (HB) is assumed to take place between segments with hard-sphere potentials [10] and a LJ potential is used in the latter [33]. The LJ potential was presumably chosen over HS in SAFT-γ Mie to improve the description of systems with very small, associating molecules. An improvement in the modelling of these systems, specifically for pure water and water + methanol, can be observed when replacing the HS potential in the SAFT-VR Mie association term with a LJ or Mie potential [46]. However, a subsequent study [47] concluded that the effects of using more complicated association potential functions are often small and inconsistent for some properties of pure water and water + *n*-alkane mixtures. Given that these observations were made for systems with water, for which association is significant, it is unlikely that the difference in association potential function would have a notable effect on results in this project. This is because the considered components are much larger and have fewer association sites.

2.1.2 Formulation

The Helmholtz free energy is given by the following expression:

$$\frac{A}{Nk_{\mathrm{B}}T} = \frac{A^{\mathrm{Ideal}}}{Nk_{\mathrm{B}}T} + \frac{A^{\mathrm{Mono}}}{Nk_{\mathrm{B}}T} + \frac{A^{\mathrm{Chain}}}{Nk_{\mathrm{B}}T} + \frac{A^{\mathrm{Assoc}}}{Nk_{\mathrm{B}}T} \tag{2.3}$$

where

$$\frac{A^{\mathrm{Mono}}}{Nk_{\mathrm{B}}T} = \frac{A^{\mathrm{HS}}}{Nk_{\mathrm{B}}T} + \frac{A^{\mathrm{Disp}}}{Nk_{\mathrm{B}}T} = \frac{A^{\mathrm{HS}}}{Nk_{\mathrm{B}}T} + \frac{A^{1}}{Nk_{\mathrm{B}}T} + \frac{A^{2}}{Nk_{\mathrm{B}}T} + \frac{A^{3}}{Nk_{\mathrm{B}}T} \tag{2.4}$$

and N refers to the total number of molecules in the system, which is equal to Avogadro's number when it is assumed that the system comprises of one mole. The ideal contribution in Eq. (2.3) comprises of the Helmholtz energy of hard particles with volumes that are negligible compared to the overall volume of the system . A^{Ideal} implicitly includes translational, rotational and vibrational contributions [48]. The first term in the expression for the monomeric segments is the hard-sphere contribution, which accounts for the volume of the segments. The three terms that account for the dispersion interaction between segments are derived from the Barker and Henderson (BH) high-temperature perturbation theory [49], [50]. SAFT-VR Mie is the first variant of SAFT to use a third-order expansion instead of second order. Each term of the third-order expansion is expressed as follows:

$$\frac{A^m}{Nk_{\text{B}}T} = \frac{a_m}{(k_{\text{B}}T)^m}, \quad m = 1,2,3 \tag{2.5}$$

The first-order perturbation term, a_1, is known as the mean-attractive energy and is calculated using an analytical expression of its BH integral. The expression for the second-order term (fluctuation term) is based on an improved BH macroscopic compressibility approximation. The third-order term is calculated with an empirical expression that employs coefficients that were regressed using Monte Carlo simulations of the fluctuation term, data for vapour–liquid equilibria, and critical points [10]. Due to the nature of the regression procedure, the third-order term therefore incorporates the contributions of higher-order BH perturbations.

The chain contribution of Eq. (2.3) is calculated as in Wertheim's TPT1 [15]; however, it makes use of a Mie potential radial distribution function (RDF) instead of a hard-sphere approximation as in the Chapman et al. version [41].

$$\frac{A^{\text{Chain}}}{Nk_{\text{B}}T} = -\sum_{i=1}^{N_{\text{C}}} x_i(m_i - 1)\ln g_{ii}^{\text{Mie}}(\sigma_{ii}) \tag{2.6}$$

The association contribution is calculated with the standard TPT1 expression, which was formulated using statistical mechanical methods. The association expression given by Eq. (2.7) is analogous to the one presented in the 1989 article of Chapman et al. [16] in which the original SAFT was extended to associating molecules.

$$\frac{A^{\text{Assoc}}}{Nk_{\text{B}}T} = \sum_{i=1}^{N_{\text{C}}} x_i \sum_{a=1}^{s_i} n_{a,i}\left(\ln X_{a,i} - \frac{1}{2}X_{a,i} + \frac{1}{2}\right) \tag{2.7}$$

For a certain chemical component i, $n_{a,i}$ equals the number of hydrogen-bonding (HB) sites of type a, and s_i is the total number of different bonding sites on i. $X_{a,i}$ represents the fraction of molecules of i not partaking in association bonding at site type a, and can be calculated analytically after assuming an association scheme for the chemical component in question. This calculation depends on both the number density of the system ($\rho = \frac{N}{V}$, with N as the number of molecules and V as the total system volume) and Δ_{ab}, which characterises the bonding strength between sites a and b. Δ_{ab} is calculated with the following equation:

$$\Delta_{ab} = \sigma^3 F_{ab} I_{ab} \tag{2.8}$$

F_{ab} depends on the association energy ($\epsilon_{ab}^{\mathrm{HB}}$), and I_{ab} depends on the RDF and the association volume (K_{ab}). The association volume is calculated with the segment diameter, σ, the association distance, r_{ab}^{d}, and the association range r_{ab}^{c} (i.e. the range of attraction between HB sites). The assumption that $r_{ab}^{\mathrm{d}} = 0.4\sigma$ is usually made for the association distance, i.e. the distance between an association site and the centre of the adjacent Mie segment [10].

It is important to note that Wertheim's TPT1 introduces three constraints for association through hydrogen bonding [10]: (i) Bonding at one site is independent of bonding at other sites; (ii) multiple bonds at one site are not allowed; and (iii) ring formations due to association are not allowed. Another general limitation of TPT1, which is discussed in more detail by Müller & Gubbins [51], is that the theory does not take bonding angles into account. This limitation is applicable to both chain formation and association bonding. In the case of chain formation through covalent bonds, single bonds allow for free rotation around the bonding axis, but double and triple bonds do not. TPT1 does not make this distinction and represents all molecules as rigid elliptoids.

Furthermore, it should be noted for the application of SAFT-VR Mie that it is formulated in such a way that the valid repulsive / attractive exponent range is $5 < \lambda \leq 100$, and the valid range for the ratio of segment diameter over temperature dependent diameter is $1 < \frac{\sigma}{d} < \sqrt{2}$ [10]. While the latter bounds are rarely exceeded, the former restriction is particularly important as it provides upper and lower regression bounds for the variable-range exponent parameters.

2.1.3 Dipolar Contribution

The modular construction of SAFT-based EoS makes them easily expanded to include contributions of different intermolecular interactions. Two new variants of SAFT-VR Mie were introduced by Cripwell et al. [19], each making use of a different polar term to account for dipolar interactions: the Jog & Chapman (JC) term [52] and the Gross & Vrabec (GV) term [53]. The

performance of the GV term has been determined to be overall superior to that of the JC term in the SAFT-VR Mie framework, therefore only SAFT-VR Mie + GV is considered in this work.

The GV term introduces two model parameters: the gas-phase dipole moment in a vacuum, μ, and the number of polar segments, n_{p}. The dipole moment is characteristic of molecular shape and charge distribution, and is inferred from experimental results. The number of polar segments was originally fixed to one to correspond to one functional group being dipolar. However, it has been found by de Villiers et al. [54] for PC-SAFT that including n_{p} in the regression procedure along with the other model parameters produces superior results. The decision to include n_{p} in the regression procedure is supported by the fact that the axis of the dipole moment is aligned parallel to the molecular axis in the GV term, causing the term to produce an underestimated contribution [54]. Furthermore, it can be argued that because the charge distribution on a molecule cannot always be pinpointed to a single positive and negative charge, the phenomenon of polarity may stretch beyond a single segment. In the work by Cripwell et al. [19], [55] with SAFT-VR Mie + GV, the number of polar segments was also either regressed with the other model parameters or correlated using molecular mass and dipole moment. New SAFT-VR Mie + GV parameter sets generated in this work feature regressed n_{p} parameters.

2.2 SAFT-γ Mie

This study will focus on the recently developed SAFT-γ Mie [30] that makes use of fused heteronuclear segments. The term *heteronuclear* indicates that an individual functional group consists of segments that are unlike those of a different functional group, as opposed to *homonuclear* where the monomeric segments of a component that is being modelled are identical to one another. The "γ" indicates that the functional groups are *fused*, meaning that they can overlap within a molecule. This overlap is accounted for by a functional-group parameter called the shape factor.

Figure 2.3 illustrates an ethyl acetate molecule broken up into functional groups. The combination of 2 × CH_3, 1 × COO, and 1 × CH_2 is only one way to break ethyl acetate up into functional groups — another combination would be 1 × CH_3COO, 1 × CH_2, and 1 × CH_3. There are no concrete rules for dividing components up into groups. The choice of functional groups is a compromise between the usefulness of the individual groups (can they be used for a large variety of components?), and the accuracy of model predictions. It has been found that breaking components up into the smallest possible groups can sometimes result in reduced prediction accuracy, especially for small components. E.g., it has been found for 1-alcohols that choosing

CH_2OH over "CH_2 and OH" produces better property descriptions with SAFT-γ SW [56] and SAFT-γ Mie [34].

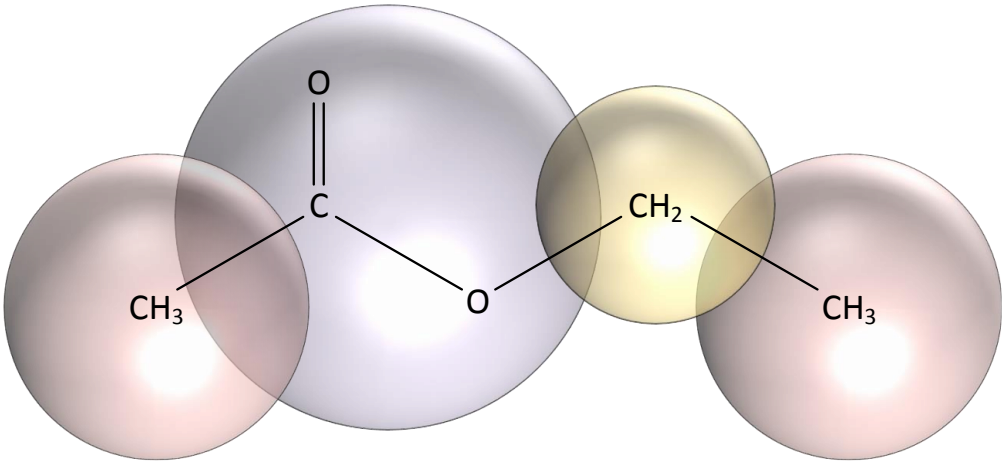

Figure 2.3: Illustration of ethyl acetate functional groups.

2.2.1 Formulation

SAFT-γ Mie model parameters can be divided into two types: group-specific parameters, and group interaction parameters. The group-specific model parameters are those that describe an attribute of a single functional group, viz. the segment number (v_k^*) which represents the number of monomeric segments of functional group k, and the shape factor (S_k) which represents the degree of overlap between those segments. The group interaction parameters refer to those that describe interactions between groups, viz. the segment diameter (σ_{kl}) which represents the centre-to-centre distance between segments of groups k and l where the Mie potential function equals zero, the dispersion energy (ϵ_{kl}) which describes the depth of the potential function between segments of groups k and l used in the dispersion and chain contributions, the attractive and repulsive exponents ($\lambda_{kl}^{\mathrm{a}}$ and $\lambda_{kl}^{\mathrm{r}}$) which characterise the steepness of the Mie potential function between segments of groups k and l, the association energy ($\epsilon_{kl,ab}^{\mathrm{HB}}$) which describes the bond energy between HB sites a and b on groups k and l, and the bonding volume ($K_{kl,ab}$) which represents the volume of association between the sites. Some of the model equations are given in this section to illustrate how group contributions are summed in SAFT-γ Mie. The complete set of model equations can be found in the seminal article by Papaioannou et al. [30], except for the modified association term equations that can be found in the Dufal et al. [33] article of 2014.

The Helmholtz energy expression of SAFT-γ Mie is the same as Eqs (2.3) and (2.4); however, the calculations of the different contributions differ. The Helmholtz energies are no longer expressed as the sum of the contribution of different components, but rather the sum of the contributions of different functional groups. Figure 2.4 illustrates the SAFT-γ Mie formulation.

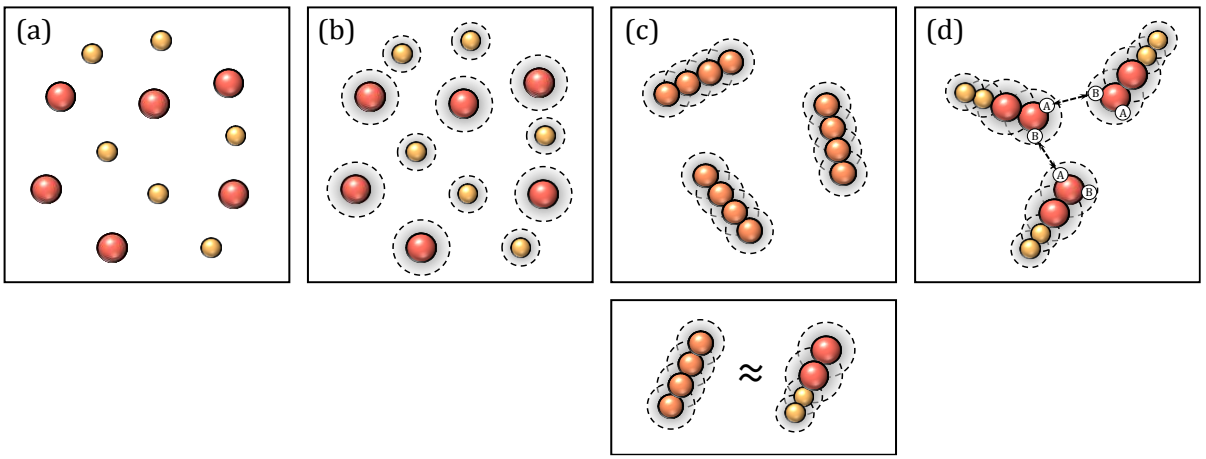

Figure 2.4: Illustration of the SAFT-γ Mie representation of (a) ideal segments, (b) dispersion interactions, (c) chain formation, and (d) association interactions. Note that the red segments belong to one group and the yellow to another, and that a group's segment number is normally an integer amount. The orange segments are characterised by average molecular parameters generated using group parameters of the red and yellow segments.

The perturbation terms of the BH third-order expansion for the dispersion contribution are calculated as follows:

$$\frac{A^m}{Nk_BT} = \left(\frac{1}{k_BT}\right)^m \left(\sum_{i=1}^{N_C} x_i \sum_{k=1}^{N_G} \nu_{k,i} \nu_k^* S_k\right) a_m, \quad m = 1,2,3 \tag{2.9}$$

and

$$a_m = \sum_{k=1}^{N_G} \sum_{l=1}^{N_G} x_{s,k} x_{s,l} a_{m,kl}\,, \quad m = 1,2,3 \tag{2.10}$$

where $\nu_{k,i}$ is the number of times functional group k appears in component i, and x_i is the mole fraction of component i. The double summation term in Eq. (2.9) calculates the mixture segment number, i.e., the mean segment number for one molecule in the system. The contribution to the mth-order perturbation term between groups k and l ($a_{m,kl}$) for all of the different functional groups in the system, N_G in total, is summed together in Eq. (2.10) to deliver the mean energy between segments in the system for the mth-order dispersion term. The term $x_{s,k}$ refers to the fraction of segments in the system that belongs to group k.

A similar method is followed in the calculation of the hard-sphere and association contributions. The chain contribution RDF is calculated exactly as in SAFT-VR Mie; however, average molecular parameters are used instead of regressed model parameters (see Figure 2.4 diagram (c)). The average molecular parameters for component i (viz. $\bar{\sigma}_{ii}$, $\bar{d}_{ii}$, $\bar{\epsilon}_{ii}$, and $\bar{\lambda}_{ii}$) are

calculated using the parameters of functional groups that occur in component *i*. The molecular fractions of the functional groups in the component are used to weigh the contributions of the group parameters to the average parameters. In essence, SAFT-γ Mie uses averaging rules in order to approximate the chain contribution in a homosegmented manner.

The association term is given by the following expression:

$$\frac{A^{\text{Assoc}}}{Nk_{\text{B}}T} = \sum_{i=1}^{N_{\text{C}}} x_i \sum_{k=1}^{N_{\text{G}}} \nu_{k,i} \sum_{a=1}^{N_{\text{ST},k}} n_{k,a} \left(\ln X_{i,k,a} + \frac{1 - X_{i,k,a}}{2} \right) \tag{2.11}$$

where N_{C} is the number of different components in the system, $N_{\text{ST},k}$ is the number of different association sites on functional group k, and $X_{i,k,a}$ is the fraction of molecules of component i that are not bonded at site a on group k.

2.2.2 Combining Rules

Most of the group interaction parameters between *unlike* groups, e.g., σ_{kl} or λ_{kl}^{r} where k and l are different functional groups, are determined using combining rules, with the exception of the dispersion energy, association energy, and association volume — these three parameters are regressed in most cases. The following combining rules are used for each of the model parameters [30].

The segment diameter is obtained from the arithmetic mean of the relevant *like* interaction parameters:

$$\sigma_{kl} = \frac{\sigma_{kk} + \sigma_{ll}}{2} \tag{2.12}$$

The same calculation is used for the temperature dependent hard-sphere diameter:

$$d_{kl} = \frac{d_{kk} + d_{ll}}{2} \tag{2.13}$$

A geometric mean that is adjusted to account for asymmetry in size is used for the dispersion energies in cases where they are not regressed:

$$\epsilon_{kl} = \frac{\sqrt{\sigma_{kk}{}^3 \sigma_{ll}{}^3}}{\sigma_{kl}{}^3} \sqrt{\epsilon_{kk}\epsilon_{ll}} \tag{2.14}$$

The repulsive and attractive exponents are calculated with the following expression:

$$\lambda_{kl} = 3 + \sqrt{(\lambda_{kk} - 3)(\lambda_{ll} - 3)} \tag{2.15}$$

The association energy is calculated using a geometric mean:

$$\epsilon^{HB}_{kl,ab} = \sqrt{\epsilon^{HB}_{kk,ab}\epsilon^{HB}_{ll,ab}} \tag{2.16}$$

The association range is calculated using an arithmetic mean:

$$r^{c}_{kl,ab} = \frac{r^{c}_{kk,ab} + r^{c}_{ll,ab}}{2} \tag{2.17}$$

The association volume is calculated with the following expression:

$$K_{kl,ab} = \left(\frac{\sqrt[3]{K_{kk,ab}} + \sqrt[3]{K_{ll,ab}}}{2}\right)^3 \tag{2.18}$$

2.2.3 Application

SAFT-γ Mie is subject to the same limitations as SAFT-VR Mie that were inherited from the TPT1. Bonding angles are not taken into consideration, contrary to the illustration in Figure 2.3. The valid ranges for λ and σ/d are also the same as for SAFT-VR Mie.

As mentioned in Section 1.1.4, SAFT-γ Mie makes the potentially limiting assumption that component properties are independent of the overall structure of a molecule. Interactions between two functional groups, e.g., $a_{m,kl}$ in Eq. (2.10), are always the same for the same parameter set irrespective of the component for which it is calculated. In reality, structural considerations (referring to both steric hindrance and conjugation) may cause the interactions between some functional groups to be different from what is otherwise expected. Note that in the context of this work, steric hindrance refers to the physical presence of groups obstructing intermolecular interactions and not the obstruction of chemical reactions. The distinction between structural configurations is particularly important when modelling isomers where the difference in group arrangement is the only thing that separates two isomeric molecules. Isomers can display noteworthy differences in phase behaviour as illustrated in Figure 2.5, which exhibits VLE data for three binary systems. Each system contains *n*-nonane and an isomer of heptanone [57].

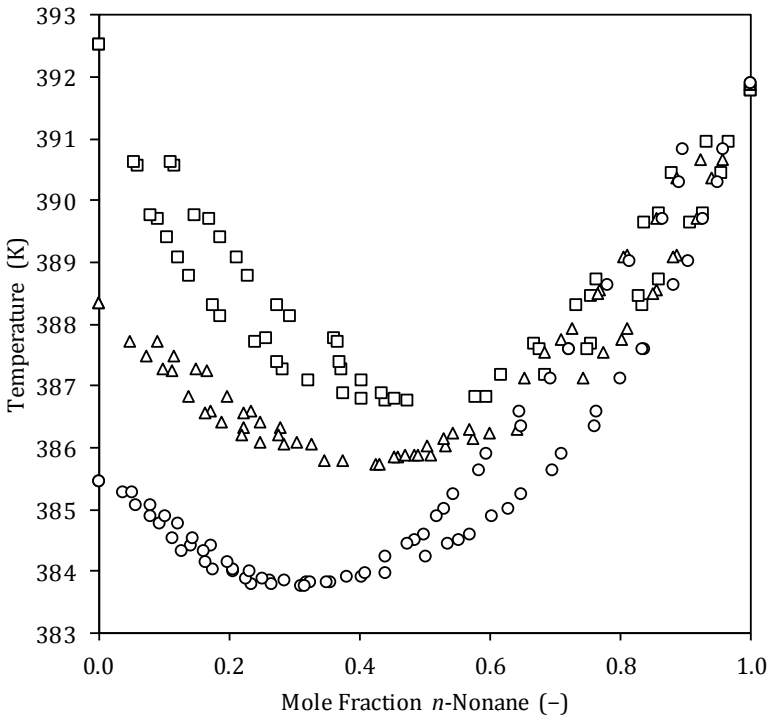

Figure 2.5: Isobaric VLE data for binary systems of *n*-nonane + 2-heptanone (□), *n*-nonane + 3-heptanone (△), and *n*-nonane + 4-heptanone (○), all at 0.400 bar.[1]

The boiling points of subsequent heptanone isomers are roughly 3, and 4 K apart. This difference in volatility causes the azeotrope compositions to differ by roughly 0.1 mole fraction *n*-nonane between the subsequent systems. This difference could have significant implications in the design of separation processes.

One key difference in the application of SAFT-γ Mie compared to SAFT-VR Mie is in the treatment of association. Association schemes are used in the SAFT-VR Mie framework, which involves making the assumptions that a molecule's different hydrogen bonds are the same, $\Delta_{ac} = \Delta_{bc}$, and that X_b, X_c, X_d, etc. can all be approximated in terms of X_a depending on the distribution of association sites on a molecule. This approach was first introduced by Huang & Radosz [40] for their revised version of the original SAFT. After implementing association schemes, the calculation of X_a becomes simplified and components require only one set of association parameters despite there being multiple different association site types on a component — in effect, the number of fitted parameters are reduced. However, in SAFT-γ Mie it is not assumed that functional groups have association schemes, and each combination of site types has its own association parameters. Figure 2.6 illustrates the different association site types for water and the carboxylic acid functional group, COOH.

[1] Reprinted (adapted) with permission from Cripwell et al. [57].

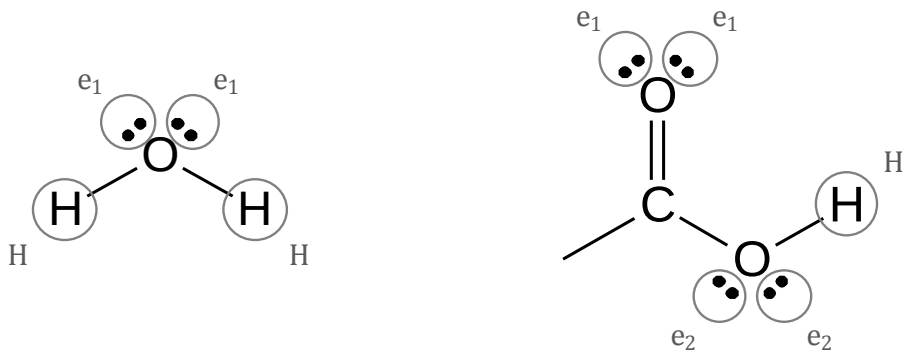

Figure 2.6: Different HB sites for water (left) and COOH (right).

Assigning HB sites to a functional group is a heuristic procedure. As a result of the choice of bonding sites for the two groups illustrated above, the different HB combinations for a system containing water and a carboxylic acid are [33], [39]:

1. $(H_2O)_{e_1} \leftrightarrow (H_2O)_H$
2. $(COOH)_{e_1} \leftrightarrow (H_2O)_H$
3. $(COOH)_{e_2} \leftrightarrow (H_2O)_H$
4. $(COOH)_H \leftrightarrow (H_2O)_{e_1}$
5. $(COOH)_{H,e_1} \leftrightarrow (COOH)_{e_1,H}$

Note that due to a strong tendency to dimerise, it is assumed that there is only one possible way for carboxylic acids to self-associate. While double hydrogen bonds are not allowed, abovementioned HB combination no. 5 is assumed to be a strong single bond between bipolar sites[1]. Another unusual choice of HB sites is presented by Dufal et al. [33] and explained by Sadeqzadeh et al. [39] for acetone. The two lone electron pairs of acetone's oxygen atom are seen as two different association sites (e_1 and e_2), despite the fact that acetone is symmetrical on either side of the carbonyl group, and a hydrogen site (H) is added adjacent to the carbonyl's carbon atom without there actually being a hydrogen atom (see Figure 2.7). This nonphysical site allocation, known as pseudo-association, allows for the strong polar interactions of acetone to be taken into consideration without an explicit polar extension in SAFT-γ Mie.

[1] Bipolar sites are allowed to associate with both positive and negative sites, as well as other bipolar sites. Note that the carboxylic acids of Dufal et al. [33] are not typical examples of how bipolar sites interact, because the user specifies that the COOH group's positive and negative sites are not allowed to self-associate, and the bipolar site is not allowed to cross-associate.

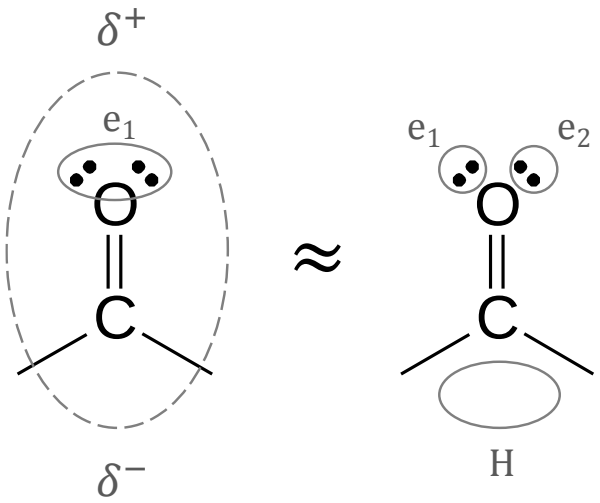

Figure 2.7: Illustration of pseudo-association for ketones.

Chapter 3: Modelling Methodology

3.1 Software

Thermodynamic modelling in this project was done using TRSolutions — software developed by the Separations Technology research group at Stellenbosch University's Department of Process Engineering. SAFT-γ Mie was implemented in TRSolutions instead of scripting it with numerical analysis software, e.g., MATLAB [58]. It was deemed more beneficial to expand the existing software so that our research group's thermodynamic modelling tools remain centralised and accessible for future researchers. Moreover, the software has an existing framework from which to work when implementing the new EoS. The existing framework includes methods to calculate various pure-component and mixture properties, and a class for thermodynamic methods that provides the basic structure in which to add new EoS.

TRSolutions was expanded to be able to store component functional-group information, identify the type and number of groups that make up components, and locate and use the correct group parameters which are stored in a newly created database. After creating the interface and procedures necessary to work with a GC formulation, the SAFT-γ Mie EoS was implemented. Its first and second derivatives with respect to composition, temperature, and volume were determined analytically and coded into the software.

3.2 Model Validation

The state function for SAFT-based EoS is defined as follows:

$$F = \frac{A^{\text{res}}}{Nk_{\text{B}}T} \tag{3.1}$$

The fidelity of the coded analytical state function derivatives was verified by comparing the percentage difference between them and numerically calculated derivatives. A comparison for the overall state function is given in Table 3.1, and the results for the individual contributions can be found in Appendix A.

Table 3.1: State function derivatives validation for 1-butanol at 300 K and 0.100 mol/L.

Derivative	Analytical	Numerical	Difference (%)
$\partial F/\partial n_i$	-13.181196017	-13.181196016	7.587E-09
$\partial F/\partial T$	0.060610806720	0.060610806774	8.909E-08
$\partial F/\partial V$	42.978683604	42.978678960	1.081E-05
$\partial^2 F/(\partial n_i \partial n_j)$	15.528851689	15.528851693	2.576E-08
$\partial^2 F/(\partial n_i \partial T)$	0.11055971503	0.11055971504	9.045E-09
$\partial^2 F/(\partial n_i \partial V)$	-155.28851684	-155.28856125	2.860E-05
$\partial^2 F/\partial T^2$	-0.00046241285792	-0.00046236761642	0.009784
$\partial^2 F/(\partial T \partial V)$	-0.49948908314	-0.49948908015	5.986E-07
$\partial^2 F/\partial V^2$	1552.8851684	1552.8857054	3.458E-05

As observed by Cripwell for SAFT-VR Mie [59], the relatively large difference for $\partial^2 F/\partial T^2$ likely stems from errors introduced when calculating a numerical derivative of a numerical integral (the temperature dependent diameter is calculated using Gauss-Legendre integration) and the functions in which it is used. Moreover, the absolute magnitude of $\partial^2 F/\partial T^2$ is very small because in many parts of the EoS, d is the only temperature dependent variable — this further inflates the percentage difference. It was therefore concluded that 0.009784% is an acceptable deviation.

The next step in validating the newly implemented SAFT-γ Mie was to reproduce property prediction absolute average deviations (AADs) published in literature for select components using the same functional-group structures and parameters. This was done for both non-associating and associating species.

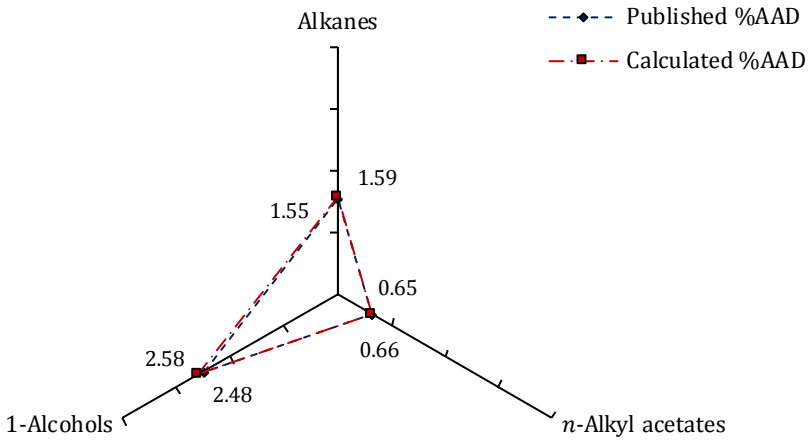

Figure 3.1: P^{vap} %AAD comparisons for model validation.

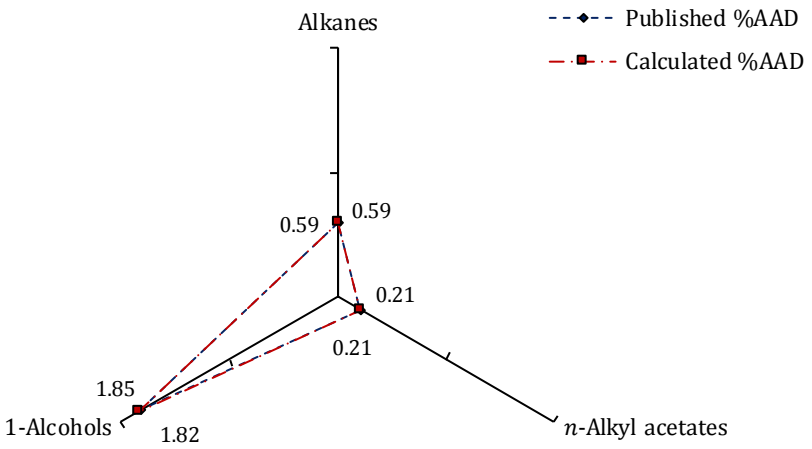

Figure 3.2: ρ^{sat} %AAD comparisons for model validation.

The same experimental data were used to calculate the deviations; the reader is referred to the references in Table 3.2 for more information about the specific pure-component data that was used. The %AADs shown on Figures 3.1 and 3.2 are arithmetic means of a range of components with varying chain lengths belonging to the homologous series. The "Published" series refers to the %AADs sourced from the references in Table 3.2, and the "Calculated" series was obtained through results generated in this work. Minor differences between the published and calculated average deviations exist because rounded parameters were used (from the references in Table 3.2), and SAFT-γ Mie in TRSolutions makes use of 12-point Gauss-Legendre integration while the literature authors may have used different numerical integration. Despite the minor differences, it is clear that the correct modelling results were obtained, since the plots on each of the figures are nearly congruent. The reader is referred to Appendix A for a per-component comparison of the published and newly calculated pure-component %AADs.

Table 3.2: References for the published %AADs presented in Figure 3.2.

Components	Short reference	Reference no.
Alkanes	Papaioannou et al. (2014)	[30]
n-Alkyl acetates	Papaioannou et al. (2014)	[30]
1-Alcohols	Hutacharoen et al. (2017)	[34]

3.3 State Function Partial Derivatives

Accurate descriptions of the derivatives listed in Table 3.1 are vital for describing the different properties of a fluid mixture. It is important to know the relationship between thermodynamic properties and the state function derivatives in order to evaluate the performance of a thermodynamic model, and it is especially important when choosing properties to include in the regression objective function so that the resulting parameters provide balanced predictions. The diagram in Figure 3.3 illustrates the relationships between properties and derivatives.

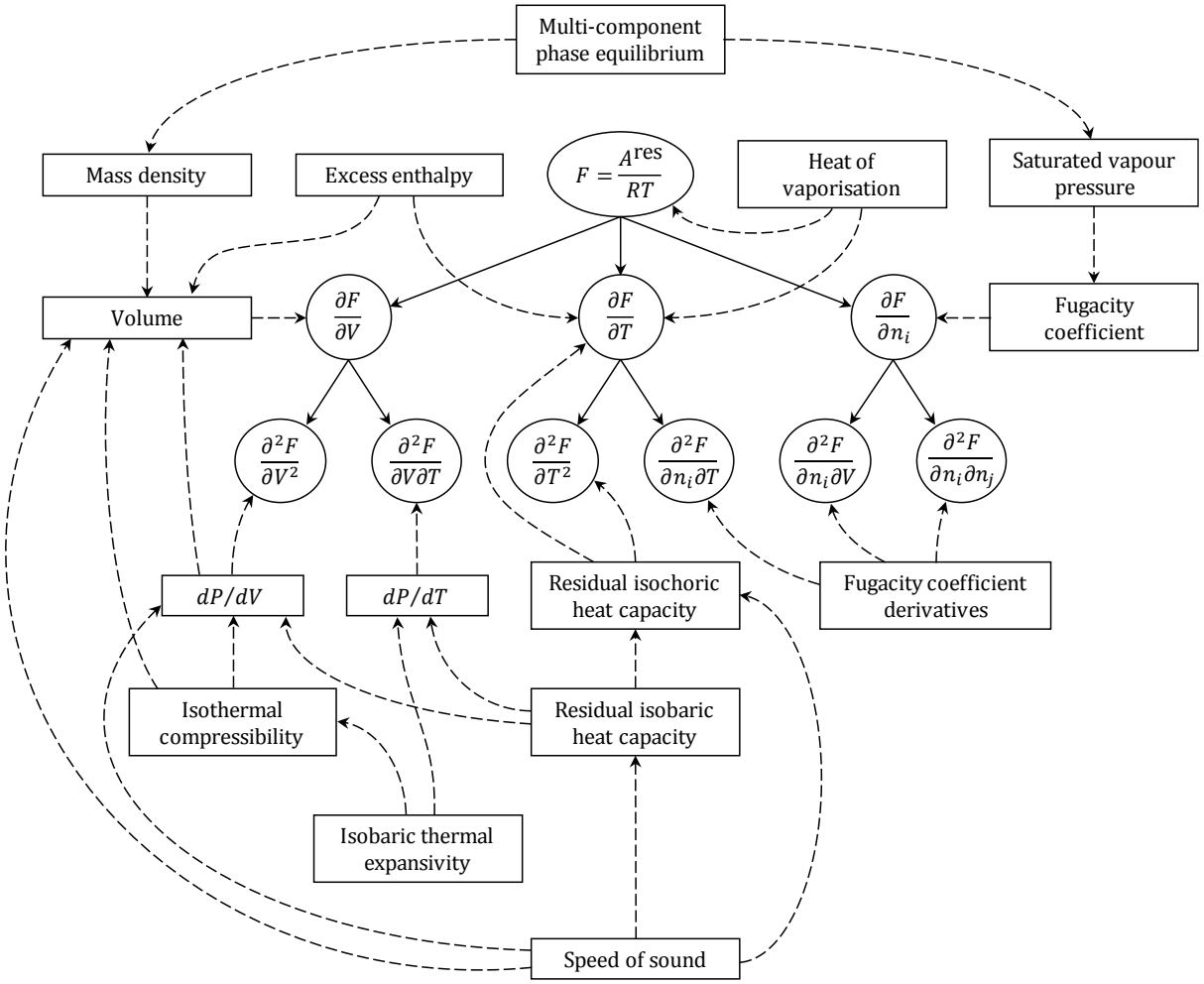

Figure 3.3: Property dependence diagram. The dashed arrows indicate dependence. Figure redrawn from de Villiers [60].

Other important applications of the state function derivatives include the use of the first- & second-order volume derivatives in an improved Newton-Raphson method implemented in the volume solver of TRSolutions (see page 93 in Michelsen & Mollerup [61]). Furthermore, the fugacity coefficient and its derivatives (calculated with the state function first & second composition derivatives) are used in the flash algorithm to solve multi-component phase equilibrium (see page 310 in Michelsen & Mollerup [61]).

3.4 Regression Procedure

3.4.1 Objective Function

The aim of the regression procedure is to minimise an objective function (OF) by iteratively adjusting the model parameters. The following equation demonstrates an OF that includes the squared errors of saturated vapour pressure, P^{vap}, saturated liquid density, ρ^{sat}, and speed of sound, u, predictions.

$$\min_{\boldsymbol{\Omega}} f_{\text{obj}} = w_1 \sum_{i=1}^{N_{P^{\text{vap}}}} \left[\frac{P_{\text{exp}}^{\text{vap}}(T_i) - P_{\text{calc}}^{\text{vap}}(T_i;\boldsymbol{\Omega})}{P_{\text{exp}}^{\text{vap}}(T_i)} \right]^2 + w_2 \sum_{i=1}^{N_{\rho^{\text{sat}}}} \left[\frac{\rho_{\text{exp}}^{\text{sat}}(T_i) - \rho_{\text{calc}}^{\text{sat}}(T_i;\boldsymbol{\Omega})}{\rho_{\text{exp}}^{\text{sat}}(T_i)} \right]^2 + w_3 \sum_{i=1}^{N_u} \left[\frac{u_{\text{exp}}(T_i,P_i) - u_{\text{calc}}(T_i,P_i;\boldsymbol{\Omega})}{u_{\text{exp}}(T_i,P_i)} \right]^2 \tag{3.2}$$

where $\boldsymbol{\Omega}$ denotes a vector of model parameters, $N_{P^{\text{vap}}}$, $N_{\rho^{\text{sat}}}$, and N_u the number of data points included for the respective properties, and w_{1-3} the regression weights for each property.

Regression weights are usually determined heuristically based on desired accuracy and error magnitudes. The quality of regressed parameters can be compromised by making the regression weights too high for properties with high errors, such as excess properties, or properties that are difficult to model, such as speed of sound. In these cases, the algorithm will skew parameters to slightly improve the predictions for these properties while greatly deteriorating the accuracy for more crucial properties, e.g., P^{vap}. It is important to take note of the number of included data points because increasing it also increases the weight of that term.

3.4.2 Group-Contribution Regression

Parameters of traditionally structured (TS), non-GC equations of state are specific to components. Intermolecular interactions are usually estimated with combining rules and can be adjusted with binary interaction parameters (BIPs) that are regressed separately with mixture data. One shortcoming of TS EoS is the need for regression with pure-component data for every component before its properties can be modelled, because such data are not always available or easily measured.

In GC equations of state, parameters are specific to functional groups. Although combining rules exist, dispersion energies and association interactions between functional groups are usually also regressed for SAFT-γ Mie since its heteronuclear nature allows these interaction parameters to be generated with pure-component data alone if the component contains both relevant functional groups. The GC formulation allows one to generate parameters very

systematically to create a database that can eventually be used to describe a vast number of components. The following steps describe the procedure for parameterising groups to model 1-alcohol + 2-ketone binary systems.

1. Generate methyl and bridging methylene (CH_3 and CH_2) group-specific and interaction parameters by including pure-component data for a range of *n*-alkanes, e.g., ethane to *n*-decane, in the OF.

2. Generate group-specific parameters for the 1-alcohol end-group (CH_2OH) and dispersion energies for CH_3–CH_2OH and CH_2–CH_2OH by including alcohol pure-component data; 1-alcohol + alkane binary data may be included to improve the resultant interaction energies.

3. Generate group-specific parameters for the 2-ketone end-group (CH_3CO) and dispersion energies for CH_3–CH_3CO and CH_2–CH_3CO by including 2-ketone pure-component data; 2-ketone + alkane binary data may also be included.

4. Generate CH_2OH–CH_3CO dispersion and association interaction parameters by including binary VLE data and other binary data (e.g., excess enthalpy).

After following the above procedure, a good GC model would allow one to predict 1-alcohol + 2-ketone systems with components that were not included in the regression. It should also be possible to use the newly regressed group parameters in more complex organic components that contain groups of different homologous series. For example, the alcohol end group (CH_2OH) could theoretically be used in the modelling of benzyl alcohol.

3.4.3 Regression Challenges

TRSolutions utilises a standard Levenberg Marquardt algorithm (LMA) [62], [63] which makes use of interpolation between the Gauss-Newton algorithm and the method of gradient descent. The algorithm is robust and fast, but it suffers from the same limitations as all other gradient based algorithms, i.e., it may converge to local minima instead of a global minimum, or with poorly chosen initial parameters it may simply diverge away from the minimum towards upper or lower bounds. Furthermore, a broad minimum may result in a mathematical optimum that is not necessarily the best practical solution. Note that the latter problem is related to the OF and is not exclusive to gradient-based regression methods.

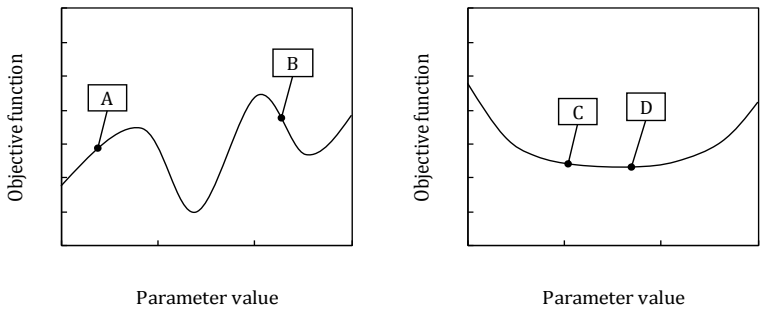

Figure 3.4: Illustration of a local minimum (left-side plot) and a broad minimum (right-side plot).

In the simple one-parameter problems illustrated in Figure 3.4, starting point "A" may lead a gradient-based regression to run into the lower bound. An OF may sometimes be smallest past one of the bounds, but the bounds are normally chosen to exclude invalid solutions, e.g., negative segment numbers. Another invalid solution would be one in which the SAFT-VR Mie or SAFT-γ Mie repulsive exponent exceeds the models' limit of 100. Starting at point "B" may cause the algorithm to get stuck at the local minimum to its right. The best solution to both problems is simply to choose a starting point that is closer to the global minimum — existing parameters for the same or similar species would make good starting points. For broad minima, as illustrated on the right-side plot, the algorithm may converge to point "D" while point "C" could be a more physically sensible solution that results in better predictions for properties that were not included in the regression. Here the best solution is to include more appropriate properties, forcing mathematical and practical optimums to coincide. However, thoughtlessly including more and more properties is impractical and demands an excessive amount of data. One may consult Figure 3.3 to select properties that embody a wider range of state function derivatives; one can also choose properties that are particularly sensitive to certain parameters to ensure that unambiguous values are obtained for those parameters.

Another way to alleviate these regression challenges is to reduce the dimensions of the parameter space by using grounded assumptions or correlations. An example of such correlation is found in the fixed polar parameter method evaluated by de Villiers et al. [54] for the simplified perturbed chain statistical associating fluid theory (sPC-SAFT) + JC & sPC-SAFT + GV, and Cripwell et al. [19] for SAFT-VR Mie + JC & SAFT-VR Mie + GV. This method involves fixing the fraction of polar segments parameter for the JC term or the number of polar segments parameter for the GV term.

In this study, the attractive exponent parameters were assumed to be $\lambda^a = 6$ in keeping with previously generated group parameters [30], [33], [34] and London's theory of dispersion [44], and the segment numbers of the new functional groups were determined heuristically based on the physical structures of the groups.

3.5 Parameters Matrix

The matrix in Figure 3.5 indicates which functional groups and group interactions relevant to this study are already parameterised, and which required the generation of new parameters. Note that all parameters used in this work can be found in Appendix B along with references.

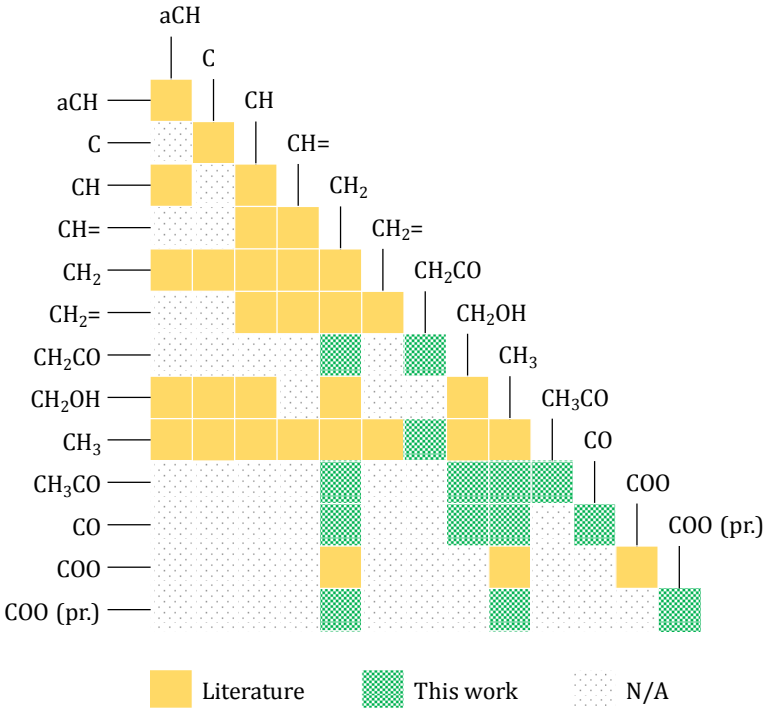

Figure 3.5: SAFT-γ Mie interaction parameters matrix. Note that the groups mentioned in the figure are fully parameterised with group-specific parameters, and a combination of two different groups is considered parameterised if their dispersion interaction energy (ϵ_{kl}/k_B) had been regressed, as well as their cross-association parameters ($\epsilon^{HB}_{kl,ab}/k_B$, and $K_{kl,ab}$), if applicable.

Literature parameters, the solid yellow squares in Figure 3.5, are used in Chapter 4 to investigate the first objective under the first hypothesis in Section 1.2, which is to identify molecular characteristics that pose a challenge for SAFT-γ Mie. Note that the FGs that occur in branched alkanes (CH and C) are not used in Chapter 4 because the modelling of branched alkanes forms part of Chapter 6. The parameters indicated with shaded green squares are new parameters presented in Chapter 5, which deals with the modelling of dipolar species. Note that some interaction parameters are not available in literature, and were not generated in this work (the dotted squares); however, systems containing these group combinations can still be modelled using combining rules.

Chapter 4: General Comparison

Pure-component and binary mixture predictions with SAFT-γ Mie are given in this chapter for increasingly complex molecules: (i) nonpolar, non-associating; (ii) polar, non-associating; and (iii) polar, associating. The standard SAFT-VR Mie of 2013 is the benchmark for all of the predictions so that the GC aspect of SAFT-γ Mie is the primary difference between the two models. This provides an initial indication of the strengths and weaknesses of SAFT-γ Mie for different applications, and specifically of which molecular characteristics pose a challenge to the SAFT-γ Mie framework. See Appendix B for the SAFT-γ Mie parameters and Appendix C for the SAFT-VR Mie Parameters.

4.1 Pure-Component Properties

Table 4.1: Pure-component property %AAD comparison between SAFT-γ Mie and SAFT-VR Mie. The bold entries indicate the lowest %AAD between the two models. P^{vap}, ρ^{sat}, and H^{vap} predictions are measured against DIPPR correlations [64], and references for the speed of sound data are given in the last column.

	P^{vap}		ρ^{sat}		H^{vap}		u		
Component	γ Mie	VR Mie	γ Mie	VR Mie	γ Mie	VR Mie	γ Mie	VR Mie	u Ref.
				n-Alkanes					
ethane	1.85	**0.65**	1.33	**0.71**	**1.97**	2.40	5.29	**4.53**	[65]
propane	1.78	**0.67**	0.96	**0.59**	**2.22**	2.26	4.84	**4.40**	[65]
n-butane	1.73	**1.14**	**0.39**	0.43	**1.75**	2.03	**3.78**	4.23	[65]
n-pentane	2.37	**1.06**	**0.30**	0.40	**1.84**	2.51	**4.36**	5.65	[65]
n-hexane	2.52	**1.27**	**0.19**	0.26	**2.24**	3.03	**2.80**	3.90	[65]
n-heptane	1.45	**0.89**	**0.20**	0.49	**1.61**	2.19	**2.83**	2.91	[65]
n-octane	1.13	**0.98**	**0.31**	0.68	**1.22**	1.65	**2.72**	2.82	[65]
n-nonane	1.24	**0.76**	**0.35**	0.55	**1.00**	1.40	4.27	**3.40**	[65]
n-decane	1.35	**0.94**	**0.31**	0.55	**1.44**	1.77	6.27	**5.36**	[65]
n-dodecane	4.07	**0.65**	0.53	**0.51**	1.36	**1.14**	5.89	**5.49**	[65]
n-pentadecane	8.11	**1.60**	**0.69**	0.76	2.66	**2.17**	3.11	**1.02**	[66]
n-eicosane	15.28	**1.68**	**0.80**	0.87	2.74	**1.69**	3.49	**0.42**	[67]
				1-Alkenes					
1-octene	1.78	**0.42**	0.10	**0.04**	**0.97**	1.00			
1-decene	1.60	**1.23**	0.11	0.11	0.86	**0.64**			
				n-Alkyl acetates					
ethyl acetate	0.53	**0.10**	0.27	**0.12**	**1.42**	2.14	9.51	**0.87**	[68]
propyl acetate	1.24	**0.48**	**0.15**	0.17	**2.72**	2.93	6.20	**1.32**	[69]
n-butyl acetate (SAFT-VR Mie Set A)	0.67	**0.38**	0.32	**0.16**	**0.83**	1.18	5.62	**1.53**	[68]
n-butyl acetate (SAFT-VR Mie Set B)	**0.67**	1.76	**0.32**	1.08	**0.83**	1.56	**5.62**	22.7	[68]

Table 4.1 (continued)

Component	P^{vap}		ρ^{sat}		H^{vap}		u		u Ref.
	γ Mie	VR Mie	γ Mie	VR Mie	γ Mie	VR Mie	γ Mie	VR Mie	
1-Alcohols									
ethanol	2.23	**0.55**	2.41	**0.09**	0.95	**0.70**			
1-propanol	5.31	**0.83**	1.48	**0.25**	**1.34**	1.48			
1-butanol	2.90	**0.70**	1.43	**0.63**	2.14	**1.48**	19.78	**17.58**	[70]
1-pentanol	2.48	**0.27**	1.27	**0.17**	**1.61**	1.63	12.97	**11.45**	[70]

Note that two SAFT-VR Mie *n*-butyl acetate parameter sets are compared to SAFT-γ Mie. Set A was regressed using only pure-component data, while Set B included a *n*-butyl acetate + *n*-octane VLE data set. The reason for regressing a second set using mixture data is discussed after the binary mixture results in Section 4.2.1. It can be seen that including the VLE set in the parameter generation deteriorated the pure-component density and especially speed of sound predictions.

SAFT-γ Mie has some difficulty matching the P^{vap} prediction accuracy of the traditionally structured SAFT-VR Mie, but for most of the components in Table 4.1 the predictions are still good. Both models were able to produce good pure-component property predictions for the acetates without having a polar contribution. SAFT-VR Mie's speed of sound predictions for the three acetates are superior (except with *n*-butyl acetate Set B), but this is expected since the three narrow-ranged speed of sound datasets were included in the SAFT-VR Mie parameter regression. Conversely, the SAFT-γ Mie pure-component predictions for 1-alcohols are relatively weak. The GC variant seems to be limited in its application to these small polar molecules where proximity effects likely play a large role. Electrostatic forces between groups may alter their charge distribution, and cause them to behave differently than what they would if they were isolated or surrounded by a different set of groups. This may explain why the structural-independence assumption of first-order GCMs limits their accuracy for small polar molecules. The absence of an explicit polar contribution could also explain the weaker 1-alcohol pure-component predictions, but neither model in Table 4.1 has a polar term, yet there is a clear difference in the P^{vap} and ρ^{sat} predictions between SAFT-γ Mie and SAFT-VR Mie.

The following discussions in this section are regarding the general behaviour of SAFT-γ Mie for pure-component predictions. Figures 4.1 and 4.2 show the percentage average deviations from P^{vap} and ρ^{sat} DIPPR correlations for the *n*-alkanes given in the previous table.

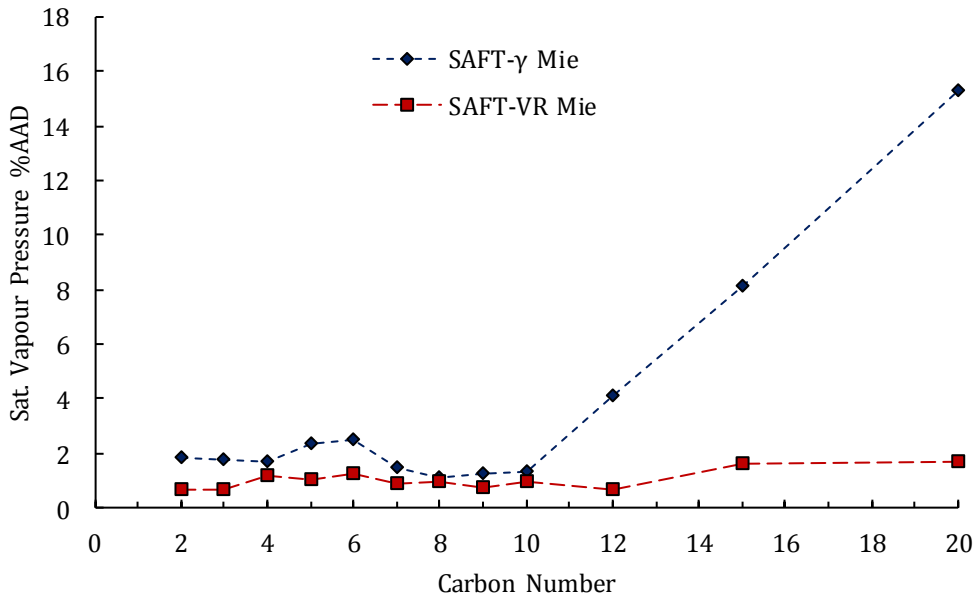

Figure 4.1: Comparison of P^{vap} prediction accuracy for *n*-alkane pure-components.

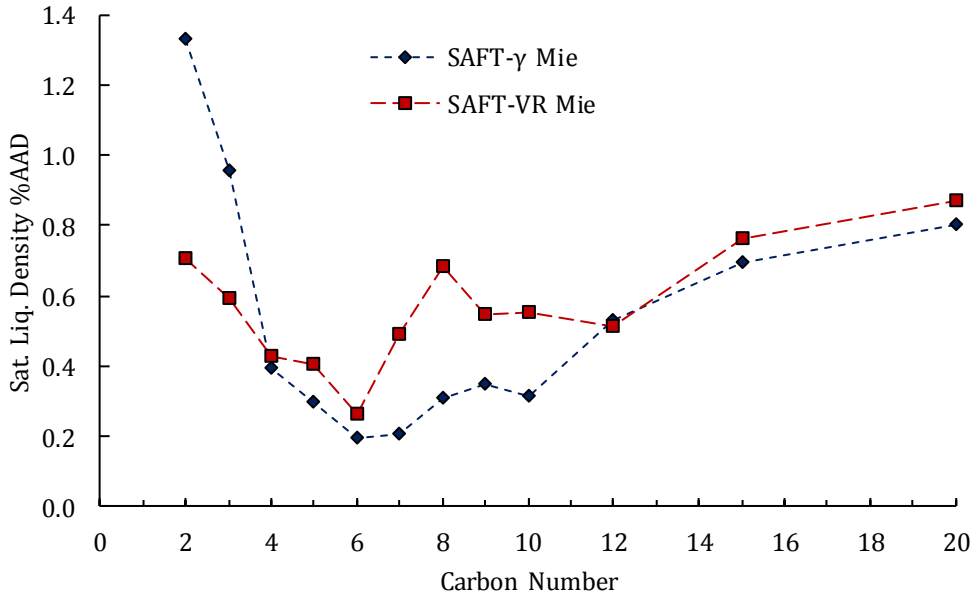

Figure 4.2: Comparison of ρ^{sat} prediction accuracy for *n*-alkane pure components.

While SAFT-γ Mie used one parameter set (spanning two functional groups and totalling 9 unique regressed parameters) to produce the alkane predictions, SAFT-VR Mie used a different set for each component (48 regressed parameters in total). The benefit of having a regressed parameter set for each component can be seen in SAFT-VR Mie's ability to produce relatively low P^{vap} prediction errors, whereas SAFT-γ Mie P^{vap} errors become proportionally greater for larger alkanes not included in the regression procedure.

It is possible that the CH_2–CH_2 attractions are overestimated in large alkanes because SAFT-γ Mie underpredicts P^{vap} (Figures D.1 and D.2 in Appendix D give the models' non-absolute errors for each alkane). As alkanes become larger, they are less likely to appear as thin linear elliptoids due to conformational isomerism — variation in a molecule's shape due to free rotation around single bonds. The irregularity in *n*-alkane shape can be quantified using the mean radius of gyration, which denotes the perpendicular distance between the molecule's centre of mass line and the mean position of carbon atoms. The mean radii of gyration for ethane up to *n*-tetradecane reported in Feng et al. [71] show a clear increase, indicating that *n*-alkanes appear wider as more carbons are added to the chain. This would not occur if longer *n*-alkanes were as linear as shorter alkanes. The addition of more CH_2 groups has a diminished effect on the change observed in pure-component properties possibly because the change in the shape of the typical molecule is not linear as it would be if the molecules were chains of perfect spheres bonded in a straight line. Figure 4.3 illustrates this with all of the *n*-butane conformational isomers superimposed on one another. SAFT-γ Mie cannot account for this nonlinear change because it adds the contributions of identical CH_2 groups with no regard for overall molecular structure. SAFT-VR Mie, on the other hand, can account for the nonlinear increase because its parameters are specifically regressed for every component.

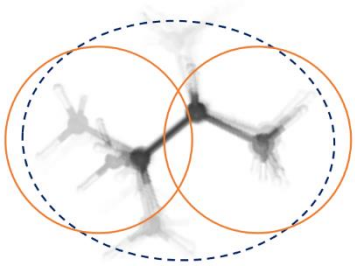

Figure 4.3: Superimposed *n*-butane conformational isomers. The orange circles represent a linear chain approximation and the dashed blue ellipse represents a more realistic molecular shape. Note that this phenomenon would be far more pronounced for long-chain *n*-alkanes.

However, it should be noted that the %AADs for *n*-alkanes are slightly misleading because the very small absolute magnitudes of P^{vap} for large alkanes inflate the relative errors. Figure 4.4 shows the difference in the absolute average errors of the two models for *n*-alkanes.

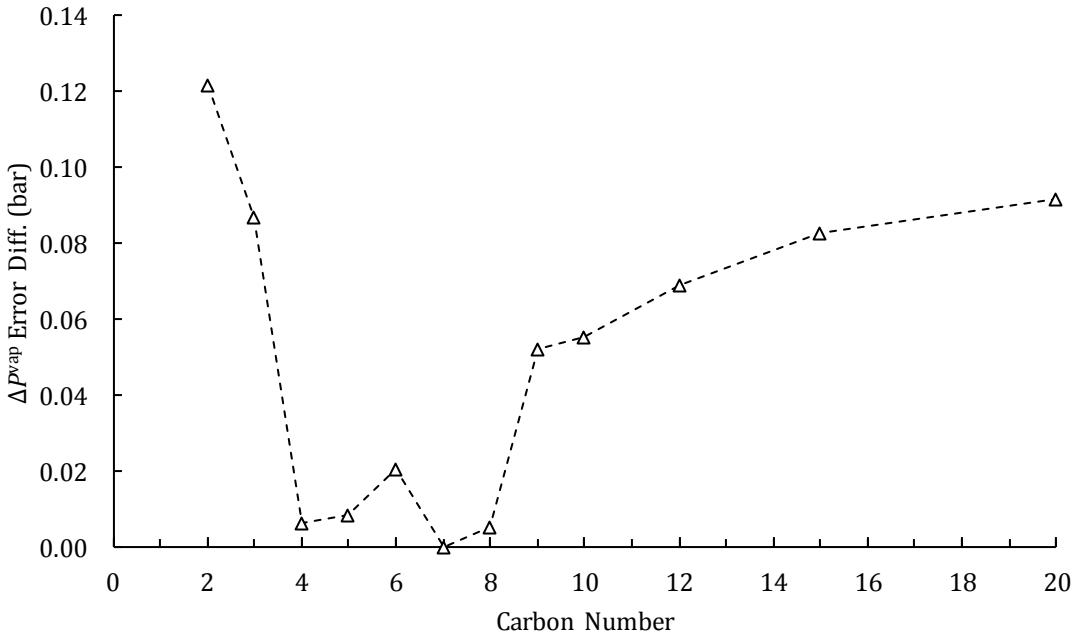

Figure 4.4: Difference in SAFT-γ Mie and SAFT-VR Mie average absolute P^{vap} errors for *n*-alkanes. ΔP^{vap} Error Diff. $= \left|(P^{vap})_{\gamma\text{ Mie, Error}}\right| - \left|(P^{vap})_{\text{VR Mie, Error}}\right|$. [1]

It can be seen from Figure 4.4 that the magnitude of the error difference is largest for ethane and that the magnitude of the errors for larger alkanes starts to level off, confirming that relative errors appear inflated. Furthermore, it can be seen that SAFT-γ Mie favours the middle alkanes. In a regression scenario where the GCM is unable to retain the same degree of accuracy for all of the components, it makes sense for the model to optimise its parameters for members in the middle of the series, because they share characteristics with both the smaller and larger members. It has been suggested that the first-order GCM's difficulty in modelling small components is due to the fact that it does not incorporate proximity effects [30], [34], but this argument is not as convincing when considering alkanes, since proximity effects are presumably less prevalent in nonpolar molecules. CH_3–CH_3 chain formation is not well-represented in the regression of alkane parameters because it only takes place in ethane. Given that SAFT-γ Mie uses average molecular parameters in the chain term, a significant portion of the chain parameters used when modelling propane is for CH_3–CH_3 *like* bonding which does not actually take place. Therefore, the homosegmented approach in the chain term may result in slightly weaker predictions for these components.

[1] The difference between the two models is given instead of the absolute error of only SAFT-γ Mie predictions to isolate the effect of GC assumptions.

4.2 Binary Mixture Properties

Binary mixture predictions provide more insight than pure-component predictions, because when modelling systems containing components of different homologous series, one can determine from results whether the correct balance between different intermolecular interactions is captured by the model and the active parameter sets. In an *n*-alkyl acetate + *n*-alkane system, both components have dispersion forces while only the ester has dipolar interactions. If a model attributes the attractive interactions between ester molecules mostly to dispersion forces, this system's VLE phase envelopes may appear similar to those of ideal systems. A clear indication of this occurrence is when an azeotrope, which appears in a real system, is absent in the model predictions. Association interactions are stronger than either dipolar or dispersion interactions; therefore, in systems with associating species the correct ratio of *unlike* to *like* interactions will also be identifiable from binary mixture predictions (referring to both phase-equilibrium and excess-property predictions). Furthermore, the modelling of binary systems is important for the evaluation of group-contribution methods, because the ratios between groups in mixtures are not the same as in pure components. For example, in the *n*-alkyl acetate + *n*-alkane system, the number of $COO–CH_2$ interactions is higher than in a pure-component *n*-alkyl acetate system. If the strength of the $COO–CH_2$ interactions is overestimated or underestimated, binary mixture predictions may aid in identifying the problem. Binary mixture VLE and excess properties are modelled in this work because, for the relevant systems, data for these properties are readily available and would allow one to identify the phenomena mentioned above. Additionally, the industry relevance of phase-equilibria predictions increases the value of evaluating model performance for VLE.

Typical binary mixture results with *n*-alkanes are shown in the following subsection. Predictions not shown here can be found in Appendix D. *n*-Alkanes were chosen as the second component in the binary mixtures because all of the necessary parameters are available in literature, and binary predictions with alkanes do not require additional interaction energies beyond those used for pure-component predictions; e.g., $\epsilon_{CH_2OH–CH_2}/k_B$ is regressed for the purpose of generating pure-component predictions and it is then not necessary to generate any other ϵ_{kl}/k_B for binary 1-alcohol + *n*-alkane predictions. The fact that the use of these interaction parameters is shared by both pure-component and binary-system modelling makes the results slightly more predictive.

4.2.1 *n*-Alkyl Acetate + *n*-Alkane

VLE (Figures 4.5 to 4.7) and excess enthalpy (Figures 4.8 to 4.10) predictions for *n*-alkyl acetates mixed with *n*-alkanes are given in this subsection.

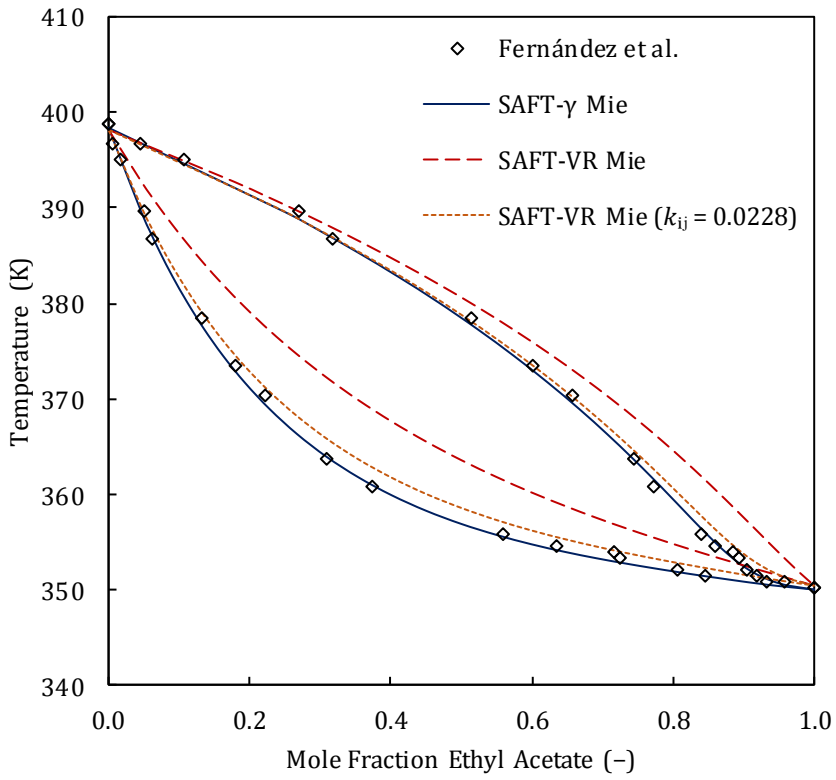

Figure 4.5: Isobaric ethyl acetate + *n*-octane VLE predictions at 1.013 bar. Data taken from Fernández et al. [72].

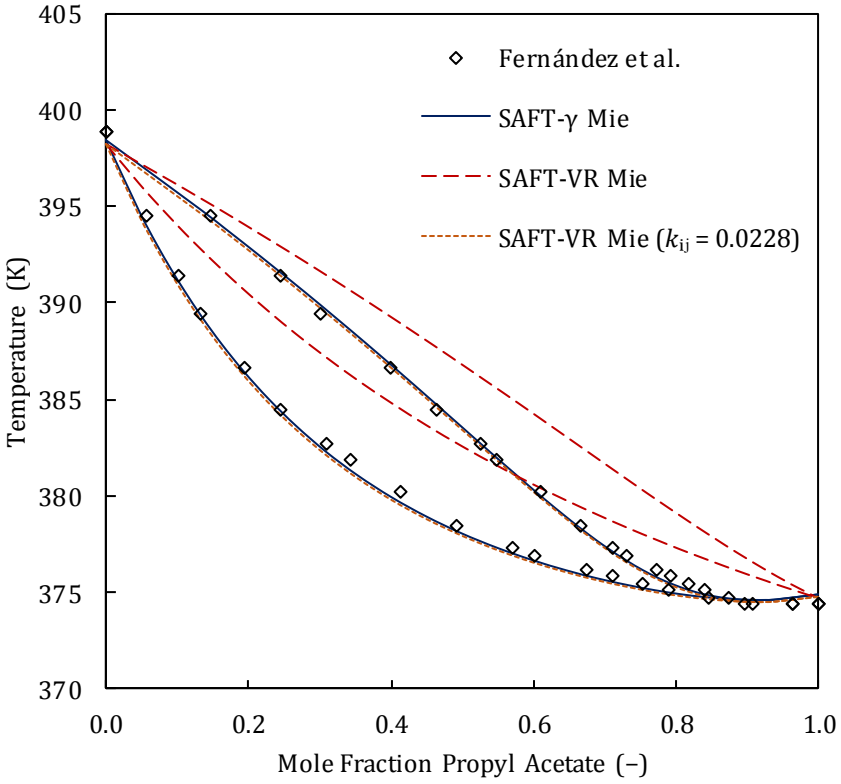

Figure 4.6: Isobaric propyl acetate + *n*-octane VLE predictions at 1.013 bar. Data taken from Fernández et al. [73].

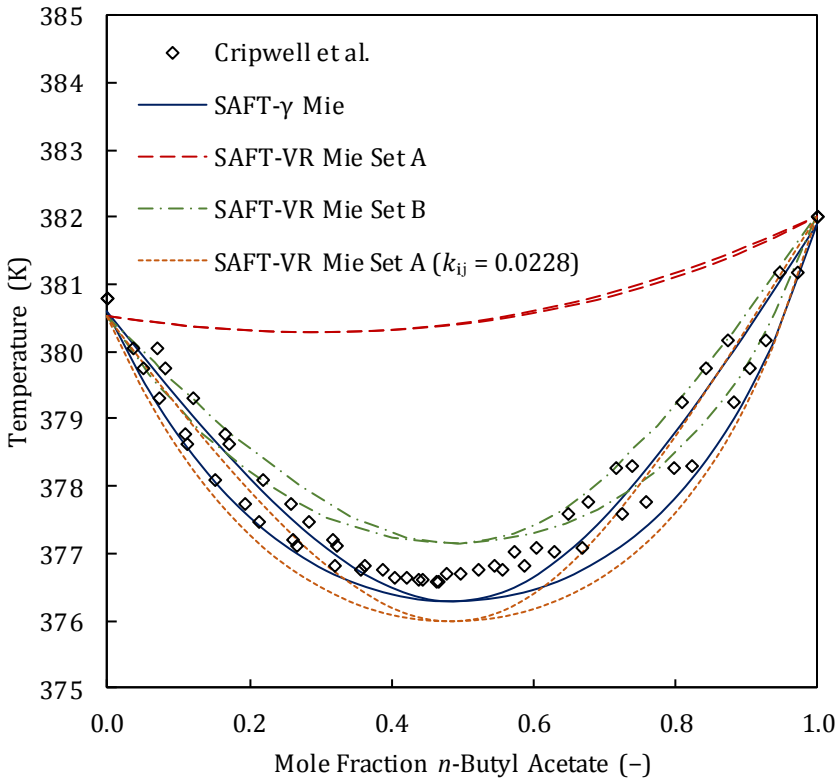

Figure 4.7: Isobaric *n*-butyl acetate + *n*-octane VLE predictions at 0.600 bar. Data taken from Cripwell et al. [74]. **N.B.**: This set was included in the SAFT-VR Mie Set B parameter regression.

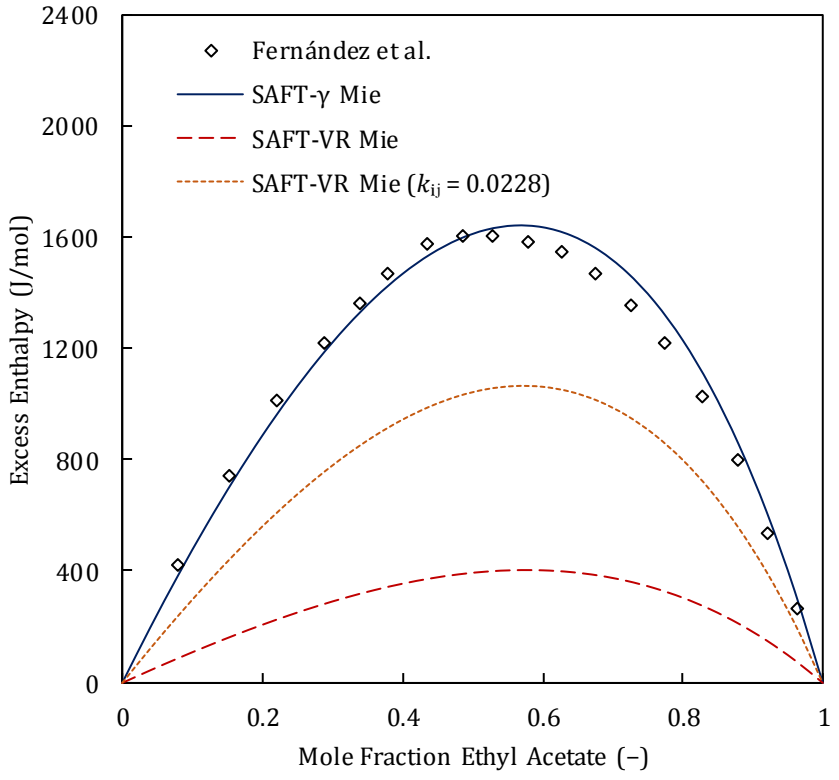

Figure 4.8: Ethyl acetate + *n*-octane excess enthalpy predictions at 298.15 K. Data taken from Fernández et al. [72].

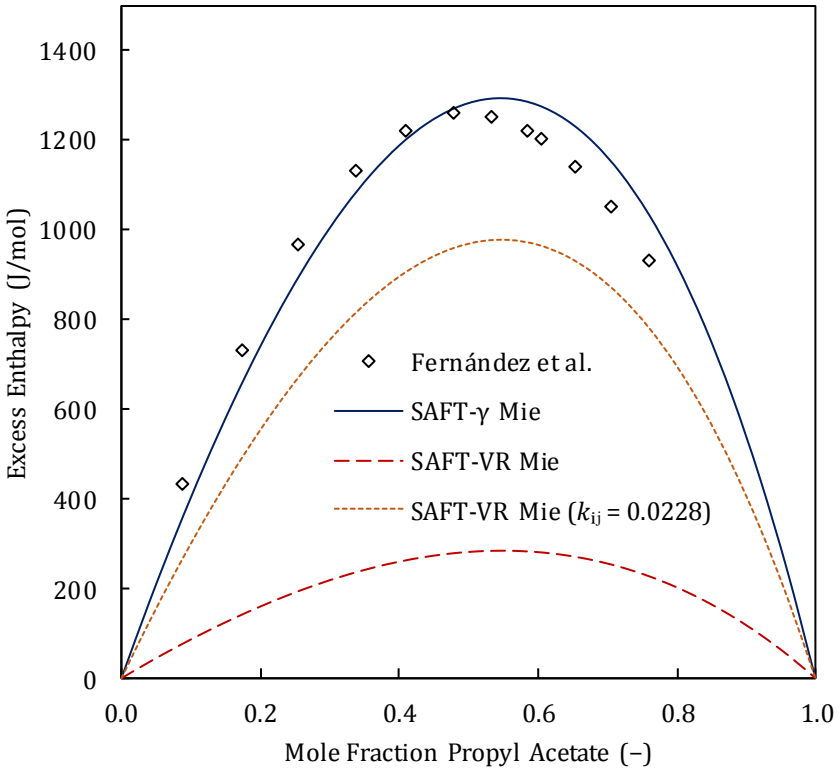

Figure 4.9: Propyl acetate + *n*-octane excess enthalpy predictions at 298.15 K. Data taken from Fernández et al. [73].

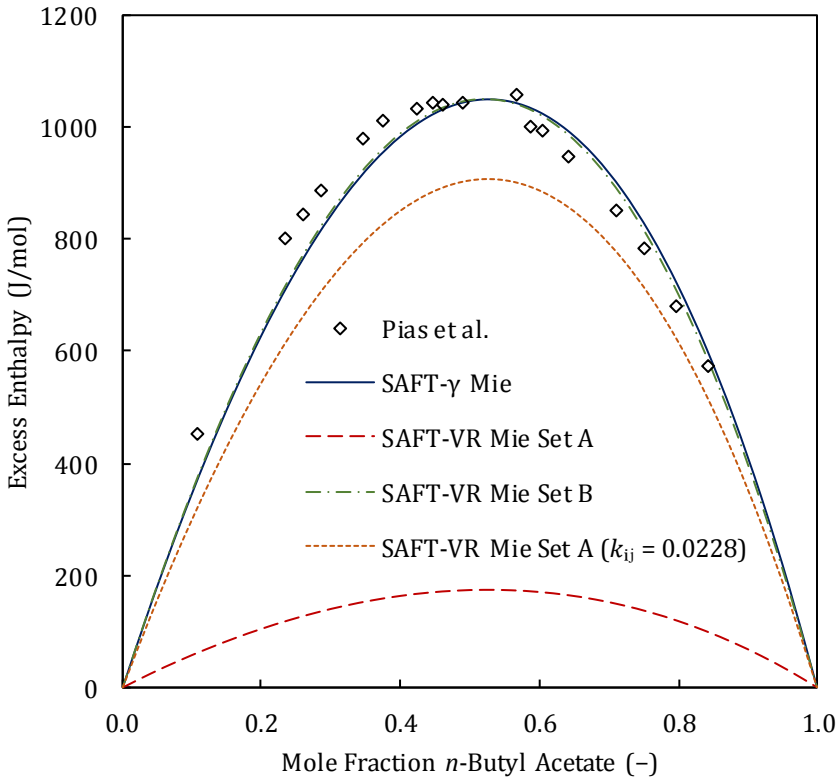

Figure 4.10: *n*-Butyl acetate + *n*-octane excess enthalpy predictions at 298.15 K. Data taken from Pias et al. [75].

SAFT-γ Mie produced exceptionally good predictions for the three acetates + *n*-alkanes, even without an explicit way to account for polarity, whereas SAFT-VR Mie (without BIPs) was unable to capture the correct mixture behaviour, despite its accuracy for the pure components. SAFT-γ Mie with its transferrable group parameters is consistent in its accuracy for VLE and excess enthalpy predictions, suggesting that it captures the correct balance between different *like* and *unlike* interactions for these systems. The accurate excess enthalpy predictions also provide confidence in the model's ability to capture the correct temperature dependence in non-associating systems.

The SAFT-VR Mie acetate parameters were regressed with only the P^{vap}, ρ^{sat}, and u data used to calculate the %AAD values in Table 4.1, while the SAFT-γ Mie parameter regression [30] included excess enthalpy data for ethyl acetate + *n*-hexane and *n*-butyl acetate + *n*-octane. A new *n*-butyl acetate parameter set (Set B) was regressed using mixture data to investigate whether SAFT-VR Mie's poor performance is due to an inadequate regression method. While the Set B VLE prediction seen in Figure 4.7 is much closer to the SAFT-γ Mie prediction, including the VLE set in the parameter regression notably deteriorated the pure-component predictions. This suggests that the standard SAFT-VR Mie lacks the flexibility to model acetates as accurately as SAFT-γ Mie likely because it cannot account for polar interactions. The regression of COO–CH_3 and COO–CH_2 interaction energies may give the GC model an advantage over SAFT-VR Mie. A BIP was applied to the SAFT-VR Mie predictions to see whether one shared parameter, that adjusts dispersion interaction energies between components, would be able to bring about an improvement in accuracy. The value was determined heuristically by inspecting BIPs that were regressed with the VLE sets given in this section. Both the VLE and excess enthalpy SAFT-VR Mie predictions with $k_{ij} = 0.0228$ are closer to the SAFT-γ Mie results (more predictions are given in Appendix D, Section D.2). The SAFT-VR Mie BIP of $k_{ij} = 0.0228$ would result in a smaller interaction energy between components *i* and *j*. It can be deduced that when polar interactions are lumped with dispersion interactions, intermolecular dispersion interactions become overestimated when combining rules are used without BIPs, because the combining rule alone cannot distinguish between polar and dispersion forces. This would then result in the model to overpredict similarity between the different components. In SAFT-γ Mie, this phenomenon is counteracted by the regressed interaction energies of COO–CH_3 and COO–CH_2, which have smaller values than those that would be obtained if the combining rule was used.

4.2.2 1-Alcohol + *n*-Alkane

VLE (Figures 4.11 to 4.13) and excess property (Figures 4.14 to 4.16) predictions for 1-alcohols mixed with *n*-alkanes are given in this subsection.

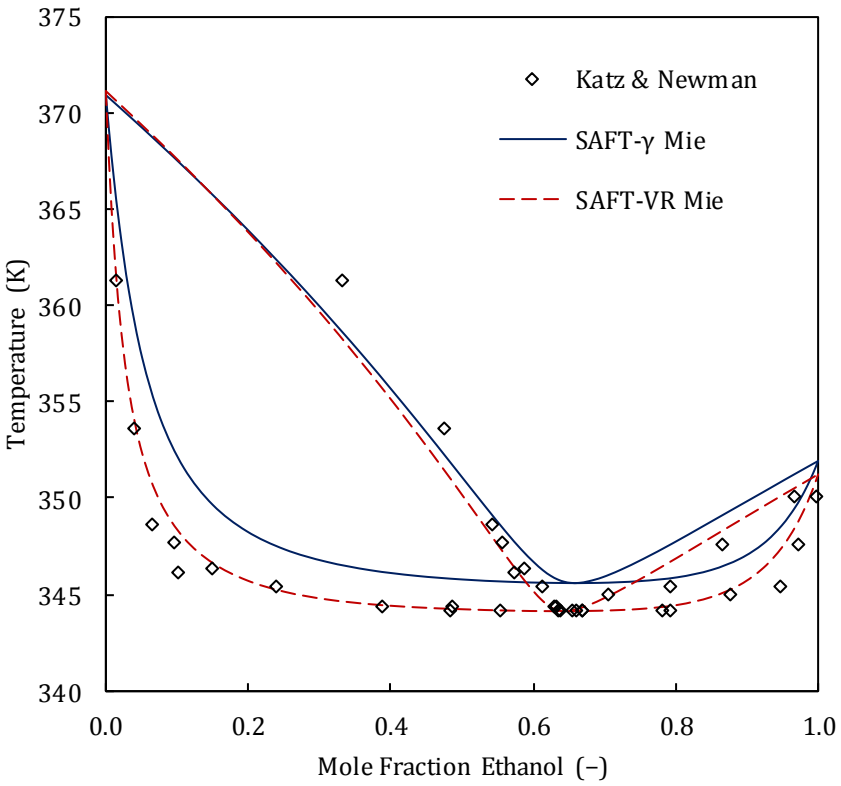

Figure 4.11: Isobaric ethanol + *n*-heptane VLE predictions at 1.01 bar. Data taken from Katz & Newman [76].

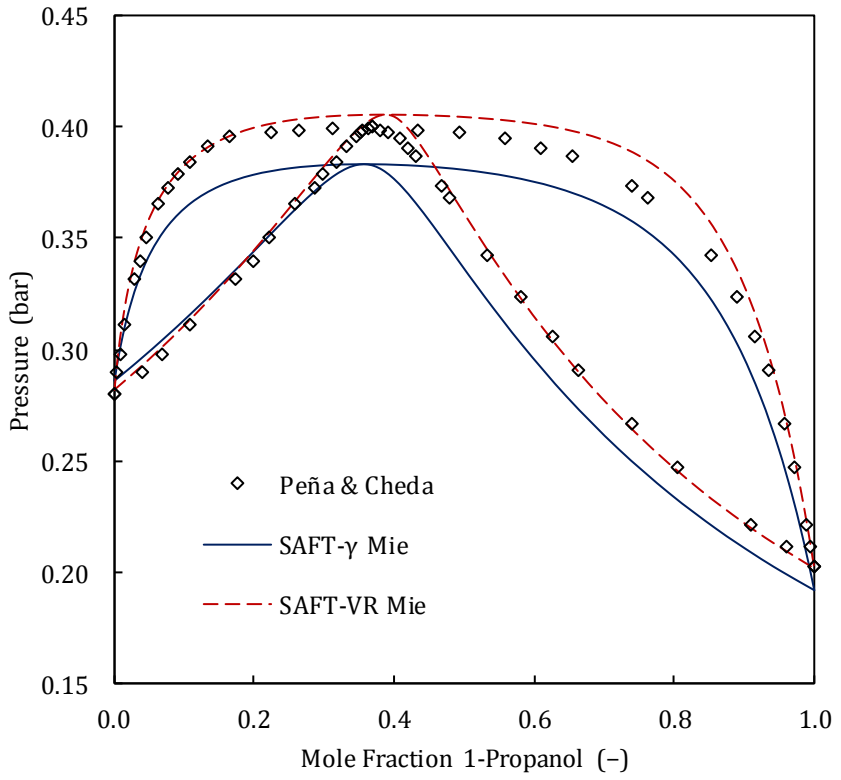

Figure 4.12: Isothermal 1-propanol + *n*-heptane VLE predictions at 333 K. Data taken from Peña & Cheda [77].

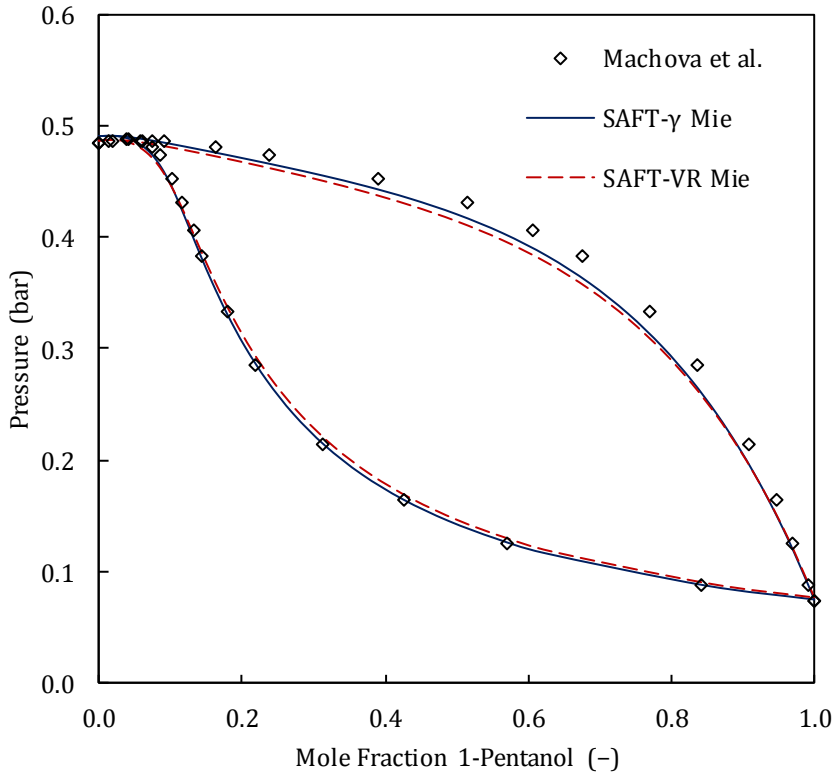

Figure 4.13: Isothermal 1-pentanol + *n*-heptane VLE predictions at 348.15 K. Data taken from Máchová et al. [78].

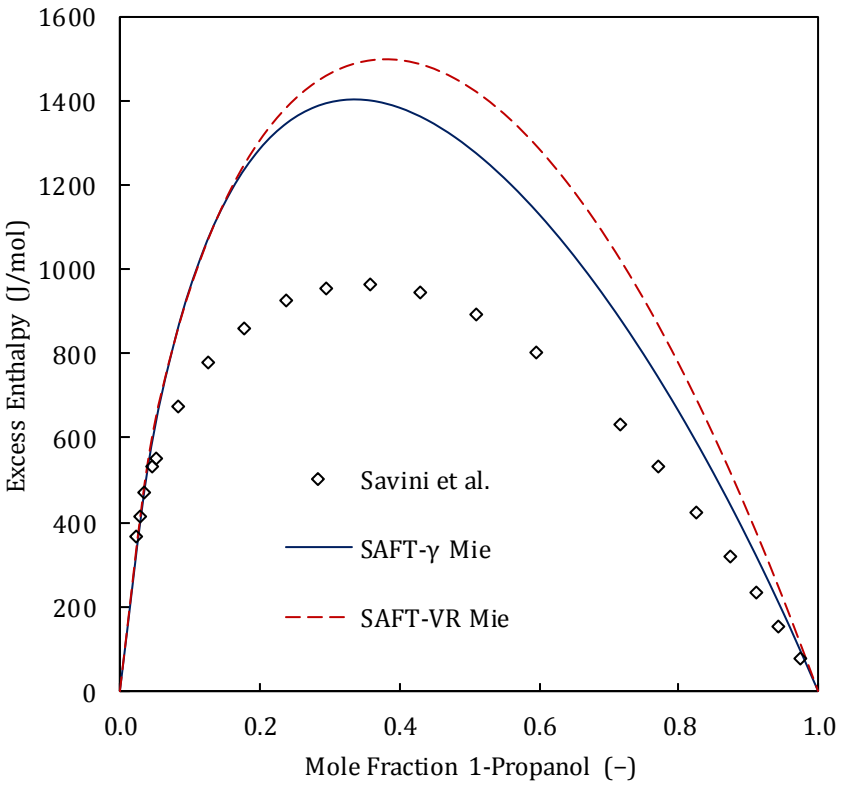

Figure 4.14: 1-Propanol + *n*-heptane excess enthalpy predictions at 318 K. Data taken from Savini et al. [79].

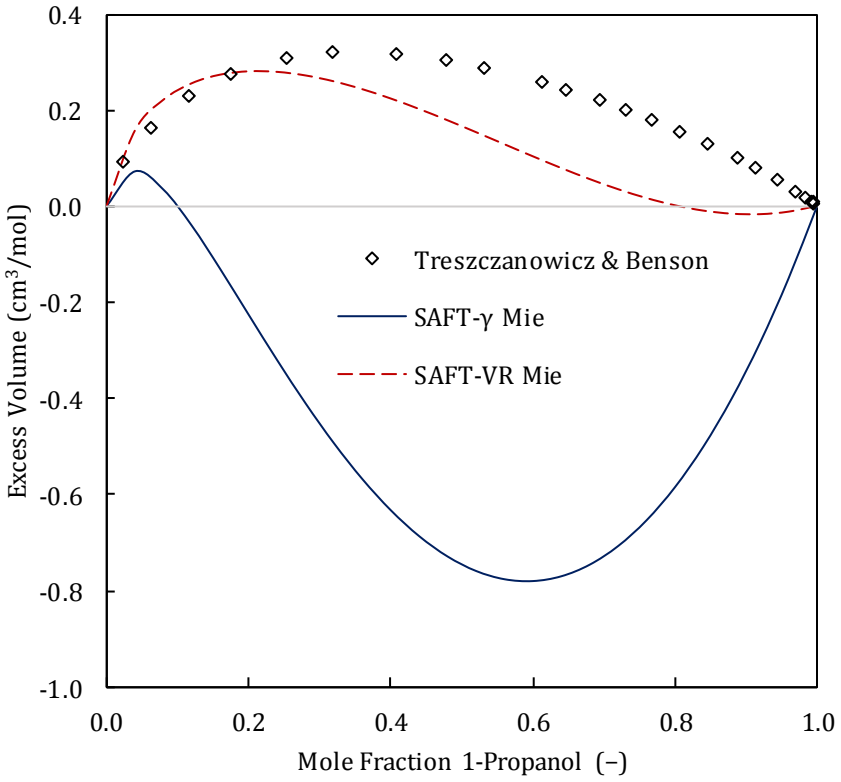

Figure 4.15: 1-Propanol + *n*-heptane excess volume predictions at 298.15 K & 1.0 bar. Data taken from Treszczanowicz & Benson [80].

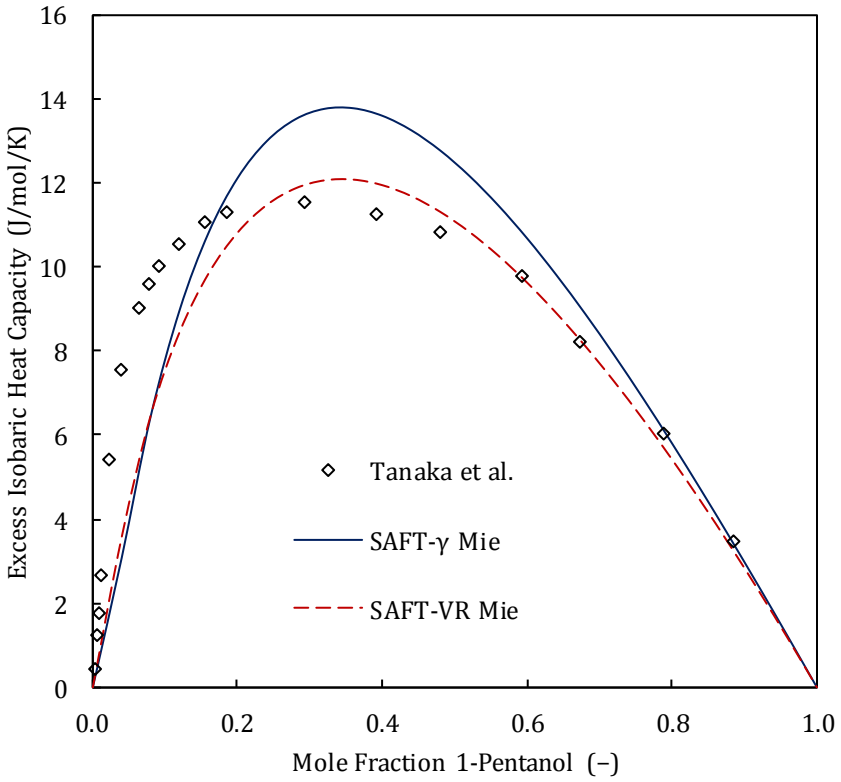

Figure 4.16: 1-Pentanol + *n*-heptane excess isobaric heat capacity predictions at 298.15 K. Data taken from Tanaka et al. [81].

As with the pure-component results, SAFT-VR Mie produced superior predictions, especially for the smaller 1-alcohols. It can be seen by comparing Figure 4.13 with Figures 4.11 and 4.12 that the difference between SAFT-VR Mie and SAFT-γ Mie predictions becomes less notable as the size of the alcohol increases. This is in agreement with the trend seen in Table 4.1, where SAFT-γ Mie's pure-component property %AADs decrease as alcohols become longer. Based on all of the predictions in Subsection 4.2.2, it seems that SAFT-γ Mie overestimates the ratio of *unlike* to *like* interactions in the 1-alcohol + *n*-alkane systems. SAFT-VR Mie favours excess volume (Figure 4.15) and heat capacity (Figure 4.16) predictions while SAFT-γ Mie somewhat favours excess enthalpy (Figure 4.14); nevertheless, the qualitative descriptions are similar.

4.3 Chapter Summary

Overall, SAFT-γ Mie performs slightly weaker than SAFT-VR Mie for pure-component P^{vap} predictions. The absolute difference between the P^{vap} predictions of the two models indicates that the GC assumptions introduce some inaccuracies for the smallest and largest *n*-alkanes, but pure-component predictions for the nonpolar, non-associating species are still satisfactory.

Excellent acetate ester predictions were obtained with SAFT-γ Mie as opposed to SAFT-VR Mie, which is unable to capture the ester–alkane binary VLE phase behaviour. The regressed binary interaction energies between the COO group and the CH_3 and CH_2 groups give SAFT-γ Mie an advantage. However, the ester modelling includes only three *n*-alkyl acetates, and thus far it is unknown whether the same level of accuracy can be obtained for different ester isomers. In the following chapter, various isomers of polar components were modelled to determine whether the position of the functional group has an effect on model performance.

Among the species considered in Chapter 4, the greatest difference in performance for pure-component predictions between SAFT-γ Mie and SAFT-VR Mie can be observed for 1-alcohols. While the dipolar moments of the considered 1-alcohols and *n*-alkyl acetates are similar, the alcohol molecules are considerably smaller. It can also be seen that results improve as the length of the alcohol increases. It appears as though the dipolar interactions of smaller polar molecules make their modelling more difficult for a GC EoS where the environment of the functional group is ignored, especially in the absence of an explicit polar contribution. Polar, non-self-associating components that are smaller than the alkyl acetates were modelled in the next chapter to single out or disprove polarity as the cause of the weaker predictions, especially in regard to pure-component properties.

Chapter 5: Non-Associating Dipolar Organics

The main goal of this chapter is to investigate whether the GCM assumptions put SAFT-γ Mie at a disadvantage compared to SAFT-VR Mie when modelling dipolar components. Non-associating dipolar components are the focus, because it was seen from the 1-alcohol predictions in Chapter 4 that SAFT-γ Mie may produce less accurate results for smaller dipolar organics. In addition to the aforementioned goal, the modelling of these components provides a platform to investigate the treatment of polar interactions in SAFT-γ Mie and the modelling consistency between isomers. In this chapter, the application of SAFT-γ Mie was therefore expanded to 2-ketones, 3-ketones, and *n*-alkyl propanoate esters.

5.1 Polarity in SAFT-γ Mie

SAFT-γ Mie does not currently have a polar contribution. Polarity can be treated in three ways: (i) lumped with the variable dispersion interaction parameters, as in Papaioannou et al. [30]; (ii) approximated as association interactions; or (iii) accounted for with a new polar contribution. This work will follow the second approach, as in Dufal et al. [33], where polar interactions are approximated as association at additional "H" and "e_1" sites — the pseudo-association approach mentioned in Chapter 2, Section 2.2.3. The first series considered in this chapter is 2-ketones, which have higher dipole moments than acetates and 1-alcohols, are relatively small, and do not self-associate. The "e_2" electron site on ketones is only active for cross-association while the "H" and "e_1" sites are always active (the "H" and "e_1" sites are also allowed to cross-associate to account for dipole-dipole interactions between different species). The pseudo-association method is chosen as it will likely produce better results than lumping polarity with the dispersion forces, because the extra parameters should offer a mathematical advantage, and it is readily implemented in the current SAFT-γ Mie. The regression of additional parameters is a downside of this approach because the increased parameter-space dimensionality could make parameterisation more difficult, and pseudo-association is not as physically appropriate as a fundamental polar term. Nevertheless, these parameters can be generated at the same time as the dispersion energy interaction parameters so that the number of regressions and the amount of data required remain the same.

One of the goals of this chapter is to investigate whether an explicit polar contribution is needed by comparing SAFT-γ Mie predictions with pseudo-association to SAFT-VR Mie + GV. If SAFT-γ Mie is unable to predict the right behaviour in systems containing polar components, adding an explicit polar contribution should definitely be considered.

5.2 2-Ketones with CO Group

The new SAFT-γ Mie parameters presented in Table 5.3 and Table 5.4 were regressed for a ketone functional group defined as one carbon atom with two open single bonds, double bonded to an oxygen atom with two lone electron pairs (see Figure 5.1). This structure was chosen to make the group small and versatile. The CH_3 and CH_2 parameters used in conjunction with the new CO parameters were sourced from the original work by Papaioannou et al. [30], while the 1-alcohol (CH_2OH) parameters used in the binary mixture predictions are from Hutacharoen et al. [34]. A summary of all the new and previously published SAFT-γ Mie parameters that are relevant to this work can be found in Appendix B, and the SAFT-VR Mie + GV parameters can be found in Appendix C.

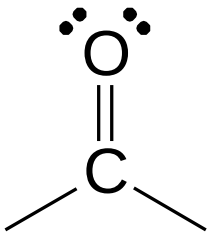

Figure 5.1: Diagrammatic representation of CO functional group.

Tables 5.1 and 5.2 summarise the data that were included in the regression for the CO group parameters and the CO–CH_2OH interaction parameters.

Table 5.1: Data included in the new 2-ketone (CO) regression. N_P refers to the number of data points.

Type	Components	Temperature[a]	Pressure	N_P	Weight	Reference
P^{vap}	2-butanone → 2-nonanone	$0.5T_C$ – $0.9T_C$	Equilibrium	180	5	[64]
ρ^{sat}	2-butanone → 2-nonanone	$0.5T_C$ – $0.9T_C$	Equilibrium	180	7	[64]
u	2-octanone	433.2 K	0.1 – 160 MPa	9	1	[82]
H^E	2-heptanone + *n*-heptane	298.15 K	1.013 bar	20	1	[83]
VLE	*n*-hexane + 2-butanone	333.15 K	Equilibrium	12	10	[84]

[a]The P^{vap} and ρ^{sat} temperature range minima and maxima are given as fractions of the component's critical temperature, T_C.

Table 5.2: Data included in the new CO–CH_2OH interaction parameter regression.

Type	Components	Temperature	Pressure	N_P	Weight	Reference
H^E	2-butanone + 1-butanol	313.15 K	1.013 bar	16	1	[85]
VLE	1-butanol + 2-pentanone	Equilibrium	1.013 bar	14	20	[86]

The regression was completed for different integer-value segment numbers: $\nu^*_{CO} = 1$, 2, and 3. Although $\nu^*_{CO} = 2$ was chosen based on the physical structure of the group, the regression was also done for $\nu^*_{CO} = 1$ and 3, which subsequently confirmed that the logical choice resulted in the lowest value of the minimised regression OF.

Table 5.3: New 2-ketone (CO) functional-group non-association SAFT-γ Mie parameters.

Parameter	Group k	Group l	Value	Units
ν^*_k	CO		2.0000	
S_k	CO		0.44504	
σ_{kl}	CO	CO	3.0471	Å
λ^a_{kl}	CO	CO	6.0000	
λ^r_{kl}	CO	CO	6.2561	
ϵ_{kl}/k_B	CO	CO	200.71	K
ϵ_{kl}/k_B	CO	CH_3	223.68	K
ϵ_{kl}/k_B	CO	CH_2	278.15	K
ϵ_{kl}/k_B	CO	CH_2OH	318.31	K

Table 5.4 New 2-ketone (CO) functional-group association SAFT-γ Mie parameters.

Parameter	Group k	Site a	Group l	Site b	Value	Units
$\epsilon^{HB}_{kl,ab}/k_B$	CO	H	CO	e_1	1100.1	K
$\epsilon^{HB}_{kl,ab}/k_B$	CO	H	CH_2OH	e_1	930.61	K
$\epsilon^{HB}_{kl,ab}/k_B$	CO	e_1	CH_2OH	H	812.03	K
$\epsilon^{HB}_{kl,ab}/k_B$	CO	e_2	CH_2OH	H	994.74	K
$K_{kl,ab}$	CO	H	CO	e_1	717.23	Å^3
$K_{kl,ab}$	CO	H	CH_2OH	e_1	385.52	Å^3
$K_{kl,ab}$	CO	e_1	CH_2OH	H	1069.0	Å^3
$K_{kl,ab}$	CO	e_2	CH_2OH	H	625.16	Å^3

The parameterisation was carried out by regressing all of the CO group-specific parameters first (the first six parameters listed in Table 5.3, excluding ν_k^* and $\lambda_{kl}^{\mathrm{a}}$) using the combining rule to calculate dispersion interaction energies between CO–CH_3 and CO–CH_2. A follow-up regression was then done to determine the interaction energies while keeping the other parameters constant. This was done to alleviate the challenges of working in an extremely large parameter space — difficulties due to local minima had been encountered during prior parameterisation attempts with all parameters included at once. Based on the argument for why regressing interaction energies is important for acetates (given at the end of Section 4.2.1), not regressing the interaction energies as part of the initial regression should not be problematic for the ketones because pseudo-association should be able to account for polarity while the dispersion parameters only account for dispersion interactions. There is therefore no apparent reason for why the combining rule cannot be used.

As with the acetone parameters of Dufal et al. [33], the pseudo-association parameters of the new ketone group comprise of a lower association energy and higher association range compared to the alcohol CH_2OH association parameters of 2097.9 K and 62.309 $Å^3$. This is reassuring because polar interactions are in fact much weaker than association interactions and they take place over a much longer range, whereas association interactions are more like weaker covalent bonds. H-atoms tend to behave bivalently to link two sufficiently electronegative atoms, thus hydrogen bonding takes place when molecules are close enough so that electron clouds can overlap.

The repulsive exponent obtained for the CO group is very small, especially compared to λ^{r} obtained by Papaioannou et al. [30] for the carboxylate group (COO) which does not have pseudo-association. It is speculated by Papaioannou et al. that the COO group's polar interactions are lumped with the variable range dispersion interactions. The reverse may be taking place for the new CO group. It is possible that a portion of the dispersion interactions is being lumped with pseudo-association to produce parameters that will fit the data. On the other hand, speculations regarding the physical meaning of group parameters should be undertaken with caution as these parameters only belong to groups — the characteristics of molecules as a whole may be very different from those of its constituent groups. What is important is that none of the parameters exceed their logical bounds.

5.2.1 Pure-Component Properties

Figures 5.2, 5.3, and 5.4 present comparisons in %AAD between the two models for P^{vap}, ρ^{sat}, and H^{vap} pure-component predictions, respectively. The average deviations of P^{vap}, ρ^{sat}, and H^{vap} were calculated using DIPPR correlations [64].

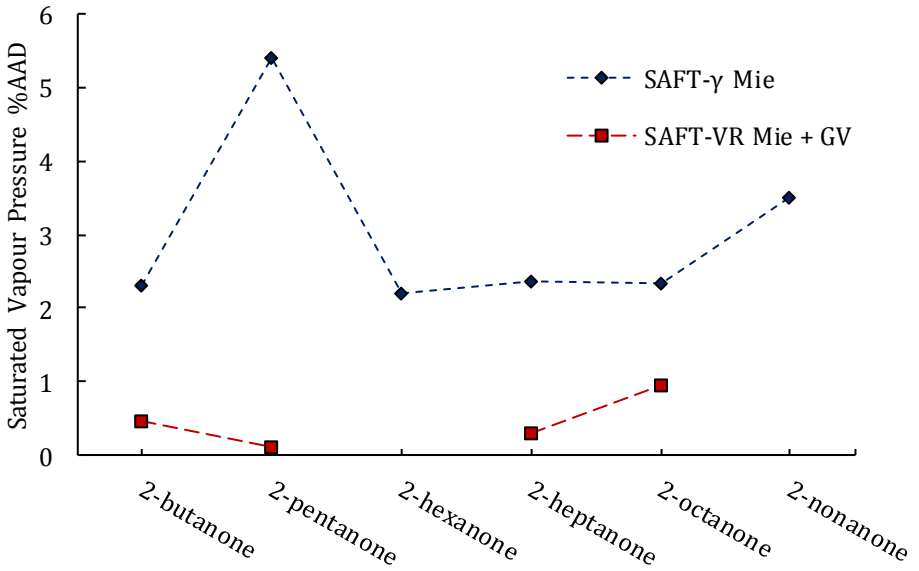

Figure 5.2: 2-Ketone P^{vap} prediction %AADs with CO group.

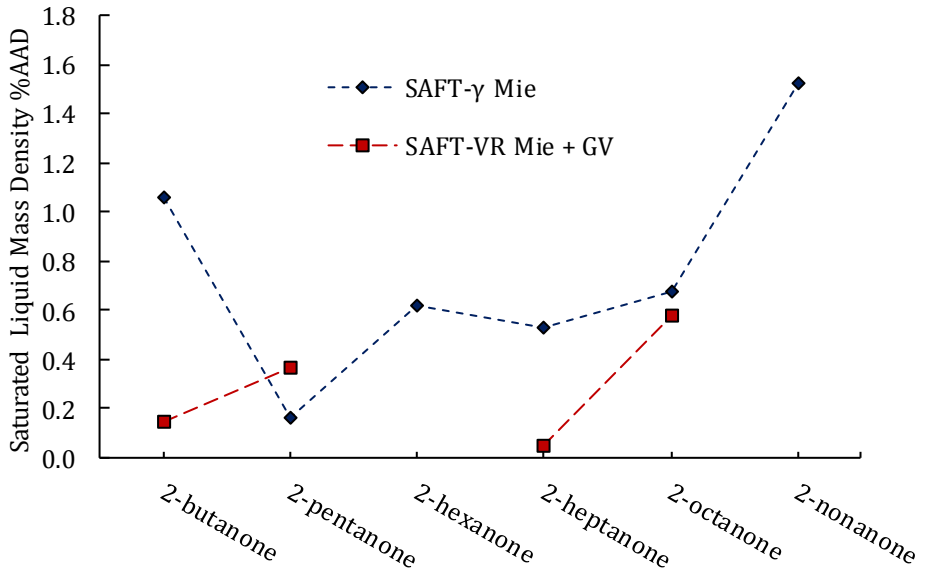

Figure 5.3: 2-Ketone ρ^{sat} prediction %AADs with CO group.

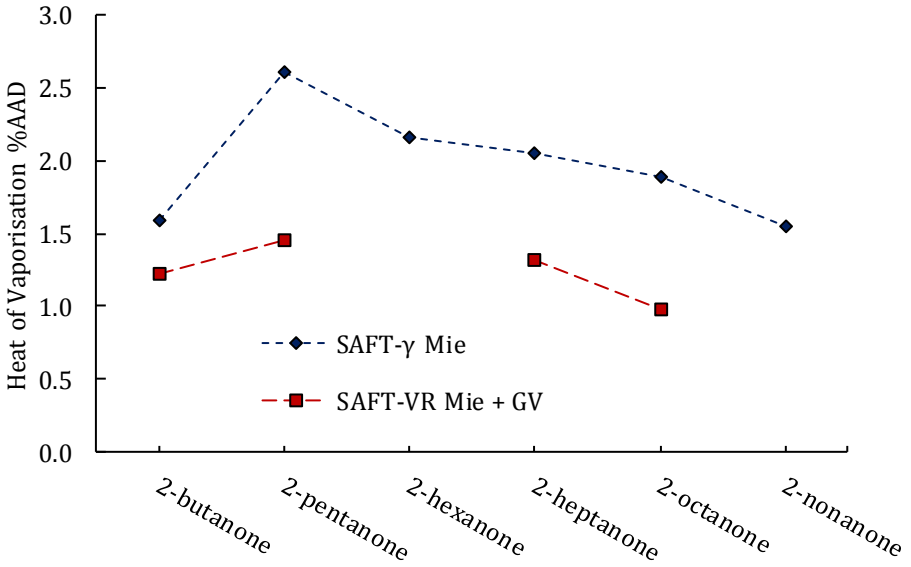

Figure 5.4: 2-Ketone H^{vap} (c) prediction %AADs with CO group.

A comparison for speed of sound predictions is given in Table 5.5.

Table 5.5: Speed of sound %AADs for 2-ketones with new CO group.

Component	SAFT-γ Mie	SAFT-VR Mie + GV	T (K)	P (bar)	Reference
2-butanone	**1.07**	3.50	293.15 - 323.15	1.0	[87]
2-pentanone	**1.57**	4.04	293.15 - 303.15	1.0	[88]
2-heptanone	**3.49**	6.02	293.15 - 303.15	1.0	[88]
2-octanone	**1.41**	3.16	433.15	1.0 - 1600	[82]

Based on Figures 5.2 to 5.4, the SAFT-γ Mie pure-component predictions leave more to be desired, especially for P^{vap}, while SAFT-VR Mie + GV provides excellent prediction accuracy for P^{vap}, ρ^{sat}, and H^{vap}. Conversely, SAFT-γ Mie provides better speed of sound predictions despite the fact that the data were included in the SAFT-VR Mie + GV parameter regression for each of the 2-ketones. This confirms that the transferability of SAFT-γ Mie's parameters extends to speed of sound predictions, and that the inclusion of one sufficiently large speed of sound dataset in the group parameter regression is adequate. A visual comparison of the two models' performance is given in Figure 5.5.

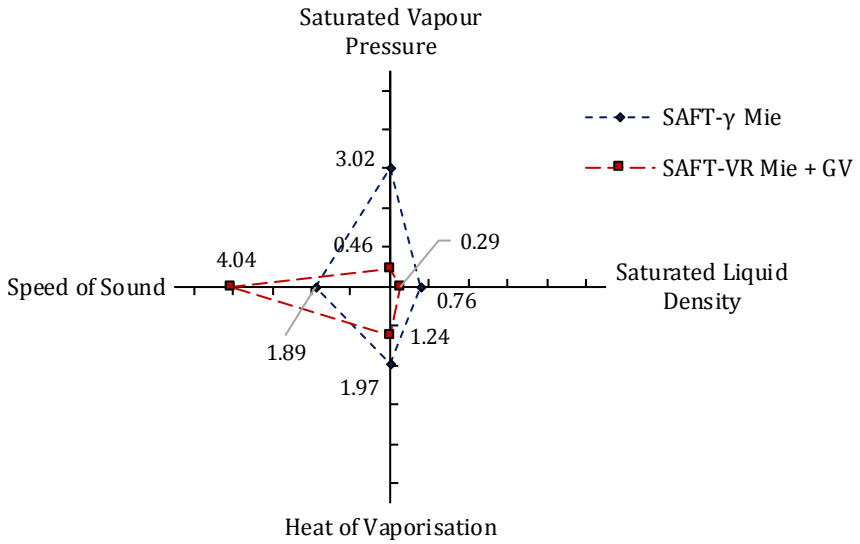

Figure 5.5: 2-Ketone pure-component mean %AADs with CO group. The %AADs are the mean values of those in Figures 5.2 to 5.4, and Table 5.5.

The datapoints of the SAFT-VR Mie + GV series in Figure 5.5 lie closer to the centre of the radial plot, giving a visual indication of how much of an advantage the TS model has over SAFT-γ Mie in regard to P^{vap}, ρ^{sat}, and H^{vap}. Accurate pure-component property predictions are crucial because the pure-component descriptions inevitably influence desired mixture property predictions, especially the properties of very dilute mixtures. Figure 5.5 suggests that a component-specific TS model, such as SAFT-VR Mie + GV, may be preferred over SAFT-γ Mie if precise 2-ketone pure-component or dilute-mixture predictions are required, given that appropriate data are available for the component-specific parameterisation of the relevant species.

5.2.2 2-Ketone + *n*-Alkane VLE

n-Alkanes were chosen as the secondary components in these binary predictions for the same reasons mentioned in Section 4.2: The interaction parameters are already available, and fewer interaction parameters means that results are more predictive. Figures 5.6 to 5.9 exhibit typical 2-ketone + *n*-alkane VLE predictions of SAFT-VR Mie + GV and SAFT-γ Mie using the new CO group.

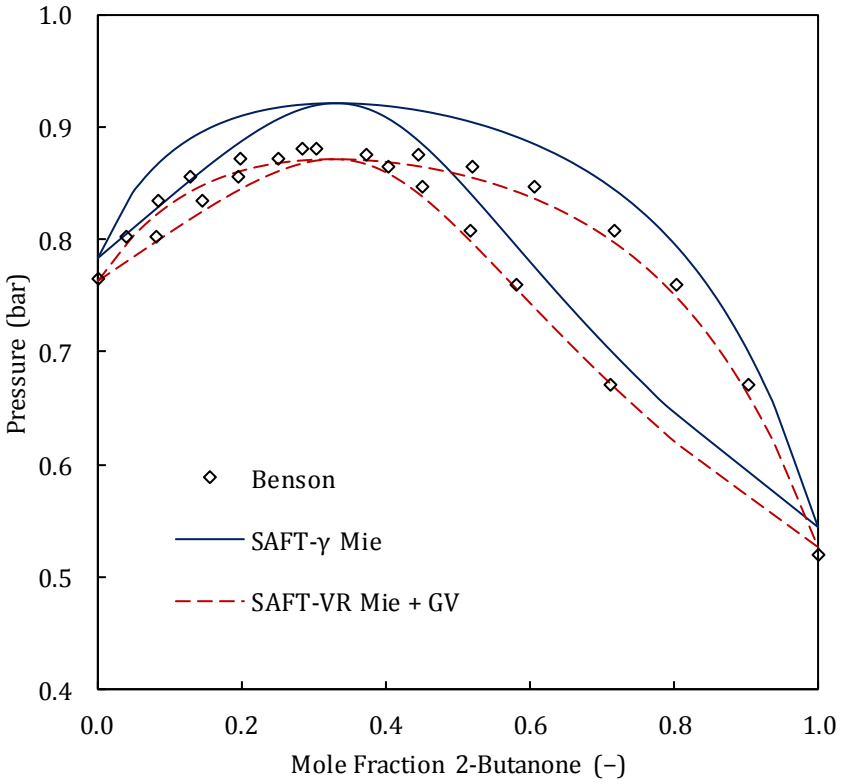

Figure 5.6: Isothermal 2-butanone + *n*-hexane VLE predictions with CO group at 333 K. Data taken from Benson [89]. **N.B.**: This set was included in the SAFT-γ Mie CO group regression.

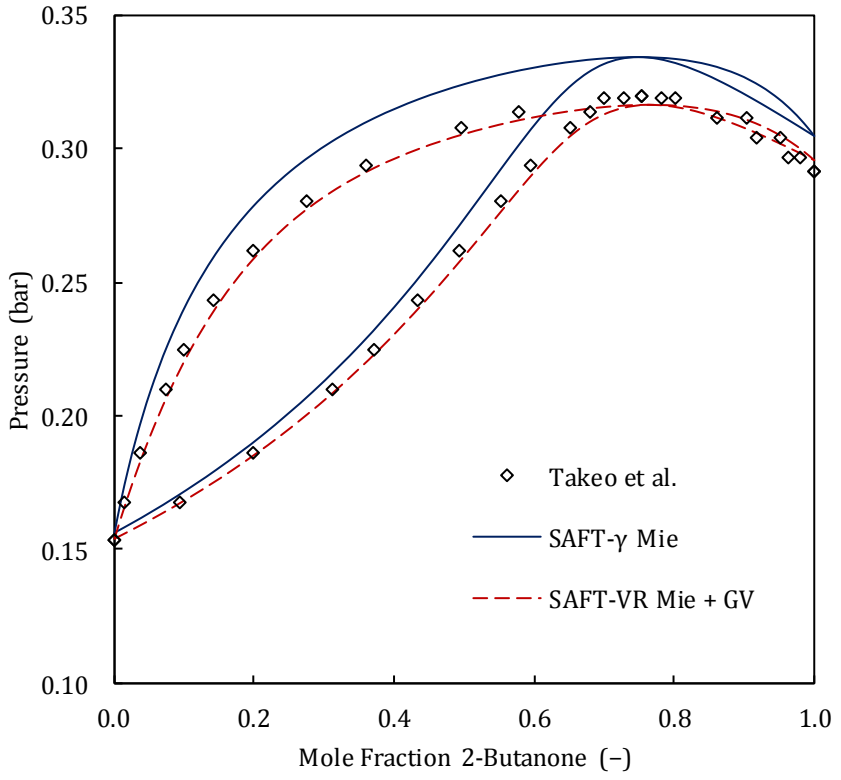

Figure 5.7: Isothermal 2-butanone + *n*-heptane VLE predictions with CO group at 318.2 K. Data taken from Takeo et al. [90].

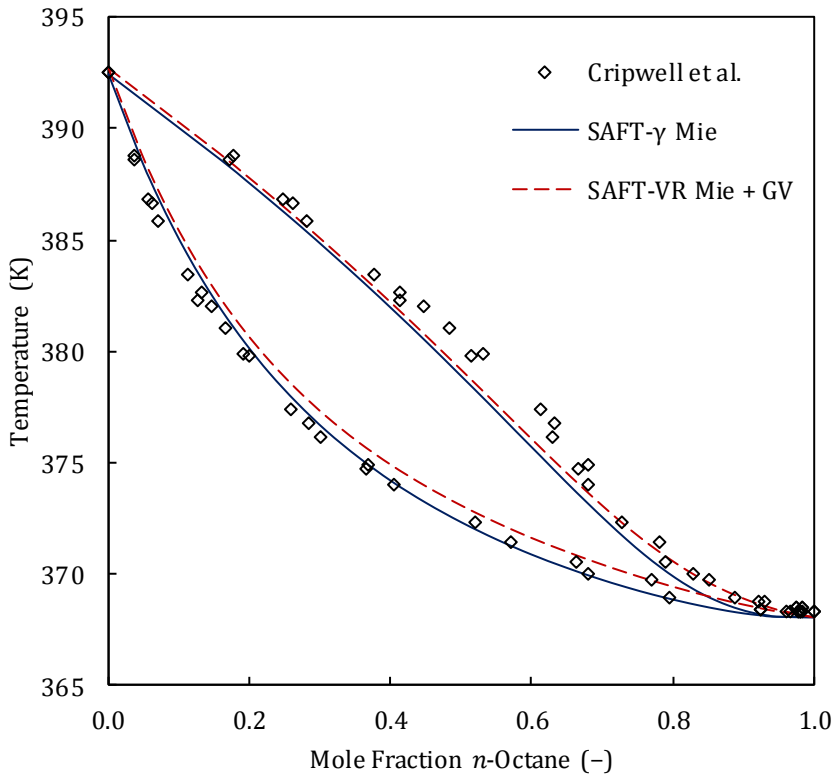

Figure 5.8: Isobaric *n*-octane + 2-heptanone VLE predictions with CO group at 0.400 bar. Data taken from Cripwell et al. [57].

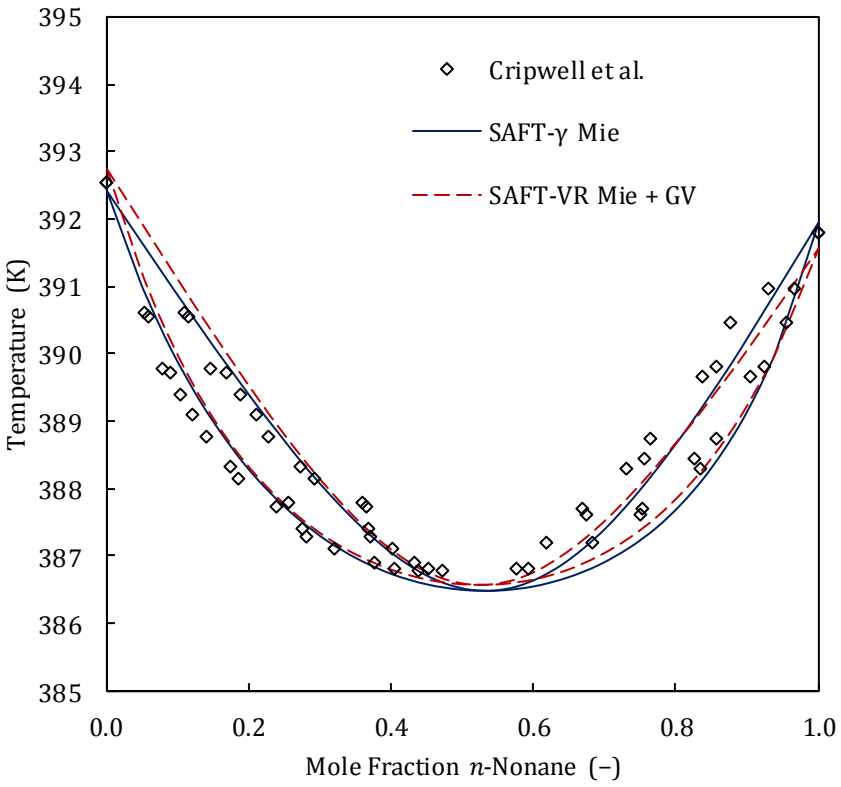

Figure 5.9: Isobaric *n*-nonane + 2-heptanone VLE predictions with CO group at 0.400 bar. Data taken from Cripwell et al. [57]. **N.B.**: This set was included in the SAFT-VR Mie + GV parameter regression [19].

Both thermodynamic models are able to predict the correct phase envelopes for the 2-butanone systems in Figures 5.6 and 5.7, but SAFT-γ Mie overpredicts the equilibrium pressures. Note that the pure-component vapour pressures are also overestimated, suggesting that better pure-component descriptions may be required before better VLE descriptions can be obtained; this is particularly apparent in Figure 5.7 where predictions at the ketone-rich compositions are notably less accurate. Both models provide similar predictions for the other systems (Figures 5.8 and 5.9), indicating that they are consistent for 2-ketones of different sizes. SAFT-γ Mie with pseudo-association seems to provide qualitatively sound VLE predictions for binary systems where the ketone is mixed with a nonpolar, non-associating species.

5.2.3 Other 2-Ketone + *n*-Alkane Mixture Properties

Predictions with SAFT-VR Mie + GV and SAFT-γ Mie using the new CO group are given for excess isobaric heat capacity in Figure 5.10, excess enthalpy in Figures 5.11 and 5.12, and speed of sound in Figure 5.13.

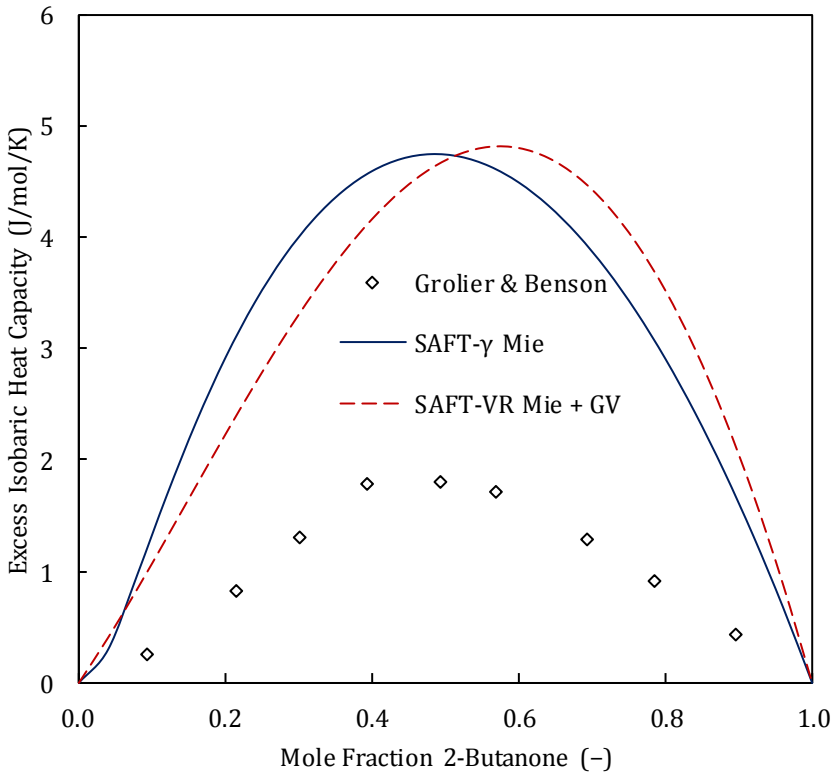

Figure 5.10: + 2-Butanone + *n*-heptane excess isobaric heat capacity predictions with CO group at 298.15 K & 1.013 bar. Data taken from Grolier & Benson [91].

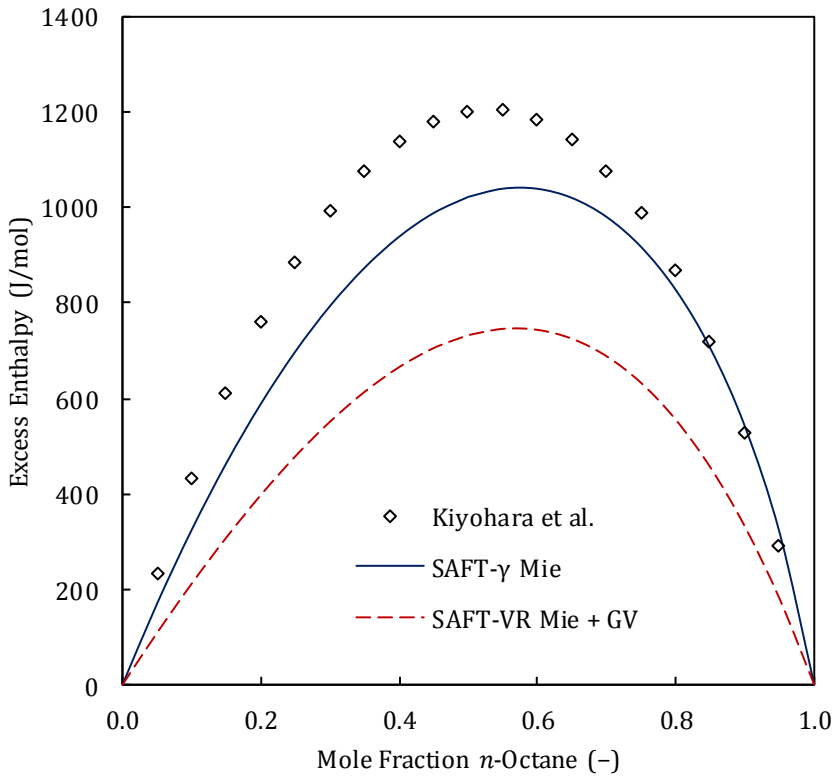

Figure 5.11: *n*-Octane + 2-pentanone excess enthalpy predictions with CO group at 298.15 K. Data taken from Kiyohara et al. [92].

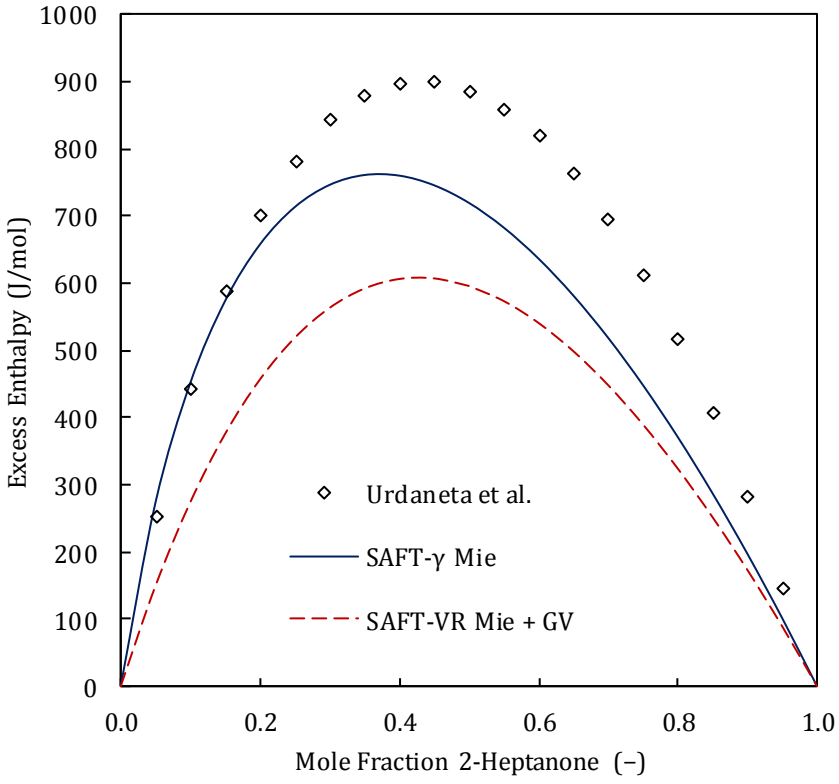

Figure 5.12: 2-Heptanone + *n*-heptane excess enthalpy predictions with CO group at 298.15 K. Data taken from Urdaneta et al. [83]. **N.B.**: This set was included in the SAFT-γ Mie CO group regression.

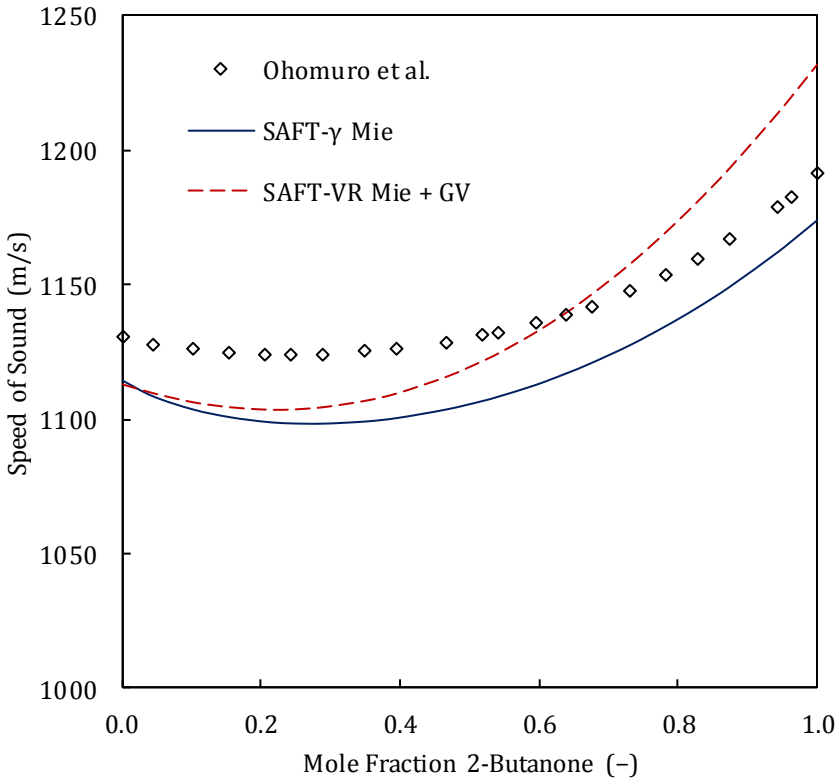

Figure 5.13: 2-Butanone + *n*-heptane speed of sound predictions with CO group at 298.15 K. Data taken from Ohomura et al. [93].

Both models overpredict the excess isobaric heat capacities (Figure 5.10) for 2-butanone + *n*-heptane to a similar extent, and underpredict the excess enthalpies (Figures 5.11 and 5.12). Despite that the excess enthalpies are underestimated, SAFT-γ Mie is once again able to reproduce the same level of accuracy for systems with 2-ketones of different chain lengths while using the same set of transferrable group parameters. SAFT-γ Mie's excess enthalpy and 2-butanone + *n*-heptane speed of sound (Figure 5.13) predictions are slightly superior with better composition dependence. An advantage of the GCM is that, to include higher derivative properties in the regression, one requires data for only one or two of the components — this may be why SAFT-γ Mie's 2-ketone temperature and second-derivative property descriptions are mostly better. Most of the SAFT-VR Mie + GV 2-ketone parameters were regressed without second-derivative property data, or with sets of very narrow temperature ranges, because data for these properties are scarce. Specifically, the SAFT-VR Mie + GV speed of sound predictions in Figure 5.13 were made with 2-butanone parameters generated without speed of sound data.

The next section investigates whether the interactions between the new CO group and another polar group are captured accurately by SAFT-γ Mie with the pseudo-association method. The other group in this case is the CH_2OH 1-alcohol group of Hutacharoen et al. [34], which does not make use of pseudo-association. However, interactions between its HB sites and the CO group's pseudo-association "H" and "e_1" sites should account for the intercomponent dipole-dipole interactions of 2-ketone + 1-alcohol systems.

5.2.4 2-Ketone + 1-Alcohol Predictions

Phase equilibrium (Figures 5.14 to 5.18) and excess enthalpy (Figures 5.19 and 5.20) predictions for 2-ketones mixed with 1-alcohols are given in this subsection.

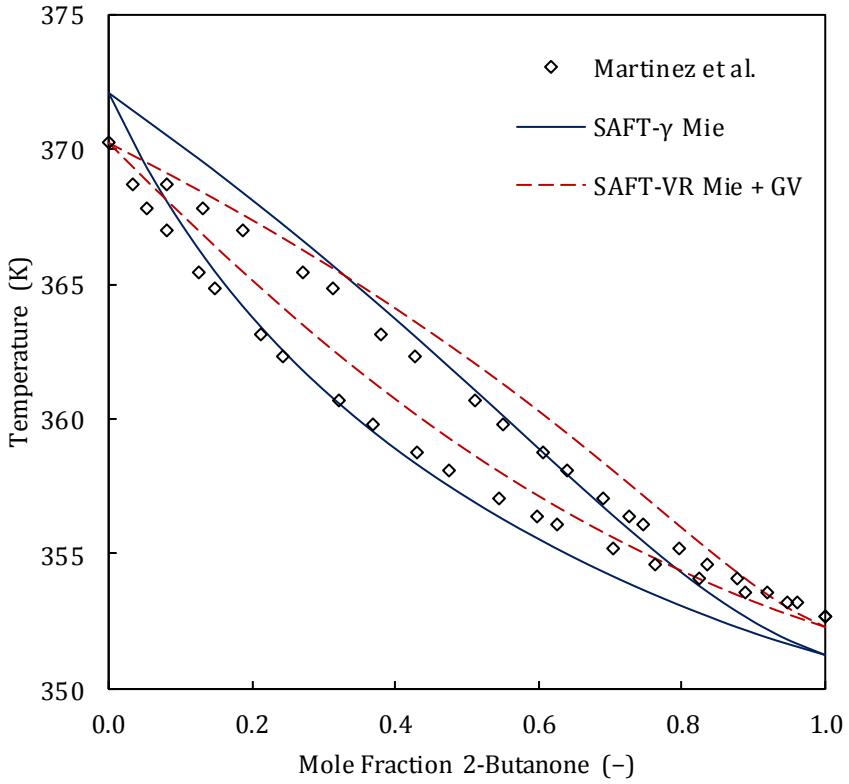

Figure 5.14: Isobaric 2-butanone + 1-propanol VLE predictions with CO group at 1.013 bar. Data taken from Martinez et al. [94].

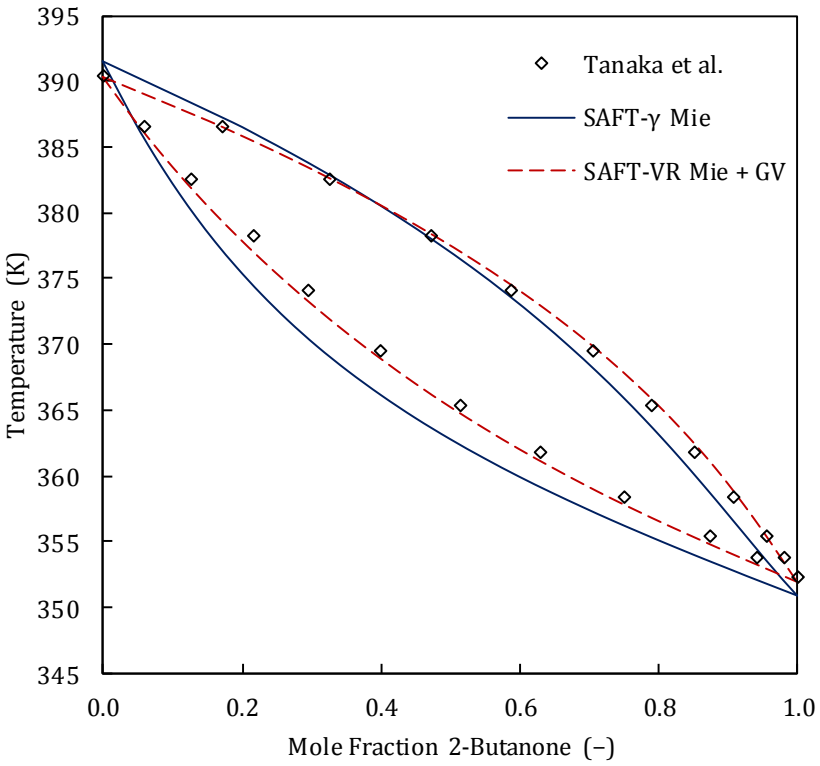

Figure 5.15: Isobaric 2-butanone + 1-butanol VLE predictions with CO group at 1.000 bar. Data taken from Tanaka et al. [95]. **N.B.**: This set was included in the SAFT-VR Mie + GV 2-butanone association parameter regression.

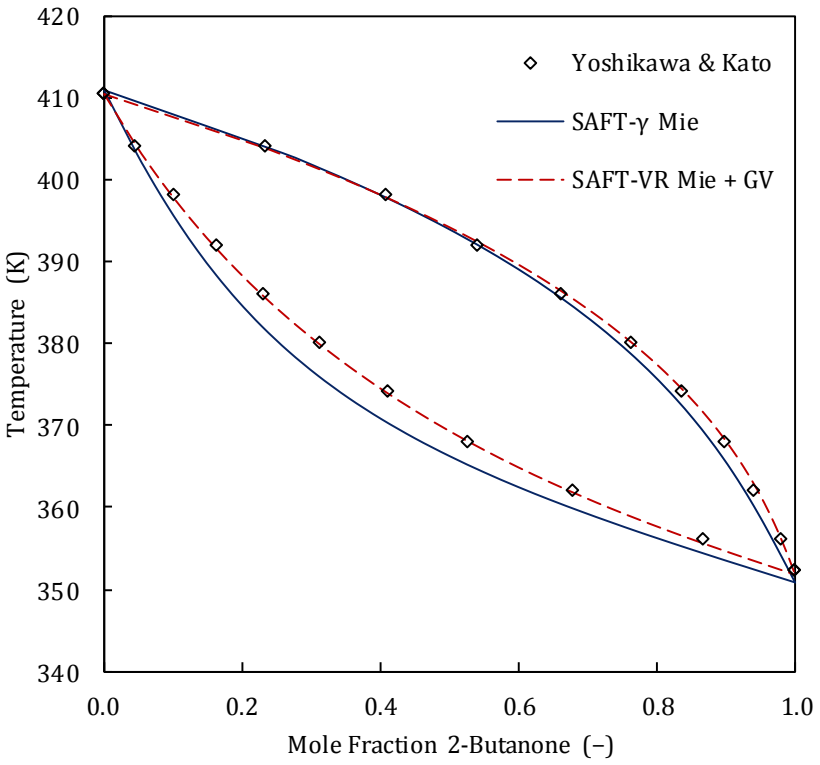

Figure 5.16: Isobaric 2-butanone + 1-pentanol VLE predictions with CO group at 1.00 bar. Data taken from Yoshikawa & Kato [96].

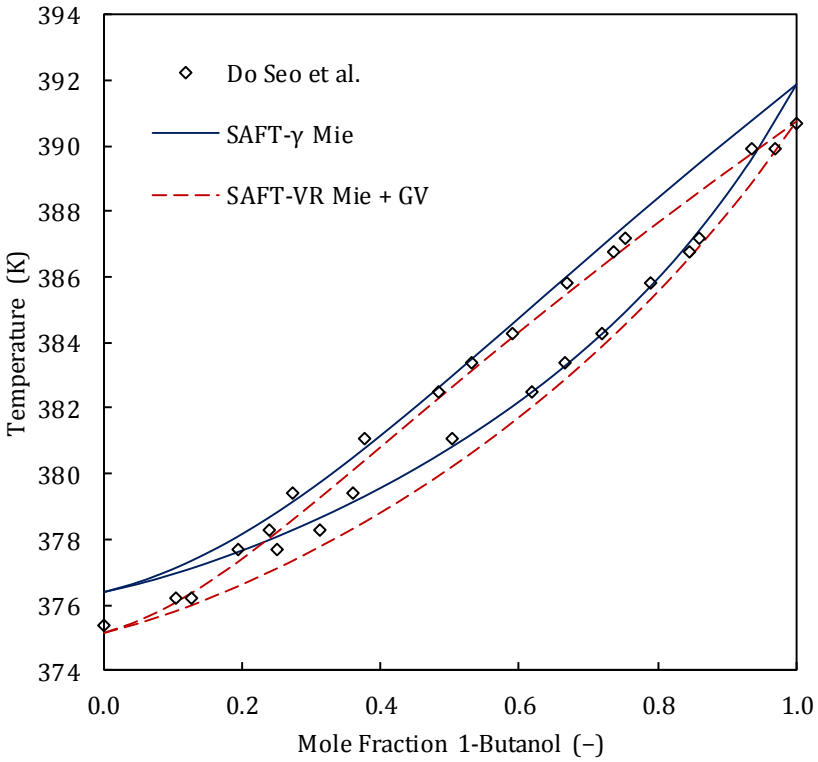

Figure 5.17: Isobaric 1-butanol + 2-pentanone VLE predictions with CO group at 1.013 bar. Data taken from Do Seo et al. [86]. **N.B.**: This set was included in the SAFT-γ Mie CO–CH_2OH group interaction parameter regression.

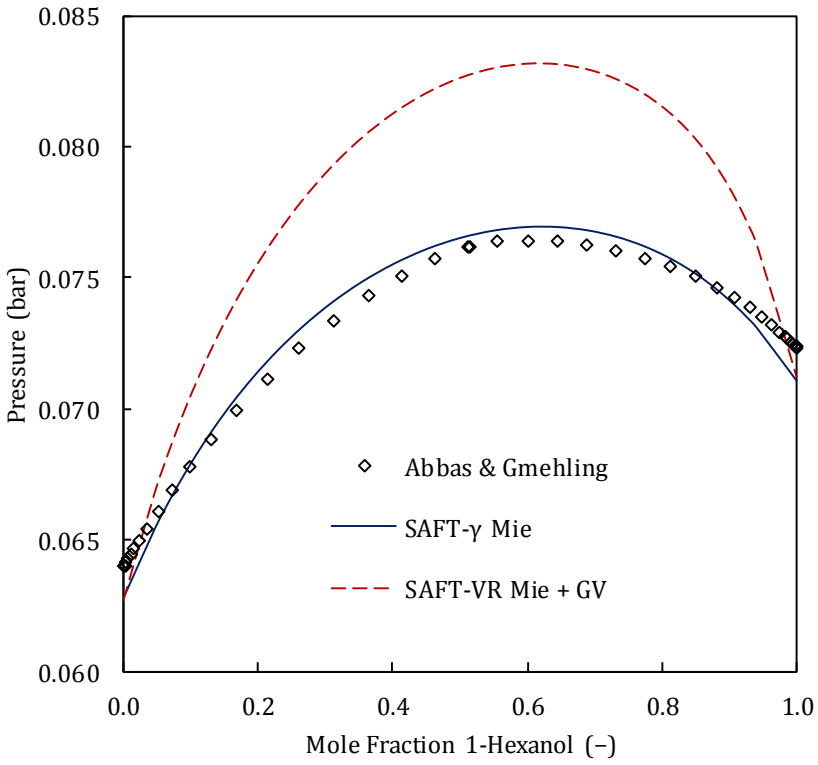

Figure 5.18: Isothermal 1-hexanol + 2-octanone liquid equilibrium pressure predictions with CO group at 363.15 K. Data taken from Abbas & Gmehling [97].

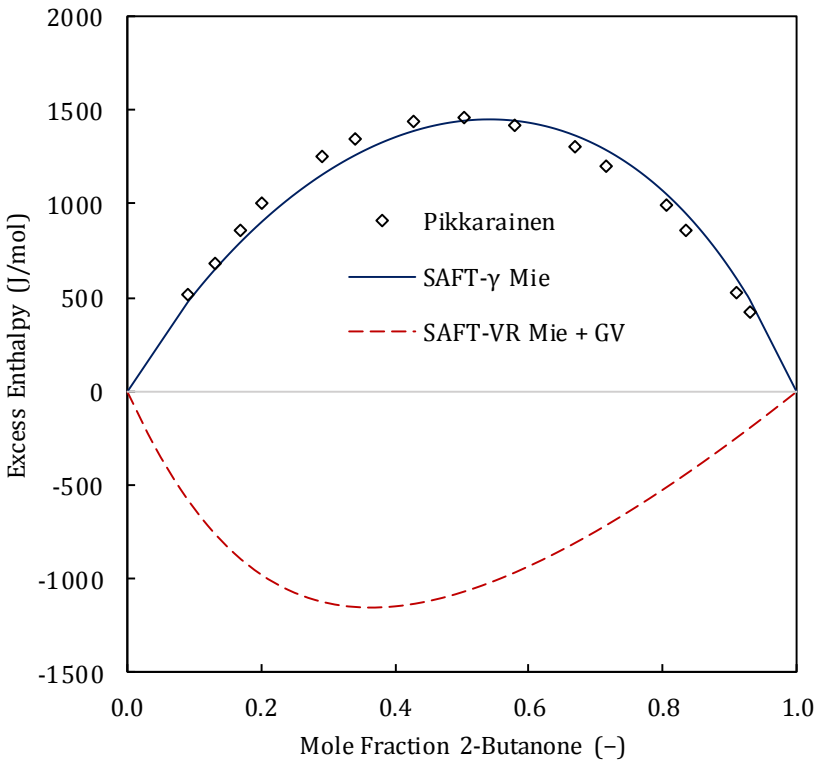

Figure 5.19: 2-Butanone + 1-butanol excess enthalpy predictions with CO group at 313.15 K. Data taken from Pikkarainen [85]. **N.B.**: This set was included in the regression for SAFT-γ Mie CO–CH_2OH group interaction parameters and SAFT-VR Mie + GV 2-butanone association parameters.

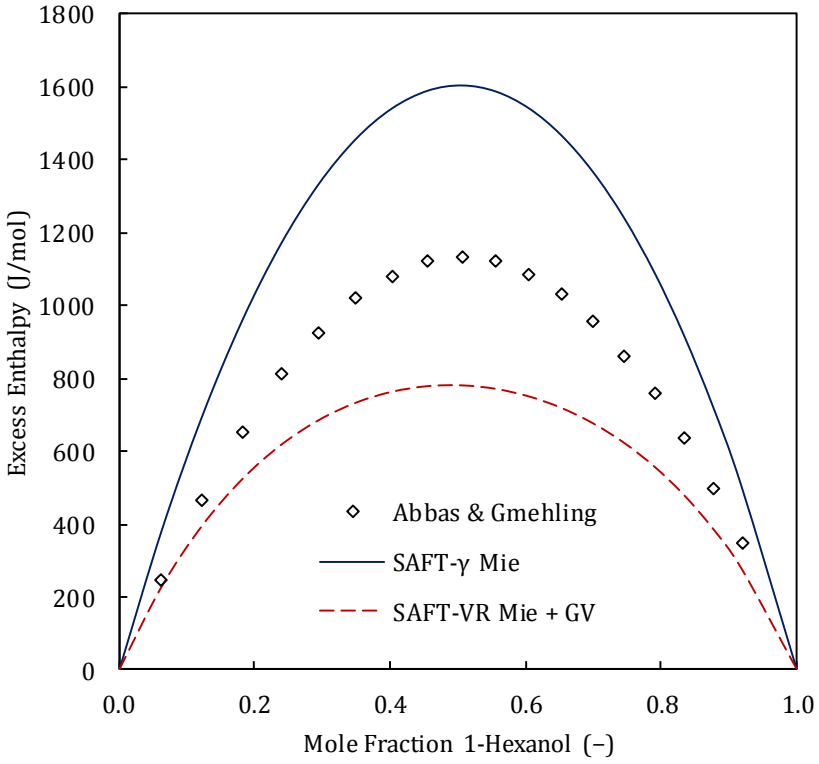

Figure 5.20: 1-Hexanol + 2-octanone excess enthalpy predictions with CO group at 413.15 K. Data taken from Abbas & Gmehling [97]. Note that nonpolar 1-hexanol SAFT-VR Mie parameters were used.

SAFT-VR Mie + GV produced slightly better phase-equilibrium descriptions for the 1-alcohol + 2-ketone systems shown in Figures 5.14 to 5.17 as a result of its accuracy for the pure-component P^{vap}. However, SAFT-γ Mie seems to be able to capture the nature of interactions in the system and produce qualitatively correct phase envelopes.

Although it is valuable to see that SAFT-γ Mie is able to generate consistent VLE results for 2-ketone + 1-alcohol systems with varying alcohol lengths (Figures 5.14 to 5.17), those results are only for 2-butanone and 2-pentanone. Predictions of 1-hexanol + 2-octanone liquid equilibrium pressures were included to confirm whether mixture results for a longer ketone would be similar. New 2-octanone SAFT-VR Mie + GV parameters were determined to facilitate a comparison between the two models because no 2-octanone SAFT-VR Mie + GV parameters had been published as of yet. These new parameters were generated by including P^{vap} [64], ρ^{sat} [64], and u [82] pure-component data in the regression OF, weighed 4:4:1, respectively. The newly regressed 2-octanone SAFT-VR Mie parameters do not produce the correct equilibrium pressure shown in Figure 5.18. This does not necessarily indicate a weakness in the EoS; it is more likely that parameter degeneracy occurred due to the high degrees of freedom caused by SAFT-VR Mie + GV's large parameter space. On the contrary, SAFT-γ Mie results for the 1-hexanol + 2-octanone system are consistent with those of the smaller ketones. The GC approach reduces a model's susceptibility to parameter degeneracy because it is able to draw on data sets of more than one component to produce reliable parameters.

The SAFT-VR Mie + GV excess enthalpy prediction in Figure 5.19 shows incorrect heat of mixing behaviour. The model predicts that the system undergoes exothermic mixing instead of endothermic, indicating that the cross-association between the two species are likely overestimated. The same predicted behaviour is not seen for 1-hexanol + 2-octanone (Figure 5.20), once again suggesting that SAFT-VR Mie + GV is subject to parameter degeneracy. This usually takes place when a broad OF minimum is obtained, as illustrated in Figure 3.4. The parameters that minimise the OF are likely very accurate for the included properties, but significantly less so for properties that were not included, which is excess enthalpy in this case. The OF can be improved by including more or better suited properties, but data scarcity can make this option unavailable. An alternative is to reduce the order of the parameter space by using grounded assumptions or correlations to fix parameters, but doing so may reduce the quality of modelling results. A more detailed breakdown of parameter degeneracy can be found in the 2018 article of Cripwell et al. [55] in which discretised regression was used to prove that an OF minimum does not always correspond to a mixture AAD minimum.

5.3 Discussion: Polar Interactions

Work in the previous Chapter 4 showed that SAFT-γ Mie is able to produce accurate results for acetates, where dipolar interactions are weaker compared to those of ketones. It is also shown that prediction quality decreases for small, highly polar molecules, likely due to limitations of the first-order GC approach. In this chapter SAFT-γ Mie is not able to attain the same level of accuracy for 2-ketone systems as SAFT-VR Mie + GV, despite the extra parameters introduced by the pseudo-association approach. Due to the stronger polarity, proximity effects are likely more prevalent in ketones; therefore, replacing the pseudo-association approach with a more rigorous group-based polar contribution without accounting for structure might not bring about the desired improvement. Nevertheless, the potential benefits of adding a polar term should not be overlooked for two reasons: (i) A polar contribution has a fundamental basis whereas pseudo-association does not; and (ii) adding the GV polar contribution has improved the prediction strength of the cubic-plus-association (CPA) EoS [98], sPC-SAFT [54], [99], and SAFT-VR Mie [19].

5.4 Isomers

SAFT-γ Mie is a first-order GCM where the contribution of one functional group is assumed to be independent of its adjacent groups, thus it cannot distinguish between isomers. Figures 5.21 and 5.22 illustrate the problem by comparing predictions of SAFT-γ Mie and SAFT-VR Mie + GV Polar. The SAFT-γ Mie predictions were generated with the CO group of Section 5.2 and the SAFT-VR Mie + GV predictions were generated with individual parameter sets for each of the isomers.

The SAFT-VR Mie + GV predictions for 3-heptanone and 4-heptanone are relatively inaccurate compared to the 2-heptanone predictions. It is possible that the SAFT-VR Mie parameters for these isomers are of a lower quality because pure-component data are scarce. The perfect GC EoS would allow one to circumvent this problem by using data of different isomers to regress parameters for a mutual functional group. In theory, one should then be able to use this group to predict the properties of different isomers because all of them contain the same group. Unfortunately, this is not possible if the GC EoS does not have an intrinsic way to take structure or group arrangement into account, as in the current SAFT-γ Mie.

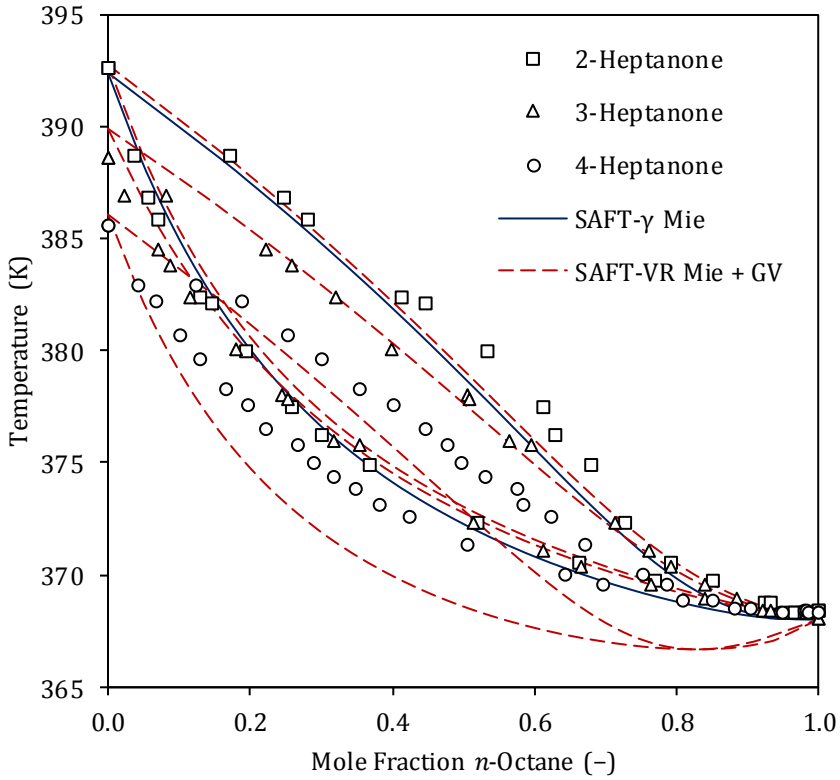

Figure 5.21: Binary VLE predictions of the 2-, 3-, and 4-heptanone isomers with *n*-octane using the CO group of Section 5.2 for SAFT-γ Mie. Data taken from Cripwell et al. [57].

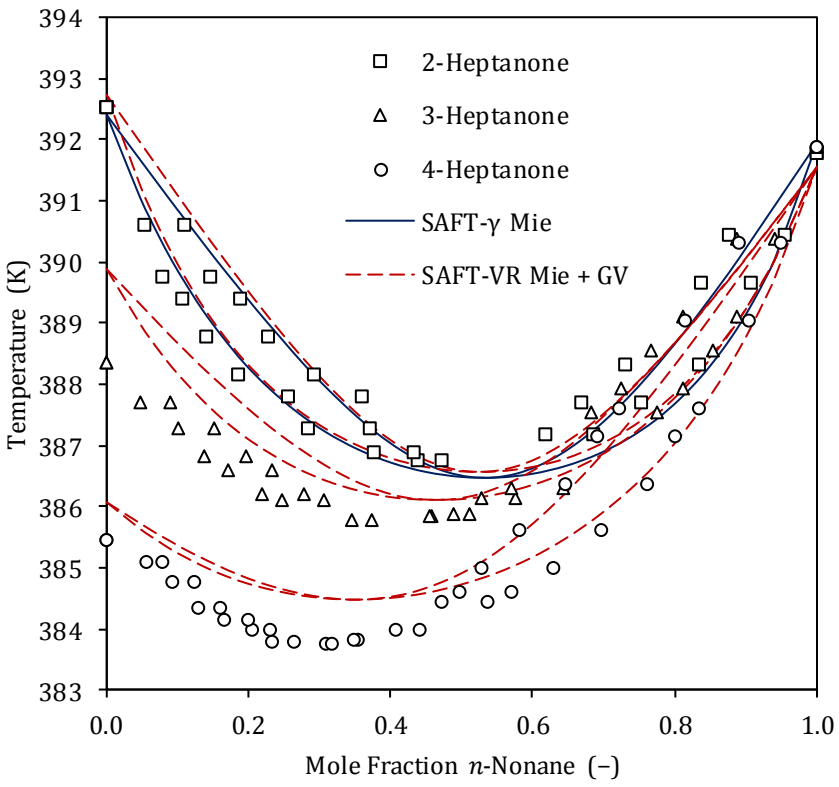

Figure 5.22: Binary VLE predictions of the 2-, 3-, and 4-heptanone isomers with *n*-nonane using the CO group of Section 5.2 for SAFT-γ Mie. Data taken from Cripwell et al. [57].

Three simple ways to improve ketone isomer descriptions with the current SAFT-γ Mie are to:

(i) regress parameters for a CO group using data for all of the different isomers;

(ii) create new functional groups (e.g., CH_3CO and CH_2CO in Figure 5.23) to define different isomers; or

(iii) formulate a way to correlate the predictions (e.g., by adjusting one or more of the FG parameters) based on the position of the functional group in the molecule.

All three proposed methods have flaws. The problem with the first is that, while predictions may improve for the 3-ketone and 4-ketone isomers, 2-ketone predictions will deteriorate. Given that pure-component descriptions for the 2-ketones are already fairly weak, this method is not viable. The second method suffers from the same limitation as a TS EoS because separate 3-ketone and 4-ketone pure-component data would be required for parameter regression. The third method of introducing an empirical correlation would be restricted to linear isomers, it may subtract from the model's credibility as an EoS based on fundamentals, and it is unlikely to outperform the method of introducing new groups, since the addition of more parameters per component provides a mathematical advantage. Two more elaborate methods which account for molecular structure, namely the addition of second-order groups and a heterosegmented chain term, may also improve descriptions. These are discussed in Sections 5.4.4 and 6.4, respectively.

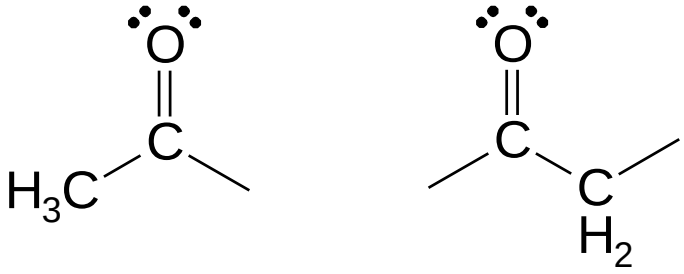

Figure 5.23: Diagrammatic representation of CH_3CO group (left) and CH_2CO group (right).

The widely used original UNIFAC activity coefficient model makes use of larger, separate groups (as in Figure 5.23) to distinguish between isomers. Since UNIFAC's introduction, different methods for dealing with its isomer problem were explored. Marcolli & Peter [100] proposed using different interaction parameters based on the type of molecule in which the groups are located, and these parameters are determined with mixture data. This method still greatly relies on the availability of data and is essentially the same as creating new groups but regressing only interaction parameters while reusing group-specific parameters. Alternatively, Chen et al. [101] introduced a method to adjust the UNIFAC group surface parameter based on molecular conformations and group contact numbers. The original UNIFAC surface parameter already makes use of an average assumed contact number of 10; implementing a similar method in SAFT-γ Mie would pose the challenge of identifying an appropriate parameter to adjust, especially

since its statistical-mechanical formulation does not currently contain any information about overall molecular structure.

For the purpose of this investigation, new functional groups were created to distinguish between ketone and ester isomers. The CH_3CO group is used for 2-ketones and CH_2CO for 3-ketones. A new functional group for propanoate esters, COO (pr.), is introduced in Section 5.4.3. This method of defining new groups is robust and is preferred over the correlation approach mainly because formulating a fundamentally based correlation would require dedication and can be done as a separate study.

5.4.1 2-Ketones with CH_3CO Group

Parameters for the new, larger ketone end-group were regressed using the same data given in Tables 5.1 and 5.2, and the dispersion interaction energies were also generated with a follow-up regression.

Table 5.6: New 2-ketone (CH_3CO) functional-group non-association SAFT-γ Mie parameters.

Parameter	Group k	Group l	Value	Units
ν_k^*	CH_3CO		2.0000[a]	
S_k	CH_3CO		0.76442	
σ_{kl}	CH_3CO	CH_3CO	3.4518	Å
λ_{kl}^{a}	CH_3CO	CH_3CO	6.0000	
λ_{kl}^{r}	CH_3CO	CH_3CO	8.2034	
ϵ_{kl}/k_B	CH_3CO	CH_3CO	209.33	K
ϵ_{kl}/k_B	CH_3CO	CH_3	233.09	K
ϵ_{kl}/k_B	CH_3CO	CH_2	298.36	K
ϵ_{kl}/k_B	CH_3CO	CH_2OH	319.57	K

[a]As with the CO group, the segment number was fixed at $\nu_{CO}^* = 2$.

Table 5.7 New 2-ketone (CH_3CO) functional-group association SAFT-γ Mie parameters.

Parameter	Group k	Site a	Group l	Site b	Value	Units
$\epsilon^{HB}_{kl,ab}/k_B$	CH_3CO	H	CH_3CO	e_1	1083.5	K
$\epsilon^{HB}_{kl,ab}/k_B$	CH_3CO	H	CH_2OH	e_1	876.27	K
$\epsilon^{HB}_{kl,ab}/k_B$	CH_3CO	e_1	CH_2OH	H	784.25	K
$\epsilon^{HB}_{kl,ab}/k_B$	CH_3CO	e_2	CH_2OH	H	1011.5	K
$K_{kl,ab}$	CH_3CO	H	CH_3CO	e_1	546.87	Å^3
$K_{kl,ab}$	CH_3CO	H	CH_2OH	e_1	323.80	Å^3
$K_{kl,ab}$	CH_3CO	e_1	CH_2OH	H	952.81	Å^3
$K_{kl,ab}$	CH_3CO	e_2	CH_2OH	H	585.46	Å^3

The pure-component AADs for the CO and CH_3CO groups are very similar, as shown in Figure 5.24 below. New predictions were expected to be slightly better since the CH_3CO group makes up a larger portion of ketone molecules, giving the regression algorithm more flexibility to match the experimental data.

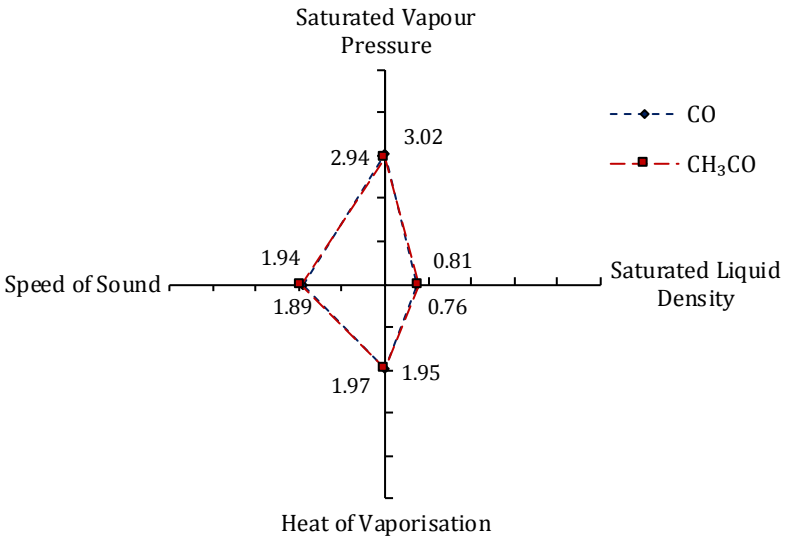

Figure 5.24: 2-Ketone pure-component mean %AADs for SAFT-γ Mie predictions with CO and CH_3CO groups.

Typical binary mixture results with the new group are shown in the next four figures. For 2-ketone + *n*-alkane systems (Figures 5.25 and 5.26), very similar VLE results were obtained, and the excess enthalpy predictions improved slightly. The 2-ketone + 1-alcohol results (Figures 5.27 and 5.28) are nearly identical for the two groups.

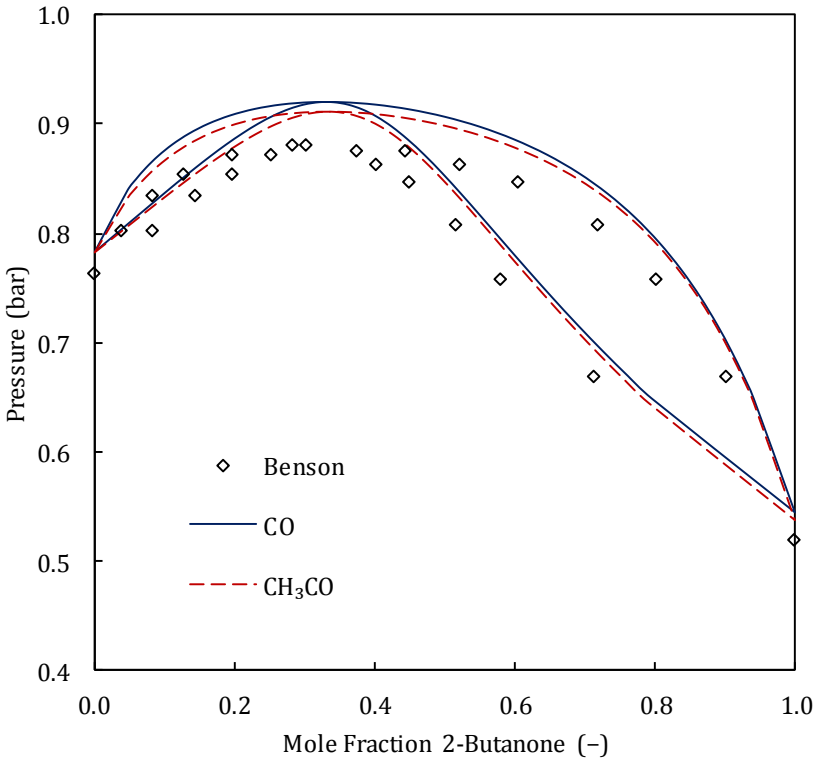

Figure 5.25: Isothermal 2-butanone + *n*-hexane VLE predictions with SAFT-γ Mie CO and CH_3CO groups at 333.15 K. Data taken from Benson [89]. **N.B.**: This set was included in the parameter regression of both groups.

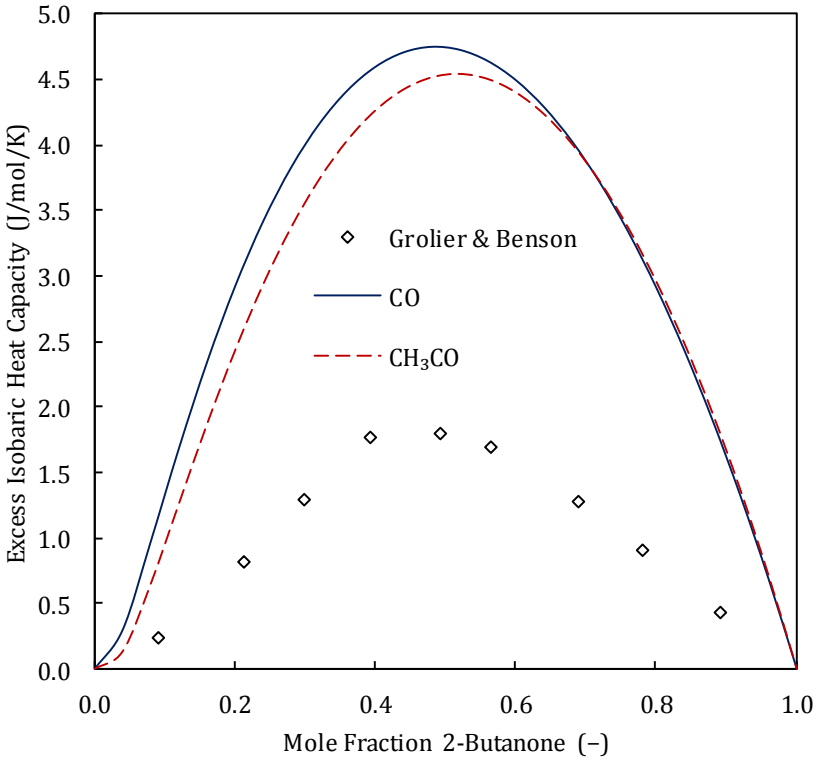

Figure 5.26: 2-Butanone + *n*-heptane excess isobaric heat capacity predictions with SAFT-γ Mie CO and CH_3CO groups at 298.15 K & 1.013 bar. Data taken from Grolier & Benson [91].

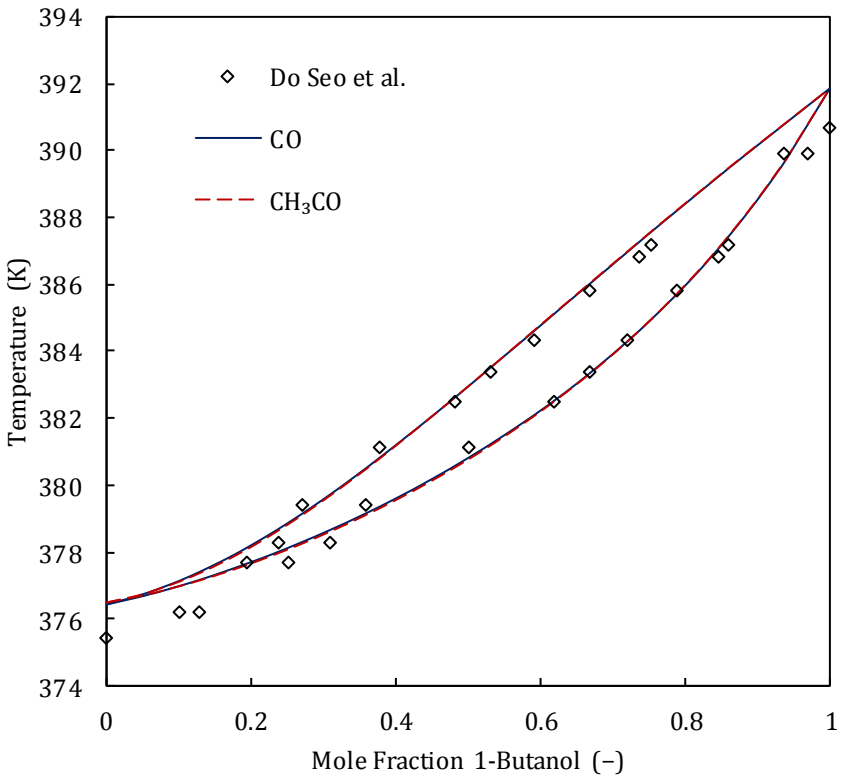

Figure 5.27: Isobaric 1-butanol + 2-pentanone VLE predictions with SAFT-γ Mie CO and CH_3CO groups at 1.013 bar. Data taken from Do Seo et al. [86].

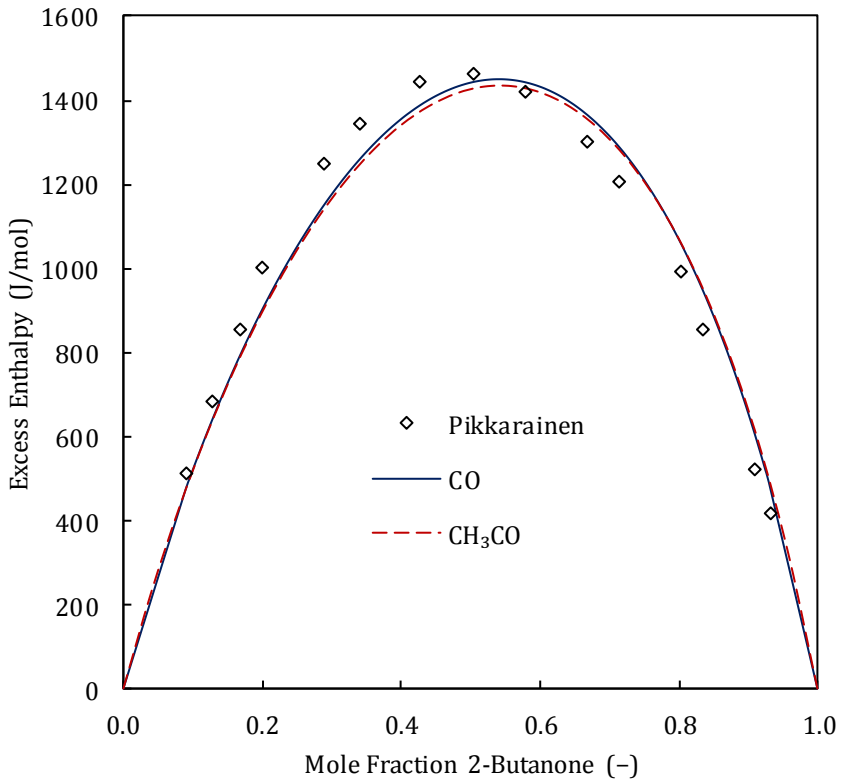

Figure 5.28: 2-Butanone + 1-butanol excess enthalpy predictions with SAFT-γ Mie CO and CH_3CO groups at 313.15 K. Data taken from Pikkarainen [85].

5.4.2 3-Ketones with CH_2CO Group

Table 5.8: Data included in the new 3-ketone (CH_2CO) regression.

Type	Components	Temperature	Pressure	N_P	Weight	Reference
P^{vap}	3-pentanone → 3-nonanone	$0.5T_C$ – $0.9T_C$	Equilibrium	150	6	[64]
ρ^{sat}	3-pentanone → 3-nonanone	$0.5T_C$ – $0.9T_C$	Equilibrium	150	8	[64]
H^E	*n*-hexane + 3-pentanone	298.15 K	1.013 bar	20	0.5	[92]
VLE	*n*-nonane + 3-heptanone	Equilibrium	0.400 bar	34	5	[57]

Two different sets of SAFT-γ Mie parameters were regressed for 3-ketones. The first (Set A) was generated by doing a follow-up regression to determine the CH_2CO–CH_3 and CH_2CO–CH_2 interaction energy values with results close to the combining rule values. After observing poor VLE prediction results with Set A, a second (Set B) was generated with the interaction energies included in the initial regression along with the other FG-specific parameters.

Table 5.9: New 3-ketone (CH_2CO) functional-group non-association SAFT-γ Mie parameters.

Parameter	Group *k*	Group *l*	Set A Value	Set B Value	Units
v_k^*	CH_2CO		2.0000	2.0000	
S_k	CH_2CO		0.60764	0.64470	
σ_{kl}	CH_2CO	CH_2CO	3.3536	3.2832	Å
λ_{kl}^a	CH_2CO	CH_2CO	6.0000	6.0000	
λ_{kl}^r	CH_2CO	CH_2CO	7.5335	7.5162	
ϵ_{kl}/k_B	CH_2CO	CH_2CO	212.33	182.19	K
ϵ_{kl}/k_B	CH_2CO	CH_3	234.11	279.88	K
ϵ_{kl}/k_B	CH_2CO	CH_2	295.76	295.92	K

Table 5.10 New 3-ketone (CH_2CO) functional-group association SAFT-γ Mie parameters.

Parameter	Group *k*	Site *a*	Group *l*	Site *b*	Set A Value	Set B Value	Units
$\epsilon_{kl,ab}^{HB}/k_B$	CH_2CO	H	CH_2CO	e_1	1098.3	921.10	K
$K_{kl,ab}$	CH_2CO	H	CH_2CO	e_1	870.98	413.49	Å^3

Note that the pseudo-association parameters for Set B are smaller, which could indicate that circumventing the combining rule and using regressed dispersion interaction energies

causes a portion of the polar interactions to be lumped with dispersion (as for the acetates in Chapter 4). In this case, the combination of both pseudo-association and regressed dispersion energies account for the polar interactions.

5.4.2.1 Pure-Component Properties

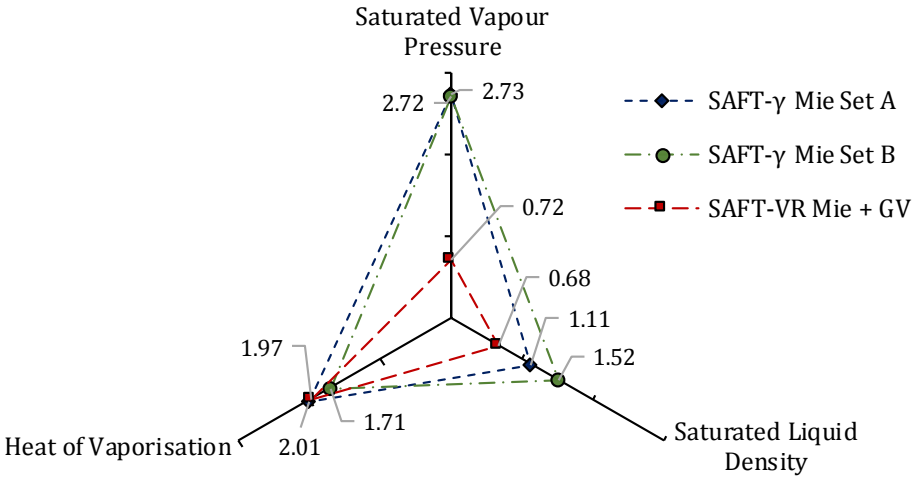

Figure 5.29: 3-Ketone pure-component mean %AADs with CH_2CO group. %AADs are an average of 3-pentanone → 3-nonanone absolute deviations. The average deviations were calculated using model predictions and DIPPR correlations [60].

5.4.2.2 3-Ketone + *n*-Alkane Mixture Properties

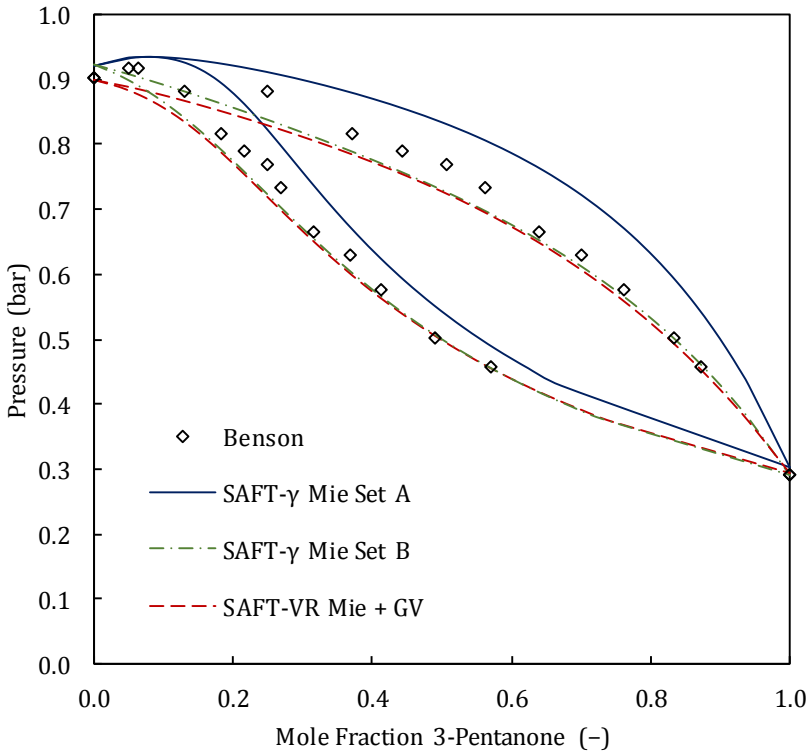

Figure 5.30: Isothermal 3-pentanone + *n*-hexane VLE predictions with CH_2CO group at 338.15 K. Data taken from Benson [89].

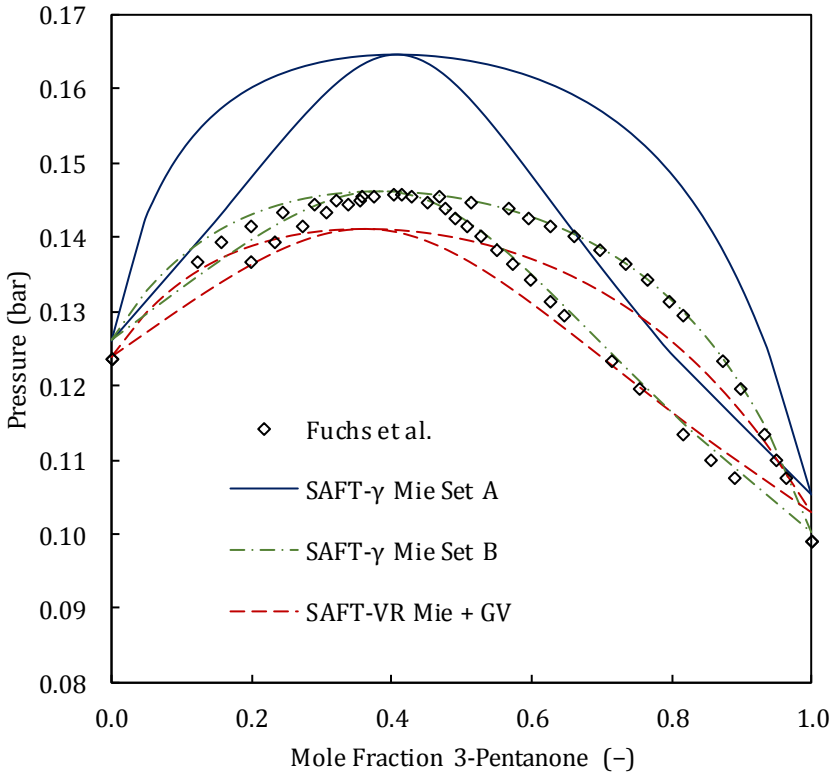

Figure 5.31: Isothermal 3-pentanone + *n*-heptane VLE predictions with CH_2CO group at 313.2 K. Data taken from Fuchs et al. [102].

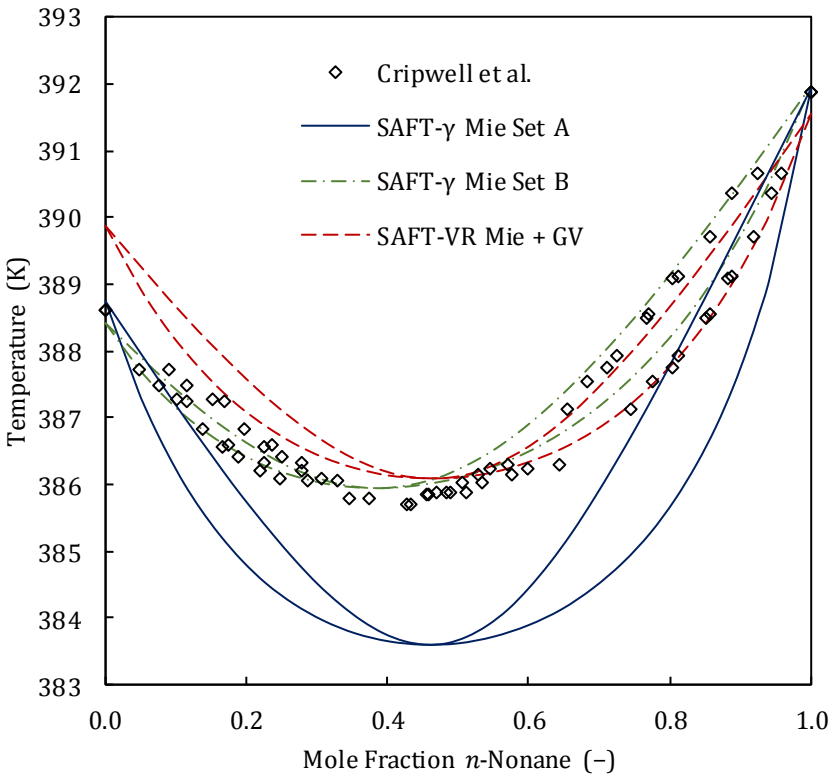

Figure 5.32: Isobaric *n*-nonane + 3-heptanone VLE predictions with CH_2CO group at 0.400 bar. Data taken from Cripwell et al. [57]. **N.B.**: This set was included in the SAFT-γ Mie CH_2CO group regression.

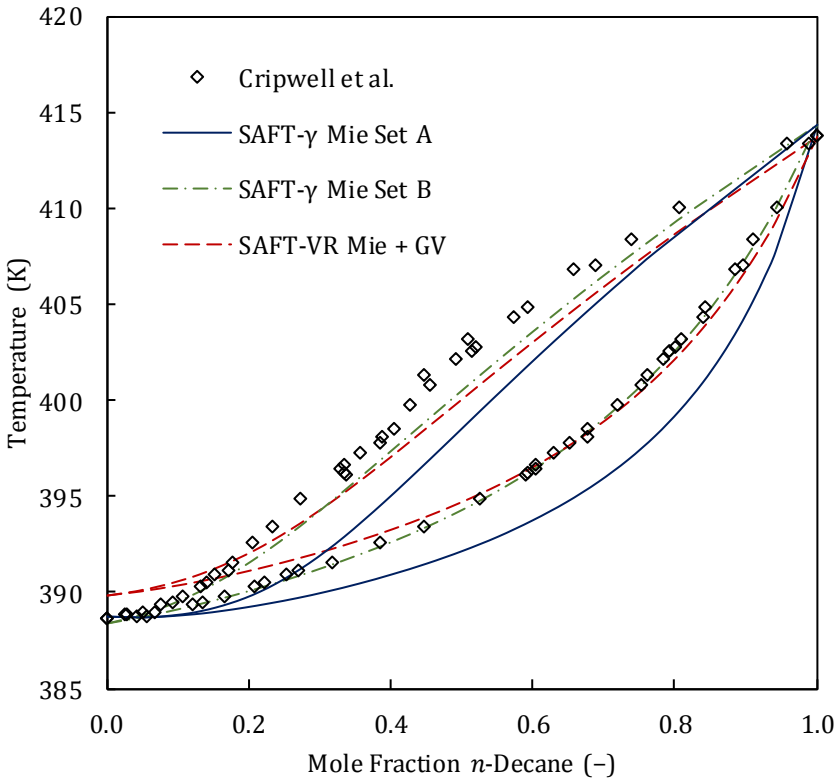

Figure 5.33: Isobaric *n*-decane + 3-heptanone VLE predictions with CH_2CO group at 0.400 bar. Data taken from Cripwell et al. [57].

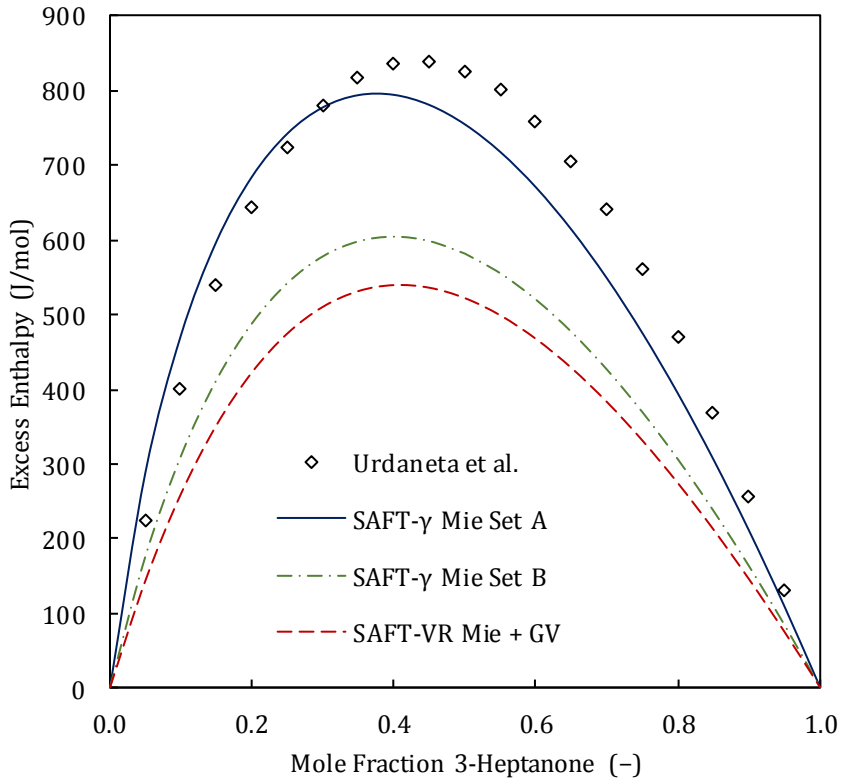

Figure 5.34: 3-Heptanone + *n*-heptane excess enthalpy predictions with CH_2CO group at 298.15 K. Data taken from Urdaneta et al. [83].

5.4.2.3 Discussion

SAFT-γ Mie with Set A is mainly unable to predict mixture VLE behaviour of systems containing 3-ketones, but after including the dispersion interaction energies as part of the initial CH_2CO group regression and circumventing the combining rule, Eq. (2.14), Set B produced substantially improved VLE descriptions while only pure-component ρ^{sat} and mixture H^E predictions slightly worsened. Another parameter set was also produced for 2-ketones (a "Set B" for the CH_3CO group) in order to see whether more balanced predictions could be obtained. The previously encountered regression difficulties were avoided by choosing more appropriate starting parameters. The results in Appendix D do not show the same level of improvement; therefore, it appears that using the dispersion energy combining rule is especially not appropriate for non-methyl ketones.

The traditionally structured SAFT-VR Mie + GV also does not replicate the accuracy it achieves for 2-ketones, possibly because data scarcity resulted in weaker parameters, or the reduced linearity of the position three isomer poses an obstacle for the EoS, which models all components as linear chains. If the problem was purely data related, one would expect the GC EoS, which is less dependent on component-specific datasets, to outperform SAFT-VR Mie. However, no concrete deductions can be made since both models failed to produce well-balanced pure-component and mixture results.

In the SAFT-γ Mie hard-sphere and dispersion contributions, it is assumed that the probability of different groups interacting with one another is only governed by the size and fraction of the groups in the system, and that it is not influenced by molecular structure. In the solution-of-groups approach, the groups are essentially free-floating spheres as shown in diagrams (a) and (b) in Figure 2.4. In the case of 2-ketones, where CH_3CO is a terminal group, this is a fair assumption; however, the CH_2CO functional group in 3-ketones is located between CH_3 and CH_2 groups. A group that is sandwiched between two other groups cannot interact equally with other molecules from all directions (see Figure 5.35 for a conceptual explanation). The only way that SAFT-γ Mie can account for the lower probability of intermolecular CH_2CO interactions is by adjusting model parameters. This phenomenon may also explain why it is necessary to regress the dispersion energies for CH_2CO–CH_3 and CH_2CO–CH_2 to obtain adequate results. Further investigation is done with *n*-alkyl propanoates to see whether the same observations can be made for a shifting ester group.

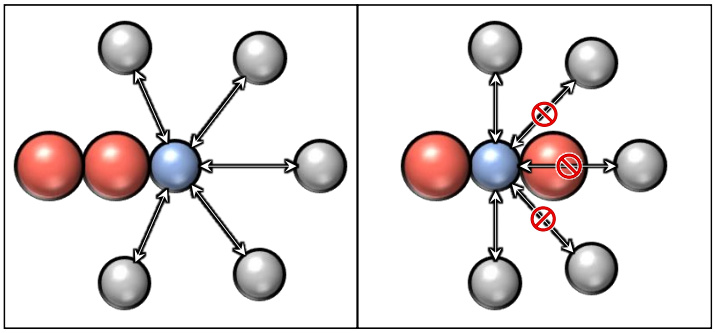

Figure 5.35: Illustrations of a defining functional group (blue) undergoing intermolecular interactions (arrows) with groups that are not part of the same molecule (grey). The left-side image shows the defining group in a terminal position, and the right-side image shows it in a nonterminal position.

5.4.3 *n*-Alkyl Propanoates

In this subsection, a new functional group is introduced for propanoate esters: COO (pr.). This new group contains the exact same atomic constituents as the COO group of Papaioannou et al. [30]. The goal is to see how the modelling results for these esters compare to the *n*-alkyl acetate results; therefore, the COO (pr.) group was parameterised without using pseudo-association in keeping with the COO group. Table 5.11 presents the data included in the COO (pr.) parameter regression, and the resultant parameters are given in Table 5.12. The COO (pr.) group segment number was fixed to one in keeping with the COO group parameters and the physical shape of the group.

Table 5.11: Data included in the new *n*-alkyl propanoate group regression.

Type	Components	Temperature	Pressure	N_P	Weight	Reference
P^{vap}	ethyl → *n*-butyl propanoate	$0.5T_C$ – $0.9T_C$	Equilibrium	90	5	[64]
ρ^{sat}	ethyl → *n*-butyl propanoate	$0.5T_C$ – $0.9T_C$	Equilibrium	90	7	[64]
H^E	ethyl propanoate + *n*-heptane	298.15 K	1.013 bar	16	0.5	[103]
VLE	propyl propanoate + *n*-octane	Equilibrium	0.600 bar	26	5	[74]

Table 5.12: New *n*-alkyl propanoate group SAFT-γ Mie parameters.

Parameter	Group k	Group l	Set A Value	Set B Value	Units
ν_k^*	COO (pr.)		1.0000	1.0000	
S_k	COO (pr.)		0.69109	0.74807	
σ_{kl}	COO (pr.)	COO (pr.)	3.9343	3.7187	Å
$\lambda_{kl}^{\mathrm{a}}$	COO (pr.)	COO (pr.)	6.0000	6.0000	
$\lambda_{kl}^{\mathrm{r}}$	COO (pr.)	COO (pr.)	100.00	28.676	
$\epsilon_{kl}/k_{\mathrm{B}}$	COO (pr.)	COO (pr.)	820.12	669.77	K
$\epsilon_{kl}/k_{\mathrm{B}}$	COO (pr.)	CH_3	510.64	428.30	K
$\epsilon_{kl}/k_{\mathrm{B}}$	COO (pr.)	CH_2	548.62	451.23	K

As with the ketone parameters, two parameter sets were regressed. The dispersion interaction energies of Set A were regressed by a follow-up regression while all of the parameters of Set B were regressed at the same time. It can be noted that during the regression procedure, the repulsive exponent of Set A reached the upper boundary of 100.

5.4.3.1 Pure-Component Properties

Pure-component results generated with the two SAFT-γ Mie COO (pr.) parameter sets are given in Table 5.13, and a visual comparison is given in Figure 5.36.

Table 5.13: Pure-component %AAD for *n*-alkyl propanoate esters with new COO (pr.) group. P^{vap}, ρ^{sat}, and H^{vap} predictions are measured against DIPPR correlations [64].

	P^{vap}		ρ^{sat}		H^{vap}		u		
Component	Set A	Set B	Set A	Set B	Set A	Set B	Set A	Set B	u Ref.
ethyl propanoate	6.39	0.59	1.37	0.61	5.55	3.03	13.65	5.12	[65]
propyl propanoate	5.37	2.48	1.18	0.32	3.28	1.30			
n-butyl propanoate	3.62	1.88	1.65	1.00	1.82	0.90			

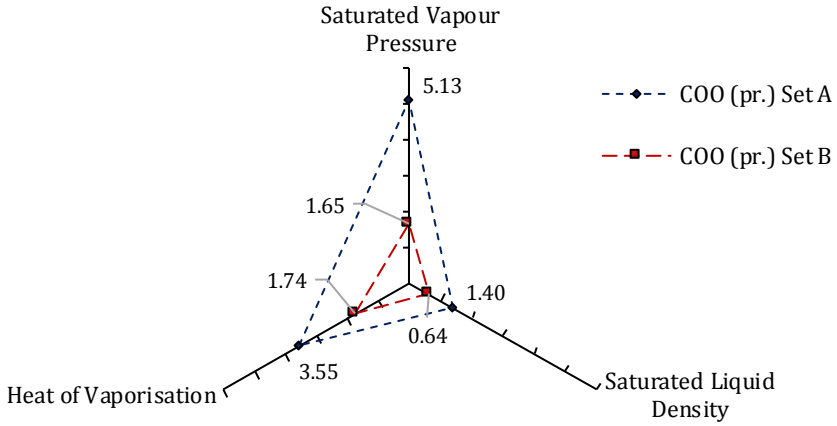

Figure 5.36: *n*-Alkyl propanoate pure-component mean %AADs with SAFT-γ Mie COO (pr.) group. %AADs are an average of ethyl → *n*-butyl propanoate absolute deviations.

The sequential regression parameters (Set A) produced proportionally worse pure-component predictions, except for the P^{vap} of ethyl propanoate, which is far worse compared to Set B. Regressing dispersion interaction energies allows the model to partially account for proximity effects. Furthermore, the same argument about why it is necessary to regress group interaction energies in acetates (as in the end of Section 4.2.1) can be applied: Using the combining rule when the polar group's polarity is lumped in with dispersion will result in inflated *unlike* dispersion energies; therefore, the regression of dispersion interaction energies is necessary to prevent interactions between polar and nonpolar groups from being too strong. This could also explain why the model struggled to reach an optimal parameter set within the given bounds during the regression of COO (pr.) Set A where the repulsive exponent reached the upper bound of 100.00.

5.4.3.2 *n*-Alkyl Propanoate + *n*-Alkane Mixture Properties

Predictions with SAFT-γ Mie using the new COO (pr.) group parameter sets are given for VLE in Figures 5.37 and 5.38, excess properties in Figures 5.39 and 5.40, and speed of sound in Figure 5.41.

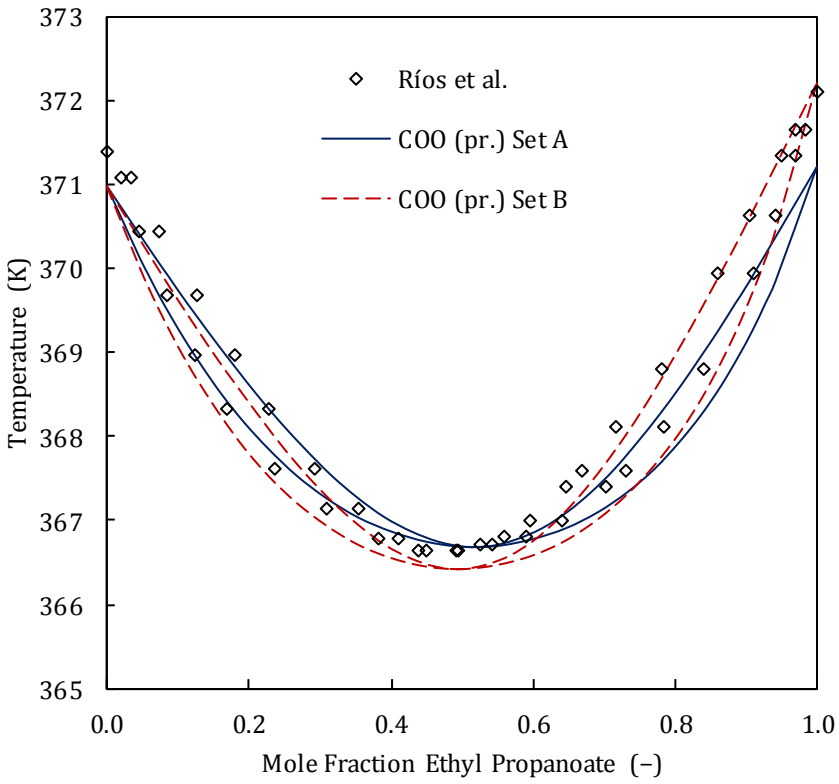

Figure 5.37: Isobaric ethyl propanoate + *n*-heptane VLE predictions with SAFT-γ Mie COO (pr.) group at 1.013 bar. Data taken from Ríos et al. [104].

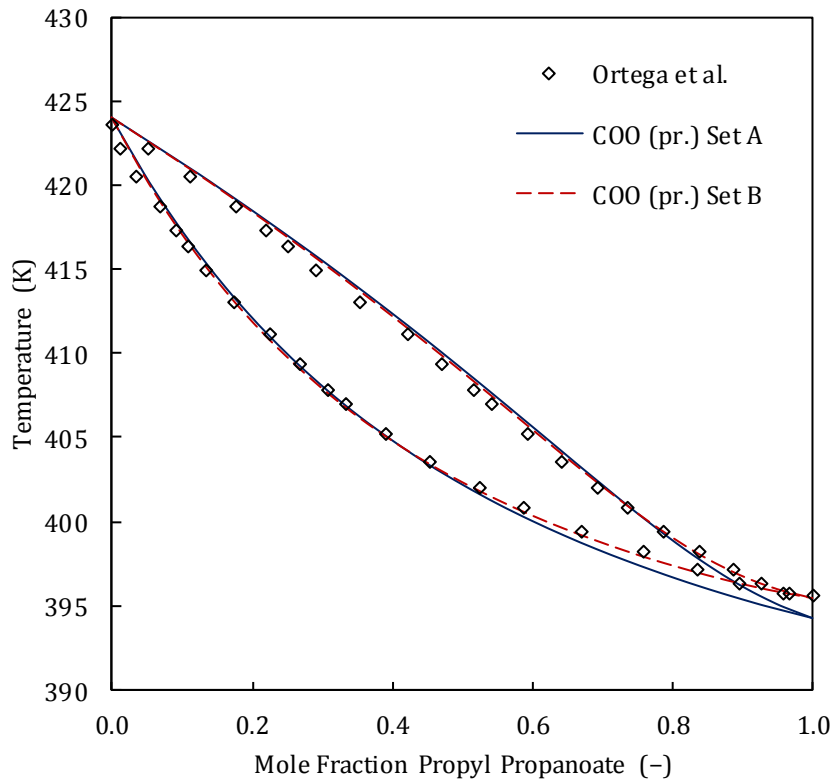

Figure 5.38: Isobaric propyl propanoate + *n*-nonane VLE predictions with SAFT-γ Mie COO (pr.) group at 1.013 bar. Data taken from Ortega et al. [105].

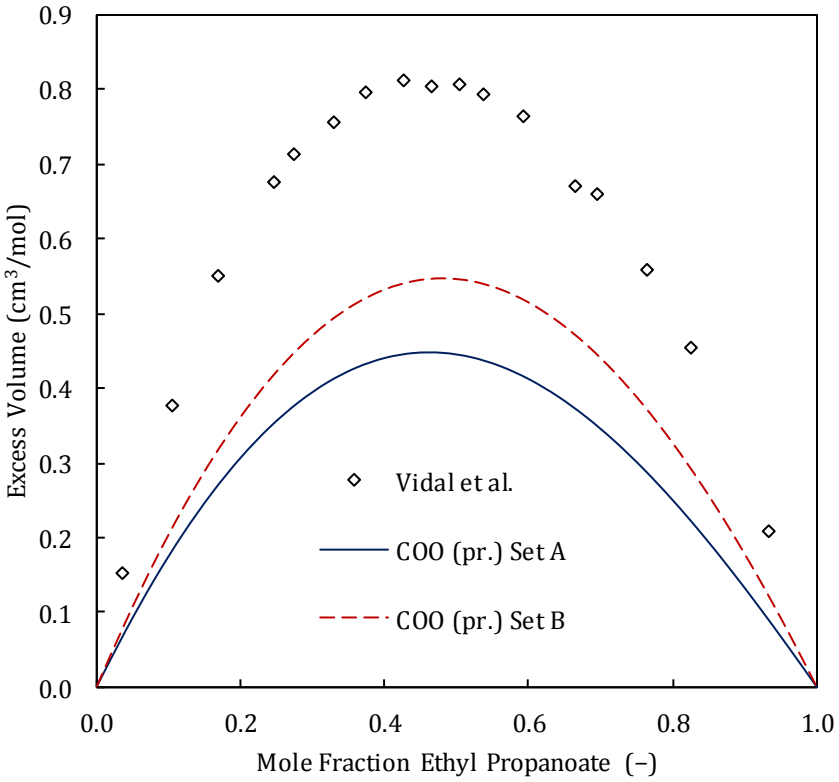

Figure 5.39: Ethyl propanoate + *n*-heptane excess volume predictions with SAFT-γ Mie COO (pr.) group at 298.15 K & 1.013 bar. Data taken from Vidal et al. [103].

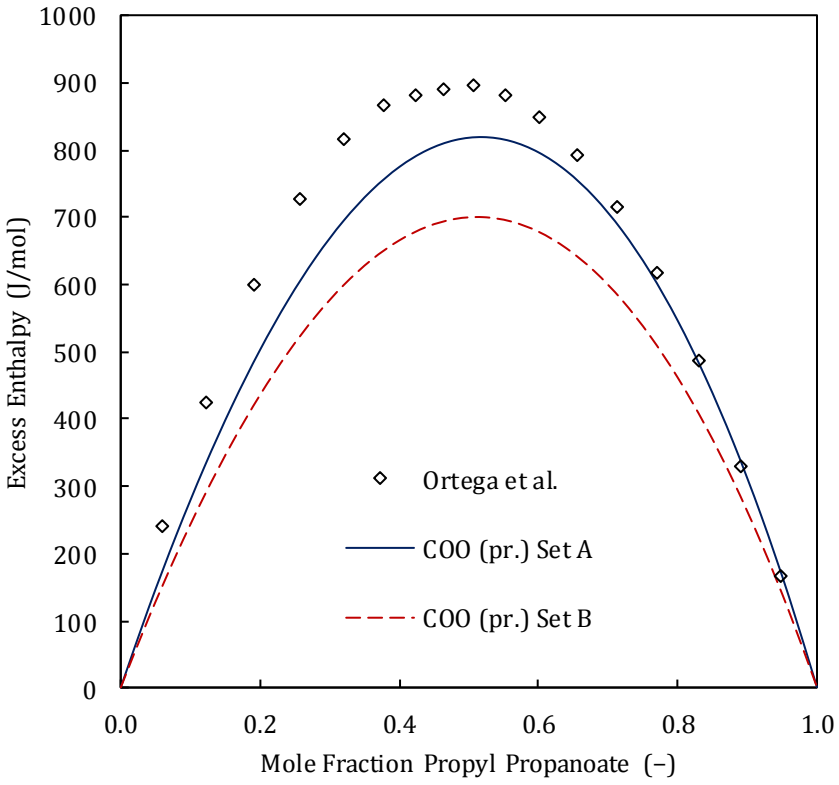

Figure 5.40: Propyl propanoate + *n*-heptane excess enthalpy predictions with SAFT-γ Mie COO (pr.) group at 298.15 K. Data taken from Ortega et al. [106].

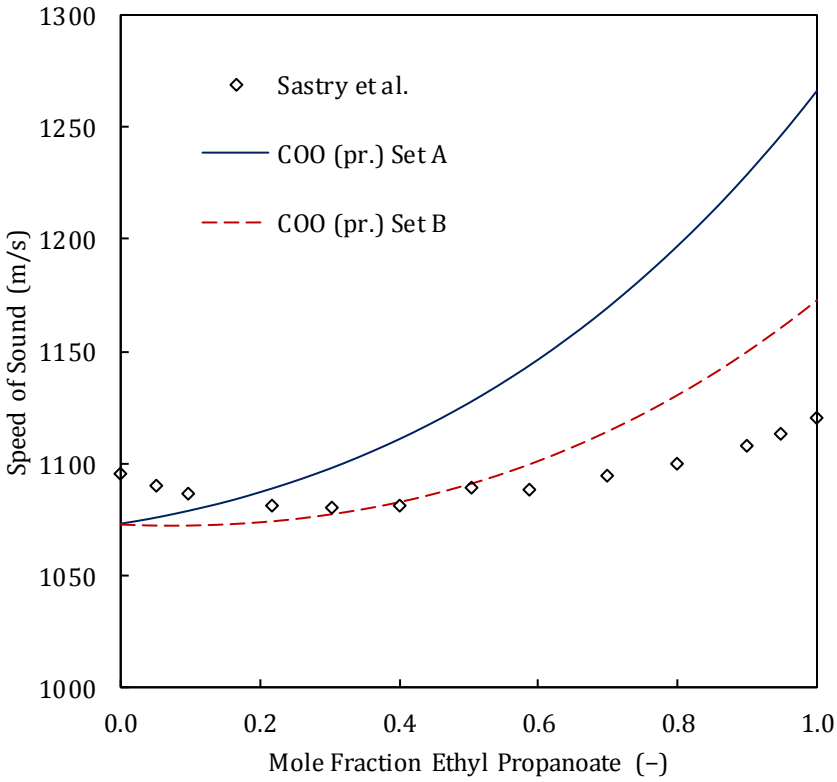

Figure 5.41: Ethyl propanoate + *n*-heptane speed of sound predictions with SAFT-γ Mie COO (pr.) group at 308.15 K & 1.013 bar. Data taken from Sastry et al. [107].

5.4.3.3 Discussion

As with the 3-ketones, parameter Set B produced significantly improved results. However, the improvements were observed for pure-component properties instead of VLE. SAFT-γ Mie behaves similarly to nonpolar SAFT-VR Mie when interaction energies are not included in the first regression; recall that the *n*-butyl acetate SAFT-VR Mie parameters (Set B in Table 4.1), which were generated with VLE data, also produced weaker pure-component predictions. This once again reaffirms that interaction energies must be regressed when polar interactions are lumped with dispersion, specifically in the absence of pseudo-association.

Although the SAFT-γ Mie propanoate results are more accurate compared to the ketone results, pure-component and excess-property predictions are not on par with the acetate results of Chapter 4, suggesting that modelling polar components becomes more difficult for SAFT-γ Mie as the defining functional group moves away from the terminal position.

5.4.4 Second-Order Groups

A potential limitation of SAFT-γ Mie was noted in Hutacharoen et al. [34]: For a small polar molecule, the assumption that group contributions are independent of the molecule in which the groups reside is inadequate because proximity effects are more pronounced. If that is the case,

accounting for polarity within groups alone (either by pseudo-association or a group-based polar contribution) would not suffice. Including smaller polar molecules in the regression of group parameters would likely degrade the quality of predictions for larger polar molecules made with these parameters. The introduction of second-order groups may improve predictions for these components while at the same time allowing the model to distinguish between isomers. Unlike first-order groups, second-order groups may have mutual atomic descriptors within a component. The mutual descriptors can be shared between it and either other second-order groups or first-order groups. It is also possible to build a polar contribution upon second-order groups. First-order GCMs, such as SAFT-γ Mie, add the contributions of a single set of groups which makes up the exact sum of the molecule's atoms, whereas second-order GCMs add the contributions of either second-order groups or both first- and second-order groups.

Benson's second-order GC method [108] details a large collection of groups of which the contributions are added in a similar manner as in first-order GCMs. Groups are segmented in single- or double-atomic parts where some members are shared between neighbouring groups. The following example illustrates the compositions of 2-pentanone and 3-pentanone.

2-pentanone:

$$\begin{aligned} CH_3COCH_2CH_2CH_3 \rightarrow\ & [C\text{–}(CO)(H)_3] + [CO\text{–}(C)_2] + [C\text{–}(C)(CO)(H)_2] \\ & + [C\text{–}(C)_2(H)_2] \ + [C\text{–}(C)(H)_3] \end{aligned} \tag{5.1}$$

3-pentanone:

$$CH_3CH_2COCH_2CH_3 \rightarrow 2[C\text{–}(C)(H)_3] + 2[C\text{–}(C)(CO)(H)_2] + [CO\text{–}(C)_2] \tag{5.2}$$

The groups, given in square brackets, consist of a polyvalent centre and its ligands, which are given in parentheses. It is clear that this method, which allows for shared atomic descriptors, is able to distinguish between isomers. An example of where this method was used to improve upon the modelling of critical temperatures and heats of vaporisation can be found in a 2006 article by Dalmazzone et al. [109]. However, the problem with this method in the context of SAFT-γ Mie is that it is not compatible with the existing first-order groups. It cannot be added as an extension to SAFT-γ Mie, and implementing it in the VR Mie framework would involve creating a completely new EoS.

Another more popular method is the one proposed by Constantinou & Gani [110] in which the contributions of first-order groups (similar to the SAFT-γ Mie groups) are summed, followed by the summation of second-order group contributions. This is also the method referenced by Papaioannou et al. [30] as an example of a second-order GCM. Here, the selection of second-order groups is based on conjugation and the *ABC method* proposed by Mavrovouniotis [111]. 2-Hexene

and 3-hexene group contributions are given below. The structural equations are followed by diagrammatic representations.

2-hexene:

$$\begin{aligned} &CH_3CH{=}CHCH_2CH_2CH_3 \\ &\rightarrow [2 \times CH_3 + CH{=}CH + 2 \times CH_2]_{\text{first-order}} \\ &+ [CH_3{-}CH{=}CH + CH_2{-}CH{=}CH]_{\text{second-order}} \end{aligned} \tag{5.3}$$

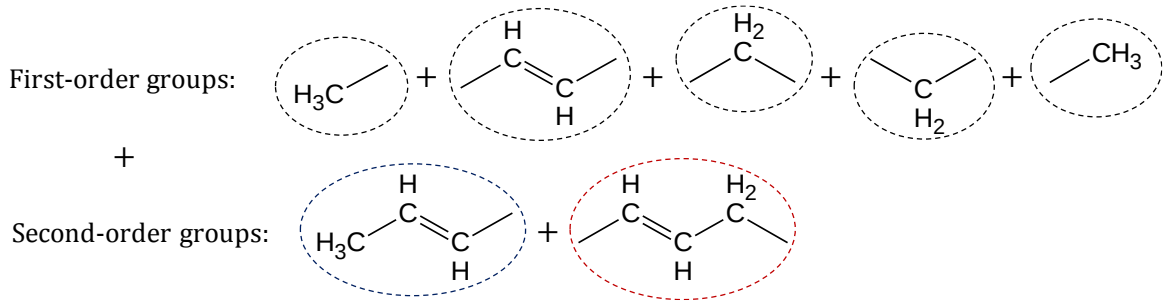

Figure 5.42: Diagrammatic breakdown of 2-hexene first- and second-order groups.

3-hexene:

$$\begin{aligned} &CH_3CH_2CH{=}CHCH_2CH_3 \\ &\rightarrow [2 \times CH_3 + CH{=}CH + 2 \times CH_2]_{\text{first-order}} \\ &+ [2 \times CH_2{-}CH{=}CH]_{\text{second-order}} \end{aligned} \tag{5.4}$$

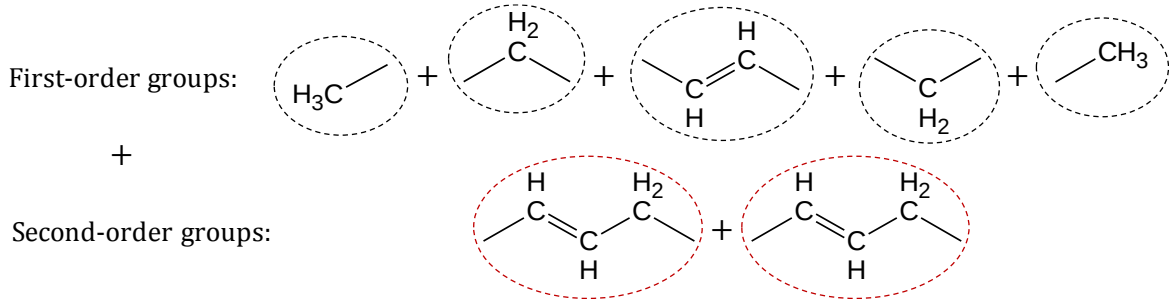

Figure 5.43: Diagrammatic breakdown of 3-hexene first- and second-order groups.

The hexene isomers in Figures 5.42 and 5.43 comprise of the same first-order groups, but the second-order group contributions differ. Note that the sum of the second-order groups does not have to make up the entire molecule; contributions of the second-order groups are only added as an adjustment to the first-order summation. Most second-order GCMs have been developed for pure-component property estimation, and the most convenient way to analyse different second-order methods is to apply them to relatively simple thermodynamic correlations that can only be used to predict one property. However, the method of Constantinou & Gani has been used by Tihic et al. [112] to generate sPC-SAFT parameters for the modelling of polymers.

Implementing a second-order group extension into SAFT-γ Mie falls beyond the scope of this work. The Sadeqzadeh et al. article of 2016 [39] states that the authors' future work will include the introduction of a second-order GCM to improve the quality of SAFT-γ Mie modelling and to add the ability to distinguish between isomers.

5.5 Chapter Summary

The ketone pure-component modelling results in this chapter are not as accurate as the acetate results in Chapter 4, even with pseudo-association. The P^{vap} %AADs more closely resemble those for 1-alcohols, suggesting that modelling smaller, highly polar molecules is a challenge for SAFT-γ Mie. Pseudo-association produced qualitatively accurate results for all of the binary VLE predictions with 2-ketones; the less accurate pure-component predictions are likely a result of the structural-independence assumption made in SAFT-γ Mie, and not due to the lack of a polar term.

New functional groups were defined to model 3-ketones and propanoates because SAFT-γ Mie cannot distinguish between isomers using the same groups. It was found that the position of the functional group has an effect on modelling results. Higher ρ^{sat} %AADs were obtained for 3-ketones compared to 2-ketones, and the propanoate pure-component predictions are less accurate than those for the acetates. It is speculated that the solution-of-groups formulation is less accurate for real molecules where the functional group is sandwiched between two other groups. Nevertheless, the GC approach provides a more convenient method for the parameterisation of polar isomers compared to the traditionally structured EoS. The group parameters produced mostly the same degree of accuracy between the different components for phase-equilibrium and second-derivative dependant property predictions.

Although it is likely that the reduction in pure-component prediction accuracy observed in this chapter is because of the model not considering proximity effects, the disregarding of physical structure may also have an adverse effect. Both of these factors can partially be corrected for by the addition of a second-order group extension. Additionally, a second-order group extension would allow SAFT-γ Mie to distinguish between isomers while using the same first-order groups.

The next chapter will focus on branched alkanes. In the absence of polar interactions that may cause proximity effects, the importance of physical structure and the arrangement of chemical bonds are emphasised.

Chapter 6: Branched Species

The model fluids in this chapter, branched alkanes, provide a strenuous test for the predictive capabilities of SAFT-γ Mie because the group-contribution method adds groups in a linear manner, whereas in reality the addition of branches influences the shape and volume of a species nonlinearly. The only groups specific to branched alkanes are CH and C shown in Figure 6.1, both of which include the carbon where branches are connected to the alkane backbone. The SAFT-γ Mie CH and C group parameters used in this chapter are those determined by Dufal et al. [33]. These groups usually make up a small part of the molecules, therefore the CH and C groups that were generated specifically for branched alkanes have a smaller contribution to predictions compared to the CH_3 group. Consequently, it is important that the GC assumption holds true in order to obtain accurate results, because the parameters for the CH_3 group that are used for the methyl branches were determined using only *n*-alkane data where the CH_3 group only occurs at the end of linear chains.

Figure 6.1: Diagrammatic representation of CH group (left) and C group (right).

6.1 Pure-Component Properties

Pure-component properties are primarily considered in this chapter because of a lack of mixture data, specifically a lack of binary data that would allow for a systematic evaluation of the effects of increasing backbone length, shifting branch positions, increasing branch number, and increasing branch length. Because the branched alkane family comprises of a large variety of possible component characteristics, it is expected that a systematic evaluation with binary mixture data would be difficult. Nonetheless, the information gained by looking at pure-component predictions is adequate for investigating the effects of molecular structure. The added benefit of including binary mixture plots (being able to identify the correct balance between different intermolecular interactions) is hardly applicable in the case of branched alkanes where dispersion interactions are predominant.

Note that SAFT-VR Mie parameters were only generated for components where u data were available. Generating SAFT-VR Mie parameters without u data may produce biased results when modelling P^{vap} and ρ^{sat}. In Tables 6.1 to 6.5, the bold entries indicate which EoS produced the smallest deviation.

6.1.1 Increasing Backbone Length

In this subsection, the effect of increased linearity on SAFT-γ Mie's prediction accuracy is considered. Table 6.1 presents a comparison between SAFT-γ Mie and SAFT-VR Mie pure-component predictions for 2-methylalkanes of increasing carbon backbone length.

Table 6.1: 2-Methylalkane pure-component %AAD for SAFT-γ Mie and SAFT-VR Mie. P^{vap}, ρ^{sat}, and H^{vap} predictions are measured against DIPPR correlations [64].

	P^{vap}		ρ^{sat}		H^{vap}		u		
Component	γ Mie	VR Mie	γ Mie	VR Mie	γ Mie	VR Mie	γ Mie	VR Mie	u Ref.
2-methylpropane	0.93		2.14		2.34				
2-methylbutane	6.82	**0.26**	0.63	**0.17**	**0.98**	2.11	8.71	**2.49**	[113]
2-methylpentane	2.26	**0.21**	0.43	**0.13**	**1.50**	1.77	4.87	**1.24**	[114]
2-methylhexane	0.54	**0.28**	0.67	**0.20**	1.89	**1.66**	5.66	**0.90**	[115]
2-methylheptane	2.00		0.86		1.75				
2-methyloctane	2.77	**0.90**	0.40	**0.38**	0.68	**0.62**	5.48	**1.68**	[116]
2-methlynonane	2.77	**0.34**	0.51	**0.15**	**1.44**	1.50	5.48	**1.21**	[116]
2-methyldecane	3.18	**0.90**	0.71	**0.59**	**0.63**	0.87	5.60	**0.86**	[116]

The SAFT-γ Mie saturated liquid density and heat of vaporisation predictions are relatively accurate compared to the predictions for other species (see Table 4.1). The vapour pressure predictions are weaker and show the same trend as for the alkanes: Prediction strength is focussed around the middle components that share characteristics with the smaller and larger molecules (see Figure 6.2). Methylpropane is an exception; good P^{vap} predictions were obtained while the ρ^{sat} predictions are less accurate. Methylpropane is different from the other 2-methylalkanes because it does not contain any CH_2 groups. This suggests that the contributions of some groups or group interactions favour or deteriorate the predictions of certain properties. It cannot be said with certainty how different contributions affect the prediction of different properties; however, this imbalance would not exist if the group-contribution assumption (as implemented in SAFT-γ Mie) was completely accurate.

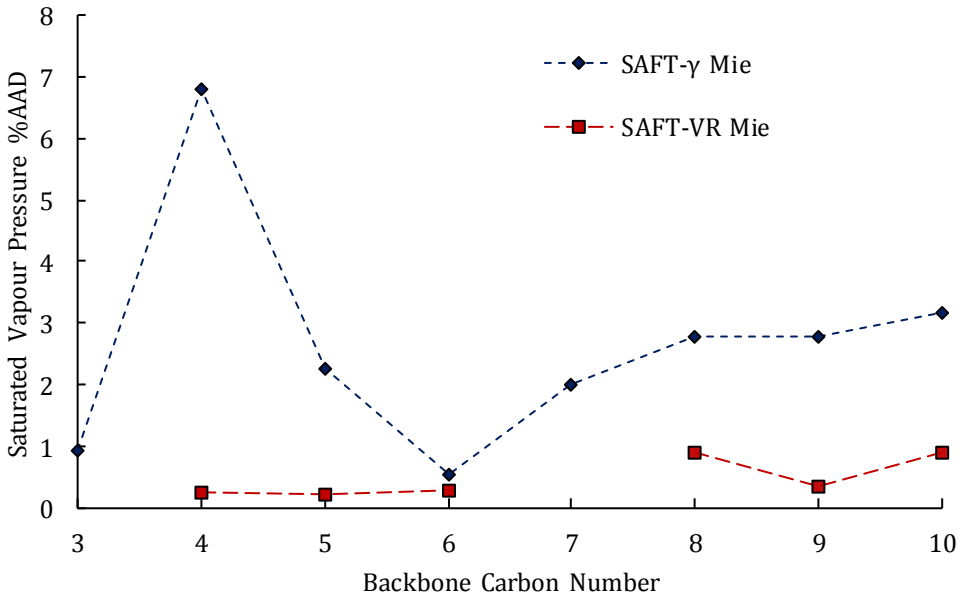

Figure 6.2: Comparison of P^{vap} prediction accuracies for 2-methylalkanes.

Table 6.2: 2,2-Dimethylalkane pure-component %AAD for SAFT-γ Mie and SAFT-VR Mie.

	P^{vap}		ρ^{sat}		H^{vap}		u		
Component	γ Mie	VR Mie	γ Mie	VR Mie	γ Mie	VR Mie	γ Mie	VR Mie	u Ref.
2,2-dimethylpropane	20.05	**0.35**	5.68	**0.32**	9.40	**1.74**	**1.05**	2.16	[117]
2,2-dimethylbutane	7.88		9.48		4.15				
2,2-dimethylpentane	6.43	**0.08**	8.94	**0.17**	3.63	**1.44**	7.28	**2.73**	[118]
2,2-dimethylhexane	5.40	**0.26**	8.03	**0.16**	2.96	**1.29**	7.18	**1.26**	[115]
2,2-dimethylheptane	6.59		7.45		3.60				
2,2-dimethyloctane	4.98		7.52		2.35				

The predictions for 2,2-dimethylalkanes are weak, but as the molecules become larger and more like linear *n*-alkanes, predictions improve slightly. SAFT-γ Mie also constantly underpredicts the densities. This is a surprising result, since one may expect a model that presents molecules as linear chains to overpredict densities — linear molecules tend to have higher densities than branched molecules with the same molecular mass. It is apparent that the regression of a single transferrable C group is not enough to correct for SAFT-γ Mie's inaccuracies for 2,2-dimethylalkanes. SAFT-VR Mie can somewhat make up for the fact that it only models linear chains, because the regression of its component-specific parameters for branched alkanes tends to produce smaller segment numbers and larger segment diameters than for *n*-alkanes of similar molecular mass. Therefore, the SAFT-VR Mie prediction %AADs in Table 6.2 are significantly smaller.

6.1.2 Shifting Branch Positions and Increasing the Number of Branches

The combining rule was used to estimate the SAFT-γ Mie dispersion interaction energy between C and CH in components where both groups occur.

Table 6.3: Branched alkane isomer pure-component %AAD for SAFT-γ Mie and SAFT-VR Mie.

Component	P^{vap}		ρ^{sat}		H^{vap}		u		u Ref.
	γ Mie	VR Mie	γ Mie	VR Mie	γ Mie	VR Mie	γ Mie	VR Mie	
Dimethylpentane									
2,2-dimethylpentane	6.43	**0.08**	8.94	**0.17**	3.63	**1.44**	7.28	**2.73**	[118]
2,3-dimethylpentane	29.37	**0.47**	6.14	**0.66**	4.20	**1.51**	12.70	**2.15**	[114]
2,4-dimethylpentane	1.86	**0.34**	1.40	**0.44**	2.40	**1.43**	10.01	**0.60**	[115]
3,3-dimethylpentane	26.06		11.65		5.00				
Dimethylhexane									
2,2-dimethylhexane	5.40	**0.26**	8.03	**0.16**	2.96	**1.29**	7.18	**1.26**	[115]
2,3-dimethylhexane	17.51		4.90		2.21				
2,4-dimethylhexane	1.85		1.24		2.04				
2,5-dimethylhexane	2.30	**0.24**	1.02	**0.16**	2.13	**1.28**	8.81	**1.13**	[115]
3,3-dimethylhexane	18.61		12.68		3.90				
3,4-dimethylhexane	24.83		6.48		3.50				
Dimethyloctane									
2,2-dimethyloctane	4.98		7.52		2.35				
2,3-dimethyloctane	8.57		3.61		1.02				
2,4-dimethyloctane	13.87		0.35		4.08				
2,5-dimethyloctane	7.39		1.77		2.85				
2,6-dimethyloctane	2.54		0.81		1.81				
2,7-dimethyloctane	4.00		1.28		2.02				
Trimethylpentane									
2,2,4-trimethylpentane	7.11	**0.38**	9.00	**0.15**	4.80	**1.30**	9.47	**2.80**	[115]
2,3,4-trimethylpentane	44.23	**0.67**	8.79	**0.36**	6.78	**1.32**	17.54	**1.52**	[115]

The results obtained for dimethylalkanes where the branches are located on opposite sides of the backbone, e.g., 2,5-dimethylhexane, are significantly more accurate than the results for alkanes where the branches are located next to each other, e.g., 2,3-dimethylpentane. Although Dufal et al. [33] do not specify which components were included in the regression of the CH group parameters, it can be deduced that the regression procedure only included components where the branches are next to one another, leading to the significant difference in accuracy based on branch position.

Table 6.4 compares the modelling results for alkanes of the same molecular mass with an increasing number of branches. The branched alkanes were selected so that the branches are located close to the terminal end and connected to neighbouring carbon atoms (two CH functional groups are used), except in the case of dimethylpropane and trimethylbutane where two branches are connected at the same carbon (the C functional group is used).

Table 6.4: Pure-component %AAD for components with equivalent molecular masses and an increasing number of branches.

Component	P^{vap}		ρ^{sat}		H^{vap}		u		u Ref.
	γ Mie	VR Mie	γ Mie	VR Mie	γ Mie	VR Mie	γ Mie	VR Mie	
				C_5H_{12}					
n-pentane	2.37	**1.06**	**0.30**	0.40	**1.84**	2.51	**4.36**	5.65	[65]
2-methylbutane	6.82	**0.26**	0.63	**0.17**	**0.98**	2.11	8.71	**2.49**	[113]
2,2-dimethylpropane	20.05	**0.35**	5.68	**0.32**	9.40	**1.74**	1.05	**2.16**	[117]
				C_7H_{16}					
n-heptane	1.45	**0.89**	**0.20**	0.49	**1.61**	2.19	**2.83**	2.91	[65]
2-methylhexane	0.54	**0.28**	0.67	**0.20**	1.89	**1.66**	5.66	**0.90**	[115]
2,3-dimethylpentane	29.37	**0.47**	6.14	**0.66**	4.20	**1.51**	12.70	**2.15**	[114]
2,2,3-trimethylbutane	31.55	**0.52**	14.02	**0.18**	5.85	**1.46**	14.50	**1.17**	[118]
				C_8H_{18}					
n-octane	1.13	**0.98**	**0.31**	0.68	**1.22**	1.65	**2.72**	2.82	[65]
2-methylheptane	2.00		0.86		1.75				
2,3-dimethylhexane	17.51		4.90		2.21				
2,3,4-trimethylpentane	44.23	**0.67**	8.79	**0.36**	6.78	**1.32**	17.54	**1.52**	[114]

SAFT-γ Mie produced less accurate results as the number of branches increases, while SAFT-VR Mie retained its accuracy. This supports the notion that the contributions of either the CH or CH_3 groups are not adequate to be used in all branched molecules, particularly when the branches are located close to one another.

Table 6.5 shows isobaric heat capacity predictions for some of the heptane isomers considered in this chapter. SAFT-γ Mie produced slightly more accurate predictions, as it often does for temperature derivative properties such as H^{vap}, C_P, and u, despite being significantly less accurate for the P^{vap} and ρ^{sat} predictions.

Table 6.5: Saturated liquid C_P %AAD comparison for C_7H_{16} isomers.

Component	SAFT-γ Mie	SAFT-VR Mie	Temp. (K)	Reference
n-heptane	**0.84**	1.25	243.0 – 513.0	[65]
2-methylhexane	**1.93**	2.55	160.4 – 301.2	[119]
2,2-dimethylpropane	**5.38**	5.89	154.7 – 298.4	[119]
2,4-dimethylpentane	**1.45**	3.36	160.8 – 307.1	[119]
2,2,3-trimethylbutane	**3.50**	7.65	253.0 – 313.3	[119]

6.2 Binary Mixture Properties

The following figure of binary VLE predictions for the benzene + 2,2,4-trimethylpentane system at five different temperatures is representative of what was typically seen for branched alkane mixture predictions. Similar accuracy was obtained for different branched alkane mixtures (presented in Section D.6 in Appendix D).

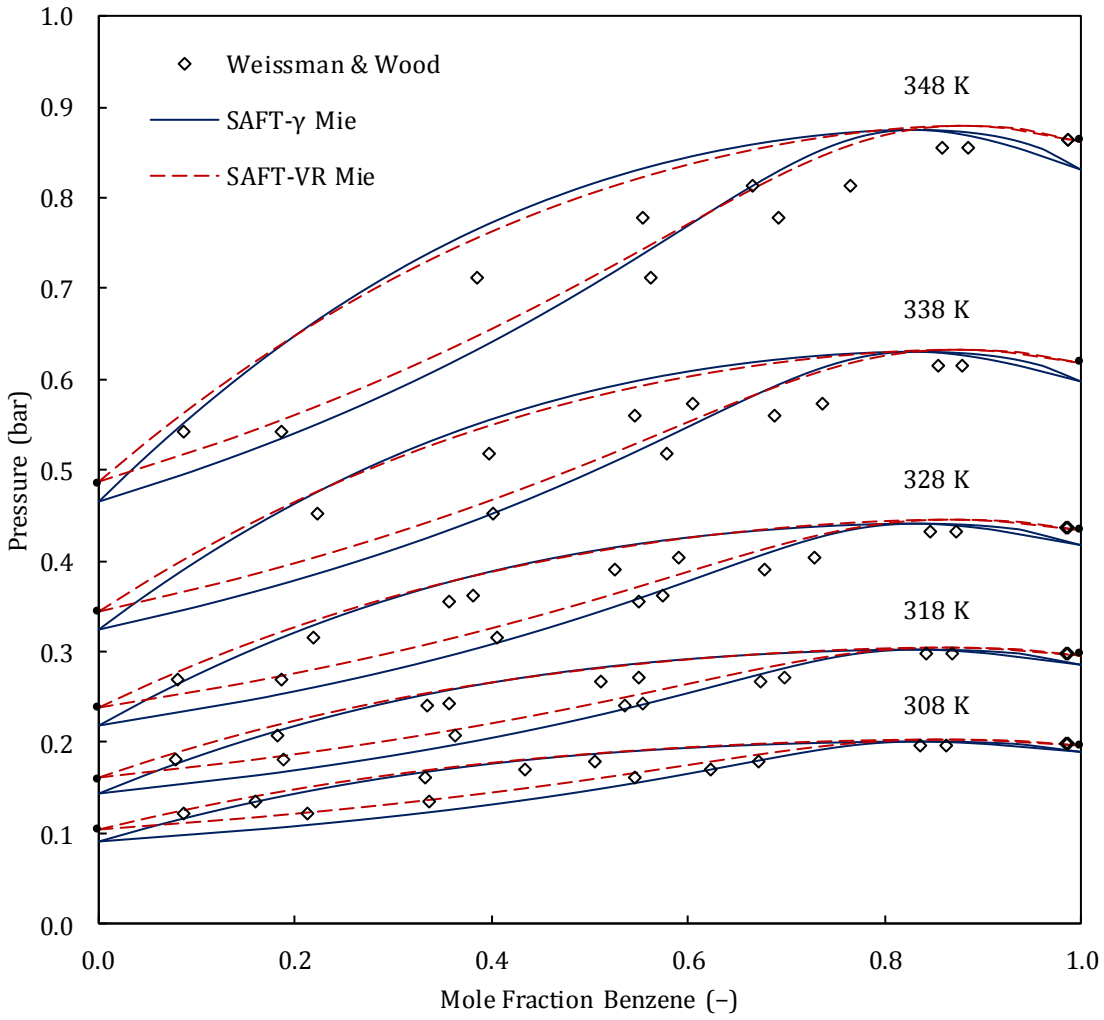

Figure 6.3: : Isothermal benzene + 2,2,4-trimethylpentane VLE predictions at 308, 318, 328, 338, and 348 K. Data taken from Weissman & Wood [120]. Black dots indicate pure-component vapour pressures calculated with DIPPR correlations [64].

Both models generated similar predictions of branched alkane VLE, with SAFT-VR Mie being slightly more accurate overall. The fact that the SAFT-γ Mie predictions closely resemble the SAFT-VR Mie predictions lends some confidence in the GCM's predictive capability, especially since the aCH–C and C–CH dispersion interaction energies were calculated with the combining rule.

6.3 Discussion

Although most of the mixture predictions are relatively good, the pure-component P^{vap} and ρ^{sat} results in this section emphasise the importance of molecular structure. The CH_3 parameters were regressed in components where the group is bonded to CH_2 instead of CH or C as in branched alkanes. A component modelled in SAFT-γ Mie will exhibit the properties of the group configuration for which the parameters were regressed because, as seen from the chain term's homosegmented formulation, the EoS does not explicitly take group arrangement into account. Consider the following two equations; the first denotes the contact RDF used in the chain term for SAFT-γ Mie, and the second for SAFT-VR Mie.

$$\left(g_{ii}^{\text{Mie}}(\bar{\sigma}_{ii})\right)^{\gamma\text{ Mie}} = g_{d,ii}^{\text{HS}}(\bar{\sigma}_{ii}) \exp\left[\frac{\frac{\bar{\epsilon}_{ii}}{k_{\text{B}}T} g_{1,ii}(\bar{\sigma}_{ii}) + \left(\frac{\bar{\epsilon}_{ii}}{k_{\text{B}}T}\right)^2 g_{2,ii}(\bar{\sigma}_{ii})}{g_{d,ii}^{\text{HS}}(\bar{\sigma}_{ii})}\right] \tag{6.1}$$

$$\left(g_{ii}^{\text{Mie}}(\sigma_{ii})\right)^{\text{VR Mie}} = g_{d,ii}^{\text{HS}}(\sigma_{ii}) \exp\left[\frac{\frac{\epsilon_{ii}}{k_{\text{B}}T} g_{1,ii}(\sigma_{ii}) + \left(\frac{\epsilon_{ii}}{k_{\text{B}}T}\right)^2 g_{2,ii}(\sigma_{ii})}{g_{d,ii}^{\text{HS}}(\sigma_{ii})}\right] \tag{6.2}$$

Note that the two equations are identical with the exception of the overbars on the SAFT-γ Mie parameters, which indicate that these are average molecular parameters. The same goes for the RDF expansion terms located in Eqs (6.1) and (6.2). Average molecular parameters are component-specific parameters calculated using equations, similar to mixing rules, that weigh a group's contribution to the parameters according to the portion of the molecule that is made up by that group. E.g., the average dispersion energy is calculated with

$$\bar{\epsilon}_{ii} = \sum_{k=1}^{N_{\text{G}}} \sum_{l=1}^{N_{\text{G}}} z_{k,i} z_{l,i} \epsilon_{kl} \tag{6.3}$$

where $z_{k,i}$ equals the fraction of the segments in component i that belongs to functional group k. In effect, SAFT-γ Mie does not consider the connections between the segments of different groups to be unique, and detailed information about the bonds between different functional groups are lost. Figure 6.4 illustrates the different bonds between groups that occur in dimethylpentane isomers that are currently considered to be identical within the SAFT-γ Mie framework.

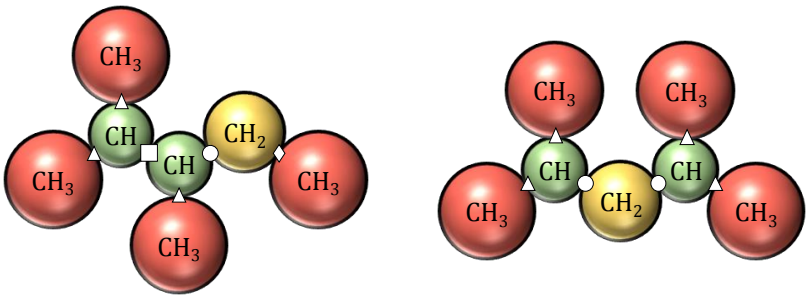

CH_3–CH_2	(◊)	:	1	CH_3–CH_2	(◊)	:	0
CH_3–CH	(△)	:	3	CH_3–CH	(△)	:	4
CH_2–CH	(○)	:	1	CH_2–CH	(○)	:	2
CH–CH	(□)	:	1	CH–CH	(□)	:	0

Figure 6.4: Diagrammatic representation of the unique bonds between functional groups in 2,3-dimethylpentane (left) and 2,4-dimethlypentane (right). The bonds between groups are represented by the small white shapes.

A rigorous method to account for bond formation between groups within chains (i.e. a fully heterosegmented approach) would result in more faithful molecular representations and allow for distinction between isomers. This approach would also be more fundamental than a second-order GC extension.

The RDF at contact could be evaluated using group interaction parameters in order to approximate chain formation between the spherical segments of *unlike* groups:

$$\left(g_{kl}^{\text{Mie}}(\sigma_{kl})\right)^{\gamma\,\text{Mie}} = g_{d,kl}^{\text{HS}}(\sigma_{kl}) \exp\left[\frac{\frac{\epsilon_{kl}}{k_\text{B}T} g_{1,kl}(\sigma_{kl}) + \left(\frac{\epsilon_{kl}}{k_\text{B}T}\right)^2 g_{2,kl}(\sigma_{kl})}{g_{d,kl}^{\text{HS}}(\sigma_{kl})}\right] \tag{6.4}$$

The next section explores the option of implementing a heterosegmented chain term using this group-specific RDF at contact.

6.4 Heterosegmented Chain Term

The following equation gives the existing homosegmented SAFT-γ Mie chain term.

$$F^{\text{Chain}} = \sum_{i=1}^{N_\text{C}} \left[n_i \left(\overbrace{\sum_{k=1}^{N_\text{G}} \nu_{k,i} \nu_k^* S_k}^{\sim m_\text{s}} - 1 \right) \left(-\ln g_{ii}^{\text{Mie}}(\bar{\sigma}_{ii}) \right) \right] \tag{6.5}$$

where the second summation term (the "−1" is not included in the summation over k) equals the total number of segments in component i (would be denoted by m_s in SAFT-VR Mie). The total

number of bonds is equal to the number of segments minus one, as in the original derivation of Chapman et al. [41]. This is true after assuming that chains consist of an integer number of spheres where each sphere is bonded to two others, with the exception of the two spheres at the ends of the chain. A conceptual interpretation of the term inside the square brackets in Eq. (6.5) is as follows: The state function contribution of complete chain formation for component i equals the state function contribution of one bond formed between two spherical segments ($-\ln g^{\text{Mie}}(\sigma)$) multiplied by the number of bonds between the spheres in one chain belonging to component i (the "number of bonds" term in parenthesis), multiplied by the number of chains (molecules) of component i. It is important to note that due to the presence of the regressed shape factor ($0 < S_k \leq 1$), the number of segments can be adjusted to a noninteger number to correct for the fact that the model does not explicitly take group overlap into account. Thus, the **number of segments** belonging to one group k in SAFT-γ Mie is equal to $\boldsymbol{\nu_k^* S_k}$ and not just ν_k^*.

A heterosegmented chain term would have to consist of two parts: an intragroup part to account for chain formation between the segments of a group, and an intergroup part to account for the bonds between groups. In the following subsection, a derivation is given for a heterosegmented chain term similar to the ones employed by the Copolymer PC-SAFT developed by Gross et al. [24], and the GC-SAFT-VR by Peng et al. [121].

6.4.1 Derivation

Figure 6.5 gives a diagrammatic representation of the intragroup bonds:

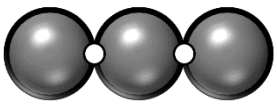

Figure 6.5: Intragroup chain formation. Note that the spheres represent segments instead of groups, and that the white dots represent the bonds between segments of the same group.

It is assumed that groups are linear chains of spherical segments. Therefore, the chain formation within groups takes on a form similar to the existing SAFT-VR Mie chain term, except that the RDF at contact is evaluated for different groups instead of components.

$$\left(F^{\text{Chain}}\right)^{\text{Intragroup}} = \sum_{i=1}^{N_C}\left[n_i \sum_{k=1}^{N_G}\left[\nu_{k,i}(\nu_k^* S_k - 1)\left(-\ln g_{kk}^{\text{Mie}}(\sigma_{kk})\right)\right]\right] \tag{6.6}$$

where $\left(-\ln g_{kk}^{\text{Mie}}(\sigma_{kk})\right)$ denotes the contribution of a singular bond between two segments belonging to group k, $(\nu_k^* S_k - 1)$ the number of bonds in the chain that makes up group k, and $\nu_{k,i}$ the number of times group k appears in component i.

The intergroup contribution consists of the sum of the bonds between groups, where each bond is assumed to take place between one spherical segment of group k and one spherical segment of group l, as shown in Figure 6.6.

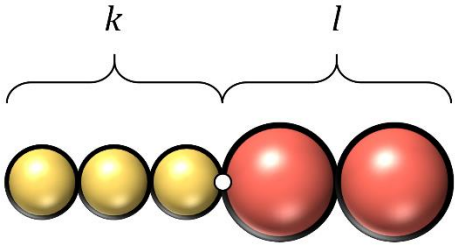

Figure 6.6: Intergroup chain formation. Note that the spheres represent segments instead of groups (the arbitrary groups k and l are made up of the yellow and red spheres, respectively), and the white dot represents an intergroup bond between groups k and l.

$$\left(F^{\text{Chain}}\right)^{\text{Intergroup}} = \sum_{i=1}^{N_C} n_i \sum_{k=1}^{N_G} \sum_{l=1}^{k} \left[\nu_{kl,i}\left(-\ln g_{kl}^{\text{Mie}}(\sigma_{kl})\right)\right] \tag{6.7}$$

where $\nu_{kl,i}$ denotes the number of times functional group k appears next to functional group l in component i. This quantity is determined by inspecting the molecule, as was done for 2,3-dimethylpentane and 2,4-dimethylpentane in Figure 6.4.

The combined heterosegmented chain term, $F^{\text{Chain}} = \left(F^{\text{Chain}}\right)^{\text{Intragroup}} + \left(F^{\text{Chain}}\right)^{\text{Intergroup}}$, is given by the following equation:

$$F^{\text{Chain}} = -\sum_{i=1}^{N_C} n_i \sum_{k=1}^{N_G} \left[\nu_{k,i}(\nu_k^* S_k - 1) \ln g_{kk}^{\text{Mie}}(\sigma_{kk}) + \sum_{l=1}^{k} \nu_{kl,i} \ln g_{kl}^{\text{Mie}}(\sigma_{kl})\right] \tag{6.8}$$

Note that the third summation only counts up to k so as to avoid counting intergroup bonds twice.

The total number of bonds in component i, $N_{\text{B},i}$, equals the sum of the intragroup and intergroup bonds:

$$N_{\text{B},i} = \overbrace{\sum_{k=1}^{N_G} \nu_{k,i}(\nu_k^* S_k - 1)}^{\text{Intragroup}} + \overbrace{\sum_{k}^{N_G} \sum_{l=1}^{k} \nu_{kl,i}}^{\text{Intergroup}} \tag{6.9}$$

After assuming that the molecules of i are all linear chains (i.e. ring formation is prohibited) [1], the number of intergroup bonds is equal to the sum of all of the functional groups in the system minus one, and (6.9) becomes

$$N_{\mathrm{B},i} = \overbrace{\sum_{k=1}^{N_\mathrm{G}} \left(\nu_{k,i}\nu_k^* S_k - \nu_{k,i}\right)}^{\text{Intragroup}} + \overbrace{\sum_{k=1}^{N_\mathrm{G}} \nu_{k,i} - 1}^{\text{Intergroup}} = \sum_{k=1}^{N_\mathrm{G}} \nu_{k,i}\nu_k^* S_k - 1 \tag{6.10}$$

This is the same number of bonds per component i that appears in the existing SAFT-γ Mie chain term. Factoring out $N_{\mathrm{B},i}$ from the second summation in (6.8) yields

$$F^{\mathrm{Chain}} = -\sum_{i=1}^{N_\mathrm{C}} n_i N_{\mathrm{B},i} \sum_{k=1}^{N_\mathrm{G}} \left[B_{k,i} \ln g_{kk}^{\mathrm{Mie}}(\sigma_{kk}) + \sum_{l=1}^{k} B_{kl,i} \ln g_{kl}^{\mathrm{Mie}}(\sigma_{kl}) \right] \tag{6.11}$$

where the bond fraction of intragroup bonds is

$$B_{k,i} = \frac{\nu_{k,i}(\nu_k^* S_k - 1)}{\sum_{l=1}^{N_\mathrm{G}} \nu_{l,i}\nu_l^* S_l - 1} = \frac{\nu_{k,i}(\nu_k^* S_k - 1)}{N_{\mathrm{B},i}} \tag{6.12}$$

and the bond fraction of intergroup bonds is

$$B_{kl,i} = \frac{\nu_{kl,i}}{\sum_{\beta=1}^{N_\mathrm{G}} \nu_{\beta,i}\nu_\beta^* S_\beta - 1} = \frac{\nu_{kl,i}}{N_{\mathrm{B},i}} \tag{6.13}$$

While the heterosegmented chain term presented in this section is mathematically consistent, the fact that the shape factor allows a group's effective number of segments to be smaller than one poses a problem. It is not physically sensible for a bond fraction to be smaller than one, or for the intragroup chain contributions to increase the Helmholtz free energy; i.e. $B_{k,i}\left(-\ln g_{kk}^{\mathrm{Mie}}(\sigma_{kk})\right) > 0$. An empirical correction is explored in the following subsection.

[1] This assumption is also made in the existing SAFT-γ Mie, even though aromatic rings are modelled as a sum of 6 aromatic groups. For a more rigorous approach, the number of bonds in benzene should be equal to the number of segments instead of $\nu_{k,i}\nu_k^* S_k - 1$; aromatic rings are therefore approximated as linear chains instead of true rings.

6.4.2 Correction

In order to prevent negative bond fractions, the shape factor is omitted from Eqs (6.12) and (6.13) to yield

$$B_{k,i} = \frac{\nu_{k,i}(\nu_k^* - 1)}{\sum_{l=1}^{N_G} \nu_{l,i}\nu_l^* - 1} \tag{6.14}$$

and

$$B_{kl,i} = \frac{\nu_{kl,i}}{\sum_{\beta=1}^{N_G} \nu_{\beta,i}\nu_\beta^* - 1} \tag{6.15}$$

This adjustment makes sense from a physical point of view. In a molecule that consists of groups with segment numbers equal to one, the intragroup chain contributions would be zero, and the intergroup bond formation would be the only contribution to the chain term. However, the adjustment results in the weight of the bond contributions to no longer correspond to the weight of the segments as calculated in the other SAFT-γ Mie contributions — if the shape factor of a certain group k, S_k, is smaller than the other groups' shape factors, the chain contribution would consider the segments of group k to take part in more bonds than what should be possible for that number of segments (which is equal to $\nu_k^* S_k$ according to the rest of SAFT-γ Mie). As of yet, it cannot be said whether this discrepancy is significant enough to result in any decrease in the model's precision because the segment "overlap" implied by the shape factors is still considered in the calculation of the packing fraction used to determine the RDF at contact (Eq. (6.4)). As a result, the probability of one group being close enough to another for chain formation to take place (calculated with the RDF at contact) and consequently the bond contributions, i.e. $-\ln g_{kk}^{\text{Mie}}(\sigma_{kk})$ and $-\ln g_{kl}^{\text{Mie}}(\sigma_{kl})$, remain in agreement with the rest of the SAFT-γ Mie formulation.

Another way to correct for the unrealisable bond fractions would be to replace the ν_k^* and S_k parameters entirely throughout the EoS with a combined m_k "chain length" parameter as employed in GC-SAFT-VR [121]:

$$m_k = \nu_k^* S_k \tag{6.16}$$

where $m_k \geq 1$. The EoS would then retain its consistency without being subject to nonsensical bond fractions and chain-formation contributions while using Eqs (6.12) and (6.13).

6.4.3 Preliminary Evaluation

A preliminary evaluation was done for 2,3-dimethylpentane and 2,4-dimethylpentane to determine whether the newly proposed chain term would allow SAFT-γ Mie to distinguish between isomers. The preliminary evaluation tests the heterosegmented chain term with the corrected bond fractions, (6.14) and (6.15), and using CH_3, CH_2, and CH parameters that were regressed for the existing SAFT-γ Mie formulation. The results of the preliminary evaluation are therefore not expected to be quantitatively accurate because the EoS no longer has the same framework.

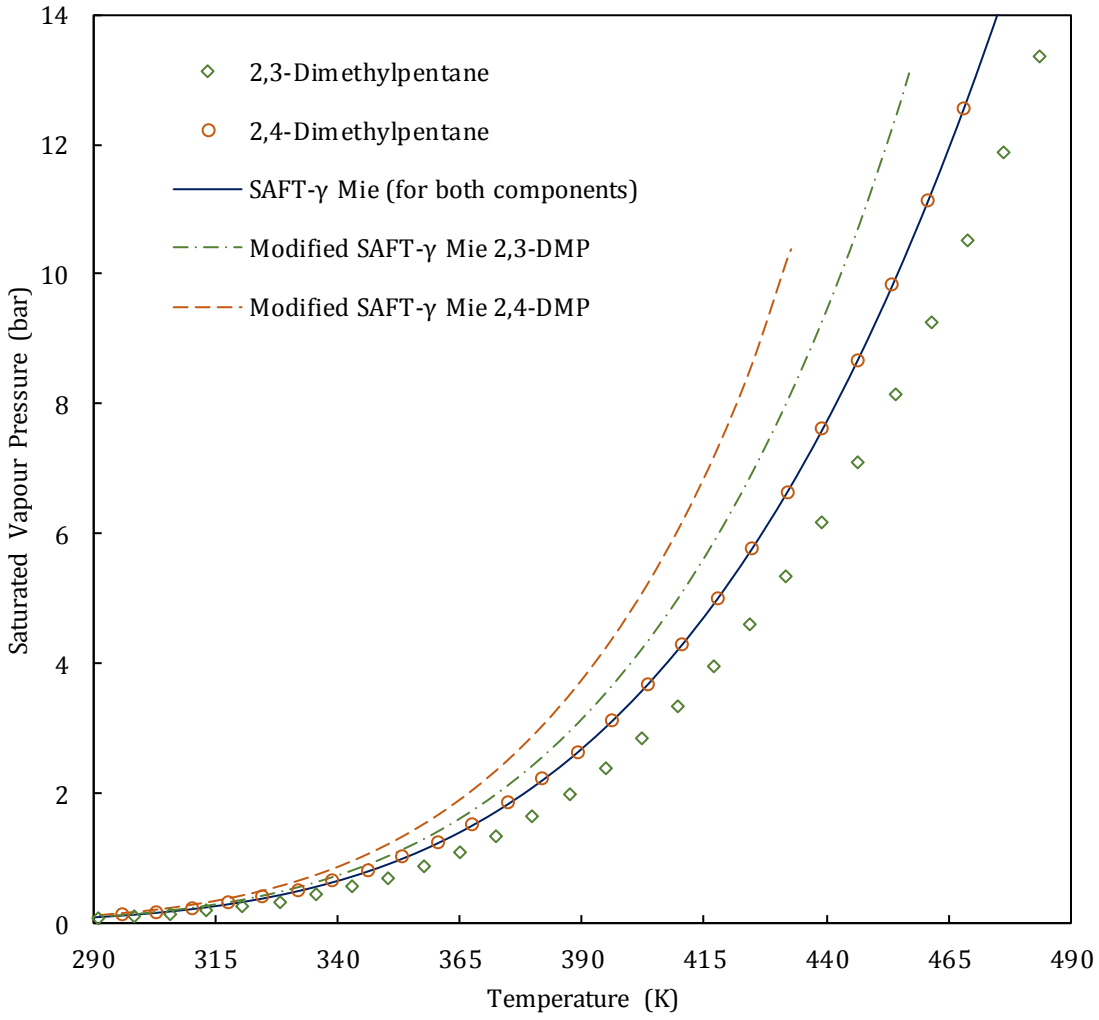

Figure 6.7: 2,3-Dimethylpentane and 2,4-dimethylpentane vapour pressure predictions with the newly proposed chain term (Modified SAFT-γ Mie) using existing SAFT-γ Mie group parameters. The markers correspond to DIPPR correlations [64].

Note that the standard SAFT-γ Mie produced the same prediction for both components and that the CH group parameters had likely been regressed using data of branched alkanes where the branch is located close to the molecule's terminal position. The modified SAFT-γ Mie variant

correctly predicts that 2,4-dimethylpentane is slightly more volatile than 2,3-dimethylpentane, and the only additional information the modification requires is the number of times groups are located next to one another — no additional (newly defined) parameters have to be regressed.

In the P^{vap} predictions made with the new chain term, the pressures are overestimated using the existing SAFT-γ Mie parameter. The 2,3-dimethylpentane and 2,4-dimethylpentane predictions were generated with hardcoded chain contributions because implementing the general form calls for much additional work that should form part of a separate project. A thorough evaluation of the modified SAFT-γ Mie would require the new chain term to be implemented for the general case, after which new functional-group parameters would have to be generated methodically for every functional group under consideration.

6.4.4 Potential Advances

In addition to allowing the model to distinguish between isomers of branched components, as shown in Figure 6.7, the chain modification will also enable distinction between isomers of dipolar components such as those investigated in Chapter 5 (2-ketones, 3-ketones, *n*-alkyl acetates, and *n*-alkyl propanoates). The chain modification could therefore be a less empirical alternative to second-order groups, and it will not require the regression of additional model parameters that do not exist in the current SAFT-γ Mie framework. Furthermore, the calculation of more robust chain-formation contributions, $g_{kl}^{\text{Mie}}(\sigma_{kl})$, could possibly increase the model's precision in general.

Chapter 7: Summary and Conclusions

7.1 Summary

The following table summarises the performance of SAFT-γ Mie vs SAFT-VR Mie.

Table 7.1: Comparative summary. The better model is indicated with "×", and "—" indicates that neither of the models are consistently better.

	SAFT-γ Mie	SAFT-VR Mie	Sections
P^{vap} (overall)		×	4.1; 5.2.1; 5.4.2.1; 6.1
ρ^{sat} (overall)	—		4.1; 5.2.1; 5.4.2.1; 6.1
First- and second-order temperature derivative properties (overall)	×		4.1; 4.2; 5.2; 5.4.2; 6.1
VLE (overall)	—		4.2; 5.2.2; 5.2.4; 5.4.2.2; 6.2
Linear, nonpolar, non-associating species	—		4.1
Larger polar molecules (esters)[a]	×		4.2.1
Smaller associating polar molecules (1-alcohols)[a]		×	4.1; 4.2.2
Smaller non-associating polar molecules (ketones)[b]		×	5.2; 5.4.2
Branched alkanes		×	6.1; 6.2
Shortest computing time		×	
Convenient modelling of new components / lower dependence on experimental data	×		

[a] Polar interactions are not treated directly
[b] Polar interactions are treated with pseudo-association in SAFT-γ Mie and the GV term in SAFT-VR Mie

The above table does not conclude the comparison between the two EoS, because many of the benefits and disadvantages of the GC formulism of SAFT-γ Mie cannot be seen from the modelling results or cannot be described quantitatively. Throughout this work it was often difficult to follow a systematic investigation due to limited data, especially speed of sound data. An advantage of the GCM became apparent in these cases because, unlike with a traditionally structured EoS, parameter generation did not require data for every component in the homologous series. The predictive capabilities of SAFT-γ Mie makes it a powerful tool, especially if one were to build a moderated database of functional group parameters such as the UNIFAC database maintained by the Dortmund Data Bank.[1]

[1] The list of UNIFAC parameters can be accessed at http://www.ddbst.com/published-parameters-unifac.html [134].

An unseen downside of SAFT-γ Mie is the computing time required to generate parameters and predictions. As the number of functional groups (N_G) increases, the number of different interaction combinations increases exponentially:

$$\text{Number of combinations } = \frac{1}{2}\left({N_G}^2 + N_G\right) \tag{7.1}$$

while assuming that $A_{kl} = A_{lk}$ for all of the different interactions. Adding more functional groups to a system in SAFT-γ Mie is equivalent to adding more components to a system in SAFT-VR Mie in terms of computing requirements. However, the increased computing time for parameterisation is less of an obstacle, because once the parameters of a functional group had been determined, there is no need to determine additional parameters to describe the individual components of its relevant homologous series, and the group can also be applied in the description of more complex molecules containing that group.

7.2 Conclusions

7.2.1 General Comparison

The results in Chapter 4 prove that the first hypothesis of this project is not true in general, and that the GC approach can be effective in a complex SAFT formulation. The hypothesis was:

> *By assuming that the characteristics of a functional group are independent of its environment, the accuracy of SAFT-γ Mie becomes generally limited.*

SAFT-γ Mie's modelling of *n*-alkanes, 1-alkenes, and *n*-alkyl acetates is comparable to that of SAFT-VR Mie and the former model's predictions of the H^{vap} property is superior — most likely due to its transferrable dispersion interaction energies. These regressed interaction energies also give the GCM an advantage over SAFT-VR Mie which is unable to correctly capture the ester + alkane VLE behaviour without an explicit polar term. While these interaction energies fulfil a role similar to k_{ij} BIPs, they can be determined using only pure-component data and can be transferred across components.

At the same time, the 1-alcohol results suggest that the hypothesis is true under certain conditions; it was speculated that the modelling of small polar components poses a challenge. Further investigation was needed to determine whether this is true, because a sample of four components is not conclusive, and due to the presence of self-association one cannot isolate polarity as the determining factor.

7.2.2 Dipolar Molecules

Chapter 5 provides further investigation of the first hypothesis and other considerations such as the modelling consistency between isomers and the performance of the pseudo-association approach. The modelling of ketones and esters provided a convenient opportunity to investigate the behaviour of SAFT-γ Mie for isomers, because sufficient binary mixture data are available and prior work had been done using SAFT-VR Mie + GV [19].

Functional groups were defined for 2-ketones, 3-ketones, and *n*-alkyl propanoates — new groups and parameters had to be generated for different isomers because the first-order GCM cannot distinguish between them using the same groups. The first hypothesis is true for smaller dipolar species: SAFT-γ Mie has difficulty with modelling these components as a result of the structural-independence assumption of the first-order GCM. The 2-ketone results match the 1-alcohol results in terms of accuracy, even with pseudo-association to treat dipolar interactions. Despite the adequate binary-system predictions, pure-component predictions leave room for improvement. The investigation was expanded to a series of 3-ketones, once again resulting in a similar level of accuracy, although density predictions worsened. Additionally, it was found that the regressed interaction energies between the functional groups are crucial to compensate for some of the underlying limitations of the GCM. Ketone isomers where the defining functional group is not located at the terminal cannot be modelled accurately with parameters generated using the dispersion energy combining rule. The propanoate results reinforce this observation; the predictions are not as accurate as for the acetates, even with the regressed interaction energies.

7.2.3 Molecular Structure and Chain Formation

This project's second hypothesis regarding molecular structure was proven true for isomers of branched alkanes. The second hypothesis was:

> *Ignoring the physical structure of the molecule in which groups occur compromises SAFT-γ Mie's accuracy for components with nonlinear structures.*

Branched alkanes are both non-associating and nonpolar, yet SAFT-γ Mie's predictions are very inconsistent, especially for the pure-component properties. Weaker predictions were obtained as the number of branches increased and for components where the branches are located close to one another. SAFT-VR Mie does not have the same inconsistency; therefore, it was deduced that the modelling difficulty is because of the first-order GCM assumption that the influence of physical structure and the arrangement of groups is negligible.

A method to account for the arrangement of groups in the chain term was proposed. It was found that a heterosegmented approach in the chain term may allow SAFT-γ Mie to correctly distinguish between isomers while using the same first-order groups. The potential disadvantages of a heterosegmented chain term are: (i) Extra molecular structure information must be specified which can be a tedious task for very complex molecules; and (ii) the calculation of the *unlike* bond interactions will greatly increase computational demands.

Chapter 8: Recommendations

8.1 Model Parameters

It is possible that the current SAFT-γ Mie CH_2 and CH_3 parameters are suboptimal. It may be valuable to do a study to determine whether more balanced and transferrable alkane parameters can be obtained. This would have a positive influence on the modelling of all organic components that contain CH_2 and CH_3 groups.

8.2 Model Improvements

The difficulties of modelling small polar components, even with pseudo-association, indicates that there are limitations inherent to the way SAFT-γ Mie is formulated. The same can be said about why the model struggles with branched alkanes. These limitations are the disregarding of steric hindrance, proximity effects, group arrangement, and bond angles — all of these effects are currently treated implicitly by being lumped with the existing model parameters.

By virtue of SAFT's modular formulation, a second-order GCM can be added as an additional contribution to the state function, or as an adjustment to any of the existing terms or parameters. Doing so will likely allow SAFT-γ Mie to counteract the limitations mentioned in the previous paragraph, and second-order groups may even provide the platform for a polar contribution. On the other hand, second-order contributions are empirical, would require the regression of additional parameters, and the creation of larger, more encompassing groups. Second-order groups would undermine both the fundamental nature of SAFT-based EoS and the predictive aspect that makes GCMs desirable.

A more fundamental alternative would be to implement a fully heterosegmented chain term in place of the current one which assumes that bonds between chains can be approximated with a molecular average. A preliminary evaluation of a newly proposed chain term proved that it is possible to distinguish between isomers using information about molecular structure. Unfortunately, implementing and fully evaluating the new chain term falls beyond the scope of this project. It is recommended that future work includes a full evaluation of the proposed chain term with (i) the corrected bond fractions and (ii) uncorrected bond fractions with the m_k parameter replacing $v_k^* S_k$ (where $m_k \geq 1$).

Although it is unclear whether an explicit group-based polar contribution would improve on the pseudo-association approach, it should still be implemented to negate the need for an approximation that has no physical basis. However, it is recommended that a dipolar term should

only be added after the model has been modified with the ability to differentiate between isomers so as to prevent the need to re-evaluate a polar term for an updated model once a heterosegmented chain term or second-order groups have been added.

8.3 Data for Parameter Generation

The addition of λ^r increases the dimension of a model's parameter space. Pure-component speed of sound data are needed to create a less ambiguous OF during the parameterisation of both SAFT-VR Mie and SAFT-γ Mie, as speed of sound predictions are known to be sensitive to the shape of the potential function [10], [122]. Even though the GCM needs significantly less pure-component data to parameterise the components of a homologous series, the scope of this investigation was still partially limited by the scarcity of speed of sound data. A larger base of speed of sound data is needed to generate SAFT-VR Mie and SAFT-γ Mie parameters more reliably.

8.4 Parameter Accessibility

A GC model greatly benefits from a regulated database of functional-group parameters in order to fully utilise the convenience of being able to describe multiple components with the same parameters. It is recommended that a regulated database be created for SAFT-γ Mie where researchers can access revised parameters and contribute to the collection.

References

[1] G. M. Kontogeorgis and G. K. Folas, *Thermodynamic Models for Industrial Application: From Classical and Advanced Mixing Rules to Association Theories*, 1st ed. John Wiley and Sons, 2010.

[2] Ø. Wilhelmsen, A. Aasen, G. Skaugen, P. Aursand, A. Austegard, E. Aursand, M. A. Gjennestad, H. Lund, G. Linga, and M. Hammer, "Thermodynamic Modeling with Equations of State: Present Challenges with Established Methods," *Industrial and Engineering Chemistry Research*, vol. 56, no. 13, pp. 3503–3515, 2017.

[3] G. Soave, "Equilibrium constants from a modified Redlich-Kwong equation of state," *Chemical Engineering Science*, vol. 27, no. 6, pp. 1197–1203, 1972.

[4] D. Y. Peng and D. B. Robinson, "A New Two-Constant Equation of State," *Industrial & Engineering Chemistry Fundamentals*, vol. 15, no. 1, pp. 59–64, 1976.

[5] H. Renon and J. M. Prausnitz, "Local Compositions in Thermodynamic Excess Functions for Liquid Mixtures," *AIChE Journal*, vol. 14, no. 1, pp. 135–144, 1968.

[6] D. S. Abrams and J. M. Prausnitz, "Statistical Thermodynamics of Liquid Mixtures: A New Expression for the Excess Gibbs Energy of Partly or Completely Miscible Systems," *AIChE Journal*, vol. 21, no. 1, pp. 116–128, 1975.

[7] A. Fredenslund, R. L. Jones, and J. M. Prausnitz, "Group-Contribution Estimation of Activity Coefficients in Nonideal Liquid Mixtures," *AIChE Journal*, vol. 21, no. 6, pp. 1086–1099, 1975.

[8] Y. S. Wei and R. J. Sadus, "Equations of State for the Calculation of Fluid Phase Equilibria," vol. 196, no. 1, pp. 169–196, 2000.

[9] B. E. Poling, G. H. Thomas, D. G. Friend, R. L. Rowley, and W. V. Wilding, "Physical and Chemical Data," in *Perry's Chemical Engineers' Handbook*, 8th ed., D. W. Perry and R. H. Green, Eds. McGraw-Hill, 2007.

[10] T. Lafitte, A. Apostolakou, C. Avendaño, A. Galindo, C. S. Adjiman, E. A. Müller, and G. Jackson, "Accurate statistical associating fluid theory for chain molecules formed from Mie segments," *Journal of Chemical Physics*, vol. 139, no. 15, 2013.

[11] M. S. Wertheim, "Fluids with Highly Directional Attractive Forces. I. Statistical Thermodynamics," *Journal of Statistical Physics*, vol. 35, no. 1, pp. 19–34, 1984.

[12] M. S. Wertheim, "Fluids with Highly Directional Attractive Forces. II. Thermodynamic Perturbation Theory and Integral Equations," *Journal of Statistical Physics*, vol. 35, no. 1, pp. 35–47, 1984.

[13] M. S. Wertheim, "Fluids with Highly Directional Attractive Forces. III. Multiple Attraction Sites," *Journal of Statistical Physics*, vol. 42, no. 3, pp. 459–476, 1986.

[14] M. S. Wertheim, "Fluids with Highly Directional Attractive Forces. IV. Equilibrium Polymerization," *Journal of Statistical Physics*, vol. 42, no. 3, pp. 477–492, 1986.

[15] M. S. Wertheim, "Fluids of dimerizing hard spheres, and fluid mixtures of hard spheres and dispheres," *The Journal of Chemical Physics*, vol. 85, no. 5, pp. 2929–2936, 1986.

[16] W. G. Chapman, K. E. Gubbins, G. Jackson, and M. Radosz, "SAFT: Equation-of-State Solution Model for Associating Fluids," *Fluid Phase Equilibria*, vol. 52, no. C, pp. 31–38, 1989.

[17] G. Mie, "Zur kinetischen Theorie der einatomigen Körper," *Annalen der Physik*, vol. 316, no. 8, pp. 657–697, 1903.

[18] T. Lafitte, D. Bessieres, M. M. Piñeiro, and J. L. Daridon, "Simultaneous estimation of phase behavior and second-derivative properties using the statistical associating fluid theory with variable range approach," *Journal of Chemical Physics*, vol. 124, no. 2, 2006.

[19] J. T. Cripwell, C. E. Schwarz, and A. J. Burger, "SAFT-VR-Mie with an incorporated polar term for accurate holistic prediction of the thermodynamic properties of polar components," *Fluid Phase Equilibria*, vol. 455, pp. 24–42, 2018.

[20] E. L. Derr and C. H. Deal, "Analytical Solutions of Groups: Correlation of Activity Coefficients Through Structural Group Parameters," in *Intern. Symp. Distill.*, 1969, vol. 32, no. 3, p. 40.

[21] D. W. van Krevelen and P. J. Hoftyzer, *Properties of Polymers: Correlations with Chemical Structure*. Elsivier: Amsterdam, 1972.

[22] R. Wittig, J. Lohmann, and J. Gmehling, "Vapor-Liquid Equilibria by UNIFAC Group Contribution. 6. Revision and Extension," *Industrial and Engineering Chemistry Research*, vol. 42, no. 1, pp. 183–188, 2003.

[23] J. N. Jaubert and F. Mutelet, "VLE predictions with the Peng-Robinson equation of state and temperature dependent k_{ij} calculated through a group contribution method," *Fluid Phase Equilibria*, vol. 224, no. 2, pp. 285–304, 2004.

[24] J. Gross, O. Spuhl, F. Tumakaka, and G. Sadowski, "Modeling Copolymer Systems Using the Perturbed-Chain SAFT Equation of State," *Industrial and Engineering Chemistry Research*, vol. 42, no. 6, pp. 1266–1274, 2003.

[25] S. Gupta and J. D. Olsont, "Industrial Needs in Physical Properties," *Industrial and Engineering Chemistry Research*, vol. 42, no. 25, pp. 6359–6374, 2003.

[26] N. D. Austin, N. V. Sahinidis, and D. W. Trahan, "Computer-aided molecular design: An introduction and review of tools, applications, and solution techniques," *Chemical Engineering Research and Design*, vol. 116, pp. 2–26, 2016.

[27] G. M. Kontogeorgis, I. Tsivintzelis, N. von Solms, A. Grenner, D. Bøgh, M. Frost, A. Knage-Rasmussen, and I. G. Economou, "Use of monomer fraction data in the parametrization of association theories," *Fluid Phase Equilibria*, vol. 296, no. 2, pp. 219–229, 2010.

[28] E. Forte, J. Burger, K. Langenbach, H. Hasse, and M. Bortz, "Multi-Criteria Optimization for Parameterization of SAFT-Type Equations of State for Water," *AIChE Journal*, vol. 64, no. 1, pp. 226–237, 2018.

[29] J. T. Cripwell, F. J. Kruger, and A. J. Burger, "Accounting for cross association in non-self-associating species using a physically consistent SAFT-VR Mie approach," *Fluid Phase Equilibria*, vol. 483, pp. 1–13, 2019.

[30] V. Papaioannou, T. Lafitte, C. Avendaño, C. S. Adjiman, G. Jackson, and E. A. Müller, "Group contribution methodology based on the statistical associating fluid theory for heteronuclear molecules formed from Mie segments," *The Journal of Chemical Physics*, vol. 140, no. 5, 2014.

[31] S. Tamouza, J. P. Passarello, P. Tobaly, and J. C. De Hemptinne, "Group contribution method with SAFT EOS applied to vapor liquid equilibria of various hydrocarbon series," *Fluid Phase Equilibria*, vol. 222–223, pp. 67–76, 2004.

[32] S. Tamouza, J. P. Passarello, P. Tobaly, and J. C. De Hemptinne, "Application to binary mixtures of a group contribution SAFT EOS (GC-SAFT)," *Fluid Phase Equilibria*, vol. 228–229, pp. 409–419, 2005.

[33] S. Dufal, V. Papaioannou, M. Sadeqzadeh, T. Pogiatzis, A. Chremos, C. S. Adjiman, G. Jackson, and A. Galindo, "Prediction of Thermodynamic Properties and Phase Behavior of Fluids and Mixtures with the SAFT-γ Mie Group-Contribution Equation of State," *Journal of Chemical and Engineering Data*, vol. 59, no. 10, pp. 3272–3288, 2014.

[34] P. Hutacharoen, S. Dufal, V. Papaioannou, R. M. Shanker, C. S. Adjiman, G. Jackson, and A. Galindo, "Predicting the Solvation of Organic Compounds in Aqueous Environments: From Alkanes and Alcohols to Pharmaceuticals," *Industrial and Engineering Chemistry Research*, vol. 56, no. 38, pp. 10856–10876, 2017.

[35] S. Z. S. Al Ghafri, G. C. Maitland, and J. P. M. Trusler, "Phase Behavior of the System (Carbon Dioxide + *n*-Heptane + Methylbenzene): A Comparison between Experimental Data and SAFT-γ-Mie Predictions," *Journal of Chemical and Engineering Data*, vol. 62, no. 9, pp. 2826–2836, 2017.

[36] A. Lymperiadis, C. S. Adjiman, A. Galindo, and G. Jackson, "A group contribution method for associating chain molecules based on the statistical associating fluid theory (SAFT-γ)," *Journal of Chemical Physics*, vol. 127, no. 23, p. 234903, 2007.

[37] A. Lymperiadis, C. S. Adjiman, G. Jackson, and A. Galindo, "A generalisation of the SAFT-γ group contribution method for groups comprising multiple spherical segments," *Fluid Phase Equilibria*, vol. 274, pp. 85–104, 2008.

[38] U. Weidlich and J. Gmehling, "A Modified UNIFAC Model. 1. Prediction of VLE, h^E, and γ^∞," *Industrial and Engineering Chemistry Research*, vol. 26, no. 7, pp. 1372–1381, 1987.

[39] M. Sadeqzadeh, V. Papaioannou, S. Dufal, C. S. Adjiman, G. Jackson, and A. Galindo, "The development of unlike induced association-site models to study the phase behaviour of aqueous mixtures comprising acetone, alkanes and alkyl carboxylic acids with the SAFT-γ Mie group contribution methodology," *Fluid Phase Equilibria*, vol. 407, pp. 39–57, 2016.

[40] S. H. Huang and M. Radosz, "Equation of State for Small , Large , Polydisperse , and Associating Molecules," pp. 2284–2294, 1990.

[41] W. G. Chapman, K. E. Gubbins, and G. Jackson, "Phase equilibria of associating fluids: Chain molecules with multiple bonding sites," *Molecular Physics*, vol. 65, no. 5, pp. 1057–1079, 1988.

[42] J. M. Prausnitz, R. N. Lichtenthaler, and E. G. de Azevedo, "Intermolecular Forces, Corresponding States and Osmotic Systems," in *Molecular Thermodynamics of Fluid-Phase Equilibria*, 3rd ed., Prentice-Hall PTR, 1999, p. 57.

[43] F. London, "Zur Theorie und Systematik der Molekularkräft," *Zeitschrift für Physik*, vol. 63, no. 3–4, pp. 245–279, 1930.

[44] F. London, "The General Theory of Molecular Forces," *Transactions of the Faraday Society*, vol. 33, pp. 8–26, 1937.

[45] J. E. Lennard-Jones, "On the Determination of Molecular Fields," *Proceedings of the Royal Society of London*, vol. 106, no. 738, pp. 463–477, 1924.

[46] S. Dufal, T. Lafitte, A. J. Haslam, A. Galindo, G. N. I. Clark, C. Vega, and G. Jackson, "The A in SAFT: Developing the contribution of association to the Helmholtz free energy within a Wertheim TPT1 treatment of generic Mie fluids," *Molecular Physics*, vol. 113, no. 9–10, pp. 948–984, 2015.

[47] J. M. Garrido, E. Cea-klapp, and I. Polishuk, "Some Observations Regarding the Association Kernel of SAFT-VR- Mie. Is the Molecularly Inspired Contribution Always Necessary?," *Industrial and Engineering Chemistry Research*, vol. 57, pp. 15869–15883, 2018.

[48] L. L. Lee, "The Ideal Gas," in *Molecular Thermodynamics of Nonideal Fluids*, H. Brenner, Ed. Boston: Butterworths, 1988, p. 37.

[49] J. A. Barker and D. Henderson, "Perturbation Theory and Equation of State for Fluids. II. A Successful Theory of Liquids," *The Journal of Chemical Physics*, vol. 47, no. 11, pp. 4714–4721, 1967.

[50] J. A. Barker and D. Henderson, "What is 'liquid'? Understanding the states of matter," *Reviews of Modern Physics*, vol. 48, no. 4, pp. 587–671, 1976.

[51] E. A. Müller and K. E. Gubbins, "Molecular-Based Equations of State for Associating Fluids: A Review of SAFT and Related Approaches," *Industrial and Engineering Chemistry Research*, vol. 40, no. 10, pp. 2193–2211, 2001.

[52] P. K. Jog and W. G. Chapman, "Application of Wertheim's thermodynamic perturbation theory to dipolar hard sphere chains," *Molecular Physics*, vol. 97, pp. 307–319, 1999.

[53] J. Gross and J. Vrabec, "An Equation-of-State Contribution for Polar Components: Dipolar Molecules," *AIChE Journal*, vol. 52, pp. 1194–1204, 2006.

[54] A. J. de Villiers, C. E. Schwarz, and A. J. Burger, "Improving vapour-liquid-equilibria predictions for mixtures with non-associating polar components using sPC-SAFT extended with two dipolar terms," *Fluid Phase Equilibria*, vol. 305, no. 2, pp. 174–184, 2011.

[55] J. T. Cripwell, S. A. M. Smith, C. E. Schwarz, and A. J. Burger, "SAFT-VR Mie: Application to Phase Equilibria of Alcohols in Mixtures with *n*-Alkanes and Water," *Industrial and Engineering Chemistry Research*, vol. 57, no. 29, pp. 9693–9706, 2018.

[56] V. Papaioannou, C. S. Adjiman, G. Jackson, and A. Galindo, "Simultaneous prediction of vapour-liquid and liquid-liquid equilibria (VLE and LLE) of aqueous mixtures with the SAFT-γ group contribution approach," *Fluid Phase Equilibria*, vol. 306, no. 1, pp. 82–96, 2011.

[57] J. T. Cripwell, C. E. Schwarz, and A. J. Burger, "Vapor-Liquid Equilibria Measurements for the Nine *N*-Alkane/Ketone Pairs Comprising 2-, 3-, and 4-Heptanone with *n*-Octane, *n*-Nonane, and *n*-Decane," *Journal of Chemical and Engineering Data*, vol. 60, no. 3, pp. 602–611, 2015.

[58] "MATLAB." The MathWorks, Inc., Natick, Massachusetts, United States.

[59] J. T. Cripwell, "Improvement of the Thermodynamic Description of Polar Molecules and Their Mixtures in the SAFT Framework," Stellenbosch University, 2017.

[60] A. J. de Villiers, "Evaluation and improvement of the sPC-SAFT equation of state for complex mixtures," Stellenbosch University, 2011.

[61] M. Michelsen and J. Mollerup, *Thermodynamic Models: Fundamentals & Computational Aspects*, 2nd ed. Copenhagen: Tie-Line Publications, 2007.

[62] K. Levenberg, "A Method for the Solution of Certain Non-Linear Problems in Least Squares," *Quarterly of Applied Mathematics*, vol. 2, pp. 164–168, 1944.

[63] D. Marquart, "An Algorithm for Least-Squares Estimation of Nonlinear Parameters," *SIAM Journal on Applied Mathematics*, vol. 11, no. 2, pp. 431–441, 1963.

[64] "DIPPR® 801 Database, Design Institute for Physical Properties of the American Institute of Chemical Engineers," *American Institute of Chemical Engineers*. [Online]. Available: https://www.aiche.org/dippr/events-products/801-database.

[65] W. E. Acree and J. S. Chickos, "Phase Transition Enthalpy Measurements of Organic and Organometallic Compounds," *NIST Chemistry WebBook, NIST Standard Reference Database Number 69*. .

[66] J. L. Daridon, H. Carrier, and B. Lagourette, "Pressure Dependence of the Thermophysical Properties of *n*-Pentadecane and *n*-Heptadecane," *International Journal of Thermophysics*, vol. 23, no. 3, pp. 697–708, 2002.

[67] S. Dutour, J. Daridon, and B. Lagourette, "Speed of sound , density , and compressibilities of liquid eicosane and docosane at various temperatures and pressures," *High Temperatures - High Pressures*, vol. 33, pp. 371–378, 2001.

[68] A. Pal, H. Kumar, R. Maan, and H. K. Sharma, "Volumetric and Ultrasonic Studies of Molecular Interactions in *n*-Alkoxypropanols + Alkyl Acetates Mixtures at Different Temperatures," *Journal of Chemical and Engineering Data*, vol. 58, no. 11, pp. 3190–3200, 2013.

[69] M. K. Patwari, R. K. Bachu, S. Boodida, and S. Nallani, "Densities, Viscosities, and Speeds of Sound of Binary Liquid Mixtures of Sulfolane with Ethyl Acetate, *n*-Propyl Acetate, and *n*-Butyl Acetate at Temperature of (303.15, 308.15, and 313.15) K," *Journal of Chemical and Engineering Data*, vol. 54, no. 3, pp. 1069–1072, 2009.

[70] Y. A. Neruchev, M. F. Bolotnikov, and V. V. Zotov, "Исследования Скорости Ультразвука в Органических Жидкостях на Линии Насыщения," *Теплофизика Высоких Температур*, vol. 43, no. 2, pp. 274–316, 2005.

[71] H. Feng, W. Gao, Z. Sun, B. Lei, G. Li, and L. Chen, "Molecular Dynamics Simulation of Diffusion and Structure of Some n-Alkanes in near Critical and Supercritical Carbon Dioxide at Infinite Dilution," *Journal of Physical Chemistry B*, vol. 117, no. 41, pp. 12525–12534, 2013.

[72] L. Fernández, P. Estafanía, J. Ortega, and J. Wisniak, "Measurements of the Excess Properties and Vapor-Liquid Equilibria at 101.32 kPa for Mixtures of Ethyl Ethanoate + Alkanes (from C_5 to C_{10})," *Journal of Chemical and Engineering Data*, vol. 55, pp. 5519–5533, 2010.

[73] L. Fernández, J. Ortega, E. Pérez, F. Toledo, and J. Canosa, "Multiproperty Correlation of Experimental Data of the Binaries Propyl Ethanoate + Alkanes (Pentane to Decane). New Experimental Information for Vapor-Liquid Equilibrium and Mixing properties," *Journal of Chemical and Engineering Data*, vol. 58, no. 3, pp. 686–706, 2013.

[74] J. T. Cripwell, C. E. Schwarz, and A. J. Burger, "Vapor–Liquid Equilibria Measurements for the Five Linear C_6 Esters with *n*-Octane," *Journal of Chemical and Engineering Data*, vol. 61, pp. 2353–2362, 2016.

[75] L. Pias, M. I. Paz-Andrade, F. Sarmiento, E. Rodriguez-Nunez, and J. Fernandez, "Excess Molar Enthalpies of Butyl Acetate + an n-Alkane at 298.15 K *," *Fluid Phase Equilibria*, vol. 28, no. 2, pp. 183–189, 1986.

[76] K. Katz and M. Newman, "Vapor-Liquid Equilibria for Ethyl Alcohol – *n*-Heptane at Low Pressure," *Industrial & Engineering Chemistry Research*, vol. 48, no. 1, pp. 137–141, 1956.

[77] M. D. Peña and D. R. Cheda, "Equilibrio liquido—vapor. III. Los sistemas *n*-propanol + *n*-hexano a 50°C y *n*-propanol + *n*-heptano a 60°C," *Anales de la Real Sociedad Española de Química*, vol. 66, pp. 747–755, 1970.

[78] I. Máchová, J. Linek, and I. Wichterle, "Vapour-Liquid Equilibria in the Heptane - 1-Pentanol and Heptane - 3-Methyl-1-Butanol Systems at 75, 85 and 95 °C," *Fluid Phase Equilibria*, vol. 41, no. 3, pp. 257–267, 1988.

[79] C. G. Savini, D. R. Winterhalter, and H. C. van Ness, "Excess Enthalpies of 1-Propanol+ Heptane Mixtures," *Int. Data Ser., Sel. Data Mixtures, Ser. A*, vol. 11, 1976.

[80] A. J. Treszczanowicz and G. C. Benson, "Excess volumes for n-alkanols + n-alkanes I. Binary mixtures of methanol, ethanol, n-propanol, and n-butanol + n-heptane," *The Journal of Chemical Thermodynamics*, vol. 9, no. 12, pp. 1189–1197, 1977.

[81] R. Tanaka, S. Toyama, and S. Murakami, "Heat capacities of $\{xC_nH_{2n+1}OH + (1 - x)C_7H_{16}\}$ for n = 1 to 6 at 298.15 K," *The Journal of Chemical Thermodynamics*, vol. 18, no. 1, pp. 63–73, 1986.

[82] V. A. Atoyan and I. A. Mamedov, "Speed and Absorption of Sounds, Viscosity and Density of Methylhexylketone in Relation to the Temperature and Pressure," *Izv. Vyssh. Uchebn. Zaved., Neft Gaz.*, vol. 18, pp. 74–78, 1975.

[83] O. Urdaneta, Y. P. Handa, and G. C. Benson, "Thermodynamic properties of binary mixtures containing ketones: V. Excess enthalpies of an isomeric heptanone + *n*-heptane," *Journal of Chemical Thermodynamics*, vol. 11, pp. 857–860, 1979.

[84] D. O. Hanson and M. van Winkle, "Alteration Of The Relative Volatility Of Hexane-1-Hexene By Oxygenated And Chlorinated Solvents," *Journal of Chemical and Engineering Data*, vol. 12, no. 3, pp. 319–325, 1967.

[85] L. Pikkarainen, "Excess Enthalpies of Binary Solvent Mixtures of 2-Butanone with Aliphatic Alcohols," *Thermochimica Acta*, vol. 114, no. 2, pp. 239–244, 1987.

[86] M. Do Seo, Y. Jo Kim, J. Sung Lim, and J. Won Kang, "Measurement and correlation of the isobaric vapor-liquid equilibrium for mixtures of alcohol+ketone systems at atmospheric pressure," *Korean Journal of Chemical Engineering*, vol. 29, no. 1, pp. 103–110, 2012.

[87] M. A. Varfolomeev, I. T. Rakipov, B. N. Solomonov, and W. Marczak, "Speed of Sound, Density, and Related Thermodynamic Excess Properties of Binary Mixtures of Butan-2-one with C1–C4 *n*-Alkanols and Chloroform," *Journal of Chemical and Engineering Data*, vol. 61, no. 3, pp. 1032–1046, 2016.

[88] A. Cobos, F. Hevia, J. A. González, I. García De La Fuente, and C. Alonso Tristán, "Thermodynamics of amide + ketone mixtures. 1. Volumetric, speed of sound and refractive index data for *N*,*N*-dimethylformamide + 2-alkanone systems at several temperatures," *The Journal of Chemical Thermodynamics*, vol. 98, pp. 21–32, 2016.

[89] G. C. Benson, "Excess Gibbs energy and liquid-vapor equilibrium in 2-butanone + normal alkane (C_6-C_8, C_{12}, C_{16}) binary mixtures," *Int. DATA Ser., Sel. Data Mixtures, Ser. A*, vol. 1, pp. 31–40, 1980.

[90] M. Takeo, K. Nishii, T. Nitta, and T. Katayama, "Isothermal Vapor-Liquid Equilibria for Two Binary Mixtures of Heptane with 2-Butanone and 4-4-Methyl-2-Pentanone Measured by a Dynamic Still with a Pressure Regulation," *Fluid Phase Equilibria*, vol. 3, pp. 123–131, 1979.

[91] J. E. Grolier and G. C. Benson, "Thermodynamic properties of binary mixtures containing ketones. VIII. Heat capacities and volumes of some *n*-alkanone + *n*-alkane mixtures at 298.15 K," *Canadian Journal of Chemistry*, vol. 64, no. 5, pp. 949–953, 1984.

[92] O. Kiyohara, P. Handa, and G. C. Benson, "Thermodynamic properties of binary mixtures containing ketones III . Excess enthalpies some aliphatic ketones "," no. 17398, pp. 453–460, 1979.

[93] K. Ohomuro, K. Tamura, and S. Murakami, "Speeds of sound, excess molar volumes, and isentropic compressibilities of '$x$$CH_3COC_2H_5$+(1 - x)C_7H_{16}'',...,'" *The Journal of Chemical Thermodynamics*, vol. 19, no. 2, pp. 163–169, 1987.

[94] N. F. Martínez, E. Lladosa, M. C. Burguet, and J. B. Montón, "Isobaric vapour-liquid equilibria for binary systems of 2-butanone with ethanol, 1-propanol, and 2-propanol at 20 and 101.3 kPa," *Fluid Phase Equilibria*, vol. 270, no. 1–2, pp. 62–68, 2008.

[95] H. Tanaka, T. Muramatsu, and M. Kato, "Isobaric Vapor-Liquid Equilibria for Three Binary Systems of 2-Butanone with 3-Methyl-1-butanol, 1-Butanol, or 2-Butanol," *Journal of Chemical and Engineering Data*, vol. 37, no. 2, pp. 164–166, 1992.

[96] H. Yoshikawa and M. Kato, "Vapor-Liquid Equilibria for Three Binary Systems Made of Methyl Ethyl Ketone with Acetone, Methyl Acetate, or *N*-Amyl Alcohol," *Journal of Chemical and Engineering Data*, vol. 36, no. 1, pp. 57–60, 1991.

[97] R. Abbas and J. Gmehling, "Vapour-liquid equilibria, azeotropic data, excess enthalpies, activity coefficients at infinite dilution and solid-liquid equilibria for binary alcohol-ketone systems," *Fluid Phase Equilibria*, vol. 267, no. 2, pp. 119–126, 2008.

[98] A. J. de Villiers, C. E. Schwarz, and A. J. Burger, "Extension of the CPA equation of state with dipolar theories to improve vapour-liquid-equilibria predictions," *Fluid Phase Equilibria*, vol. 312, no. 1, pp. 66–78, 2011.

[99] J. T. Cripwell, C. E. Schwarz, and A. J. Burger, "Polar (s)PC-SAFT: Modelling of polar structural isomers and identification of the systematic nature of regression issues," *Fluid Phase Equilibria*, vol. 449, pp. 156–166, 2017.

[100] C. Marcolli and T. Peter, "Water activity in polyol / water systems: new UNIFAC parameterization," *Atmospheric Chemistry and Physics, European Geosciences Union*, vol. 5, no. 6, pp. 1545–1555, 2005.

[101] J. Chen, Z. Li, and Y. Li, "A method for predicting VLE and H^E of chain-like isomers using a modified UNIFAC model," *Fluid Phase Equilibria*, vol. 74, no. C, pp. 47–65, 1992.

[102] R. Fuchs, L. Krenzer, and J. Gaube, "Excess Properties of Binary Mixtures Composed of a Polar Component and an Alkane," *Berichte der Bunsengesellschaft für physikalische Chemie*, vol. 88, no. 7, pp. 642–649, 1984.

[103] M. Vidal, J. Ortega, and J. Plácido, "Thermodynamic properties of (an ethyl ester + *n*-alkane)," *The Journal of Chemical Thermodynamics*, vol. 29, no. 1, pp. 47–74, 1997.

[104] R. Ríos, J. Ortega, L. Fernández, I. De Nuez, and J. Wisniak, "Improvements in the Experimentation and the Representation of Thermodynamic Properties (iso-*p* VLE and y^E) of Alkyl Propanoate + Alkane Binaries," *Journal of Chemical and Engineering Data*, vol. 59, no. 1, pp. 125–142, 2014.

[105] J. Ortega, C. González, and S. Galván, "Vapor-Liquid Equilibria for Binary Systems Composed of a Propyl Ester (Ethanoate, Propanoate, Butanoate) + an *n*-Alkane (C_7, C_9)," *Journal of Chemical and Engineering Data*, vol. 46, no. 4, pp. 904–912, 2001.

[106] J. Ortega, M. Vidal, and J. Plácido, "Thermodynamic properties of (a propyl ester + *n*-alkane)," *Journal of Chemical Thermodynamics*, vol. 31, no. 8, pp. 1025–1044, 1999.

[107] N. V. Sastry, N. J. Jain, A. George, and P. Bahadur, "Viscosities, speeds of sound and excess isentropic compressibilities of binary mixtures of alkyl alkanoate-hydrocarbons at 308.15 K and 318.15 K," *Fluid Phase Equilibria*, vol. 163, no. 2, pp. 275–289, 1999.

[108] S. W. Benson, "Methods for the Estimation of Thermochemical Data," in *Thermochemical Kinetics: Methods for the Estimation of Thermodynamical Data and Rate Parameters*, 2nd ed., New York: John Wiley & Sons, 1976, pp. 19–72.

[109] D. Dalmazzone, A. Salmon, and S. Guella, "A second order group contribution method for the prediction of critical temperatures and enthalpies of vaporization of organic compounds," *Fluid Phase Equilibria*, vol. 242, no. 1, pp. 29–42, 2006.

[110] L. Constantinou and R. Gani, "New Group Contribution Method for Estimating Properties of Pure Compounds," *AIChE Journal*, vol. 40, no. 10, pp. 1697–1710, 1994.

[111] M. L. Mavrovouniotis, "Estimation of Properties from Conjugate Forms of Molecular Structures: The ABC Approach," *Industrial and Engineering Chemistry Research*, vol. 29, no. 9, pp. 1943–1953, 1990.

[112] A. Tihic, G. M. Kontogeorgis, N. Von Solms, M. L. Michelsen, and L. Constantinou, "A Predictive Group-Contribution Simplified PC-SAFT Equation of State: Application to Polymer Systems," *Industrial and Engineering Chemistry Research*, vol. 47, pp. 5092–5101, 2008.

[113] T. Walter, U. Bardelmeier, and A. Wuerflinger, "Ultrasonic Studies of Rotational Isomerism and P, V, T Data of 2-Methylbutane at Elevated Pressures," *Berichte der Bunsengesellschaft für physikalische Chemie*, vol. 96, pp. 717–721, 1992.

[114] F. Plantier and J. L. Daridon, "Speed of Sound of 2-Methylpentane, 2,3-Dimethylpentane, and 2,2,4-Trimethylpentane from (293.15 to 373.15) K and up to 150 MPa," *Journal of Chemical and Engineering Data*, vol. 50, no. 6, pp. 2077–2081, 2005.

[115] A. M. Awwad and R. A. Pethrick, "Adiabatic Compressibility of Branched Chain Hydrocarbons - Pentanes and Hexanes," *Journal of Molecular Liquids*, vol. 25, pp. 115–127, 1983.

[116] D. J. Luning Prak, E. K. Brown, and P. C. Trulove, "Density, Viscosity, Speed of Sound, and Bulk Modulus of Methyl Alkanes, Dimethyl Alkanes, and Hydrotreated Renewable Fuels," *Journal of Chemical and Engineering Data*, vol. 58, no. 7, pp. 2065–2075, 2013.

[117] A. Lainez, J. A. Zollweg, and W. B. Streett, "Speed-of-sound measurements for liquid *n*-pentane and 2,2-dimethylpropane under pressure," *Journal of Chemical Thermodynamics*, vol. 22, pp. 937–948, 1990.

[118] E. B. Freyer, J. C. Hubbard, H. Donald, and Andrews, "Sonic Studies of the Physical Properties of Liquids. I. The Sonic Interferometer. The Velocity of Sound in Some Organic Liquids and Their Compressibilities," *Journal of the American Chemical Society*, vol. 51, no. 3, pp. 759–770, 1929.

[119] H. M. Huffman, M. E. Gross, D. W. Scott, and J. P. McCullough, "Low Temperature Thermodynamic Properties of Six Isomeric Heptanes," *Journal of Physical Chemistry*, vol. 65, no. 3, pp. 495–503, 1961.

[120] S. Weissman and S. E. Wood, "Vapor-Liquid Equilibrium of Benzene–2,2,4-Trimethylpentane Mixtures," *The Journal of Chemical Physics*, vol. 32, p. 1153, 1960.

[121] Y. Peng, K. D. Goff, M. C. dos Ramos, and C. McCabe, "Developing a predictive group-contribution-based SAFT-VR equation of state," *Fluid Phase Equilibria*, vol. 277, no. 2, pp. 131–144, 2009.

[122] S. Dufal, T. Lafitte, A. Galindo, G. Jackson, and A. J. Haslam, "Developing Intermolecular-Potential Models for Use with the SAFT-VR Mie Equation of State," *AIChE Journal*, vol. 61, no. 9, pp. 2891–2912, 2015.

[123] F. J. Toledo-Marante, J. Ortega, M. Chaar, and M. Vidal, "Thermodynamic properties of (a butyl ester + *n*-alkane)," *Journal of Chemical Thermodynamics*, vol. 32, no. 8, pp. 1013–1036, 2000.

[124] C. Berro and A. Péneloux, "Excess Gibbs Energies and Excess Volumes of 1-Butanol–*n*-Heptane and 2-Methyl-1-Propanol–*n*-Heptane Binary Systems," *Journal of Chemical and Engineering Data*, vol. 29, no. 2, pp. 206–210, 1984.

[125] H. C. van Ness, C. A. Soczek, and N. K. Kochar, "Thermodynamic Excess Properties for Ethanol–*n*-Heptane," *Journal of Chemical and Engineering Data*, vol. 12, no. 3, pp. 346–351, 1967.

[126] J. L. Fortier and G. C. Benson, "Excess heat capacities of binary liquid mixtures determined with a Picker flow calorimeter," *The Journal of Chemical Thermodynamics*, vol. 8, no. 5, pp. 411–423, 1976.

[127] T. H. Nguyen and G. A. Ratcliff, "Heats of Mixing of *n*-Alcohol–*n*-Alkane Systems at 15° and 55°C," *Journal of Chemical and Engineering Data*, vol. 20, no. 3, pp. 252–255, 1975.

[128] S. E. M. Hamam, M. K. Kumaran, and G. C. Benson, "Excess enthalpies of some binary mixtures: (a C_5-alkanol+*n*-heptane) at 298.15 K," *The Journal of Chemical Thermodynamics*, vol. 16, no. 11, pp. 1013–1017, 1984.

[129] W. E. Vaughan and F. C. Collins, "P-V-T-x Relations of the System Propane-Isopentane," *Industrial & Engineering Chemistry*, vol. 34, no. 7, pp. 885–890, 1942.

[130] C. L. Ho and R. R. Davison, "Vapor-Liquid Equilibriums for the Binary Systems *n*-Hexane with 2-Methylpentane, 3-Methylpentane, and 2,4-Dimethylpentane," *Journal of Chemical and Engineering Data*, vol. 24, no. 4, pp. 293–296, 1979.

[131] T. E. Vittal Prasad, N. Sriram, A. N. Raju, and D. H. L. Prasad, "(Vapor + liquid) equilibria of binary mixtures formed by *iso*-octane with a variety of compounds at 95.8 kPa," *Journal of Chemical Thermodynamics*, vol. 38, no. 2, pp. 119–122, 2006.

[132] E. K. Liu and R. R. Davison, "Vapor-Liquid Equilibria for the Binary Systems *n*-Octane with 2-Methylpentane, 3-Methylpentane, and 2,4-Dimethylpentane," *Journal of Chemical and Engineering Data*, vol. 26, no. 1, pp. 85–88, 1981.

[133] S. S. Chen and B. J. Zwolinski, "Excess Thermodynamic Functions of Binary Mixtures of Normal and Isomeric Alkanes (C5 and C6)," *Journal of the Chemical Society, Faraday Transactions 2*, vol. 70, pp. 1133–1142, 1974.

[134] Dortmund Data Bank 2019, "Parameters of the Original UNIFAC Model." [Online]. Available: http://www.ddbst.com/published-parameters-unifac.html.

Appendix A: SAFT-γ Mie Code Validation

A.1 Derivatives Comparison

$$\frac{dF(x)}{dx} = \frac{F(x+\Delta) - F(x-\Delta)}{2\Delta} \tag{A.1}$$

Two-point numerical differentiation (the equation above) was used to calculate the values in the "Numerical" columns of Tables A.1 to A.5. The difference between the analytical and numerical derivatives are given in the following tables for 1-butanol at a temperature of 300 K and a volume of 0.100 L/mol.

Table A.1: Hard-sphere term derivatives validation

Derivative	Analytical	Numerical	Difference (%)
$\partial F/\partial n_i$	20.693803972	20.693803971	4.832E-09
$\partial F/\partial T$	-0.0016615643913	-0.0016615643927	8.426E-08
$\partial F/\partial V$	-136.8160171	-136.8160221	3.655E-06
$\partial^2 F/(\partial n_i \partial n_j)$	52.575501040	52.575501039	1.902E-09
$\partial^2 F/(\partial n_i \partial T)$	-0.006386229538	-0.006386228435	1.727E-05
$\partial^2 F/(\partial n_i \partial V)$	-525.75501040	-525.75501068	5.326E-08
$\partial^2 F/\partial T^2$	3.4209297006E-06	3.4209295553E-06	4.247E-06
$\partial^2 F/(\partial T \partial V)$	0.047246651467	0.047246654204	5.793E-06
$\partial^2 F/\partial V^2$	5257.550104	5257.550479	7.133E-06

Table A.2: Dispersion term derivatives validation

Derivative	Analytical	Numerical	Difference (%)
$\partial F/\partial n_i$	-26.120483105	-26.120483104	3.828E-09
$\partial F/\partial T$	0.045262366545	0.045262366566	4.640E-08
$\partial F/\partial V$	134.6637943	134.6637940	2.228E-07
$\partial^2 F/(\partial n_i \partial n_j)$	-21.559756531	-21.559756528	1.391E-08
$\partial^2 F/(\partial n_i \partial T)$	0.095722716853	0.095722716847	6.268E-09
$\partial^2 F/(\partial n_i \partial V)$	215.59756531	215.59754953	7.319E-06
$\partial^2 F/\partial T^2$	-0.00031655012980	-0.00031626450764	0.09023
$\partial^2 F/(\partial T \partial V)$	-0.5046035031	-0.5046035030	1.982E-08
$\partial^2 F/\partial V^2$	-2155.9756531	-2155.9754897	7.579E-06

Table A.3: Chain term derivatives validation

Derivative	Analytical	Numerical	Difference (%)
$\partial F/\partial n_i$	-2.6348725696	-2.6348725671	9.488E-08
$\partial F/\partial T$	-0.0033528993646	-0.0033528993776	3.877E-07
$\partial F/\partial V$	22.498463993	22.498464628	2.822E-06
$\partial^2 F/(\partial n_i \partial n_j)$	-9.5857279603	-9.5857279181	4.402E-07
$\partial^2 F/(\partial n_i \partial T)$	-0.0024170400497	-0.0024170447865	1.960E-04
$\partial^2 F/(\partial n_i \partial V)$	95.857279603	95.857281076	1.537E-06
$\partial^2 F/\partial T^2$	2.3675146521E-05	2.3434769750E-05	1.015
$\partial^2 F/(\partial T \partial V)$	-0.009358593149	-0.009358594445	1.385E-05
$\partial^2 F/\partial V^2$	-958.57279603	-958.57282346	2.862E-06

Table A.4: Association term derivatives validation

Derivative	Analytical	Numerical	Difference (%)
$\partial F/\partial n_i$	-5.1196443139	-5.1196442832	5.997E-07
$\partial F/\partial T$	0.020362903930	0.020362903996	3.241E-07
$\partial F/\partial V$	22.632442432	22.632442423	3.977E-08
$\partial^2 F/(\partial n_i \partial n_j)$[a]		-5.9011648603	
$\partial^2 F/(\partial n_i \partial T)$	0.023640267769	0.023640267353	1.760E-06
$\partial^2 F/(\partial n_i \partial V)$	59.011648648	59.011646716	3.274E-06
$\partial^2 F/\partial T^2$	-0.00017295880435	-0.00017295880460	1.445E-07
$\partial^2 F/(\partial T \partial V)$	-0.032773638388	-0.032773637635	2.298E-06
$\partial^2 F/\partial V^2$	-590.11648648	-590.11388518	4.408E-04

[a]The second composition derivative of the association state function contribution is calculated through numerical differentiation only.

Table A.5: Combined state function derivatives validation

Derivative	Analytical	Numerical	Difference (%)
$\partial F/\partial n_i$	-13.181196017	-13.181196016	7.587E-09
$\partial F/\partial T$	0.060610806720	0.060610806774	8.909E-08
$\partial F/\partial V$	42.978683604	42.978678960	1.081E-05
$\partial^2 F/(\partial n_i \partial n_j)$	15.528851689	15.528851693	2.576E-08
$\partial^2 F/(\partial n_i \partial T)$	0.11055971503	0.11055971504	9.045E-09
$\partial^2 F/(\partial n_i \partial V)$	-155.28851684	-155.28856125	2.860E-05
$\partial^2 F/\partial T^2$	-0.00046241285792	-0.00046236761642	0.009784
$\partial^2 F/(\partial T \partial V)$	-0.49948908314	-0.49948908015	5.986E-07
$\partial^2 F/\partial V^2$	1552.8851684	1552.8857054	3.458E-05

A.2 %AAD Comparisons

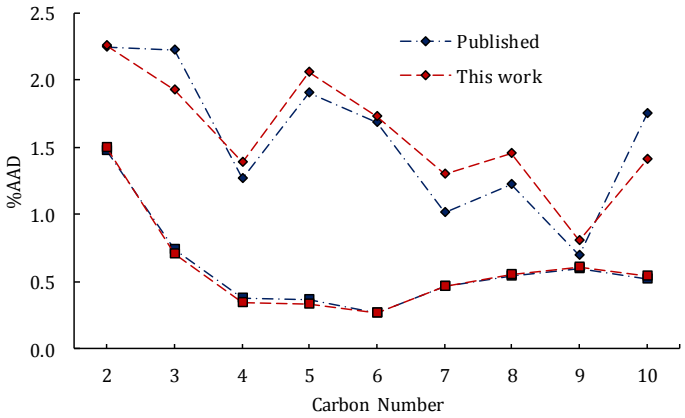

Figure A.1: Comparison of published and calculated %AADs for *n*-alkanes. The diamonds correspond to P^{vap} and the squares to ρ^{sat}.

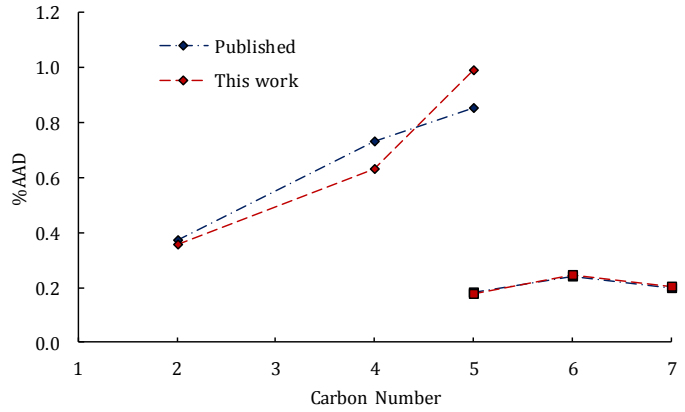

Figure A.2: Comparison of published and calculated %AADs for *n*-alkyl acetates. The carbon number on the x-axis refers to the length of the *n*-alkyl branch. The diamonds correspond to P^{vap} and the squares to ρ^{sat}.

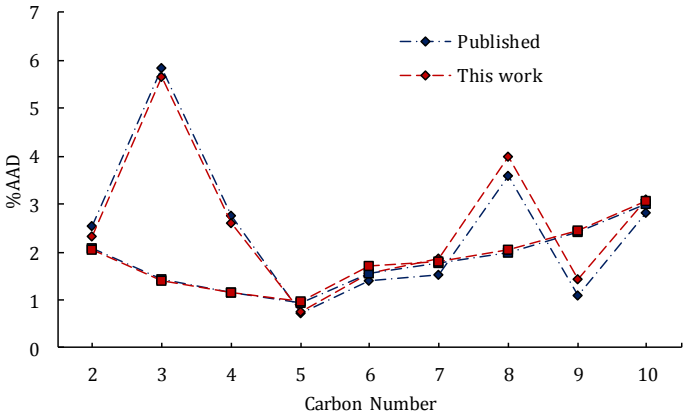

Figure A.3: Comparison of published and calculated %AADs for 1-alcohols. The diamonds correspond to P^{vap} and the squares to ρ^{sat}.

Appendix B: SAFT-γ Mie Parameters

Two sets were generated for the functional groups parameterised in this work. The best one was chosen and added to the summary tables.

Table B.1: Summary of functional-group-specific parameters.

Group k	ν_k^*	S_k	σ_{kk} (Å)	λ_{kk}^{a}	λ_{kk}^{r}	ϵ_{kk}/k_B (K)	$n_{k,H}$	n_{k,e_1}	n_{k,e_2}	Ref.
aCH	1	0.32184	4.0578	6.0000	14.756	371.53				[33]
C	1	0.04072	5.6571	6.0000	8.0000	50.020				[33]
CH	1	0.07210	5.2950	6.0000	8.0000	95.621				[33]
CH=	1	0.20037	4.7488	6.0000	15.974	952.54				[33]
CH_2	1	0.22932	4.8801	6.0000	19.871	473.39				[30]
CH_2=	1	0.44887	4.3175	6.0000	20.271	300.90				[33]
CH_2CO	2	0.64470	3.2832	6.0000	7.5162	182.19	1	1	1	This work
CH_2OH	2	0.58538	3.4054	6.0000	22.699	407.22	1	2		[34]
CH_3	1	0.57255	4.0773	6.0000	15.050	256.77				[30]
CH_3CO	2	0.76442	3.4518	6.0000	8.2034	209.33	1	1	1	This work
CO	2	0.44504	3.0471	6.0000	6.2561	200.71	1	1	1	This work
COO	1	0.65264	3.9939	6.0000	31.189	868.92				[30]
COO (pr.)	1	0.74807	3.7187	6.0000	28.676	669.77				This work

Table B.2: Summary of functional-group dispersion interaction parameters.

Group k	Group l	ϵ_{kl}/k_B (K)	Ref.	Group k	Group l	ϵ_{kl}/k_B (K)	Ref.
aCH	aCH	371.53	[33]	CH	CH_2	506.21	[33]
aCH	CH	441.43	[33]	CH	CH_3	387.48	[33]
aCH	CH_2	415.64	[33]	CH=	CH=	952.54	[33]
aCH	CH_3	305.81	[33]	CH=	CH_2	459.40	[33]
C	C	50.020	[33]	CH=	CH_2=	275.75	[33]
C	CH_2	300.07	[33]	CH=	CH_3	252.41	[33]
C	CH_3	339.91	[33]	CH_2	CH_2	473.39	[30]
CH	CH	95.621	[33]	CH_2	CH_2=	386.80	[33]

Table B.2 (continued)

Group k	Group l	ϵ_{kl}/k_B (K)	Ref.	Group k	Group l	ϵ_{kl}/k_B (K)	Ref.
CH_2	CH_2CO	295.92	This work	CH_2OH	CH_3	333.20	[34]
CH_2	CH_2OH	423.17	[34]	CH_2OH	CH_3CO	319.57	This work
CH_2	CH_3	350.77	[30]	CH_2OH	CO	318.31	This work
CH_2	CH_3CO	298.36	This work	CH_3	CH_3CO	233.09	This work
CH_2	CO	278.15	This work	CH_3	CO	223.68	This work
CH_2	COO	498.86	[30]	CH_3	COO	402.75	[30]
CH_2	COO (pr.)	451.23	This work	CH_3	COO (pr.)	428.30	This work
CH_2=	CH_2=	300.90	[33]	CH_3CO	CH_3CO	209.33	This work
CH_2CO	CH_2CO	182.19	This work	CO	CO	200.71	This work
CH_2CO	CH_3	279.88	This work	COO	COO	868.92	[30]
CH_2OH	CH_2OH	407.22	[34]	COO (pr.)	COO (pr.)	669.77	This work

Table B.3: Summary of functional-group association interaction parameters

Group k	Site a	Group l	Site b	$\epsilon^{HB}_{kl,ab}/k_B$ (K)	$K_{kl,ab}$ (Å^3)	Ref.
CH_2CO	H	CH_2CO	e_1	921.10	413.49	This work
CH_2OH	H	CH_2OH	e_1	2097.9	62.309	[34]
CH_2OH	e_1	CH_3CO	H	876.27	323.80	This work
CH_2OH	H	CH_3CO	e_1	784.25	952.81	This work
CH_2OH	H	CH_3CO	e_2	1011.5	585.46	This work
CH_2OH	e_1	CO	H	930.61	385.52	This work
CH_2OH	H	CO	e_1	812.03	1069.0	This work
CH_2OH	H	CO	e_2	994.74	625.16	This work
CH_3CO	H	CH_3CO	e_1	1083.5	546.87	This work
CO	H	CO	e_1	1100.08	717.23	This work

Appendix C: SAFT-VR Mie Parameters

Table C.1: SAFT-VR Mie parameters

Component	m_s	σ (Å)	λ^a	λ^r	ϵ/k_B (K)	$\epsilon^{HB}_{kl,ab}/k_B$ (K)	r^c_{ab}/σ	Ref.
ethane	1.4373	3.7257	6.0000	12.400	206.12	0	0	[10]
propane	1.6845	3.9056	6.0000	13.006	239.89	0	0	[10]
n-butane	1.8514	4.0887	6.0000	13.650	273.64	0	0	[10]
n-pentane	1.9606	4.2928	6.0000	15.847	321.94	0	0	[10]
n-hexane	2.1097	4.4230	6.0000	17.203	354.38	0	0	[10]
n-heptane	2.3949	4.4282	6.0000	17.092	358.51	0	0	[10]
n-octane	2.6253	4.4696	6.0000	17.378	369.18	0	0	[10]
n-nonane	2.8099	4.5334	6.0000	18.324	387.55	0	0	[10]
n-decane	2.9976	4.5890	6.0000	18.885	400.79	0	0	[10]
n-dodecane	3.2519	4.7484	6.0000	20.862	437.72	0	0	[10]
n-pentadecane	3.9325	4.7738	6.0000	20.822	444.51	0	0	[10]
n-eicosane	4.8794	4.8788	6.0000	22.926	475.76	0	0	[10]
1-octene	2.8113	4.2743	6.0000	14.078	319.29	0	0	This work
1-decene	3.1964	4.4010	6.0000	15.311	350.04	0	0	This work
ethanol	2.0929	3.3648	6.0000	10.183	202.25	2740.9	0.40219	–[a]
1-propanol	2.3356	3.5612	6.0000	10.179	227.66	2746.2	0.35377	[10]
1-butanol	2.4377	3.7856	6.0000	11.660	278.92	2728.1	0.32449	[10]
1-pentanol	2.4568	4.014	6.0000	12.633	308.76	2632.72	0.3411	[55]
1-hexanol	2.1719	4.4301	6.0000	13.704	364.84	3105.6	0.28342	This work
ethyl acetate	3.6095	2.8246	6.0000	13.738	289.60	0	0	–[b]
propyl acetate	2.9197	3.7921	6.0000	14.419	309.66	0	0	–[b]
n-butyl acetate (Set A)	2.7739	4.0945	6.0000	17.657	370.54	0	0	–[b]
n-butyl acetate (Set B)	1.6639	5.0888	6.0000	33.658	572.87	0	0	This work
benzene	1.9163	4.0549	6.0000	14.798	372.59	0	0	[10]
2-methylbutane	1.6100	4.6269	6.0000	18.660	371.08	0	0	This work
2-methylpentane	1.9596	4.5459	6.0000	17.487	360.02	0	0	This work
2-methylhexane	2.0804	4.6769	6.0000	19.231	393.73	0	0	This work

[a] Unpublished internal parameters regressed with P^{vap}, ρ^{sat}, u, and monomer fraction IR spectroscopy data
[b] Unpublished internal parameters regressed with P^{vap}, ρ^{sat}, and u

Table C.1 (continued)

Component	m_s	σ (Å)	λ^a	λ^r	ϵ/k_B (K)	$\epsilon^{HB}_{kl,ab}/k_B$ (K)	r^c_{ab}/σ	Ref.
2-methylheptane	2.5104	4.5291	6.0000	17.078	366.30	0	0	This work
2-methyloctane	2.8146	4.5265	6.0000	18.592	382.74	0	0	This work
2-methlynonane	2.6980	4.7894	6.0000	21.343	433.78	0	0	This work
2-methyldecane	3.1857	4.6251	6.0000	19.816	410.01	0	0	This work
2,2-dimethylpropane	1.5668	4.6833	6.0000	17.208	339.09	0	0	This work
2,2-dimethylpentane	1.8660	4.8505	6.0000	19.330	402.95	0	0	This work
2,3-dimethylpentane	1.8443	4.8460	6.0000	20.193	426.25	0	0	This work
2,4-dimethylpentane	1.8123	4.9315	6.0000	21.370	424.91	0	0	This work
2,2-dimethylhexane	2.0181	4.9396	6.0000	21.104	429.42	0	0	This work
2,5-dimethylhexane	2.1357	4.8400	6.0000	20.402	415.61	0	0	This work
2,2,3-trimethylbutane	1.5103	5.2382	6.0000	22.319	472.79	0	0	This work
2,2,4-trimethylpentane	1.8340	5.1052	6.0000	21.113	439.83	0	0	This work
2,3,4-trimethylpentane	1.8326	5.0691	6.0000	21.723	464.26	0	0	This work

Note that the SAFT-VR Mie parameters generated in this work were regressed with P^{vap}, ρ^{sat}, and u data weighed 4:4:1, respectively. DIPPR correlations [64] were used for P^{vap} and ρ^{sat}, and the speed of sound datasets are those used to calculate the %AADs given in the body of the thesis.

Table C.2: SAFT-VR Mie + GV Polar parameters

Component	m_s	σ (Å)	λ^a	λ^r	ϵ/k_B (K)	$\epsilon^{HB}_{kl,ab}/k_B$ (K)	r^c_{ab}/σ	n_p	μ (D)	Ref.
2-butanone	2.6027	3.6138	6.0000	11.957	257.89	2968.2[a]	0.24806[a]	1.4308	2.76	[19]
2-pentanone	2.5546	3.8842	6.0000	14.202	309.10	2968.2[a]	0.24806[a]	1.5814	2.77	[19]
2-heptanone	3.4465	3.8386	6.0000	11.911	276.97	0	0	1.9211	2.61	[19]
2-octanone	3.1353	4.1697	6.0000	15.698	343.80	2968.2[a]	0.24806[a]	3.2393	2.7	This work
3-pentanone	2.3494	4.0097	6.0000	16.124	342.83	0	0	1.5258	2.82	[19]
3-heptanone	3.0839	3.9978	6.0000	14.653	325.04	0	0	1.8486	2.81	[19]
3-nonanone	3.8983	3.9619	6.0000	13.628	314.53	0	0	0.83463	2.6	This work
4-heptanone	2.5293	4.3476	6.0000	18.149	386.85	0	0	2.333	2.68	[19]
1-propanol	1.8962	3.8621	6.0000	9.9271	221.26	2900.0	0.3149	2.80	1.7	[55]
1-butanol	2.4050	3.8075	6.0000	11.106	261.48	2779.6	0.32998	1.4963	1.67	This work
1-pentanol	2.3796	4.0621	6.0000	12.554	307.13	2661.9	0.3362	1.8315	1.7	[55]

[a]The association parameters for 2-ketones were regressed for this work with 2-butanone + 1-butanol VLE data from Tanaka et al. [95] (weight = 20) and 2-butanone + 1-butanol excess enthalpy data from Pikkarainen [85] (weight = 1).

Appendix D: Supporting Results

D.1 *n*-Alkane Saturation Property Accuracy Comparisons

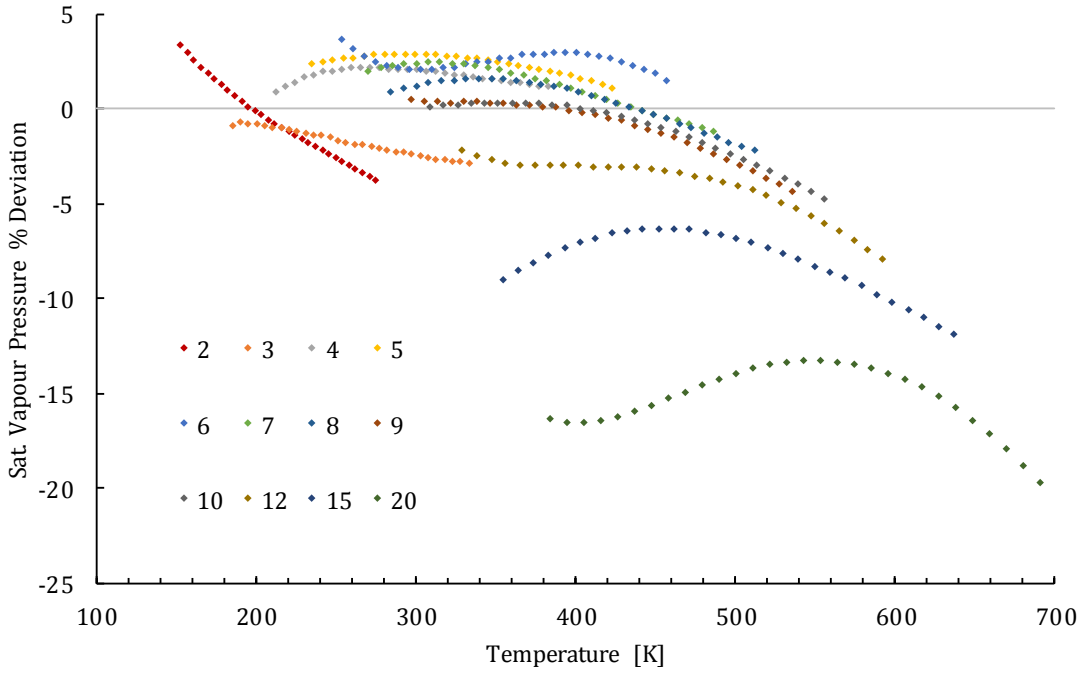

Figure D.1: SAFT-γ Mie P^{vap} % deviation from DIPPR correlations [64] for *n*-alkanes. Component carbon numbers are given in the legend.

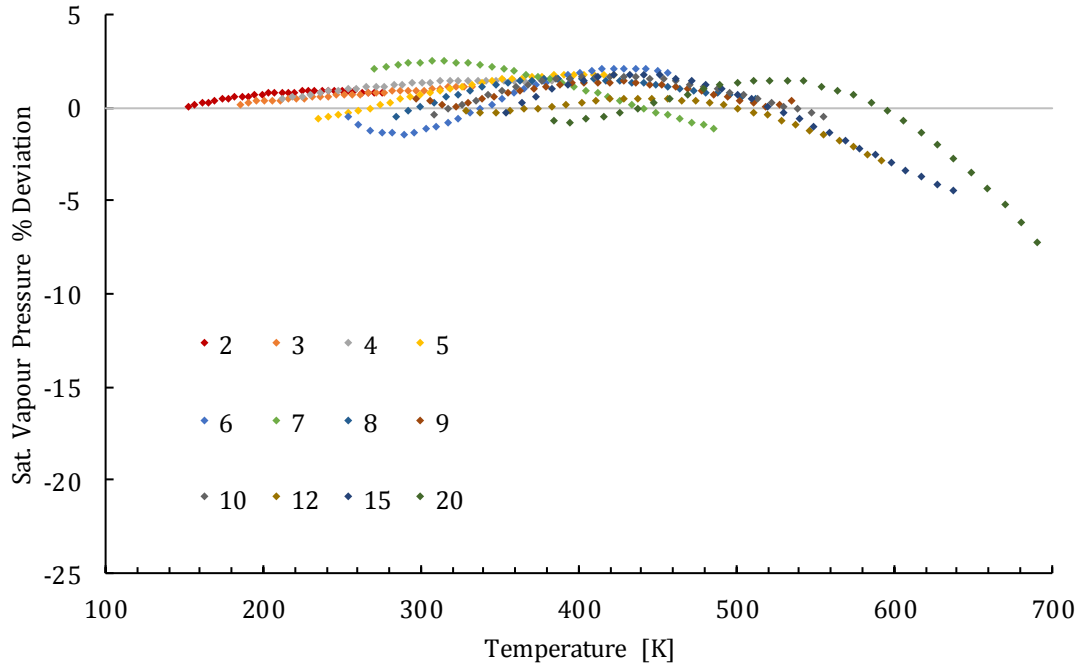

Figure D.2: SAFT-VR Mie P^{vap} % deviation from DIPPR correlations [64] for *n*-alkanes. Component carbon numbers are given in the legend.

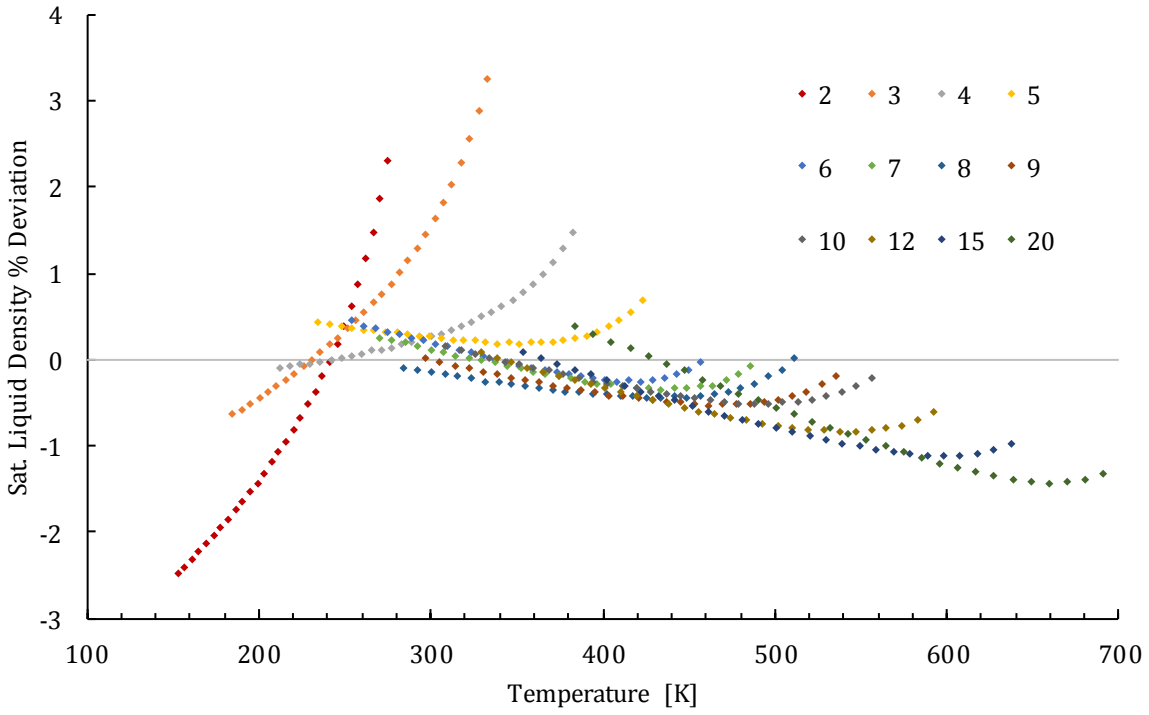

Figure D.3: SAFT-γ Mie ρ^{sat} % deviation from DIPPR correlations [64] for *n*-alkanes. Component carbon numbers are given in the legend.

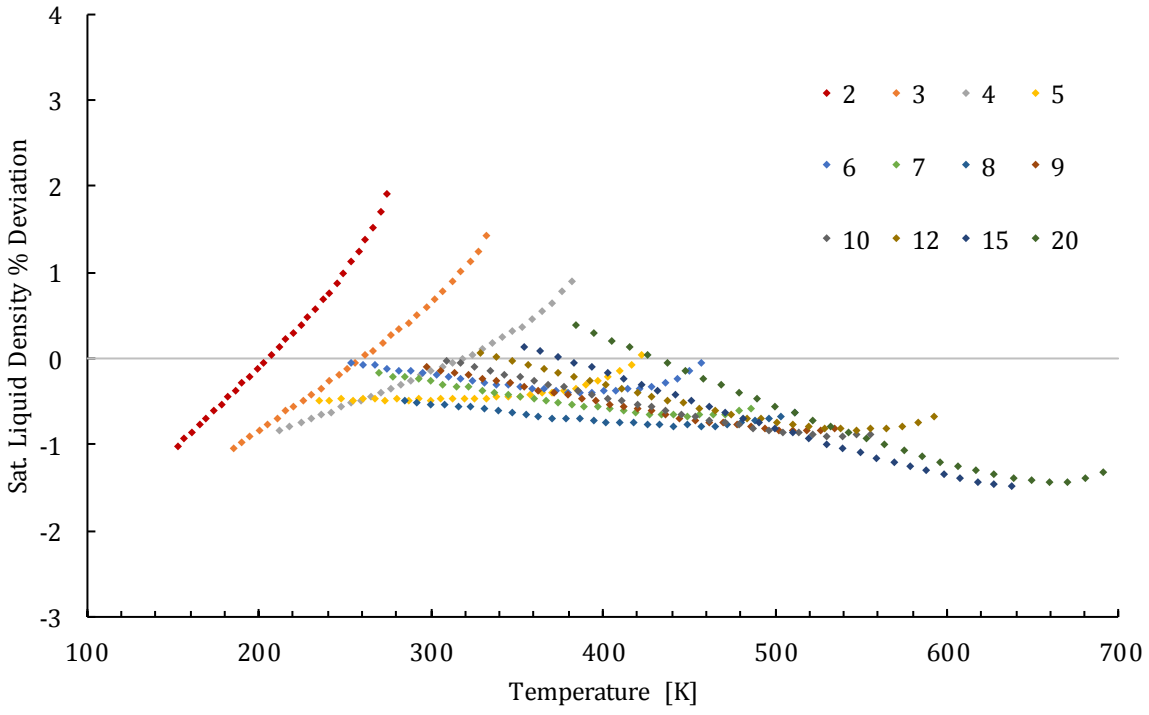

Figure D.4: SAFT-VR Mie ρ^{sat} % deviation from DIPPR correlations [64] for *n*-alkanes. Component carbon numbers are given in the legend.

It can be noted for both P^{vap} and ρ^{sat} that the trend in temperature dependence of the errors is very similar for the two models that utilise the same statistical-mechanical framework.

D.2 *n*-Alkyl Acetate + *n*-Alkane Binary Mixture Properties

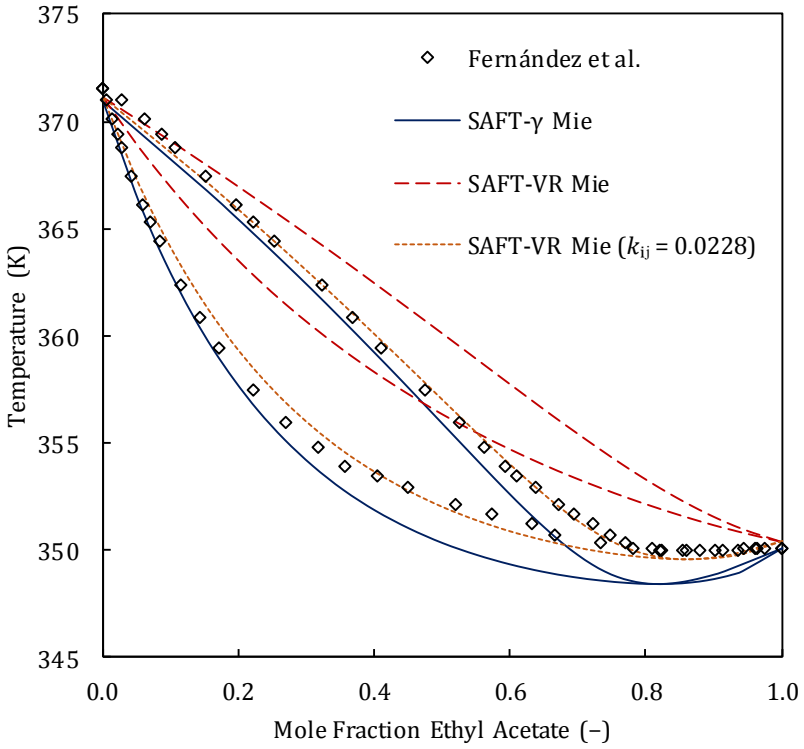

Figure D.5: Isobaric ethyl acetate + *n*-heptane VLE predictions at 1.013 bar. Data taken from Fernández et al. [72].

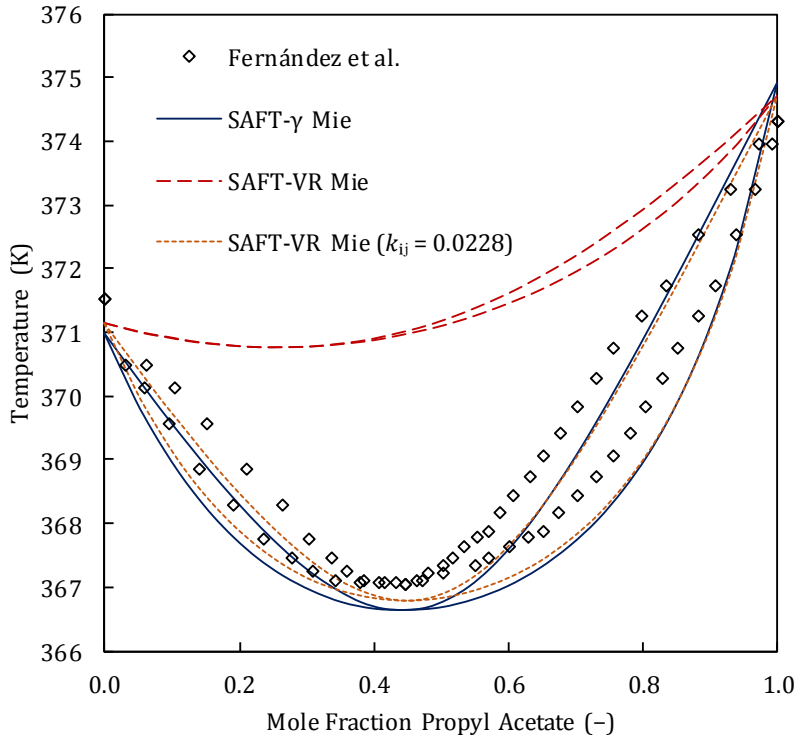

Figure D.6: Isobaric propyl acetate + *n*-heptane VLE predictions at 1.013 bar. Data taken from Fernández et al. [73].

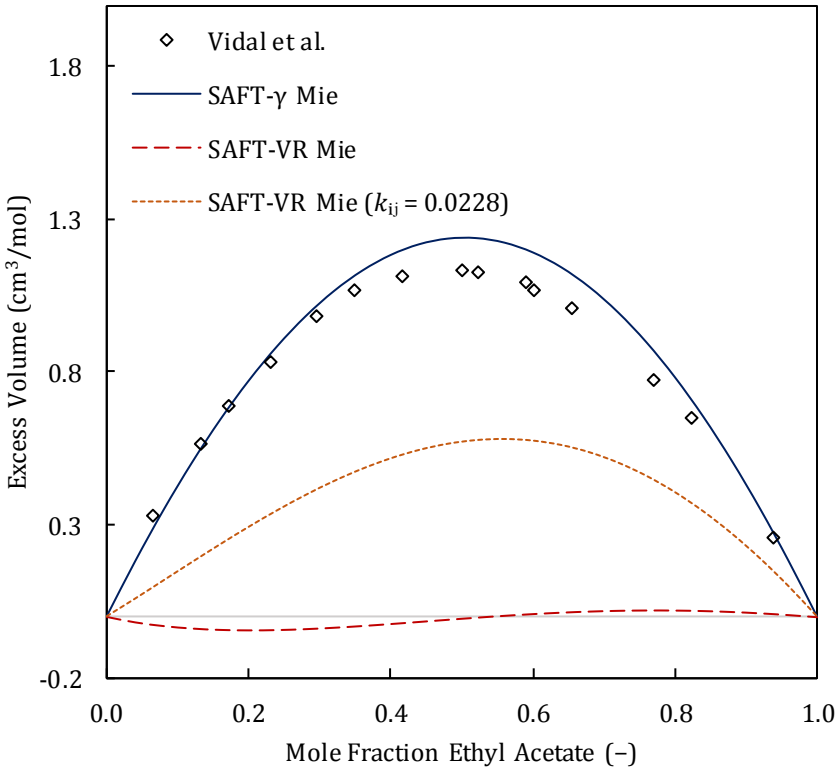

Figure D.7: Ethyl acetate + *n*-heptane excess volume predictions at 298.15 K & 1.013 bar. Data taken from Vidal et al. [103].

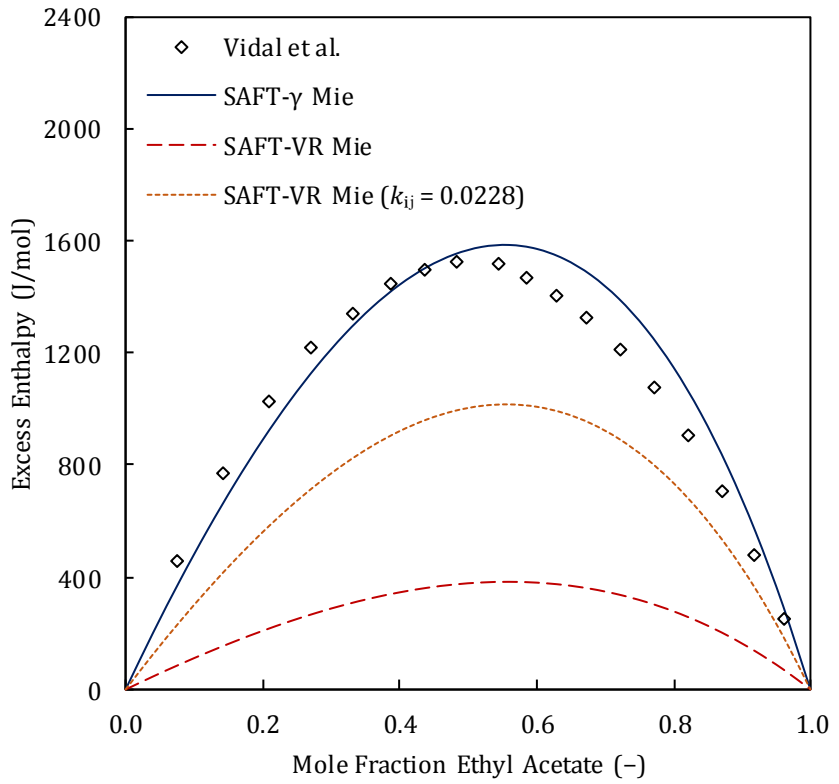

Figure D.8: Ethyl acetate + *n*-heptane excess enthalpy predictions at 298.15 K. Data taken from Vidal et al. [103].

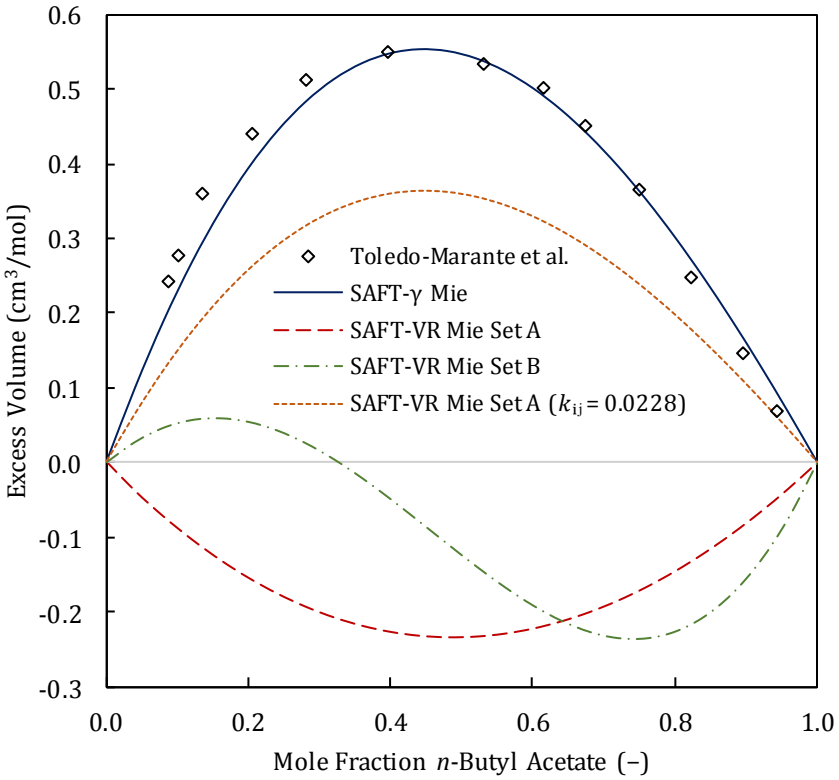

Figure D.9: *n*-Butyl acetate + *n*-heptane excess volume predictions at 298.15 K & 1.013 bar. Data taken from Toledo-Marante et al. [123].

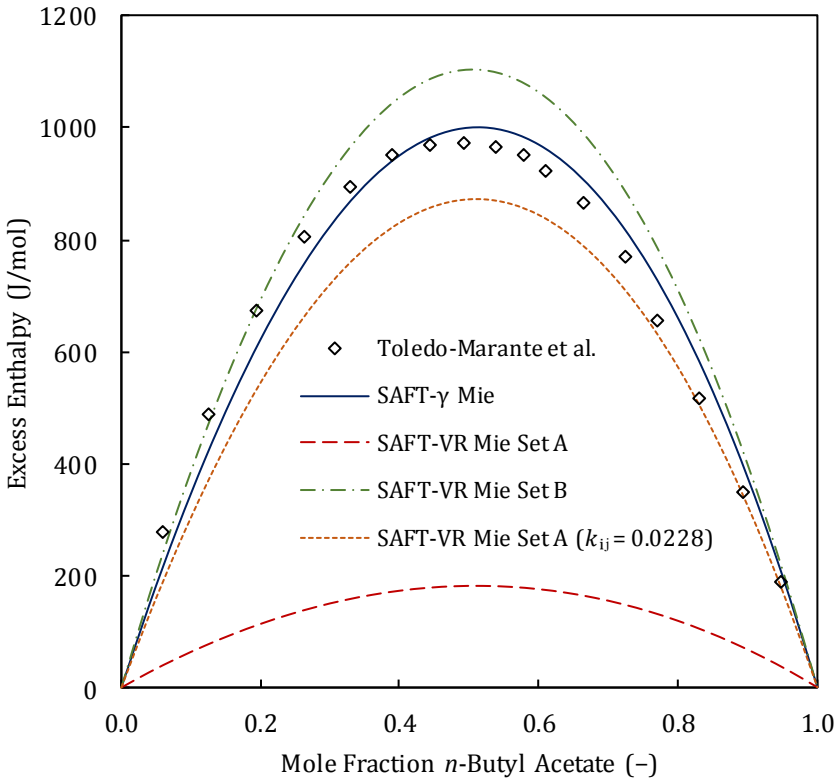

Figure D.10: *n*-Butyl acetate + *n*-heptane excess enthalpy predictions at 298.15 K. Data taken from Toledo-Marante et al. [123].

D.3 1-Alcohol + *n*-Alkane Binary Mixture Properties

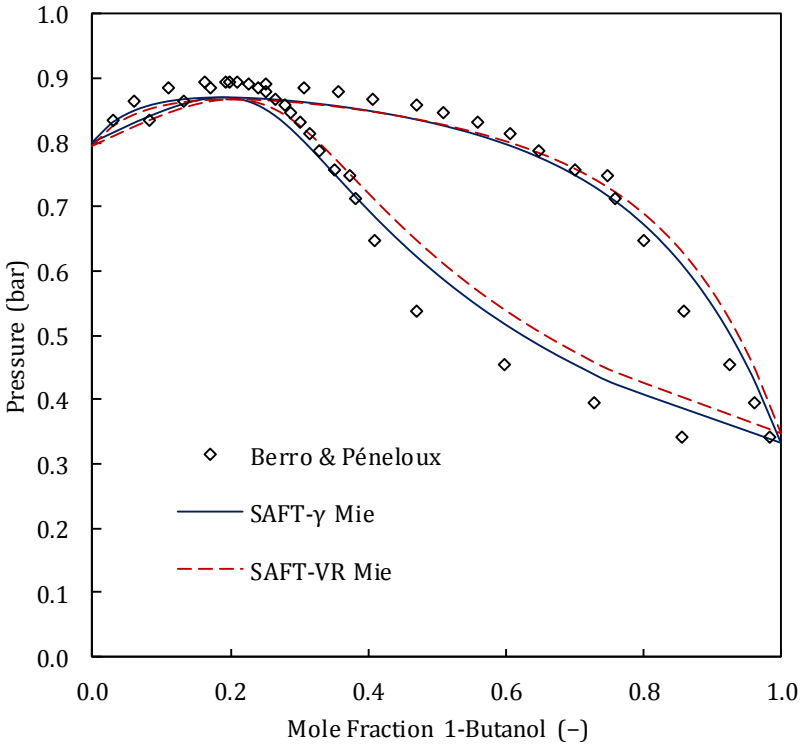

Figure D.11: Isothermal 1-butanol + *n*-heptane VLE predictions at 363.15 K. Data taken from Berro & Péneloux [124].

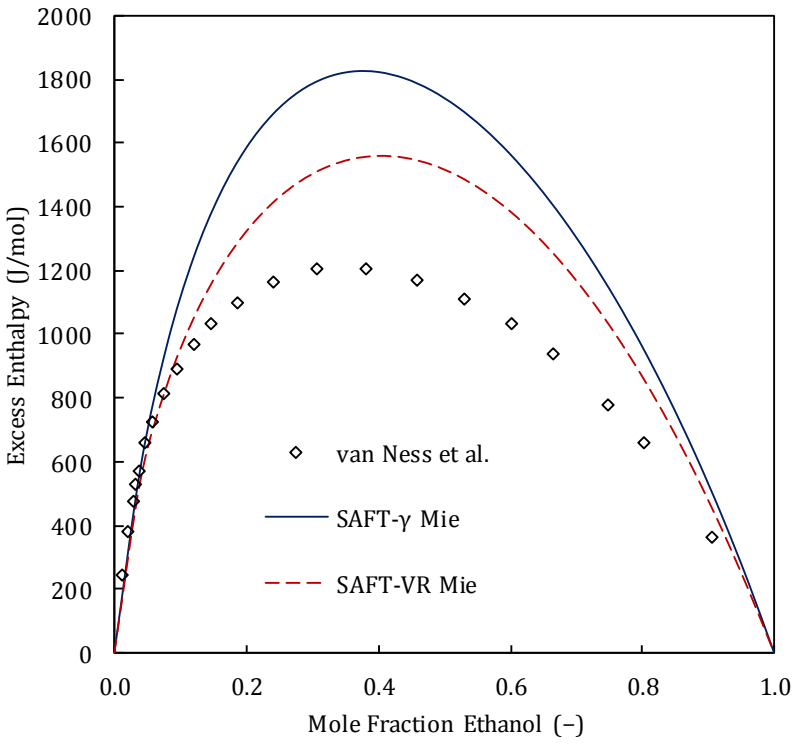

Figure D.12: Ethanol + *n*-heptane excess enthalpy predictions at 333 K. Data taken from van Ness et al. [125].

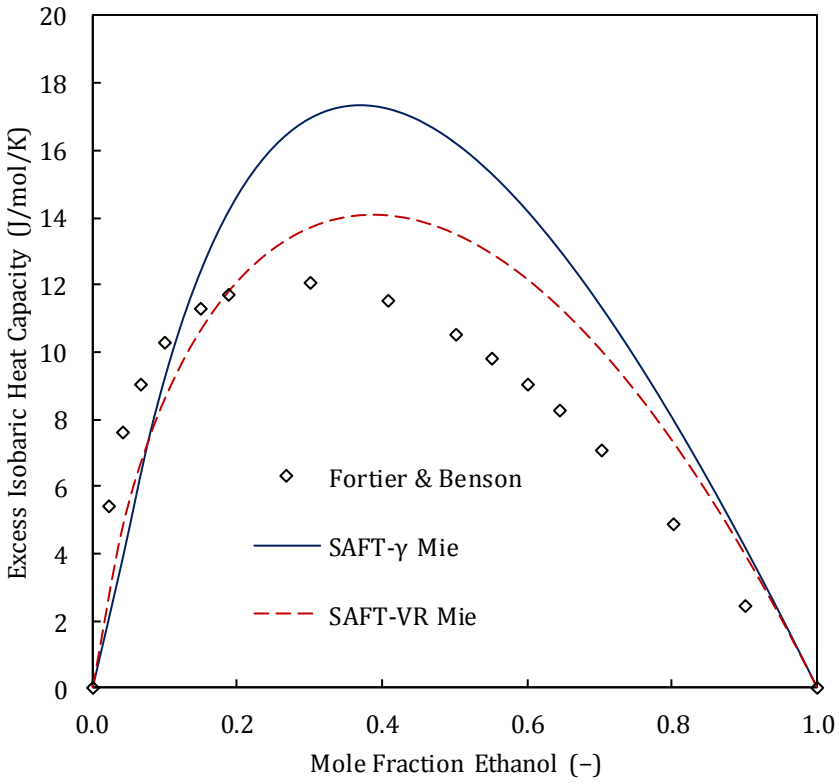

Figure D.13: Ethanol + *n*-heptane excess isobaric heat capacity predictions at 298.15 K & 1.013 bar. Data taken from Fortier & Benson [126].

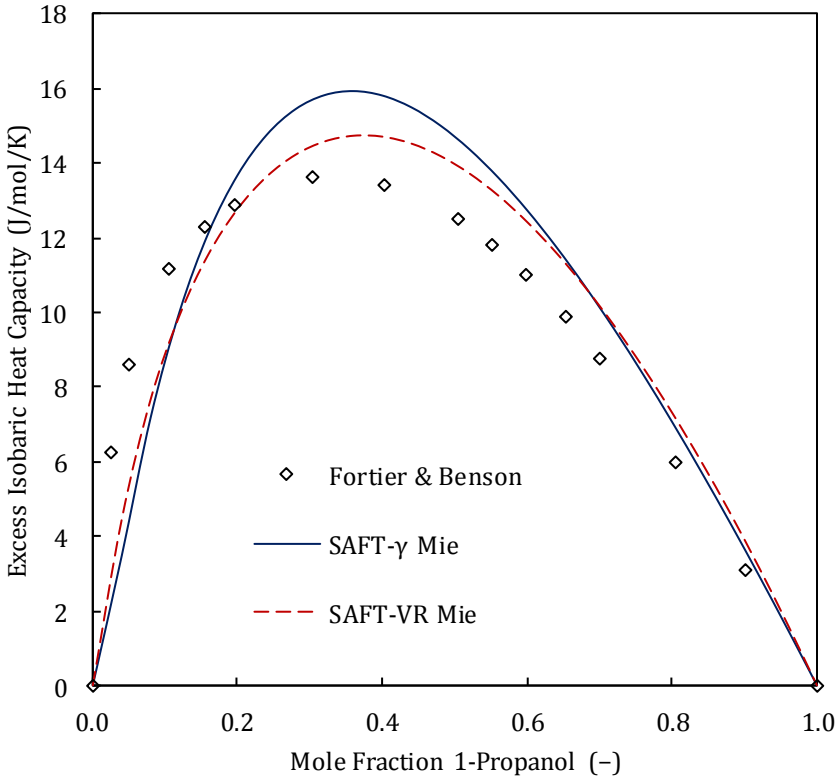

Figure D.14: 1-Propanol + *n*-heptane excess isobaric heat capacity predictions at 298.15 K & 1.013 bar. Data taken from Fortier & Benson [126].

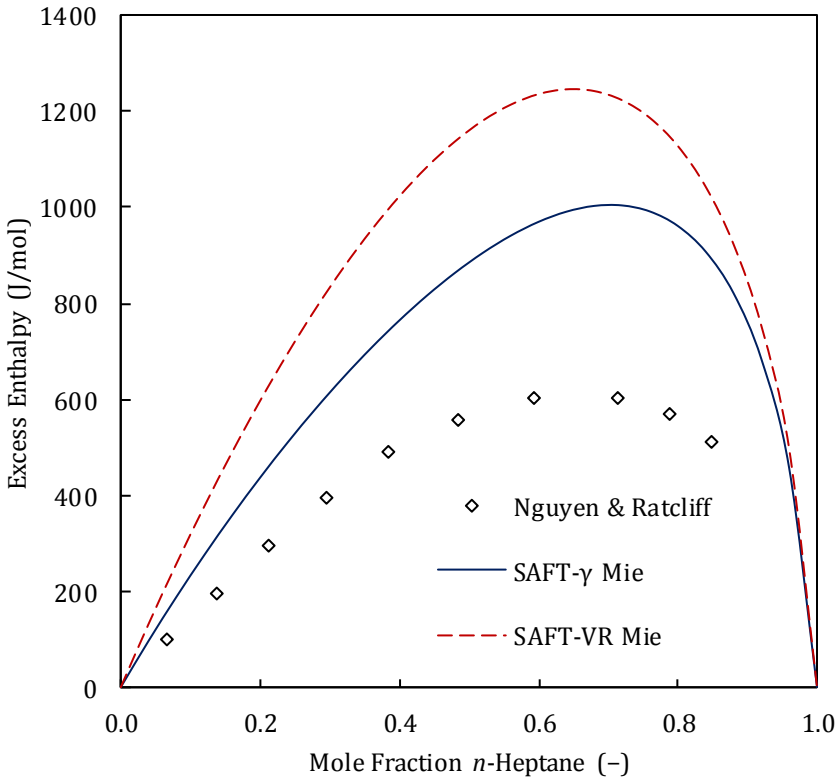

Figure D.15: *n*-Heptane + 1-butanol excess enthalpy predictions at 298 K. Data taken from Nguyen & Ratcliff [127].

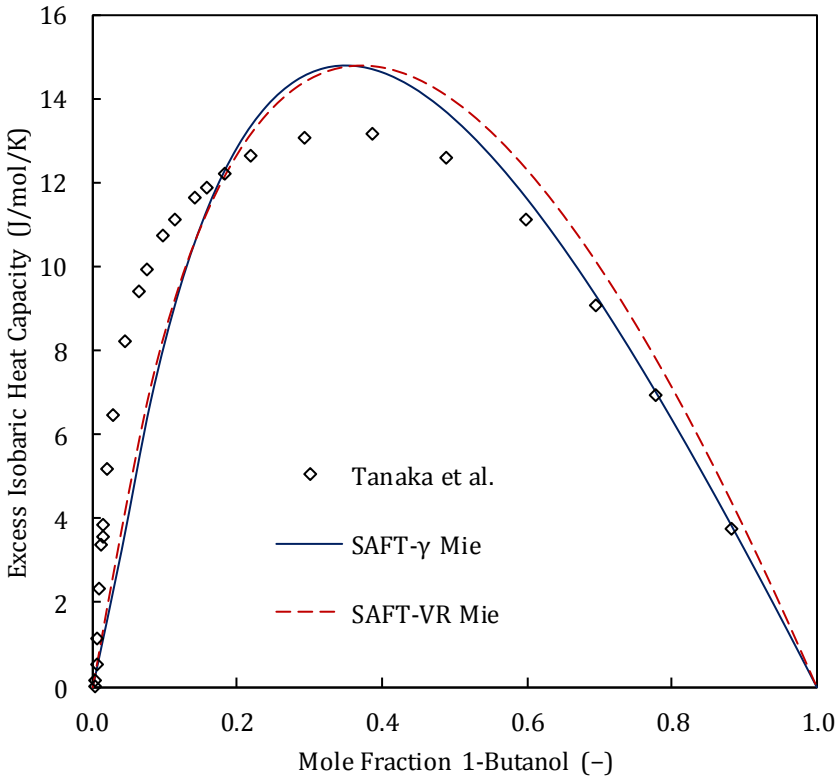

Figure D.16: 1-Butanol + *n*-heptane excess isobaric heat capacity predictions at 298.15 K & 1.013 bar. Data taken from Tanaka et al. [81].

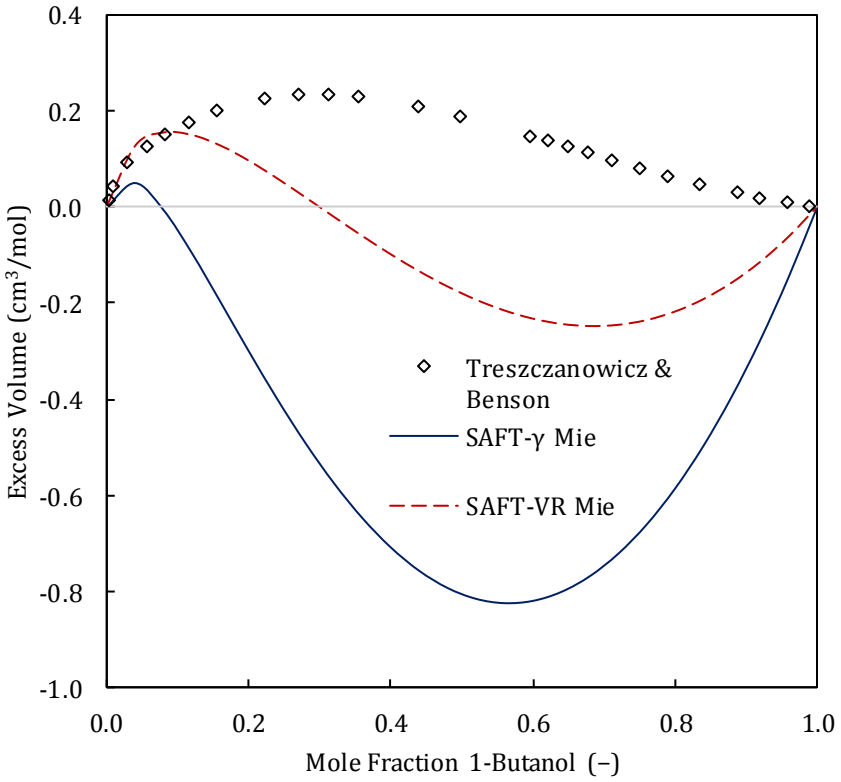

Figure D.17: 1-Butanol + *n*-heptane excess volume predictions at 298.15 K & 1.013 bar. Data taken from Treszczanowicz & Benson [80].

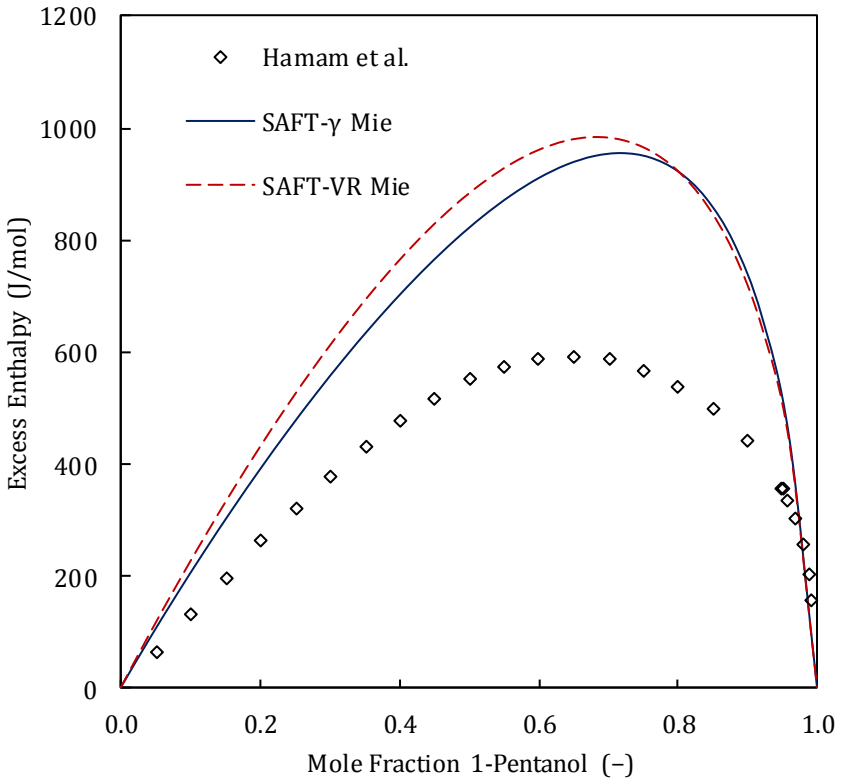

Figure D.18: 1-Pentanol + *n*-heptane excess enthalpy predictions at 298.15 K. Data taken from Hamam et al. [128].

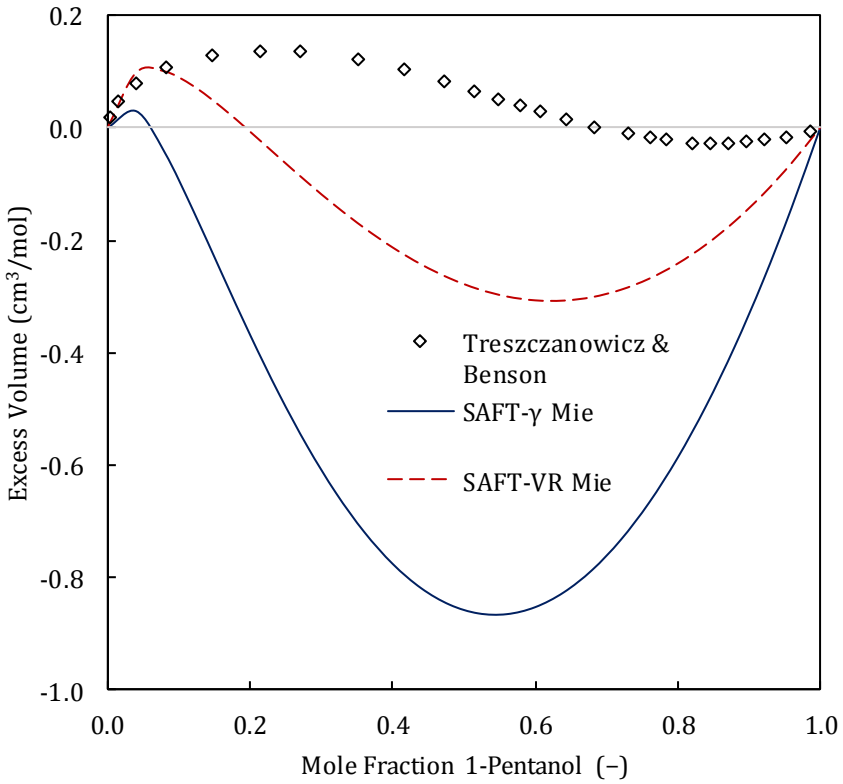

Figure D.19: 1-Pentanol + *n*-heptane excess volume predictions at 298.15 K & 1.013 bar. Data taken from Treszczanowicz & Benson [80].

D.4 2-Ketone Group Alternative Parameters

The following parameters were regressed with the same OF as those presented in Chapter 5, but the interaction dispersion energies were generated at the same time as the group-specific parameters.

Table D.1: New 2-ketone (CH_3CO) functional-group non-association SAFT-γ Mie parameters. Set A is the same parameters presented in Chapter 5 and Set B was generated with all of the parameters included in one regression procedure (excluding v_k^* and λ_{kl}^{a}).

Parameter	Group k	Group l	Set A Value	Set B Value	Units
v_k^*	CH_3CO		2.0000	2.0000	
S_k	CH_3CO		0.76442	0.63562	
σ_{kl}	CH_3CO	CH_3CO	3.4518	3.7005	Å
λ_{kl}^{a}	CH_3CO	CH_3CO	6.0000	6.0000	
λ_{kl}^{r}	CH_3CO	CH_3CO	8.2034	10.357	
ϵ_{kl}/k_B	CH_3CO	CH_3CO	209.33	303.93	K
ϵ_{kl}/k_B	CH_3CO	CH_3	233.09	280.17	K
ϵ_{kl}/k_B	CH_3CO	CH_2	298.36	348.48	K

Table D.2 New 2-ketone (CH_3CO) functional-group association SAFT-γ Mie parameters.

Parameter	Group k	Site a	Group l	Site b	Set A Value	Set B Value	Units
$\epsilon_{kl,ab}^{HB}/k_B$	CH_3CO	H	CH_3CO	e_1	1083.5	1033.0	K
$K_{kl,ab}$	CH_3CO	H	CH_3CO	e_1	546.87	282.69	$Å^3$

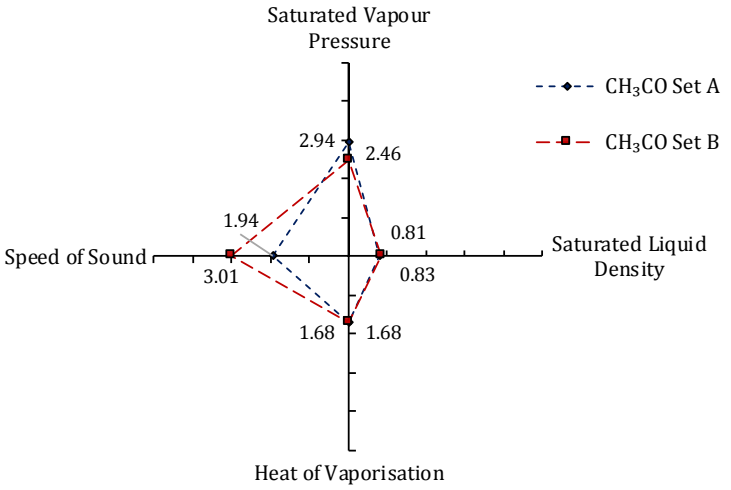

Figure D.20: 2-Ketone pure-component mean %AADs with two CH_3CO group parameter sets. %AADs are an average of 2-pentanone → 2-nonanone absolute deviations.

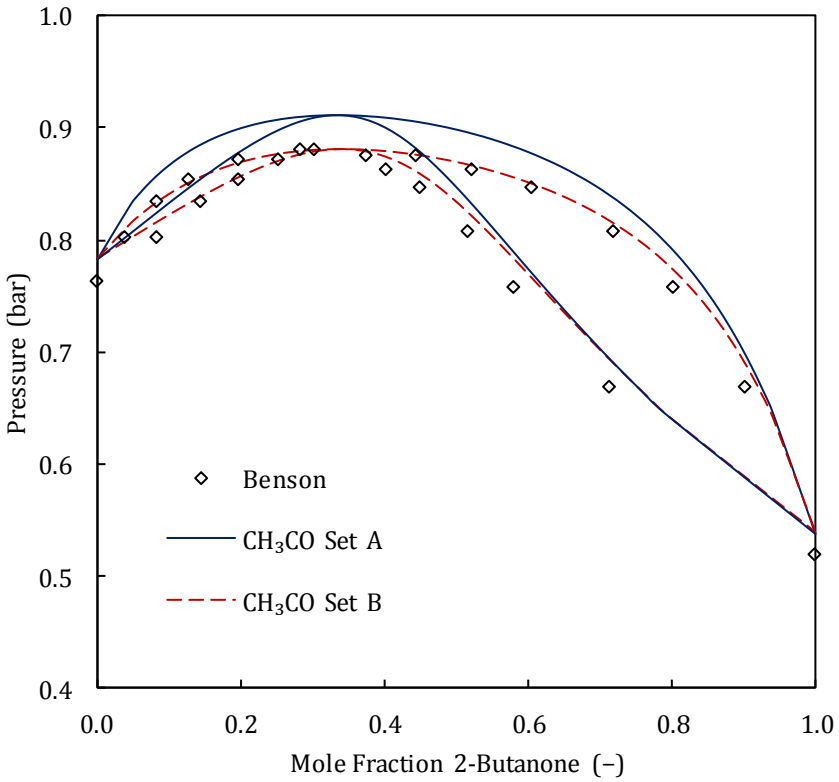

Figure D.21: Isothermal 2-butanone + *n*-hexane VLE predictions with two CH_3CO parameter sets at 333.15 K. Data taken from Benson [89]. **N.B.**: This set was included in the parameter regression.

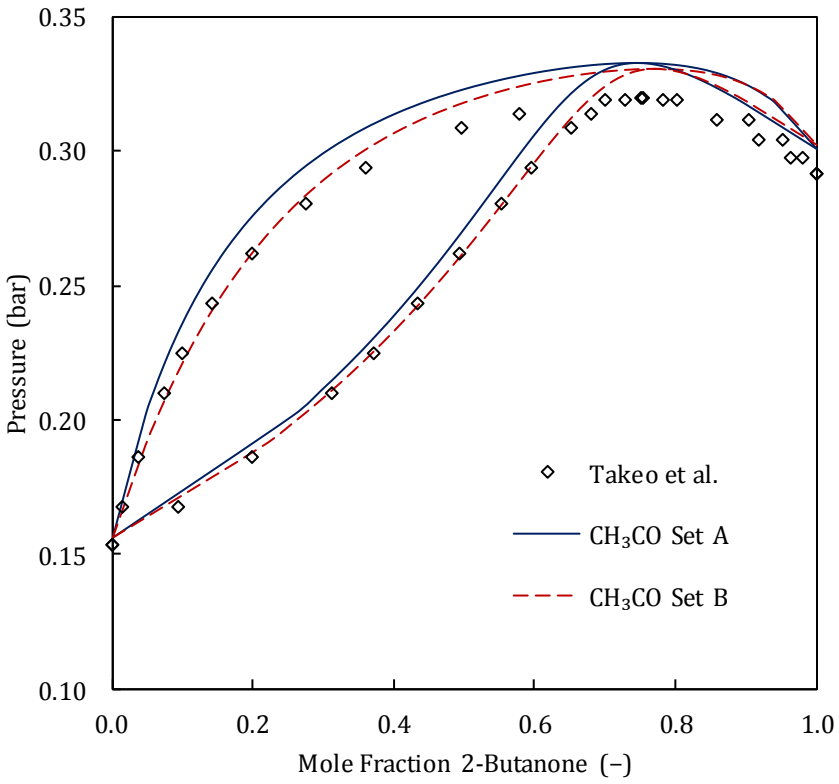

Figure D.22: Isothermal 2-butanone + *n*-heptane VLE predictions with two CH_3CO parameter sets at 318.15 K. Data taken from Takeo et al. [90].

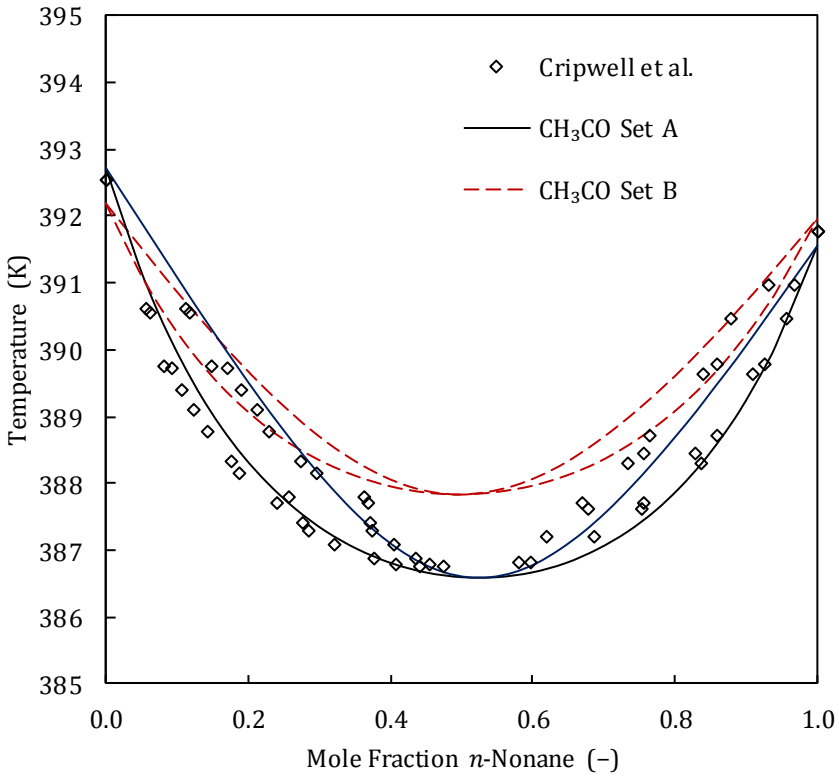

Figure D.23: Isobaric *n*-nonane + 2-heptanone VLE predictions with two CH_3CO parameter sets at 0.400 bar. Data taken from Cripwell et al. [57].

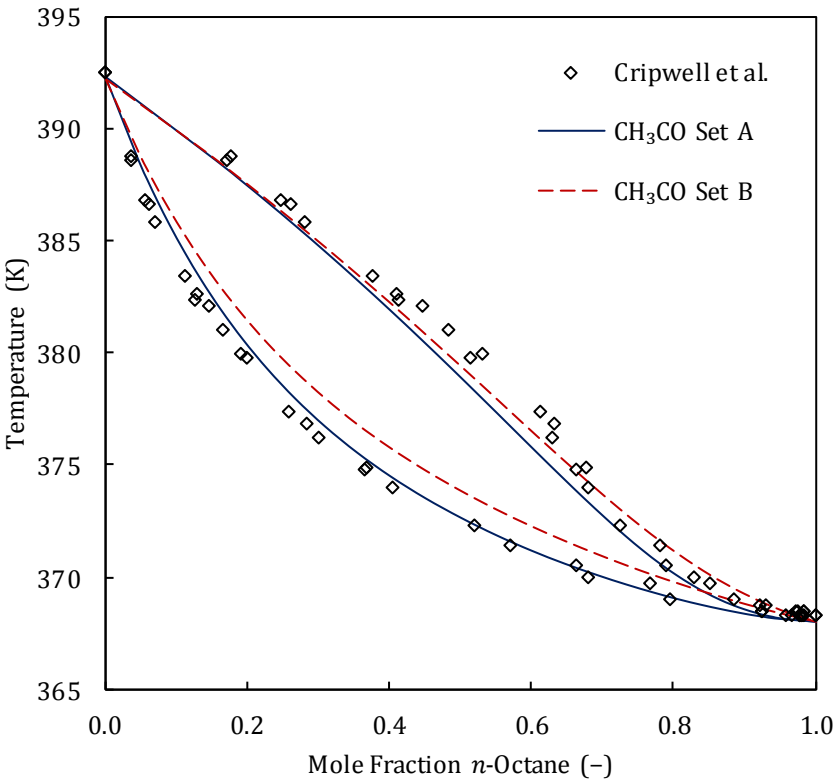

Figure D.24: Isobaric *n*-octane + 2-heptanone VLE predictions with two CH_3CO parameter sets at 0.400 bar. Data taken from Cripwell et al. [57].

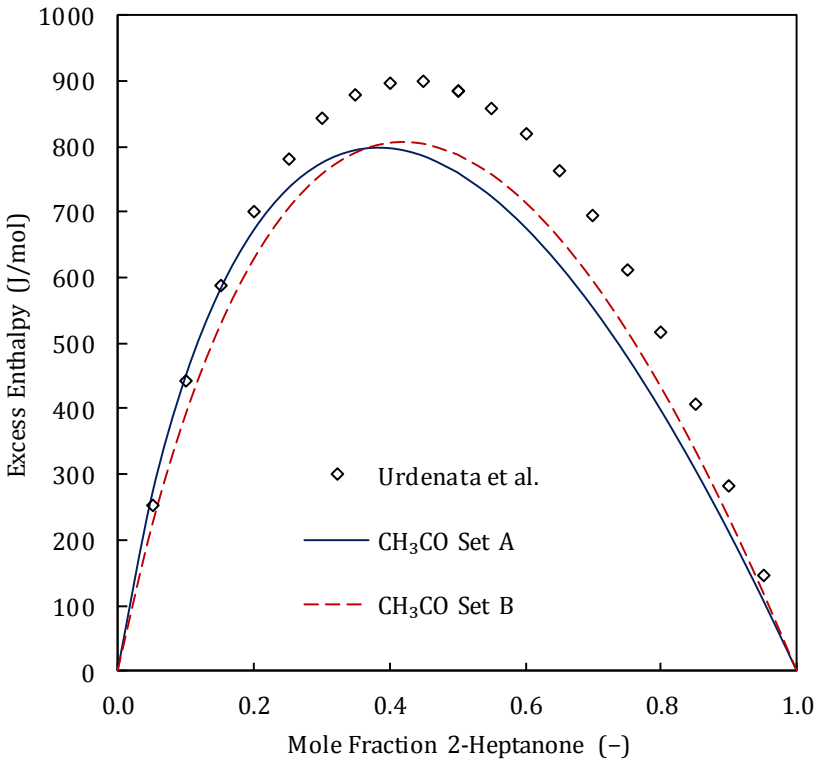

Figure D.25: 2-Heptanone + *n*-heptane excess enthalpy predictions with two CH_3CO parameter sets at 298.15 K. Data taken from Urdaneta et al. [83]. **N.B.**: This set was included in the parameter regression.

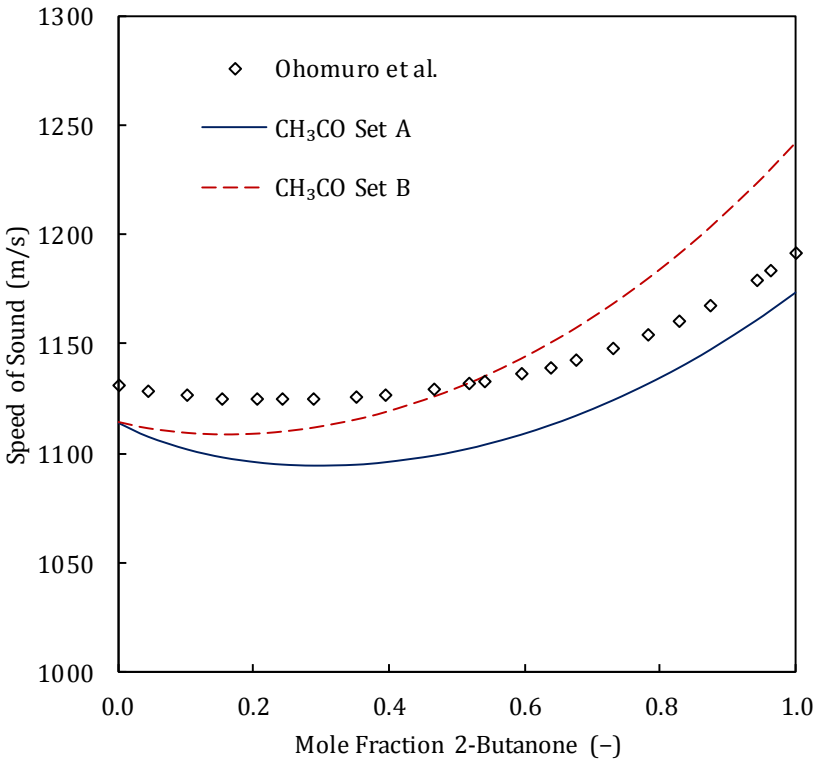

Figure D.26: 2-Butanone + *n*-heptane speed of sound predictions with two CH_3CO parameter sets at 298.15 K & 1.013 bar. Data taken from Ohomura et al. [93].

Including all of the dispersion interaction parameters for the 2-ketone group did not produce superior parameters as it did for 3-ketones. The prediction strength simply shifted between the components.

D.5 Additional *n*-Alkyl Propanoate Results

The average deviations are taken between model predictions and DIPPR correlations [64].

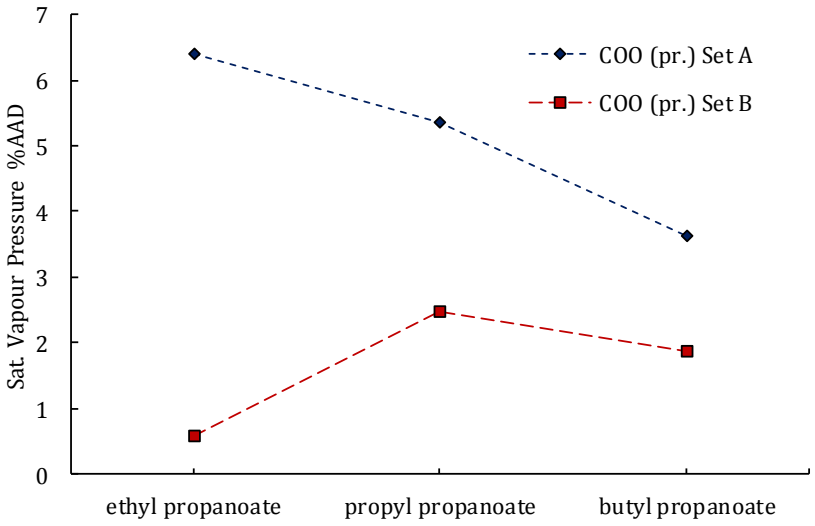

Figure D.27: : *n*-Alkyl propanoate P^{vap} prediction %AAD with COO (pr.) group.

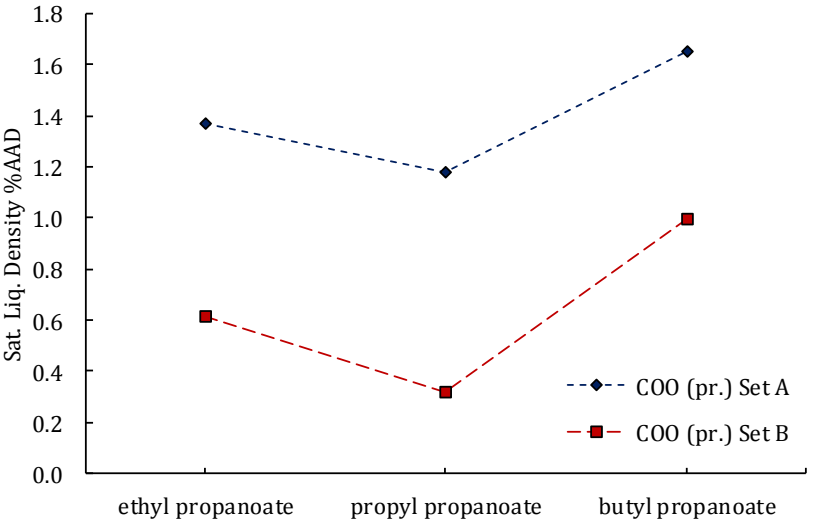

Figure D.28: *n*-Alkyl propanoate ρ^{sat} prediction %AAD with COO (pr.) group.

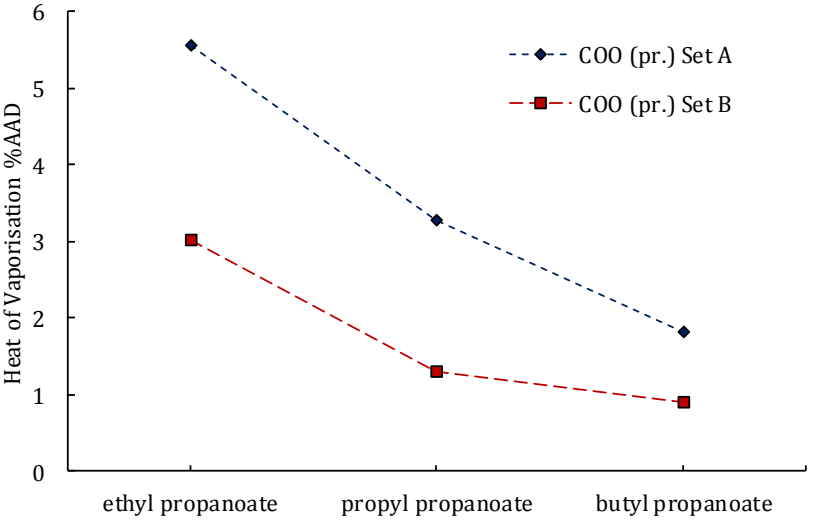

Figure D.29: *n*-Alkyl propanoate H^{vap} prediction %AAD with COO (pr.) group.

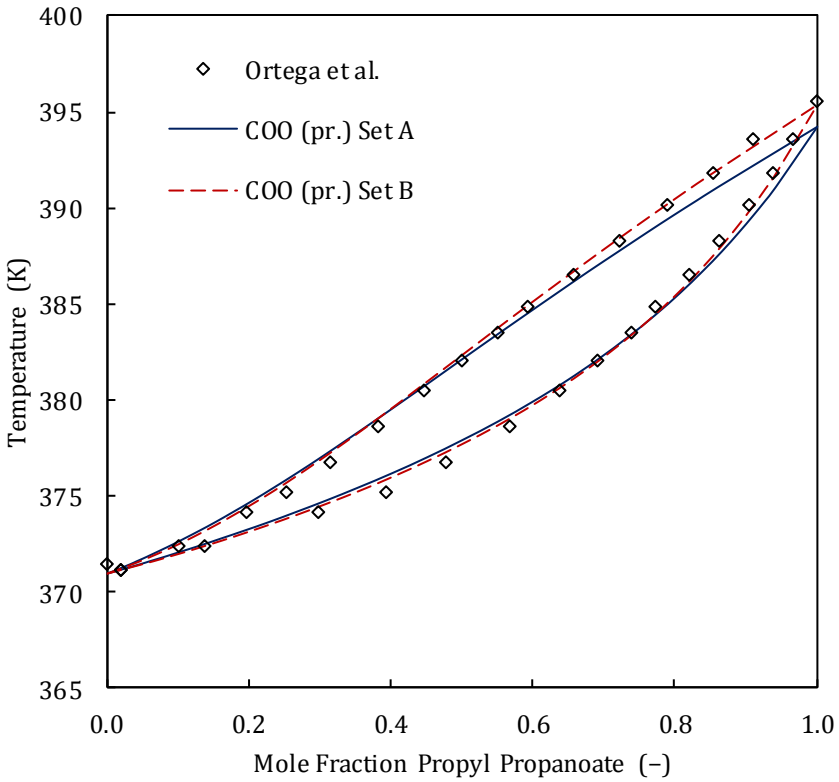

Figure D.30: Isobaric propyl propanoate + *n*-heptane VLE predictions with COO (pr.) group at 1.013 bar. Data taken from Ortega et al. [105].

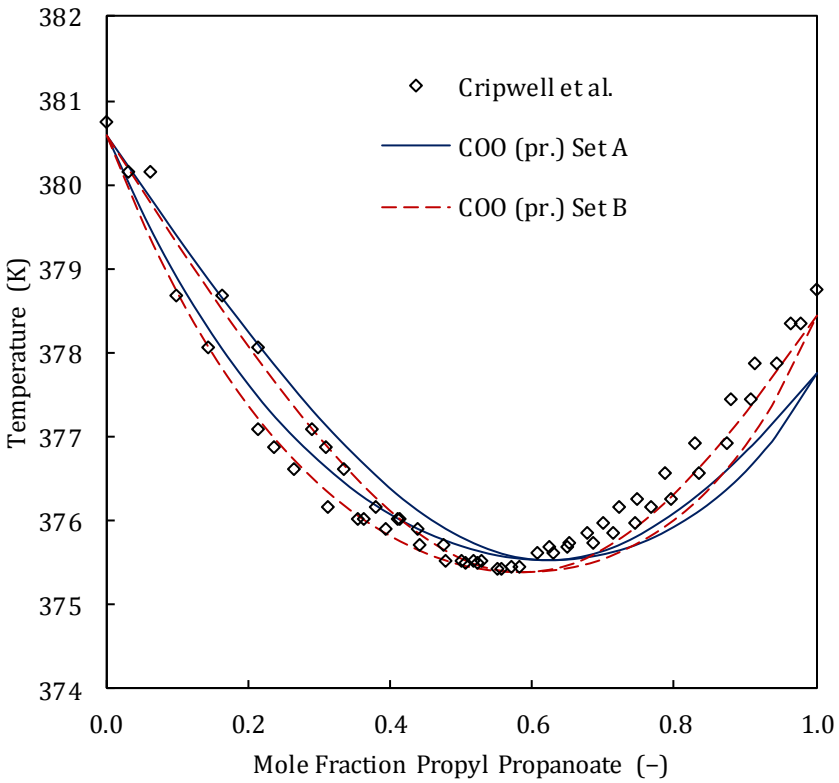

Figure D.31: Isobaric propyl propanoate + *n*-octane VLE predictions with COO (pr.) group at 1.013 bar. Data taken from Cripwell et al. [74].

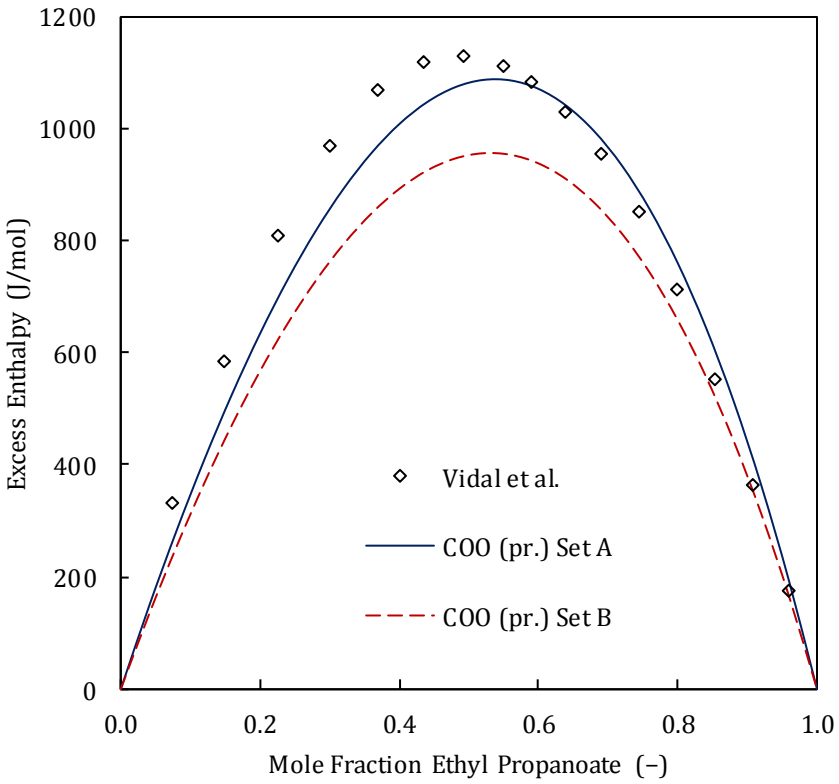

Figure D.32: Ethyl propanoate + *n*-heptane excess enthalpy predictions with COO (pr.) group at 298.15 K. Data taken from Vidal et al. [103].

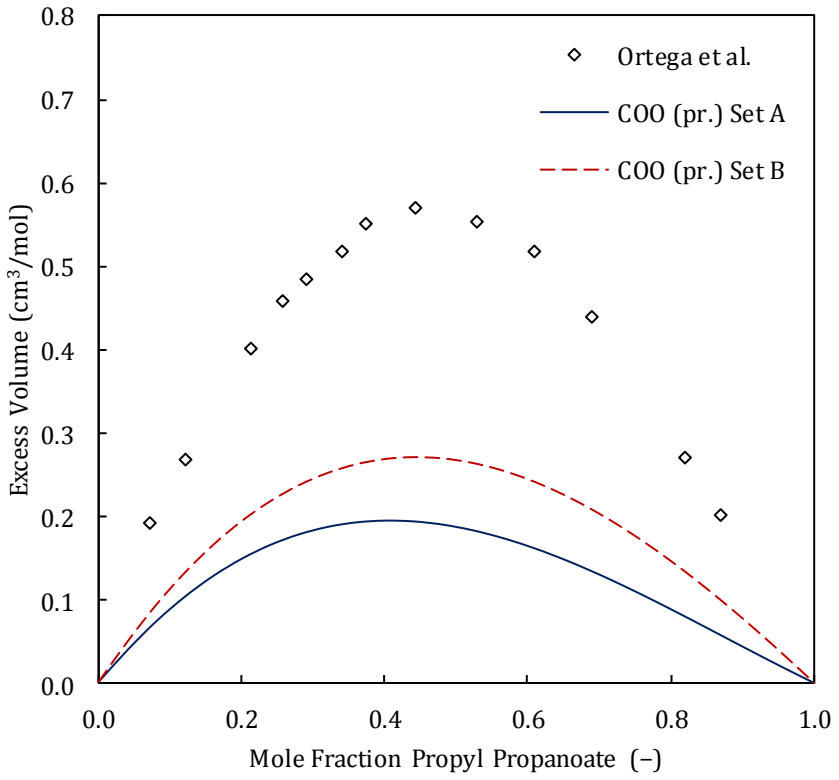

Figure D.33: Propyl propanoate + *n*-heptane excess volume predictions with COO (pr.) group at 298.15 K & 1.013 bar. Data taken from Ortega et al. [106].

D.6 Additional Branched Alkane VLE Results

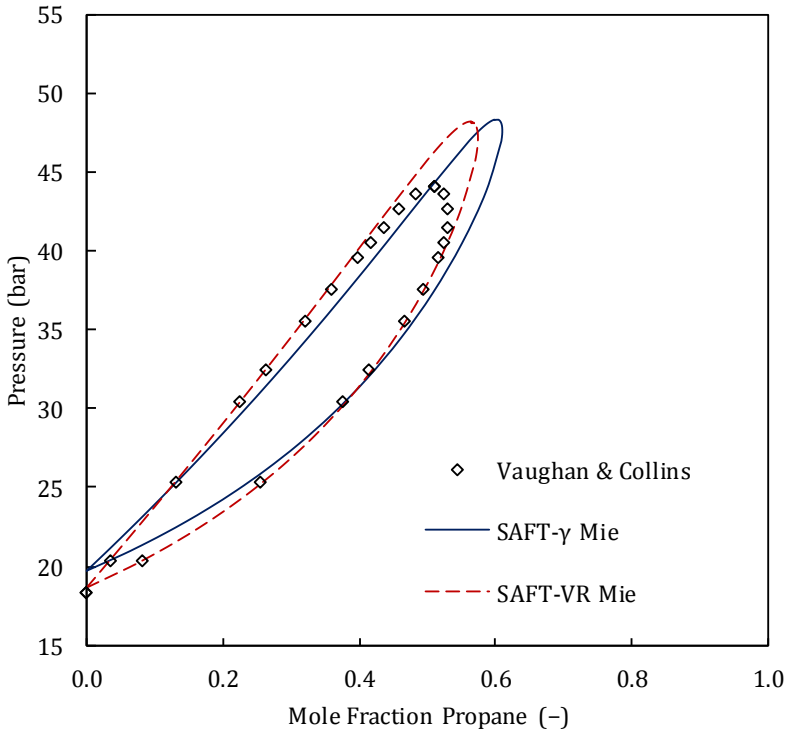

Figure D.34: Isothermal propane + 2-methylbutane VLE predictions at 423.15 K. Data taken from Vaughan & Collins [129].

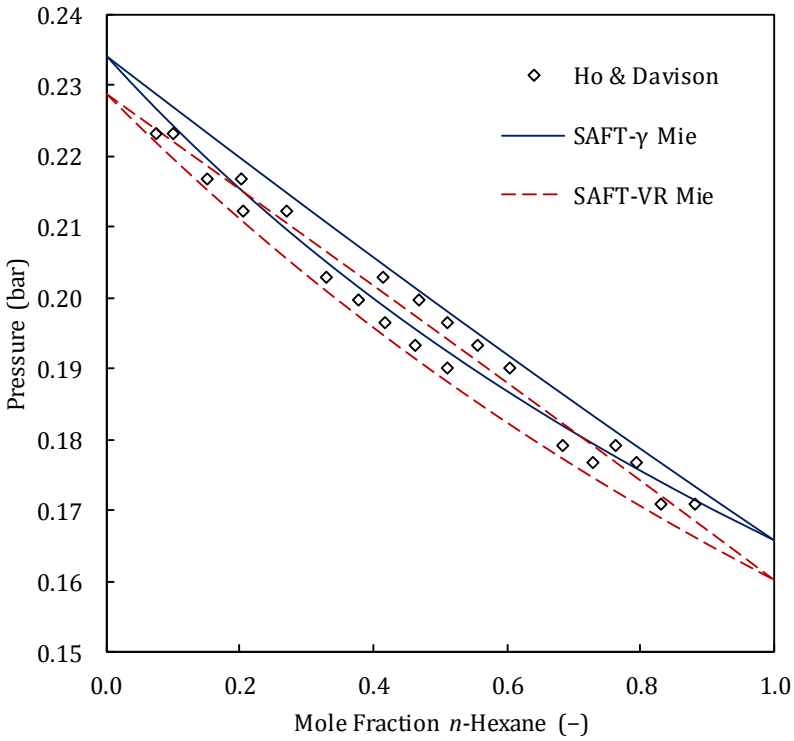

Figure D.35: Isothermal *n*-hexane + 2-methylpentane VLE predictions at 293.15 K. Data taken from Ho & Davison [130].

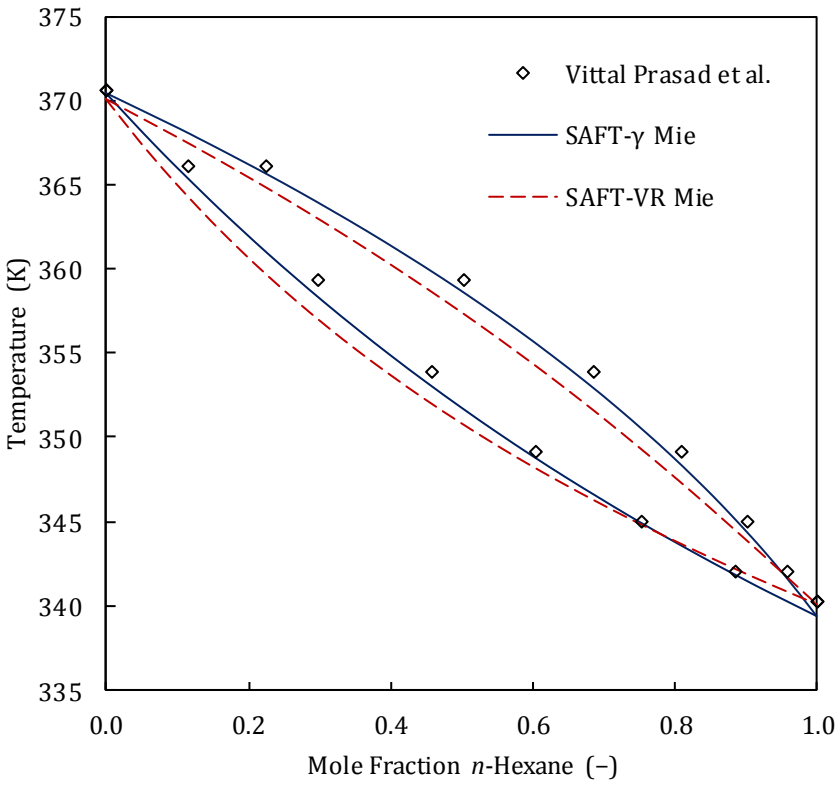

Figure D.36: Isobaric *n*-hexane + 2,2,4-trimethylpentane VLE predictions at 0.958 bar. Data taken from Vittal Prasad et al. [131].

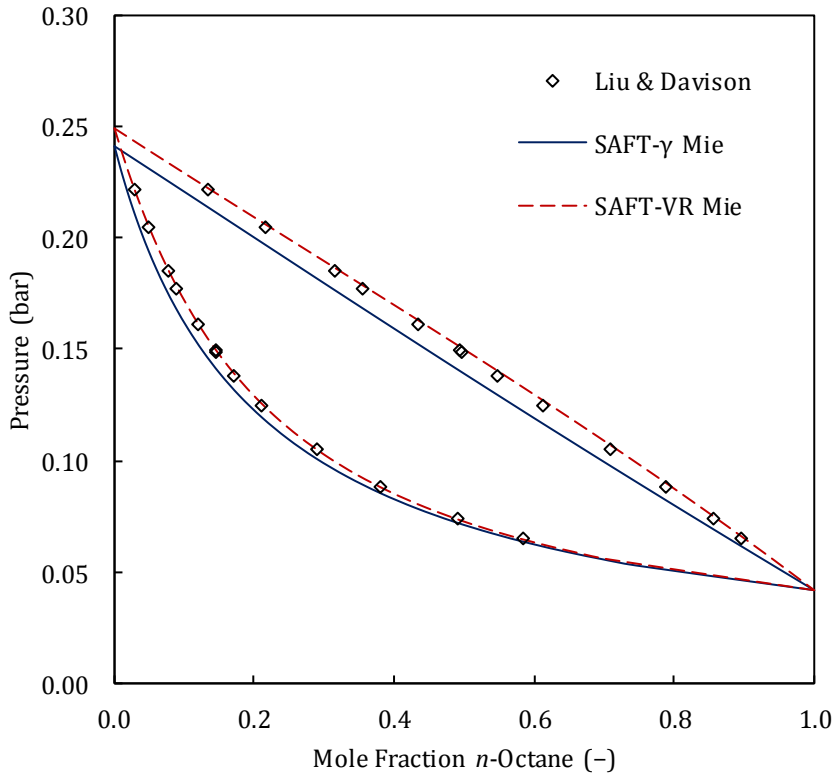

Figure D.37: Isothermal *n*-octane + 2,4-dimethylpentane VLE predictions at 313.15 K. Data taken from Liu & Davison [132].

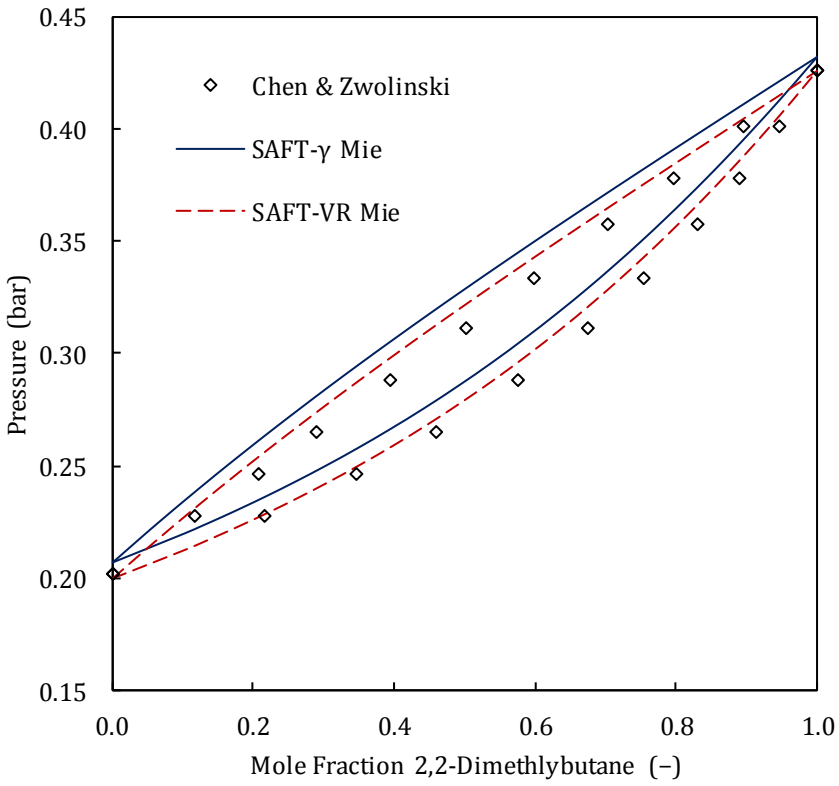

Figure D.38: Isothermal 2,2-dimethylbutane + *n*-hexane VLE predictions at 298.15 K. Data taken from Chen & Zwolinski [133].